
Theses and Dissertations

Spring 2013

Controlled polymer nanostructure and properties through photopolymerization in lyotropic liquid crystal templates

Bradley Steven Forney
University of Iowa

Follow this and additional works at: <https://ir.uiowa.edu/etd>

 Part of the [Chemical Engineering Commons](#)


Copyright 2013 Bradley Steven Forney

This dissertation is available at Iowa Research Online: <https://ir.uiowa.edu/etd/2495>

Recommended Citation

Forney, Bradley Steven. "Controlled polymer nanostructure and properties through photopolymerization in lyotropic liquid crystal templates." PhD (Doctor of Philosophy) thesis, University of Iowa, 2013.
<https://doi.org/10.17077/etd.59z0lc2p>

Follow this and additional works at: <https://ir.uiowa.edu/etd>

 Part of the [Chemical Engineering Commons](#)

CONTROLLED POLYMER NANOSTRUCTURE AND PROPERTIES THROUGH
PHOTOPOLYMERIZATION IN LYOTROPIC LIQUID CRYSTAL TEMPLATES

by
Bradley Steven Forney

An Abstract

Of a thesis submitted in partial fulfillment
of the requirements for the Doctor of
Philosophy degree in Chemical and Biochemical Engineering
in the Graduate College of
The University of Iowa

May 2013

Thesis Supervisor: Professor C. Allan Guymon

ABSTRACT

Incorporating nanotechnology into polymers has tremendous potential to improve the functionality and performance of polymer materials for use in a wide range of biomedical and industrial applications. This research uses lyotropic liquid crystals (LLCs) to control polymer structure on the nanometer scale in order to improve material properties. The overall goal of this research is to establish fundamental methods of synthesizing polymers with controlled nanostructured architectures in order to understand and utilize useful property relationships that result from the organized polymer morphologies. This work aims to establish a fundamental understanding of the reaction conditions needed to control polymer nanostructure and determine the benefits of organized polymer network structures on mechanical and transport properties.

The synthesis of nanostructured polymers for improved material performance has utilized LLCs and photopolymerization kinetics to direct polymer structure. Self-assembled LLC phases provide a useful template that may be used as a photopolymerization platform to control polymer morphology on the nanometer size scale. Photopolymerization kinetics were used as a tool to examine the thermodynamics and phase structure evolution that occurs during the polymerization reaction. Additionally, several methods were developed to control polymer morphology and prevent loss of LLC order that can occur during polymerization. LLCs were also used to generate nanocomposite polymers with two distinct polymer networks to impart improvements in material properties. Other useful property relationships including increases in mechanical integrity, greater diffusive transport, and larger water uptake were established in this research.

Finally, the LLC templating process was applied to solve performance problems associated with stimuli-sensitive polymer materials. Dramatic improvements in the response rate, dynamic range, and mechanical properties were achieved using LLCs and

photopolymerization to control polymer nanostructure. This work has established fundamental tools that can be used to understand and control the evolution of polymer structure during the polymerization reaction in order to improve polymer properties. Ultimately, the enhanced properties generated by the nanostructured polymer network can be used to improve the functionality of polymers.

Abstract Approved: _____
Thesis Supervisor

Title and Department

Date

CONTROLLED POLYMER NANOSTRUCTURE AND PROPERTIES THROUGH
PHOTOPOLYMERIZATION IN LYOTROPIC LIQUID CRYSTAL TEMPLATES

by

Bradley Steven Forney

A thesis submitted in partial fulfillment
of the requirements for the Doctor of
Philosophy degree in Chemical and Biochemical Engineering
in the Graduate College of
The University of Iowa

May 2013

Thesis Supervisor: Professor C. Allan Guymon

Graduate College
The University of Iowa
Iowa City, Iowa

CERTIFICATE OF APPROVAL

PH.D. THESIS

This is to certify that the Ph.D. thesis of

Bradley Steven Forney

has been approved by the Examining Committee
for the thesis requirement for the Doctor of Philosophy
degree in Chemical and Biochemical Engineering at the May 2013 graduation.

Thesis Committee: _____
C. Allan Guymon, Thesis Supervisor

Julie Jessop

David Rethwisch

Eric Nuxoll

Vicki Grassian

I would like to dedicate this work to my mom and dad.

ACKNOWLEDGMENTS

First and foremost, I thank my advisor Dr. Allan Guymon for his insights and support over the last four and a half years. I learned much more than general research skills from him including how to express ideas and concerns, defend my work, and generally handle myself in professional manner. I will never forget the important lessons that I have learned from my observations of and conversations with Dr. Guymon inside and outside the lab. The skills and training that I have received during my time at Iowa have prepared me for future success in research and product development.

I would like to thank my committee members Dr. Julie Jessop, Dr. David Rethwisch, Dr. Eric Nuxoll, and Dr. Vikki Grassian for their direct and indirect contributions to this work. In addition to technical knowledge, each member contributed a unique perspective to this research that pushed me to consider other opportunities in the development and application of polymers studied in this research. Moreover, the perspectives and accomplishments of my committee members has taught me the value of collaboration, the need to continually push the boundaries of my observations, and to never rest on my laurels.

I thank the Department of Chemical and Biochemical Engineering for the resources needed to complete this work and the opportunity to instruct Chemical Engineering Thermodynamics. I want to thank Linda Wheatley, Natalie Potter, and Wendy Meyers for all their help and assistance. I thank the National Science Foundation, Ciba Vision, and the Materials Research Science and Engineering Center for financial support of this project.

I have had the privilege of working with several talented undergraduates that have contributed to this research including Ben Butler, Abby Neu, Stephanie McCoy, and Barbara McMullan. I learned a lot about motivating, planning, and communicating ideas

needed to accomplish this research through my interactions with these exceptionally bright individuals. I wish each of them success in their future careers.

Many thanks go out to Lucas Sievens-Figueroa, Kwame Owusu-Adom, Jason Clapper, Soon Ki Kim, Clint Cook, Brain Dillman, Brad Tuft, Kristan Worthington, Celine Baguenard, Jon Scholte, Todd Thorson, and Jake McLaughlin. Each has contributed to my success in graduate school through helpful discussions, laughter and perspective, leading by example, happy memories, and showing me the promising future that lay ahead of me if I continue to work hard. I have fully enjoyed the time we have spent together and I consider each one of them friends and look forward to meeting up with them in the future.

Finally, I thank Katie for all of her support and patience in this process. She helps to provide the motivation for my hard work, dedication, and consistency.

ABSTRACT

Incorporating nanotechnology into polymers has tremendous potential to improve the functionality and performance of polymer materials for use in a wide range of biomedical and industrial applications. This research uses lyotropic liquid crystals (LLCs) to control polymer structure on the nanometer scale in order to improve material properties. The overall goal of this research is to establish fundamental methods of synthesizing polymers with controlled nanostructured architectures to understand and utilize useful property relationships that result from the organized polymer morphologies. This work aims to establish a fundamental understanding of the reaction conditions needed to control polymer nanostructure and determine the benefits of organized polymer network structures on mechanical and transport properties.

The synthesis of nanostructured polymers for improved material performance has utilized LLCs and photopolymerization kinetics to direct polymer structure. Self-assembled LLC phases provide a useful template that may be used as a photopolymerization platform to control polymer morphology on the nanometer size scale. Photopolymerization kinetics were used as a tool to examine the thermodynamics and phase structure evolution that occurs during the polymerization reaction. Additionally, several methods were developed to control polymer morphology and prevent loss of LLC order that can occur during polymerization. LLCs were also used to generate nanocomposite polymers with two distinct polymer networks to impart improvements in material properties. Other useful property relationships including increases in mechanical integrity, greater diffusive transport, and larger water uptake were established in this research.

Finally, the LLC templating process was applied to solve performance problems associated with stimuli-sensitive polymer materials. Dramatic improvements in the response rate, dynamic range, and mechanical properties were achieved using LLCs and

photopolymerization to control polymer nanostructure. This work has established fundamental tools that can be used to understand and control the evolution of polymer structure during the polymerization reaction in order to improve polymer properties. Ultimately, the enhanced properties generated by the nanostructured polymer network can be used to improve the functionality of polymers.

TABLE OF CONTENTS

LIST OF TABLES	x
LIST OF FIGURES	xi
CHAPTER	
1. INTRODUCTION	1
Lyotropic Liquid Crystals.....	4
Lyotropic Liquid Crystals as Structure Directing Polymerization Platforms.....	8
Photopolymerization.....	11
Initiation	14
Propagation.....	16
Termination	17
Characteristics of Thiol-ene Radical Photopolymerizations	19
Photopolymerization Kinetics in Ordered Liquid Crystalline Systems.....	21
Photopolymerization of Lyotropic Liquid Crystalline Templates – Reactive Surfactants	27
Structure-property Relationships in Nanostructured Polymer Systems	29
Transport Properties of LLC Nanostructured Polymers.....	34
Stimuli-sensitive Polymers	37
Research Summary	42
Notes	44
2. OBJECTIVES.....	50
3. MATERIALS AND EXPERIMENTAL METHODS.....	55
Materials and Sample Preparation	55
Characterization.....	58
Photopolymerization Kinetics and Structure Characterization	58
Transport Property Characterization	61
Mechanical Property Characterization	63
Notes	65
4. NANOSTRUCTURE EVOLUTION DURING PHOTOPOLYMERIZATION IN LYOTROPIC LIQUID CRYSTAL TEMPLATES	66
Introduction.....	67
Experimental.....	70
Materials.....	70
Sample Preparation.....	71
Kinetics.....	71
Characterization.....	72
Results and Discussion	73

	Nanostructure Evolution of Hexagonal Templated PEGDA (PEGDA-50).....	81
	Nanostructure Evolution of Lamellar Templated HDDA (HDDA-50).....	86
	Conclusions.....	90
	Notes	92
5.	CONTROLLED HYDROGEL NANOSTRUCTURE AND PROPERTIES THROUGH PHOTOPOLYMERIZATION IN LYOTROPIC LIQUID CRYSTALLINE TEMPLATES.....	95
	Introduction.....	96
	Experimental.....	100
	Materials	100
	Sample Preparation.....	101
	Kinetics.....	101
	Structural Characterization.....	102
	Water Uptake.....	103
	Release Profiles	103
	Mechanical Properties	104
	Results and Discussion	105
	Structural Characterization.....	105
	Physical Properties	115
	Mechanical Properties	119
	Conclusions.....	124
	Notes	126
6.	FAST DESWELLING KINETICS OF NANOSTRUCTURED POLY(<i>N</i> -ISOPROPYLACRYLAMIDE) PHOTOPOLYMERIZED IN A LYOTROPIC LIQUID CRYSTALLINE TEMPLATE.....	128
	Introduction.....	128
	Experimental.....	131
	Materials	131
	Hydrogel Synthesis.....	131
	Structural Characterization.....	132
	Network Swelling.....	133
	Deswelling Kinetics.....	133
	Mechanical Properties	133
	Results and Discussion	134
	Conclusions.....	140
	Notes	141
7.	IMPROVED STIMULI RESPONSE AND MECHANICAL PROPERTIES OF NANOSTRUCTURED POLY(<i>N</i> -ISOPROPYLACRYLAMIDE-CO-DIMETHYLSILOXANE) HYDROGELS GENERATED THROUGH PHOTOPOLYMERIZATION IN LYOTROPIC LIQUID CRYSTAL TEMPLATES	143
	Introduction.....	144
	Experimental.....	149

Materials	149
Sample Preparation.....	150
Structural Characterization.....	151
Equilibrium Water Uptake	151
Deswelling Kinetics.....	152
Mechanical Properties	153
Results and Discussion	152
Conclusions.....	164
Notes	166
8. NANOSTRUCTURED THIOL-ENE POLYMERS GENERATED THROUGH PHOTOPOLYMERIZATION IN WATER FREE LYOTROPIC LIQUID CRYSTALLINE PHASES	169
Introduction.....	170
Experimental.....	175
Results and Discussion	179
Conclusions.....	194
Notes	196
9. CONCLUSIONS AND RECOMMENDATIONS	201
BIBLIOGRPAPHY.....	212

LIST OF TABLES

Table

5.1. Summary of Physical Properties for LLC Templated and Isotropic Polyacrylamide	124
--	-----

LIST OF FIGURES

Figure

- 1.1. Representations of self-assembled lyotropic liquid crystalline phases commonly formed using surfactant in a polar solvent such as water. Shown in order of increasing surfactant concentrations are the hexagonal, bicontinuous cubic, and lamellar mesophases5
- 1.2. Representative structures of reactive and non-reactive surfactants utilized to generate lyotropic liquid crystalline phases with water. Shown are a) Polyethylene glycol hexadecyl ether, polyoxyethylene (20) cetyl ether (Brij 58), b) dodecyltrimethylammonium bromide (DTAB), acrylate functionalized quaternary ammonium surfactant, dodecyl-dimethyl-(2-prop-2-enoyloxyethyl)ammonium bromide, (C12A), and d) cationic triacrylate terminated sodium salt7
- 1.3. Representative LLC templating process used to generate a hexagonal nanostructure in organic polymers. Shown clockwise from the bottom left is (a) cross-section of the hexagonal phase, (b) segregation of polar *N*-isopropylacrylamide in the continuous water-soluble domains of the template, (c) segregation of non-polar PDMS monomers in the discontinuous oil-soluble domains of the template, (d) photopolymerization of monomers and removal of the non-reactive surfactant template10
- 1.4. Chemical structures of common radical photoinitiated polymer systems that are used in this research. Shown are a) *N,N'*-methylene bisacrylamide, b) acrylamide, c) *N*-isopropylacrylamide, d) hexanediol diacrylate, e) poly(ethylene glycol) diacrylate, f) poly(dimethyl siloxane) dimethacrylate, and g) radical photoinitiator 2,2-Dimethoxy-1,2-diphenylethan-1-one (Irgacure 651).13
- 1.5. Schematic of the radical mediated thiol-ene step growth photopolymerization reaction with alternating propagation and chain-transfer events between thiol and ene monomer20
- 1.6. Representation of the average mesh size, ξ , which largely dictates the diffusive properties of the polymer network. Shown are a) representative average mesh size for an isotropic network and b) hexagonal LLC nanostructured network36

3.1. Chemical structures of monomers, surfactants, and photoinitiators used in this study. Shown are a) <i>N,N'</i> -methylene bisacrylamide, b) acrylamide, c) <i>N</i> -isopropylacrylamide, d) hexanediol diacrylate, e) poly(ethylene glycol) diacrylate, f) poly(dimethyl siloxane) dimethacrylate, g) acrylate functionalized quaternary ammonium surfactant, dodecyl-dimethyl-(2-prop-2-enoyloxyethyl)ammonium bromide, (C12A), h) pentaerythritol tetrakis(2-mercaptoacetate) i) 1,3,5-triallyl-1,3,5-triazine-2,4,6(1H,3H,5H)-trione j) quaternary ammonium surfactant cetyltrimethylammonium bromide (CTAB), k) polyoxyethylene (2) cetyl ether (Brij 52), l) polyoxyethylene (10) cetyl ether (Brij 56), m) radical photoinitiators 2,2-Dimethoxy-1,2-diphenylethan-1-one (Irgacure 651) and n) hydroxy-2-methyl-1-phenyl-propan-1-one (Darocur 1173).....	57
4.1. Photopolymerization kinetics for LLC templated and isotropic polymer systems. Shown are (a) Polymerization rate as a function of time for 20 wt% PEGDA in EGDAC (isotropic – ●), and with 40 wt% (normal hexagonal – ▽), 50 wt% (normal hexagonal – □), 60 wt% (lamellar – ◇), and 70 wt% (lamellar – ▲) Brij 56 in water. (b) Polymerization rate as a function of time for 20 wt% HDDA in EGDAC (isotropic – ○), and with 30 wt% (normal hexagonal – ▽), 40 wt% (normal hexagonal – ■), 50 wt% (lamellar – ◇), and 60 wt% (lamellar – ▲) Brij 56 in water. Polymerization was initiated with 0.5 wt% Irgacure 651 at a light intensity of 3.27 mW/cm ²	75
4.2. Polarized light micrographs of LLC templated samples before and after photopolymerization at 10X magnification. Shown are samples of 20 wt% PEGDA with 50 wt% Brij 56 in water (a) before and (b) after polymerization and a sample of 20 wt% HDDA with 50 wt% Brij 56 in water (c) before and (d) after polymerization. Polymerization was initiated with 0.5 wt% Irgacure 651 at a light intensity of 0.5 mW/cm ²	78
4.3. SAXS profiles before and after photopolymerization of LLC templated PEGDA and HDDA. Shown are (a) SAXS profile of a 20 wt% PEGDA with 50 wt% Brij 56 in water (normal hexagonal) before polymerization (i) and after polymerization (ii) as well as Brij 56-water mixture (iii) containing the same surfactant to water ratio. (b) SAXS profile for a 20 wt% HDDA with 50 wt% Brij 56 in water (lamellar) before polymerization (i) and after polymerization (ii) as well as Brij 56-water mixture (iii) containing the same surfactant to water ratio. Polymerization was initiated with 0.5 wt% Irgacure 651 at a light intensity of 0.5 mW/cm ²	79
4.4. Photopolymerization rate and rate derivative for LLC templated and isotropic PEGDA. Shown are (a) Polymerization rate as a function of conversion of 20 wt% PEGDA in EGDAC (isotropic – ●) and with 50 wt% Brij 56 in water (normal hexagonal – ▽). (b) First derivative of polymerization rate shown in (a) with respect to conversion as a function of conversion of 20 wt% of 20 wt% PEGDA in EGDAC (isotropic – ●) and with 50 wt% Brij 56 in water (normal hexagonal – ▽). Inset shows the rate derivative between 40 and 60% conversion. Polymerization was initiated with 0.5 wt% Irgacure 651 at a light intensity of 0.5 mW/cm ²	82

- 4.5. SAXS profiles before, during, and after photopolymerization of PEGDA. Shown are (a) SAXS profile for a 20 wt% PEGDA with 50 wt% Brij 56 in water (PEGDA-50, normal hexagonal) before polymerization (i) and at 15% conversion (ii), (b) 40% (iii) and 50% conversion (iv), and (c) 55% (v) and 70% conversion (vi). Insets show higher order scattering peaks. Polymerization was initiated with 0.5 wt% Irgacure 651 at a light intensity of 0.5 mW/cm².....83
- 4.6. Photopolymerization rate and rate derivative for LLC templated and isotropic HDDA. Shown are (a) Polymerization rate as a function of conversion for 20 wt% HDDA in EGDAC (isotropic – ∇) and with 50 wt% Brij 56 in water (lamellar – ●). Inset shows rate behavior at low conversion. (b) First derivative of the polymerization rate shown in (a) with respect to conversion as a function of conversion for 20 wt% HDDA in EGDAC (isotropic – ∇) and with 50 wt% Brij 56 in water (lamellar – ●). Inset shows the rate derivative between 50 and 70% conversion. Polymerization was initiated with 0.5 wt% Irgacure 651 at a light intensity of 0.5 mW/cm².87
- 4.7. SAXS profiles before, during, and after photopolymerization of HDDA. Shown are (a) SAXS profile for 20 wt% HDDA with 50 wt% Brij 56 in water (lamellar) before polymerization (i) 10% conversion (ii) and (b) 55% conversion (iii) and 65% conversion (iv). Insets show higher order scattering peaks. All polymerization were initiated with 0.5 wt% Irgacure 651 at a light intensity of 0.5 mW/cm².88
- 5.1. Chemical structures of monomers and surfactants used in this study. Shown are (a) *N,N'*-methylenebisacrylamide, (b) acrylamide, (c) cetyltrimethylammonium bromide (CTAB) surfactant, and (d) acrylate functionalized quaternary ammonium surfactant, dodecyl-dimethyl-(2-prop-2-enoyloxyethyl)ammonium bromide, (C12A).100
- 5.2. Polarized light micrographs of 20 wt % cross-linked acrylamide templated with different concentrations of CTAB and C12A surfactants (50 wt % total) in water before and after photopolymerization. Shown are 0 wt % C12A before (a) and after (b), 5 wt % C12A before (c) and after (d), 10 wt % C12A before (e) and after (f), and 15 wt % C12A before (g) and after (h) polymerization.107
- 5.3. Small angle X-ray scattering profiles before and after photopolymerization of acrylamide (95 wt % acrylamide and 5 wt % *N,N'*-methylenebisacrylamide) templated with varying concentrations of nonreactive CTAB and polymerizable C12A surfactants. Shown are profiles of samples with a) 5:3 weight ratio CTAB:water (---), 0/50 wt % C12A/CTAB before (●), and after polymerization (○), b) 5/45 wt % C12A/CTAB before (◆) and after polymerization (◇), c) 10/40 wt % C12A/CTAB before (▲) and after polymerization (Δ), and d) 15/35 wt % C12A/CTAB before (■) and after (□) polymerization. Insets are also shown to indicate the secondary reflections that identify the hexagonal phase.....109

- 5.4. Scanning electron micrographs of 20 wt % cross-linked polyacrylamide photopolymerized in the hexagonal LLC phase formed using varying concentrations of unreactive CTAB and polymerizable C12A surfactants. Shown are cross-sections of polyacrylamide templated with (a) 0/50 wt % C12A/CTAB, (b) 5/45 wt % C12A/CTAB, (c) 10/40 wt % C12A/CTAB, (d) (c) at higher magnification, (e) 15/35 wt % C12A/CTAB, and (f) (e) at higher magnification. CTAB surfactant template was removed prior to imaging.....112
- 5.5. Polymerization rate as a function of time for 20 wt % cross-linked polyacrylamide photopolymerized in the hexagonal LLC phase formed using varying concentrations of nonreactive CTAB and polymerizable C12A surfactants. Shown are acrylamide templated with 0/50 wt % C12A/CTAB (●), 5/45 wt % C12A/CTAB (◇), 10/40 wt % C12A/CTAB (▲), and 15/35 wt % C12A/CTAB (□). Photopolymerization was initiated at a light intensity of 1.5 mW/cm² at 365 nm and 1 wt % Irgacure 651 with respect to monomer mass.114
- 5.6. Mass percentage water content as a function of time for polyacrylamide hydrogels photopolymerized in the hexagonal LLC phase formed using varying concentrations of unreactive CTAB and polymerizable C12A surfactants. Also included is the transient water uptake of isotropic polyacrylamide controls with the same basic chemical composition of LLC templated systems. Shown are 0/50 wt % C12A/CTAB (○, phase separated), 0/0 wt % C12A/CTAB (●, isotropic), 5/45 wt % C12A/CTAB (◇, phase separated), 5/0 wt % C12A/CTAB (◆, isotropic), 10/40 wt % C12A/CTAB (Δ, hexagonal), 10/0 wt % C12A/CTAB (▲, isotropic), 15/35 wt % C12A/CTAB (□, hexagonal), and 15/0 wt % C12A/CTAB (■, isotropic). CTAB surfactant was removed by solvent exchange prior to analysis.116
- 5.7. Cumulative dye release profiles as a function of time for polyacrylamide hydrogels photopolymerized in the hexagonal LLC phase formed using varying concentrations of nonreactive CTAB and polymerizable C12A surfactants. Also included are the release profiles of isotropic polyacrylamide controls with the same basic chemical composition of LLC templated systems. Shown are 0/50 wt % C12A/CTAB (○, phase separated), 0/0 wt % C12A/CTAB (●, isotropic), 5/45 wt % C12A/CTAB (◇, phase separated), 5/0 wt % C12A/CTAB (◆, isotropic), 10/40 wt % C12A/CTAB (Δ, hexagonal), 10/0 wt % C12A/CTAB (▲, isotropic), 15/35 wt % C12A/CTAB (□, hexagonal), and 15/0 wt % C12A/CTAB (■, isotropic). CTAB surfactant was removed by solvent exchange prior to analysis. Trend lines generated by least squares curve fits against equation 5.2.....118
- 5.8. Stress-strain profiles of LLC templated and isotropic polyacrylamide systems. Shown are (a) hydrated and (b) dehydrated polyacrylamide photopolymerized in the hexagonal LLC phase formed using varying concentrations of unreactive CTAB and polymerizable C12A surfactants. Also included are isotropic polyacrylamide controls with the same basic chemical composition of LLC templated counterparts. Shown are 0/50 wt % C12A/CTAB (○, phase separated), 0/0 wt % C12A/CTAB (●, isotropic), 5/45 wt % C12A/CTAB (◇, phase separated), 5/0 wt % C12A/CTAB (◆, isotropic), 10/40 wt % C12A/CTAB (Δ, hexagonal), 10/0 wt % C12A/CTAB (▲, isotropic), 15/35 wt % C12A/CTAB (□, hexagonal), and 15/0 wt % C12A/CTAB (■, isotropic). CTAB surfactant was removed by solvent exchange prior to analysis.....121

- 6.1. Small angle X-ray scattering profile of 20 wt.-% *N*-isopropylacrylamide (97.5 wt.-% *N*-isopropylacrylamide and 2.5 wt.-% *N,N'*-methylenebisacrylamide mixture) templated in the bicontinuous cubic LLC mesophase formed with 50 wt.-% polyoxyethylene (2) cetyl ether in water. Shown are SAXS profiles (i) before (●) and (ii) after (∇) photopolymerization. Inset shows higher order scattering peaks.....135
- 6.2. Equilibrium water uptake for polymer hydrogels. Shown are equilibrium percent water uptake as a function of temperature for isotropic (∇) and bicontinuous cubic LLC templated (●) PNIPAm hydrogels. (b) Weight percent water of isotropic (∇) and bicontinuous cubic LLC templated (●) PNIPAm hydrogels as a function of time after transfer from 22 to 37 °C water at time zero. Trendlines represent least squares curve fits.137
- 6.3. Stress-strain profiles for water swollen hydrogels. Shown are typical stress vs. strain curves of water swollen isotropic (∇) and bicontinuous cubic LLC templated (●) PNIPAm hydrogels at 22 °C. No statistically significant difference in compressive modulus between the isotropic (2.42 ± 0.29 kPa) and bicontinuous cubic LLC templated (2.64 ± 0.39 kPa) hydrogels is observed as determined using a *t*-test at a confidence level of 95 %.....139
- 7.1. Representative LLC templating process used to generate a hexagonal nanostructure in PDMS-PNIPAM hydrogels. Shown clockwise from the bottom left is (a) cross-section of the hexagonal phase, (b) segregation of polar *N*-isopropylacrylamide in the continuous water-soluble domains of the template, (c) segregation of non-polar PDMS monomers in the discontinuous oil-soluble domains of the template, (d) photopolymerization of monomers and removal of the non-reactive surfactant template.....154
- 7.2. Small angle X-ray scattering profiles for hexagonal LLC templated PDMS-PNIPAM hydrogels with varying concentrations of PDMS monomer before and after photopolymerization. Samples contained 50 wt % Brij 52 surfactant, 40 wt % total monomer, and 1 wt % photoinitiator with respect to monomer mass in water. Shown are (a) 0% PDMS before (●) and after (○), (b) 6.7% PDMS before (■) and after (□), (c) 12.5% PDMS before (◆) and after (◇), (d) 25.0% PDMS before (●) and after (○), (e) 33.0% PDMS before (▲) and after (Δ), (f) 50.0% PDMS before (■) and after (□) photopolymerization. PDMS concentration represents the weight percentage of the total monomer. Insets show higher order scattering reflections in greater detail.156
- 7.3. Equilibrium water uptake for polymer hydrogels. Shown are Equilibrium water uptake for (a) hexagonal LLC templated and (b) isotropic PDMS-PNIPAM hydrogels with varying concentrations of PDMS monomer at temperatures between 22 and 50 °C. Shown are LLC templated hydrogels (a) containing 0% PDMS (○), 6.7% (□), 12.5% PDMS (◇), 25% PDMS (○), 33.3% PDMS (Δ), 50% PDMS (□). Also shown are isotropic hydrogels (b) containing 0% PDMS (●), 6.7% PDMS (■), 12.5% PDMS (◆), 25% PDMS (●), 33.3% PDMS (▲), 50% PDMS (■). PDMS concentrations represent the weight percentage of the polymer that is siloxane after surfactant removal and drying. Surfactant was removed prior to analysis.....158

- 7.4. Transient water uptake profiles for polymer hydrogels. Shown are water uptake as a function of time for (a) hexagonal LLC templated and (b) isotropic PDMS-PNIPAM hydrogels with varying ratios of PDMS monomer after transfer from 22 to 37 °C water. Shown are LLC templated hydrogels containing (a) 0 % PDMS (○), 6.7 % (□), 12.5 % PDMS (◇), 25 % PDMS (○), 33.3 % PDMS (△), 50 % PDMS (□). Also shown are isotropic hydrogels containing (b) 0 % PDMS (●), 6.7 % PDMS (■), 12.5 % PDMS (◆), 25 % PDMS (●), 33.3 % PDMS (▲), 50 % PDMS (■). PDMS concentration represents the total weight percentage of the polymer that is siloxane after surfactant removal and drying. Surfactant was removed prior to analysis.161
- 7.5. Compressive modulus for polymer hydrogels. Shown are compressive modulus of hexagonal LLC templated (●) and isotropic (▲), PDMS-PNIPAM hydrogels as a function of (a) PDMS concentration and (b) equilibrium percent water uptake at 22 °C. PDMS concentration represents the total weight percentage of the polymer that is siloxane after surfactant removal and drying. Surfactant was removed prior to analysis.163
- 8.1. Chemical structures of monomers and surfactants used in this study. Shown are trifunctional ene monomer 1,3,5-triallyl-1,3,5-triazine-2,4,6(1H,3H5H)-trione (TTT) tetrafunctional thiol monomer pentaerythritol tetrakis(2-mercaptoacetate) (4-SH), and non-reactive surfactant polyoxyethylene (2) cetyl ether (Brij 52).177
- 8.2. Small angle x-ray scattering profiles for the hexagonal phase formed at 85 wt % thiol-ene mixture and 15 wt % Brij 52 surfactant i) before photopolymerization, ii) after photopolymerization, and iii) after photopolymerization and surfactant removal. Insets show higher order scattering peaks in greater detail with secondary and tertiary scattering peaks identified. The thiol-ene mixture includes 1 wt % photoinitiator and a 1:1 molar ratio of thiol and ene functional groups.182
- 8.3. Ternary phase diagram for Brij 52 surfactant, thiol monomer 4-SH, and ene monomer TTT. Symbols represent LLC phase including ■-isotropic, ●-hexagonal, ▲-cubic/lamellar, ▼-lamellar, and ►-crystalline solid. Filled symbols represent a disproportional ratio of thiol and ene monomers that would not form a robust polymer after curing where unfilled symbols represent a stoichiometric ratio of thiol and ene functional groups that are cured and used in mechanical property studies.184
- 8.4. Lattice or *d*-spacings (Å) of the primary scattering peak in ordered systems for the ternary Brij 52 surfactant, thiol monomer 4-SH, and ene monomer TTT system. Symbols represent LLC phase including ■-isotropic, ●-hexagonal, ▲-cubic/lamellar, ▼-lamellar, and ►-crystalline solid.186
- 8.5. Glass transition temperature and $\tan \delta$ for thiol-ene polymers. Shown are a) $\tan \delta$ as a function of temperature and b) storage modulus as a function of temperature for LLC templated and isotropic thiol-ene systems. Shown are a 85 wt % thiol-ene mixture cured in 15 wt % DMSO (□), an LLC templated system cured with 85 wt % thiol-ene mixture and 15 wt % Brij 52 surfactant (○), and a neat thiol-ene polymer cured as a 100 wt % mixture of thiol and ene (▲). A 1:1 molar ratio of thiol and ene functional groups were used for all thiol-ene mixtures with 1 wt % photoinitiator. Solvent and surfactant were removed prior to analysis.188

- 8.6. Glass transition temperature for LLC templated and isotropic thiol-ene polymers as a function of weight percent monomer used in the initial formulation. Shown are a hexagonal nanostructured thiol-ene copolymers templated using Brij 52 surfactant (●) and an isotropic polymer system cured in varying concentrations of DMSO. A 1:1 molar ratio of thiol and ene functional groups were used for all thiol-ene mixtures with 1 wt % photoinitiator. Brij 52 surfactant comprised the remainder of the sample formulations for the LLC templated system while the remainder of the isotropic solutions was DMSO. Solvent and surfactant were removed prior to testing.....190
- 8.7. FTIR conversion profiles of thiol and ene functional groups for LLC templated and isotropic thiol-ene systems. Shown are thiol (Δ) and ene (▲) conversion for a 85 wt % thiol-ene mixture in 15 wt % DMSO, thiol (○) and ene (●) conversion for 85 wt % thiol-ene mixture with 15 wt % Brij 52 surfactant, and thiol (□) and ene (■) conversion for a 100 wt % mixture of thiol and ene. A 1:1 molar ratio of thiol and ene functional groups were used for all thiol-ene mixtures with 1 wt % photoinitiator. Photopolymerization was initiated using 365nm light at an intensity of $2.5 \text{ mW} \cdot \text{cm}^{-2}$193

CHAPTER 1

INTRODUCTION

Control of matter on the nanometer size scale has led to dramatic increases in the performance of many useful products ranging from semiconductors, electronic displays, drug delivery vehicles, and sensors.¹⁻⁵ The growing research interest in producing nanostructured materials stems primarily from the useful properties that are attained when one or more structural dimensions are on the order of one-hundred nanometers or less.^{6,7} Many processing techniques have been developed to control the structure of organic and inorganic materials including sol-gel, nano-lithography, soft and hard templating, and self-assembly.⁸⁻¹¹ These methods have been utilized to generate materials that contain transport and mechanical properties useful in many industrial and biomedical applications. In particular, the synthesis of polymer materials containing periodic order on the sub-micrometer scale has been the subject of much research in recent years.

The significant and growing research interest in generating polymers with controlled structures is largely due to the far reaching applications in which polymers can be utilized including drug-delivery, tissue scaffolds, artificial tissues, sensors, solar cells, electronics, and separation membranes, to name a few.^{12,13} In each of these applications there are a myriad of instances in which nanometer sized structures facilitate enhanced material performance. For example, enhanced transport and modulus provided by the nanometer sized features of the polymer network has increased cell attachment and survival on tissue scaffolds, increased the rate and degree of response to changes in external conditions for stimuli-sensitive polymers, improved the separation efficiency of polymeric membranes, and improved the rate of drug release compared to polymer systems that do not contain ordered nanostructures.^{10,14-17}

Incorporation of periodic nanometer sized structures in organic polymers is well-known to increase the performance of many polymer materials. For example, Kevlar is a liquid crystalline polymer containing defined nanostructured domains and is commonly used in body armor applications.¹⁸ Much of the mechanical properties of Kevlar including the high tensile strength and impact resistance are derived from the organization of polymer chains. Other examples of increased performance based on the ordered network structure of polymers include the use of poly(hydroxybenzoic acid) derivatives and poly(ethylene terephthalate) crystalline polymer to increase the strength, solvent resistance, and barrier properties in many high performance applications such as mechanical parts, food packaging, and electrical insulation.^{19,20}

Polymers with ordered nanostructures can generate dramatic improvements in functionality that can lead to the development of a useful product whereas the isotropic analog of the self-assembled polymer may not have the properties required for proper performance. For example, the crystalline order of Kevlar imparts much of the tensile strength to the polymer making it useful for body armor applications, where the corresponding isotropic or disordered polymer network would be weaker and unsuitable for such applications.²¹ Unfortunately, a very particular and difficult to achieve stereochemistry and chemical structure of polymers is needed to achieve the thermodynamic conditions and packing geometry needed to drive the self-assembly process and generate nanostructured crystalline order in the system.^{22,23} This may limit the versatility of polymer systems because little change can be made to the polymer network without compromising or destroying the crystalline order of the polymer. For example, cross-linking or modulating polymer properties through incorporation of particular heteroatoms in the polymer backbone can alter the thermodynamics in such a manner that prevent the self-organization of the polymer chains.²⁴

This study examines a general method that may be utilized to incorporate well-defined nanometer sized morphologies in a wide range of polymers that are readily

available in order to improve material performance. Generating the desired nanostructure throughout the bulk of a polymer requires particular thermodynamic and stereochemical conditions that are attained only in a small class of polymers. It is highly desirable to expand the range of polymer chemistries in which nanostructure may be generated. Increasing the performance of a wide range of polymer materials through incorporation of nanotechnology into the polymer network can have tremendous benefits in many industrial and biomedical applications. Utilizing a templating technique that can be applied to produce nanostructure in an extensive range of polymer chemistries will greatly expand the functionality and applications of polymers.

Recently, much research has examined how to expand and optimize the functionality of polymers through incorporation of nanometer sized structures imposed on the polymer network by a templating or self-assembly process.²⁵ The use of a template is a particularly attractive method of generating nanostructure in organic polymers because the templating process may be applied to a wide variety of monomer and polymer precursors. This process greatly expands the polymer chemistries in which nanostructure can be incorporated, leading to enhanced functionality of many polymer materials by controlling polymer network morphology. There are a number of different methods of generating nanostructure in organic polymers, many of which can use a template as a polymerization platform to direct polymer structure. The organization of monomers into ordered geometries followed by polymerization to generate higher molecular weight polymers is one of the primary strategies utilized in the synthesis of polymers with controlled structures.²⁶

Two basic approaches are often used to produce or incorporate nanometer sized features into the final polymer network architecture. One technique utilizes thermodynamics to design polymers that will self-organize into particular ordered structures. Another promising technique takes advantage of the differences in solubility, absorption, or binding affinity of a moiety in order to partition and segregate copolymers,

monomers, or pre-polymers into an organized matrix. After achieving the desired order, various polymerization methods may be utilized to generate the polymer network and lock-in the original order of the matrix.²⁵ Molecular imprinting (MIP), in which a polymer is formed around a template or host molecule such as a protein or enzyme that interacts with functional groups on the monomer shows great promise in many biosensing and separation applications.²⁷ By polymerizing around a host or template molecule followed by subsequent removal of the molecule from the polymer matrix, MIP generates a specific site that contains the precise geometry and favors strong interaction and binding affinity to the template molecule, similar to the “lock and key” mechanism of enzyme binding in a biological environment. MIP illustrates the utility of a template to direct the morphology of organic polymers and produce materials with organized network structure analogues to the host or parent template structure.

Lytotropic Liquid Crystals

A particularly promising method of controlling polymer nanostructure uses self-assembling lyotropic liquid crystals (LLCs) as polymerization templates to direct polymer morphology. The LLC templating process has been utilized to generate nanostructure in a wide-range of polymer systems, resulting in materials that contain useful property relationships that are often not observed in traditional or isotropic polymer systems.^{14,15,25,28-31} The LLC templating process allows for a diverse range of morphologies to be incorporated in polymers that lack the stereochemistry or chemical structures needed to achieve a self-organized nanostructure. Additionally, the LLC templating technique provides a new method of incorporating nanostructure in polymers when traditional methods of generating nanostructure throughout the bulk such as extrusion, sheering, or melt crystallization are not feasible. LLC mesophases are

typically formed at higher concentrations of surfactant or amphiphilic molecules that self-organize into geometries with nanometer sized dimensions in the presence of a solvent such as water.³² The geometry of the self-assembled phase, also known as the mesophase, formed depends largely on the size, polarity, and concentration of surfactant molecules. Typically, spherical micelles are formed at lower surfactant concentrations and the higher dimensionally ordered hexagonal, bicontinuous cubic, and lamellar phases are formed with increasing surfactant concentration. Figure 1.1 shows a representation of typical surfactant, mesophases that are utilized as LLC surfactant templates in this research. These self-assembled phases include the hexagonal phase, characterized by a curved and columnar structure bicontinuous cubic which is best described as having a gyroid or sponge morphology, and lamellar with a flat bilayer type structure. At higher surfactant concentrations inverse phases, in which the curvature of the mesophases with respect to water is reversed, are also possible. However, such inverse phases are not utilized extensively in this research.

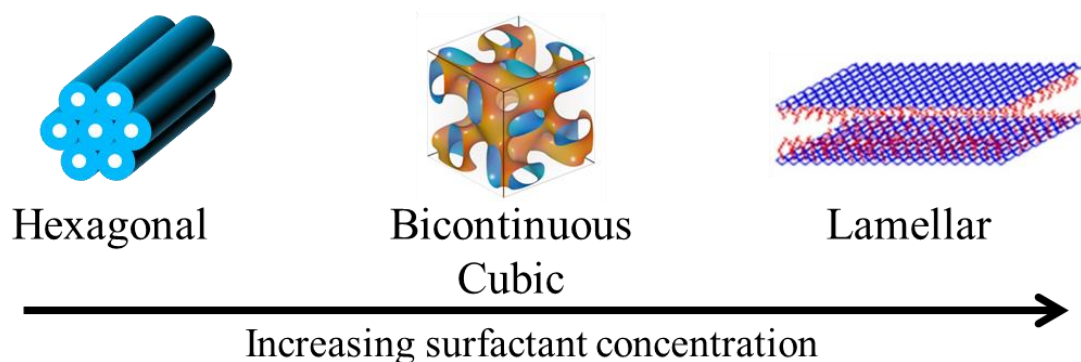


Figure 1.1. Representations of self-assembled lyotropic liquid crystalline phases commonly formed using surfactant in a polar solvent such as water. Shown in order of increasing surfactant concentrations are the hexagonal, bicontinuous cubic, and lamellar mesophases

The structure of self-assembled LLC phases can be described by the attractive and repulsive interactions between surfactant and solvent.^{33,34} Attractive forces include hydrogen bonding, hydrophobic, and van der Waals interactions which are necessary for self-assembly. On the other hand, repulsive interactions such as steric, electric double-layer, and hydration oppose the self-assembly process. The balance of attractive and repulsive forces will dictate the geometry of surfactant aggregates. Figure 1.2 shows the structure of representative surfactants and their polymerizable analogues that will be used to direct polymer structure in this research. Water will typically be used as the solvent to generate the LLC mesophases because it is highly polar and inexpensive.

The ethylene oxide repeat units of surfactant a) and ionic head group of surfactants b) – d) in Figure 1.2 can form hydrogen bonds with water and promote the self-assembly process. Likewise, the aliphatic chains of these surfactants are insoluble in water and contribute to attractive hydrophobic forces that stabilize the mesophase. In other words, the formation of self-assembled surfactant aggregates is due to the favorable interaction of the polar head groups with water and the agglomeration of hydrophobic chains to shield themselves from and minimize their contact with water. Changes in surfactant concentration often alter the LLC mesophase due to shifts in attractive and repulsive forces. Modulating surfactant concentration provides a facile method of controlling the order of LLC mesophases.³² In some cases, it is possible to change the mesophase at a given surfactant concentration by changing temperature. Different mesophases result from the minimization of repulsive forces brought about by changes in surfactant ordering. The packing parameter is often used to relate molecular structure and surfactant concentration to the morphology of surfactant aggregates.³³ This dimensionless shape parameter, also known as the critical packing parameter (CPP), is directly proportional to the effective volume of the surfactant and inversely proportional to the length of the hydrocarbon chain and effective area of the surfactant head group. An expression for the CPP (Equation 1.1) that provides a quick measure of that surfactant

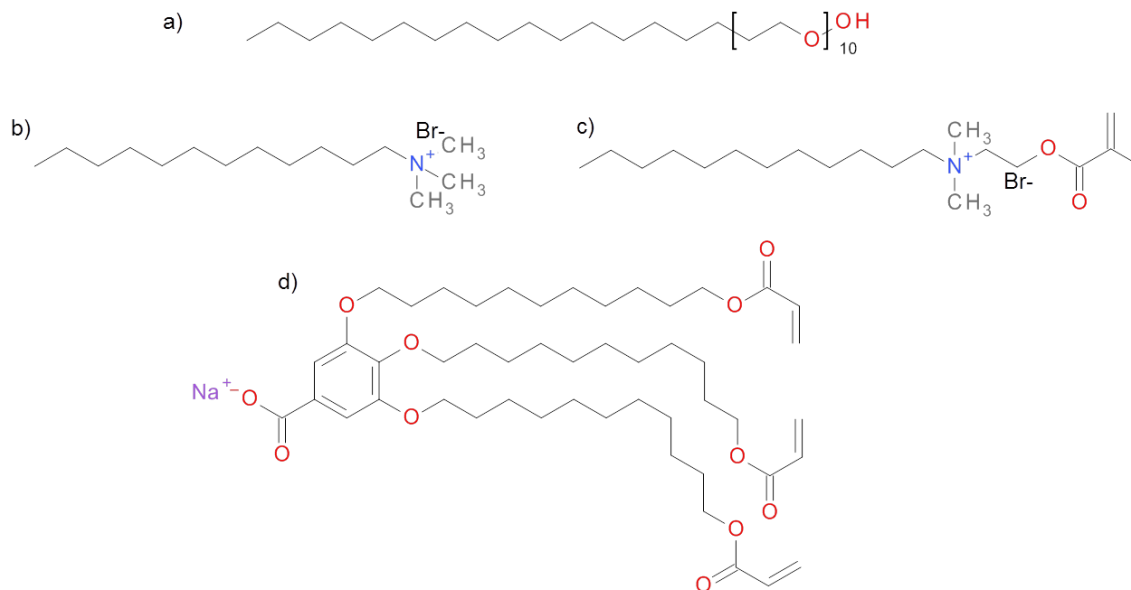


Figure 1.2. Representative structures of reactive and non-reactive surfactants utilized to generate lyotropic liquid crystalline phases with water. Shown are a) Polyethylene glycol hexadecyl ether, polyoxyethylene (20) cetyl ether (Brij 58), b) dodecyltrimethylammonium bromide (DTAB), *acrylate functionalized quaternary ammonium surfactant*, dodecyl-dimethyl-(2-prop-2-enoyloxyethyl)ammonium bromide, (C12A), and d) cationic triacrylate terminated sodium salt.

geometry that can be utilized as a first approximation to estimate the phase a particular surfactant may form is shown below

$$CPP = v/a_0l_c \quad (1.1)$$

where v is the average volume occupied by the surfactant molecule, a_0 is the effective area of the surfactant headgroup, and l_c is the effective length of the surfactant chain.³⁵

The interchain attraction, headgroup repulsion, and solvent interactions are used to determine the effective area of the headgroups, which are heavily dependent on surfactant concentrations and solvent polarity. Empirical expressions for the surfactant chain and volume of surfactant amphiphiles has been established for simple, single chains surfactants given by the following equations:

$$v = (27.4 + 26.9 n_c) \text{ \AA}^3 \quad (1.2)$$

$$l_c = (1.5 + 1.26 n_c) \text{ \AA} \quad (1.3)$$

where n_c is the number of carbon atoms in the chain. Equations 1.1 – 1.3 describe the general phase behavior of LLCs and can be used to predict and modulate phase behavior by changing external conditions. In addition to changes in surfactant concentration, the pH or ionic strength of the solvent can be modulated to change the effective areas and volumes of surfactant molecules. For example, acidic conditions can readily protonate the oxygen heteroatoms in the poly(ethylene oxide) block of the common Brij series surfactants similar in structure to Figure 1.2a, leading to an increase in the effective area of the surfactant head group, a larger surfactant volume, and a subsequent increase in the CPP.

A packing parameter equal to unity typically corresponds to the formation of a lamellar phase while the bicontinuous cubic and hexagonal mesophases are formed at progressively smaller packing parameters. Although surfactant concentration is not explicit in the packing parameter, it is directly related to the area of the surfactant head group and volume of the surfactant. Typically, an increase in surfactant concentration tends to increase the packing parameter partly by reducing the effective area of the surfactant head group due to changes in the attractive forces and competitive “binding” for water molecules with the hydrophilic head group.³³

Lyotropic Liquid Crystals as Structure Directing

Polymerization Platforms

LLC mesophases are well-suited for use as polymerization platforms to direct polymer structure on the nanometer size scale. The LLC phase structure is readily

controlled by changing surfactant size, concentration, and polarity, providing a facile method of modulating the template and subsequent polymer morphology. The self-assembled structures of LLC phases can serve as photopolymerization templates to direct the structure of organic polymers by taking advantage of the water- and oil-soluble domains of the parent mesophase. Figure 1.3 shows the general templating process that is utilized to transfer LLC nanostructure to the polymer network for a representative polar and non-polar monomer system using the hexagonal LLC phase as a parent template. If a photocurable polar monomer such as *N*-isopropylacrylamide (NIPAM) is incorporated into the LLC phase, the monomer will preferentially segregate in the water soluble domains of the parent template and adopt a geometry that directly resembles that of the self-assembled phase. Likewise, if a hydrophobic monomer such as poly(dimethylsiloxane) dimethacrylate (PDMSDMA) is added to the phase, the monomer will preferentially segregate in the oil-soluble domains of the LLC phase. In this scenario, the hydrophobic monomer PDMSDMA will segregate in the discontinuous oil-soluble domains of the LLC phase while the polar NIPAM monomer will segregate in the continuous domains of the hexagonal phase.

Although a dual monomer system containing polar and non-polar monomers is represented in Figure 1.3, the templating process may be used to template a single monomer system, or multiple monomer systems of increasing complexity consisting of multiple polar and non-polar monomers and combinations thereof. Additionally, the reactive surfactants that are shown in Figure 1.2 c) and d) may also be used to generate the LLC template to direct polymer structure and are incorporated into the final polymer network through copolymerization with templated monomers. A non-reactive surfactant template can be readily removed from the polymer networks via solvent exchange while reactive surfactants are integrated into the network structure. Photopolymerization is then utilized to cure the monomer/LLC formulation and transfer the order of the parent template to the polymer system. Ideally, the photopolymerization reaction locks in the

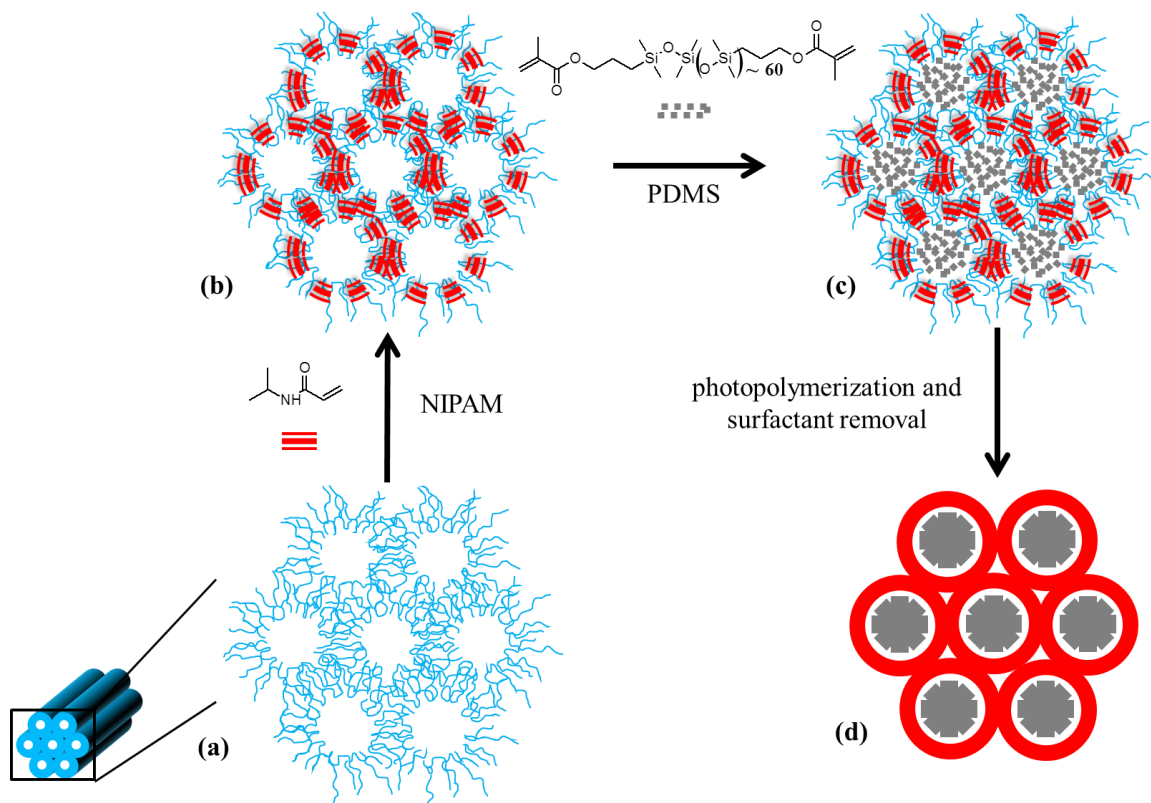


Figure 1.3. Representative LLC templating process used to generate a hexagonal nanostructure in organic polymers. Shown clockwise from the bottom left is (a) cross-section of the hexagonal phase, (b) segregation of polar *N*-isopropylacrylamide in the continuous water-soluble domains of the template, (c) segregation of non-polar PDMS monomers in the discontinuous oil-soluble domains of the template, (d) photopolymerization of monomers and removal of the non-reactive surfactant template.

order of the parent template and generates a nanostructured material with the same geometry and size scale as the original LLC template. Unfortunately, several undesirable thermodynamic consequences often accompany the polymerization reaction and prevent the successful transfer of LLC template structure to the polymer.³⁶ Thermodynamically driven phase separation events typically occur as monomer is converted to polymer, often yielding polymers with poorly ordered structures on much larger length scales compared to the original LLC template. Phase separation is a significant problem in LLC polymer templating because it opposes the control of polymer structure and properties. In many

cases, the interplay of intermolecular and thermodynamic interactions gives rise to an environment in which the polymer is more stable in the phase separated state. Successful transfer of the parent template structure to the polymer thus requires that the template remain thermodynamically stable throughout polymerization such that the polymerization rate is sufficiently rapid to kinetically trap the template structure before phase separation occurs.³⁷⁻⁴⁰

Despite the factors opposing the control of polymer nanostructure, LLC templating is still a promising method of directing polymer nanostructure for the following reasons: (1) The phase behavior of many LLC-solvent systems is well-characterized, providing numerous mesophases that may be utilized to direct polymer structure. (2) Numerous surfactants are inexpensive and commercially available. (3) The synthesis of LLC templated polymers is relatively simple and their large-scale production is expected to be more feasible than other templating methods.⁴¹ (4) Non-reactive surfactants are readily extracted from the polymer matrix by solvent exchange. The latter could be critical in tissue engineering, catalysis, and separation applications due to potential biocompatibility issues or steric interference of the surfactant. These attributes may be beneficial in the synthesis of nanostructured polymers with useful property relationships using economical surfactants for use in large scale industrial applications.

Photopolymerization

The curing method used to produce the polymer network is of considerable importance in generating nanostructured materials using the LLC templating process. There are several aspects that must be considered in order to successfully generate and retain the parent template order during the polymerization reaction. The first is the concentration dependence of LLC phase which eliminates solvent based polymerization

methods from consideration as high amounts of solvent destroy the order of the phase. Secondly, the polymerization rate should be sufficiently fast to allow for potentially thermodynamically unstable nanostructures to be kinetically trapped. Finally, the initiation rate should be independent of temperature to allow for polymerization of the LLC composite at a temperature in which the mesophase is stable. Photopolymerization is an attractive method of curing LLC templated monomer systems because the process is solvent free, the polymerization rates are inherently fast especially compared to thermal or redox initiation techniques, and the initiation rate is independent of temperature.

Photopolymerization uses light to generate the active center to initiate polymerization. This method can be utilized to generate polymer networks from a wide-range of monomer chemistries and functional groups. The past three decades have seen significant increases in the use of photopolymerization to produce polymer materials for use in coatings, integrated circuits, stereolithography, 3D printing, dental resins, and fiber optic applications, to name a few.⁴² The use of ultraviolet light to produce polymer networks may be broken down into three main classes based on the polymerization and propagation mechanism of the growing polymer chain. These methods include radical, cationic, and anionic initiations. Of these three methods, radical and cationic polymerization far outweigh the use of anionic photopolymerization to synthesize polymers due to the wide-range of monomer chemistries and cost-effectiveness of radical and cationic polymerizations comparatively.

Although cationic polymerizations have a number of advantages including insensitivity to oxygen and a wide range of monomer chemistries, the polymerization is inhibited by water.⁴³ In fact, the presence of water or hydroxyl containing species can have dramatic impacts on the polymerization mechanism and final mechanical properties of the polymer network. Because water is often used to generate the LLC phase for use as a photopolymerization template, this research primarily utilizes radical

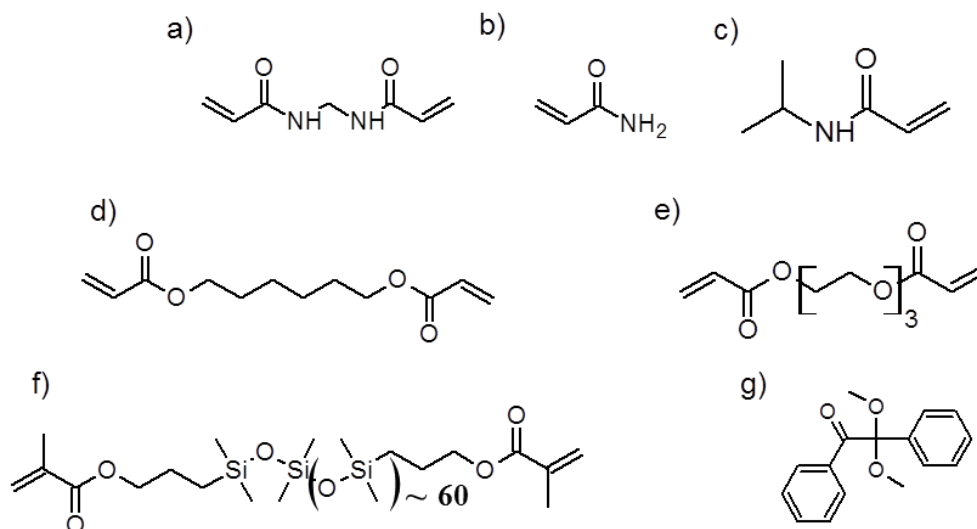


Figure 1.4. Chemical structures of common radical photoinitiated polymer systems that are used in this research. Shown are a) *N,N'*-methylene bisacrylamide, b) acrylamide, c) *N*-isopropylacrylamide, d) hexanediol diacrylate, e) poly(ethylene glycol) diacrylate, f) poly(dimethyl siloxane) dimethacrylate, and g) radical photoinitiator 2,2-Dimethoxy-1,2-diphenylethan-1-one (Irgacure 651).

photopolymerization to produce the nanostructured polymer network. A number of different monomer functionalities can be cured using radical photoinitiation including acrylate, methacrylate, acrylamide, methacrylamide, vinyl, and thiol-enes. Furthermore, a wide-range of monomer chemistries containing varying molecular weights and number of reactive functional groups on the monomer backbone that can be used to control the crosslinking density, chemistry, and final properties of the polymer network. Figure 1.4 shows representative structure of photopolymerizable monomers that are used in this research. These structures can be used in conjunction with one another to generate polymers with a wide-range of mechanical properties. Also shown in Figure 1.4 g) is the chemical structure of a common photoinitiator that is often used in this research.

With respect to radical chain polymerization, each double bond represents a functionality of two, meaning that the ene functional group can form two covalent bonds with other radically reactive ene functional groups. Photopolymerization of a monomer with a total functionality of two will form a linear polymer network. For example, the

homopolymerization of monomers in Figure 1.4b and c will predominantly form a linear polymer. As the functionality of the monomer system is increased to four or higher, the system will form a crosslinked polymer network that is, by definition, insoluble in solvent. Polymerization of the monomers containing two double bonds shown in Figure 1.4 will form a crosslinked polymer network. As the ratio of monomer functionality to molecular weight is increased, the system will become increasingly crosslinked. The three basic steps of radical chain photopolymerization include initiation, propagation, and termination. These steps are now described in greater detail:

Initiation

The first step in the polymerization process is the generation of a reactive radical species that will start the polymerization reaction. The compound that is used to begin the polymerization process is called a photoinitiator. The photoinitiator is a light sensitive compound that generates free-radicals and will initiate the polymerization by reacting with the electron rich double bonds similar in chemical structure to those shown in Figure 1.4. Upon absorption of an appropriate wavelength of UV light, a photofragmentation process generates a pair of radicals through α -cleavage of a C-C bond.⁴⁴ This class of photoinitiators is referred to as type I photoinitiators and often include aromatic carbonyl compounds, α -amino ketones, hydroxyalkylphenones, and acylphosphine oxides in the chemical structure. Type II photoinitiators are typically two component systems comprised of a radical precursor such as an aromatic ketone and a hydrogen donor. In this process a radical incapable of initiating polymerization is generated on the radical precursor which subsequently abstracts hydrogen from a hydrogen donor to produce the initiating radical species. Type I photoinitiators are predominantly used in LLC templating process primarily due to their high efficiency. Another benefit of utilizing photopolymerization to initiate polymerization in LLC

templated systems is the independence of the initiation rate on temperature. This allows the reaction to be conducted at a temperature in which the LLC phase is stable.

Selection of a photoinitiator that contains an absorption band that overlaps with the emission spectra of the curing lamp is important to achieve high monomer conversions in a reasonable time frame. One of the most common lamps that are used to cure UV reactive polymers is the mercury arc lamp. Many of the commonly used photoinitiators including Irgacure 184, Irgacure 651, Irgacure 2959, and Darocur 1173 contain absorption bands that overlap with the emission spectra of mercury arc lamps.⁴⁴ For type I photoinitiators, the absorption of a photon and cleavage into a pair of radicals is depicted by the following chemical formula



where I is the photoinitiator, $R\cdot$ is the initiating radical, and $h\nu$ represents light absorption. After generating radicals that are capable of initiating the polymerization reaction, the second step in the initiation process is the addition of the free-radical to radically reactive monomer (M). This step can be represented by:



where k_i represents the initiation rate constant for the reactive radical combining with the monomer. Equation 1.4 assumes that the pair of radicals formed by the cleavage of the photoinitiator have equal reactivity toward monomer species. However, the benzoyl radical often formed in many type I photoinitiators is the major initiating species. To account for the differences in radical reactivity a parameter called the quantum yield of initiation, ϕ , is introduced. The quantum yield of initiation represents the number of

propagating chains initiated per photon of light absorbed. The total photoinitiation rate, R_i , is given by

$$R_i = 2\phi I_a \quad (1.6)$$

where I_a is the intensity of light absorbed by the photoinitiator. Equation 1.6 accounts for the differences in radical reactivity that are observed for type I photoinitiating systems.

Propagation

The continual addition of monomer to the growing polymer chain to form a high molecular weight polymer is referred to as the propagation step as given by



where k_p is the propagation rate constant. The subscript n in equation 1.8 represents the number of monomer units added to the growing polymer chain, otherwise known as the degree of polymerization. The propagation rate constant is generally considered to be independent of polymer chain length. In typical radical chain photopolymerizations, a high-molecular weight polymer is usually formed within the first few percent conversion. The rate of propagation is given by

$$R_p = k_p [M \cdot] [M] \quad (1.9)$$

Termination

The final stage of the polymerization reaction is the termination step in which radical on the growing polymer chains react to form dead polymer. There are two basic mechanisms of termination for radical chain polymerization as given by the following equations.



where k_{tc} and k_{td} represent the rate constants for termination by combination and disproportionation, respectively. Note that chain transfer reactions to monomers or solvents are also possible, but typically deemed negligible for most species. In the development for a general rate expression for radical polymerization, it is generally assumed that the rate of formation of initiating radicals is equal to the rate of radical termination. In other words, it is assumed that the radical concentration does not change during the polymerization reaction. This is known as the pseudo steady-state assumption and allows for an analytical expression for radical concentration to be obtained through a mass balance. The general expression of the rate of polymerization is given by

$$R_p = k_p [M] \left(\frac{R_i}{2k_t} \right)^{1/2} \quad (1.12)$$

Plugging in equation 1.6 for the rate of initiation and accounting for the attenuation of light through the depth the polymer film, ϵb , using Beers law, the following general expression for the photopolymerization rate is obtained

$$R_p = k_p [M] \left(\frac{\phi I_o (1 - e^{-\epsilon b [I]})}{k_t} \right)^{1/2} \quad (1.13)$$

Several important transport considerations need to be discussed to fully describe photopolymerization behaviors that are not directly evident from the above polymerization rate equations. Although the change in k_p that can occur with increasing chain length can be neglected, the change in k_t that occurs with increasing conversion cannot be overlooked. At low conversions the viscosity of the reacting system is low and two reactive functional groups can diffuse relatively unhindered. In this stage, the polymerization rate is controlled by segmental diffusion of the polymer chains. As the polymerization progresses to higher conversions, the system viscosity increases and changes the rate limiting diffusion mechanism. With increasing viscosity the rate is controlled by how quickly two reactive species can diffuse together, and the polymerization rate is limited by translational diffusion of polymer chains among the network of other entangled polymer chains.

An important phenomenon observed in radical chain polymerization is the so called autoacceleration or Trommsdorff effect. Based on the equations above, one may expect that the polymerization rate to continually decrease throughout the polymerization reaction due to depleting monomer concentration. However, the increase in system viscosity leads to restricted diffusion of polymer chains resulting in a decrease in the termination rate parameter. This results in a significant increase in the concentration of propagating radicals and a subsequent increase in the polymerization rate.

At even higher conversions the viscosity of the system may become so large that the translation of polymer chains throughout the matrix is much slower than propagation through double bonds in the network. In other words, at higher conversions the polymerization rate is said to be reaction diffusion limited. The glass transition temperature and monomer functionality has a significant impact on the ultimate conversion and onset of the autoacceleration effect. The glass transition temperature (T_g) is the temperature at which the polymer attains sufficient thermal energy for atoms in the polymer chain to move in a coordinated manner. A rubber band at room temperature is

an example of a polymer that is above its T_g at room temperature, where a poly(styrene) petri dish is well below its T_g at room temperature. If the polymerization reaction occurs at a temperature that is below the glass transition temperature of the polymer, it is often difficult to attain complete conversion due to reaction diffusion limitations. As the ratio of monomer functionality to molecular weight is increased the onset of autoacceleration is decreased to lower conversions due to the increase in viscosity and close proximity of polymer reactive groups. Furthermore, the ultimate conversion of double bonds tends to decrease with increasing crosslinking density due to diffusion limitations during the reaction.

Characteristics of Thiol-ene Radical

Photopolymerizations

The classical radical photopolymerizations described above proceed via a chain growth mechanism and have been utilized in a range of applications including dental composites, contact lenses, and coatings applications.⁴⁵⁻⁴⁸ Unfortunately, there are several disadvantages that are associated with the classical photopolymerization of acrylates and methacrylate monomers such as high degrees of volumetric shrinkage and stress development, oxygen inhibition, and heterogeneous networks.⁴⁹⁻⁵¹ Each of these disadvantages in addition to low-gel point conversions can drive the phase separation process during radical chain photopolymerization in LLC templates. For example, the high shrinkage stress of radical chains photopolymerizations can disrupt the LLC structure by “squeezing out” or “crushing” the self-assembled surfactant aggregate structures that make up the template.

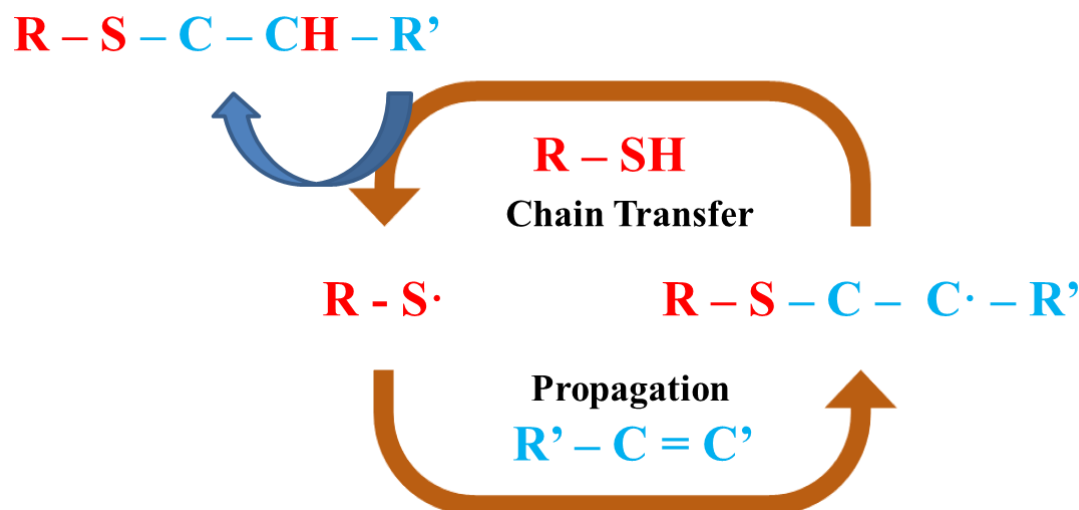


Figure 1.5. Schematic of the radical mediated thiol-ene step growth photopolymerization reaction with alternating propagation and chain-transfer events between thiol and ene monomer.

Radical mediated thiol-ene photopolymerizations proceed by an inherently different polymerization mechanism than the chain growth process. The thiol-ene photopolymerization processed by a step-growth mechanism that consists of alternating chain transfer and propagation between the thiol and ene monomers. Figure 1.5 shows a schematic of the alternating step-growth polymerization mechanism between thiol and ene monomers. Many thiol and ene monomers are commercially available with the speed of the reaction being primarily controlled by the electron density on the ene monomer.⁵² Electron rich double bonds such as vinyl ethers polymerize considerably faster than electron poor enes such as maleimides, providing a wide range of ene chemistries available to generate the required polymer properties.

A number of advantages of the thiol-ene reaction over traditional radical chain photopolymerizations could be useful in retaining the LLC nanostructure during the polymerization reaction. For example, delayed gelation, relatively low molecular weight oligomeric species up until gelation, and low crosslinking density up to gelation could be

beneficial in LLC templating.⁵³ The delay in molecular weight buildup to higher conversions may allow much of the polymerization reaction to be completed before phase separation events associated with increasing molecular weight occur. Other advantages inherent in thiol-ene photopolymerizations including fast polymerization kinetics, moderate shrinkage stress, insensitivity to oxygen, and homogeneous network formation may also be useful in retaining the LLC template nanostructure during the polymerization.⁵⁴

Photopolymerization Kinetics in Ordered Liquid Crystalline Systems

Critical to the synthesis of polymer with controlled nanometer sized pore structures is a fundamental understanding of the relationships between the thermodynamics of the system that dictate the geometry of self-assembled structures as well as the polymerization kinetics of the system that are required to retain the organized structures during polymerization.^{23,55} Much research has been conducted on the impact of kinetics on the crystallization and resulting morphology of polymers such as Kevlar and poly(ethylene).^{56,57} In these investigations, the thermodynamics of the system allow for the organization of polymer chains with periodic nanometer sized dimensions above the glass transition temperature. The kinetics at which the polymer melt is quenched or cooled below the glass transition temperature to vitrify the polymer chains and affix the ordered geometry dictate many critical parameters such as the ultimate polymer morphology, degree of disorder, and degree of crystallinity. Moreover, the structures that are preserved in the quenching process have a dramatic impact on the performance of the polymer material including significant effects on properties such as modulus, strength, relaxation time, and elongation at break.⁵⁸

The segregation effect of the parent template on the order of reactive species has a dramatic impact on the photopolymerization kinetics in the system, generating large changes in the local monomer concentration and kinetic constants. Changes in the LLC template mesophase, free volume effects, and connectivity of reactive domains impact the final polymerization rate, making the study of photopolymerization kinetics in LLC phases a sensitive tool that can be utilized to probe the order during the polymerization reaction. Before discussing particular examples of reaction kinetics in LLC templates, a general overview of the photopolymerization kinetics and underlying factors that govern polymer structure retention is provided.

The experimentally observed relationships between LLC order and photopolymerization kinetics have led to some interesting and useful insights into the factors needed to control polymer structure during the reaction. Two coupled and competing factors dictate the degree of LLC structure retained during the polymerization reaction and final working structure of the polymer.^{22,23,55,59} On one hand the thermodynamics of the system dictate the stable phase morphology of the self-assembled system. On the other hand, the reaction speed and buildup of molecular weight continually change the interaction between monomer, polymer, solvent, and surfactant. In addition to the constantly changing thermodynamic interactions that govern the stability of the self-assembled structure, the photopolymerization reaction serves to lock-in the current structure through the formation of covalent bonds and limiting species diffusion via a fast increase in system viscosity and chain entanglement.

It has been suggested that the polymerization reaction needs to be sufficiently fast in order to prevent phase separation.^{31,60-62} A thermodynamically unstable LLC structure could be kinetically trapped if the formation of covalent bonds between monomers occurs on a time scale faster than the phase separation process. If a sufficiently high concentration of covalent bonds is established such that the viscosity of the system increases and the diffusivity of monomer, polymer, and surfactant through the polymer

matrix is severely restricted, the original LLC order may be transferred to the polymer. The rapid buildup of polymer molecular weight is most readily accomplished using light to initiate the polymerization reaction as opposed to much slower thermal or redox initiated polymerization processes.

The thermodynamics of the system during the polymerization reaction must also be considered for the successful transfer of LLC parent template order to the polymer.³⁶ The polymerization reaction brings about a decrease in entropy as monomer is converted to polymer as well as dramatic differences in polymer solubility and interaction. In the confines of the parent LLC template, the increase in molecular weight gives rise to a thermodynamic driving force for phase separation.⁶³ Specifically, the growing polymer strives to increase its entropy by occupying more space in the parent LLC template. This driving force can result in the loss of the LLC structure by polymer partitioning into the surfactant rich domains that serve to direct polymer order. In this case, the reaction rate must be faster than the phase separation events in order for polymer to retain the parent template structure.

Although the thermodynamic driving force for phase separation produced by the polymerization reaction leads to an increase in polymer molecular weight and a subsequent decrease in entropy is unavoidable, it may not be sufficient to destroy the order of the phase. If the interactions between the surfactant template and the polymer are strong enough, the cohesive forces may be able to maintain the phase order.^{32,59} In other words, if the cohesive energy density is great enough to counterbalance or overcome the entropy driving force for phase disruption, the LLC structure may be transferred to the polymer. Such a LLC template is said to be thermodynamically stable in that a sufficiently high polymerization rate is not needed to preserve the LLC order. In principle, the polymerization can proceed arbitrarily slow and the structure of the LLC template would be preserved. This is in contrast to a kinetically stable LLC template in

that a minimum polymerization rate is needed to “trap” or outpace the phase separation process in order to retain the structure.

The reaction rate during polymerization in organized mesophases has received much attention in the past decade.^{29,60-62,64-68} This is largely due to the strong influence the LLC structure has on monomer segregation behavior resulting in dramatic changes in polymerization kinetics. The order imposed on reactive species can generate significant differences in the propagation and termination rates compared to classical polymerizations. In fact, due to the direct relationship between nanostructure and local order, photopolymerization kinetics can be utilized as a tool to probe the local order of the system. Changes in parent template order can lead to alterations in local monomer concentration and orientation which directly impacts the rate of polymerization and kinetic rate constants. Researchers have exploited the connection of LLC order and kinetics to monitor the evolution of polymer structure during the photopolymerization reaction. For example, the hexagonal LLC order can generate a ten-fold increase in the polymerization rate of acrylamide compared to the isotropic or traditional solution-based photopolymerization of acrylamide.⁶¹ This is a remarkable increase in rate given that each system was polymerized under the same light intensity, temperature, and photoinitiator concentration.

The degree of monomer organization and interaction with the parent surfactant template was characterized by examining the NMR quadrupolar splitting pattern of nitrogen present in the acrylamide monomer.⁶² The quadrupolar splitting pattern of the ¹⁴N nuclei provides direct evidence of induced ordering of acrylamide monomers by the presence of the LLC template. For acrylamide dissolved in water, the NMR spectra of the quadrupolar ¹⁴N nuclei showed a sharp peak with no splitting pattern indicating that the acrylamide monomer is in an isotropic environment and contains no monomer organization. As surfactant concentration is increased and the surfactant begins to aggregate to form characteristic LLC phases, splitting patterns begin to develop in the

NMR spectra. In fact, as surfactant concentration increases and LLC structure becomes more defined the splitting pattern becomes broader indicating that the acrylamide monomers are in a more ordered environment. The bicontinuous cubic phase formed at 40 wt % surfactant generates a broad peak with shoulders at the base of the peak at approximately 0.4 and 0.8 kHz. The broadness of this peak indicates that the amide nitrogen has adopted a preferential orientation in the LLC phase. The increase in orientational ordering suggests that the acrylamide monomer segregates near the polar regions in the LLC phase. Monomer segregation behavior and local ordering in the LLC templated acrylamide system leads to the observed increase in polymerization rate.

The segregation behavior of a similar acrylamide/surfactant system was also probed using NMR by characterizing the ^{13}C T_1 spin lattice relaxation times of the carbonyl, methylene, and methine carbons of the acrylamide monomers as a function of surfactant concentration.⁵² Typically, short relaxation times are indicative of hindered mobility of the functional group studied. The relaxation times of the ^{13}C nuclei were found to decrease linearly with increasing surfactant concentrations, further suggesting that the acrylamide monomers are becoming increasingly sequestered as the order of the LLC phase increases. The strong tendency for acrylamide to segregate near the polar head groups of surfactant molecules results in an increased concentration of reactive groups and a faster polymerization rate.

Similar trends of increasing polymerization rate as the LLC phase dimensionality increases from hexagonal, to bicontinuous cubic, to lamellar has been observed for the photopolymerization of poly(ethylene glycol) dimethacrylate (PEGDMA) templated with the cationic surfactant dodecyltrimethylammonium bromide (DTAB).⁶⁰ This study further demonstrates that the order of the LLC phase has a dramatic impact on the speed of the polymerization reaction with the fastest polymerization occurring in the higher dimensionally ordered lamellar phase. Previous studies of the polymerization of polar monomers indicate that an increase in local monomer concentration as well as a decrease

in termination rate drives the overall increase in polymerization rate. The confined environment limits the mobility of the propagating radical chains leading to a decrease in termination and a concurrent increase in radical concentration in more ordered LLC systems.

The ordering effects of monomers generated by the parent template also impact the rate at which active centers terminate to produce dead chains. The close proximity of reactive groups for radical systems photopolymerized in LLC phases often leads to an increase in bimolecular termination. The increased probability of termination results in an increase in the termination rate constant which serves to decrease the polymerization rate. However, because the polymerization rate is proportional to $k_p/k_t^{1/2}$ a similar increase in both rate constants will lead to an overall increase in the polymerization rate. The segregation behavior and phase structure can be examined during the polymerization reaction through characterization of the kinetic rate constants determined by a series of after-effect experiments, in which the light is shuttered and the subsequent decay in polymerization rate is used to decouple the rate constants. In general, it is common for kinetic constants in the LLC phase to be about an order of magnitude different than those observed in isotropic systems and can vary dramatically with the order of the LLC phase.^{60,64,66,67}

The termination rate generally decreases with increasing degrees of dimensional order, decreasing as the LLC phase changes from hexagonal, to bicontinuous cubic, to lamellar. For example, the termination rate constant is substantially higher in the ordered hexagonal phase compared to the much less ordered micellar phase. Although the termination rate constant is highly dependent on the local order of the parent phase, the propagation rate constant is less sensitive to changes in phase behavior. The ordering of monomer through segregation in the LLC phase tends to generate a higher apparent propagation rate constant compared to an analogous isotropic system, however changes in the phase do not dramatically change the true rate constant of propagation.

Polymerization of Lyotropic Liquid Crystalline Templates – Reactive Surfactants

Another approach in generating polymers containing LLC order involves the direct polymerization of phase forming surfactant monomers.^{16,31,68-72} In this method, researchers have taken the approach of functionalizing LLC phase forming surfactants with reactive groups that can be polymerized into a network. Examples of polymerizable surfactants that can form LLC phases followed by photopolymerization to generate nanostructured polymers are shown in Figure 1.2 c) and d). By polymerizing the LLC phase directly, the need to extract a non-reactive parent template is eliminated. This can offer numerous advantages in the processing and characterization of the materials as it may not be necessary to solvent exchange the cured polymer to remove significant quantities of unreactive material. Additionally, because any birefringence and scattering arises from the interactions between the polymerized surfactants, the structure of the working polymer can be directly characterized using diffraction techniques and light microscopy. This is in contrast to the characterization of polymers synthesized by the polymerization of monomers in a non-reactive LLC template, phase separation events or disruptions in polymer structure can allow for strong interactions between surfactant and solvent that dominate the scattering profiles or optical textures of the sample and do not represent the structure of the polymer.⁶⁵

Researchers have utilized the ability to directly characterize reactive LLC polymer structure to better understand the dynamics of phase transitions that can occur during the polymerization of reactive surfactant assemblies. In one study, the direct relationship between polymerization kinetics and local order was utilized to detect changes in the LLC phase that occur during the polymerization of a reactive quaternary ammonium surfactant.⁷² The reaction profile for the photopolymerization of the methacrylate terminated quaternary ammonium surfactant in water displayed behavior

that is very atypical of that observed in traditional or isotropic photopolymerized systems. Specifically, multiple local maxima or peaks were observed in the polymerization rate profile that can indicate changes in the segregation behavior of reactive groups.

Comparison of the x-ray diffraction profiles before and after polymerization indicated that the original hexagonal morphology changes to a lamellar phase during the polymerization reaction. Further characterization of the reaction rate profiles at higher surfactant concentrations that generated a lamellar structure before polymerization showed significantly higher polymerization rates compared to the lower dimensionally ordered hexagonal phase. The increases in reaction rate that are observed after the initial autoacceleration event were therefore due to the LLC order changing from hexagonal to lamellar during polymerization. Moreover, this work provides valuable insight into the kinetic and thermodynamic factors needed to control polymer structure during photopolymerization. For instance, from a kinetic point of view these data suggest that LLC order evolves in a manner that generates the highest reaction rate. From a thermodynamic perspective, on the other hand, the transition from the hexagonal phase to the lamellar phase during polymerization supports that the lamellar phase is the more stable morphology as the polymerization proceeds and molecular weight increases.

The effect of photopolymerization kinetics on the final structure of the polymerizable quaternary ammonium surfactant was examined by changing the initiation rate and characterizing polymer structure directly using SAXS.⁶⁸ The initiation rate was modulated by varying the light intensity used to cure the polymer as well as using photoinitiators with inherently different efficiencies. Before polymerization, two scattering reflections with a ratio characteristic of the hexagonal phase were observed. After polymerization the intensity of the primary scattering peak is significantly decreased and the ratio of scattering peaks characteristic of the hexagonal phase was lost. Interestingly, the hexagonal phase is much better retained when the initiation rate is increased through the use of a more efficient photoinitiator. The intensity of the primary

scattering peak was retained to a much larger degree when the more efficient Irgacure 651 photoinitiator was used to cure the system, indicating that the reaction kinetics have a significant impact on the nanostructure evolution for reactive LLC systems. Furthermore, when the light intensity used to cure the system was increased from 1 to 15 mW/cm² the hexagonal structure is retained after polymerization. These results support that the reaction kinetics are critical in the preservation of LLC polymer structure in order to synthesize nanostructured materials with useful properties.

Reactive surfactants may provide a thermodynamically stable platform to direct the nanostructure of light cured polymers. The wide range of phases formed using reactive surfactants can template LLC order in polymers and may facilitate structure retention through the close proximity of reactive groups and high degree of thermodynamic stability. Incorporation of reactive surfactants that retain their structure to a large degree during polymerization may provide a useful method of controlling nanostructure in LLC templated polymer systems that tend to phase separate during polymerization.

Structure-property Relationships in Nanostructured Polymer Systems

One of the key features making the development of nanostructured polymers using LLCs as structure directing polymerization templates is the improved functionality materials can achieve by generating periodic nanostructured domains in the polymer network. Significant improvements in the mechanical and transport properties for polymers with nanostructured domains are often reported in the literature.⁷³⁻⁷⁶ For example, a simultaneous increase in the strength and toughness of poly(propylene) (PP) was achieved by generating a nanostructure using a styrene-(ethylene-co-butylene)-

styrene triblock copolymer.⁷⁷ Small angle X-ray scattering profiles of the block copolymer-PP blend indicated that polymer had adopted a lamellar nanostructure as directed by the block copolymer. The addition of the copolymer led to a tenfold increase in the elongation at break and a 13-fold increase in the energy at break. The authors attributed this substantial increase in polymer toughness to the strong interactions between polymer chains.

A number of mechanisms have been identified in which ordered LLC domains can improve polymer mechanical properties. In the previous example the strong interaction between the PP and triblock copolymer generated dramatic improvements in material properties. The viscoelastic behavior of polymers including the glass transition temperature and modulus have been correlated with the cohesive energy density (CED), which represents the thermodynamic interactions between polymer chains.⁷⁸ Specifically, the CED is the theoretical energy that is required to remove a polymer chain from the local molecular environment into the vapor phase. Predictions from this model are in good agreement with experimental results. For instance, the CED predicted purely from Lennard-Jones interaction parameters predicted a modulus of 3.3×10^{10} dyne/cm², in good agreement with the experimental value of 3.3×10^{10} dyne/cm². The interaction or CED of polymer chains may be increased when arranged in a liquid crystalline structure and may explain the increase in mechanical properties that are often observed in nanostructured polymer systems.

From a thermodynamic point of view, the packing of polymer chains into organized structures can increase the activation energy needed for the polymer molecules to achieve long range coordinated molecular motion. In this manner, the packing of the polymer chains can increase the modulus of the polymer.⁷⁹ The degree of crystallinity or fraction of the polymer network that contains ordered nanostructured environments has been correlated to the modulus of the polymer. Increases in the degree of crystallinity are well-known to increase the modulus of the polymer, supporting that polymer crystalline

domains increase polymer mechanical properties by acting as filler particles. From these well-established correlations it is easy to conclude that the degree of LLC template nanostructure transferred to the polymer during polymerization will have a dramatic impact on final polymer properties.

Critical to the use of LLC templating to improve polymer properties is a successful transfer of parent template structure to the polymer. A one to one copy of the original LLC phase structure to the polymer network would generate the maximum improvement in properties. On the other hand, complete phase separation would lead to a disordered polymer network with properties that may not be measurably different from the corresponding isotropic (traditional) polymer network. In practice, the degree of structure transferred to the polymer is often between complete structure retention and complete phase separation, leading to a range or gradient in property improvements based on the degree of structure retained.

Another theory that is useful in explaining the improvement in properties that are observed in nanostructured polymer systems is based on the physical order of the polymer network and provides a complementary viewpoint in relation to thermodynamic views of property improvements. The impact of organized structures on material properties is well-characterized through relationships developed for architected foams, polymers, and ceramics.⁸⁰ For architected systems, the modulus is dependent on the mechanism of deformation of the unit cell which is largely dependent on the connectivity of the structure. In LLC systems, higher connectivities may be established by the intersection of structures that make up the LLC lattice that lead to a larger modulus. On the other hand, isotropic polymers lack a lattice structure needed to establish higher levels of connectivity and lead to lower modulus materials. The differences in mechanical properties observed between LLC nanostructured polymers and isotropic systems may be explained through such variances in lattice structure. It is likely that the increase in mechanical properties observed for LLC ordered polymers is due to the higher

connectivity of the periodic LLC lattice structures. Additionally, this same connecting and continuous structure leads to increased transport. These structure-property relationships observed in the LLC polymers represent a new class of materials with improved properties based on nanostructure which may be useful as biomaterials and tissue scaffolds with property relationships that cannot be generated using traditional polymerization techniques.

The particular geometry of the polymer structures in the polymer network also impacts the observed properties. In other words, differences in the mechanical properties between hexagonal, bicontinuous cubic, and lamellar phase have been established. The majority of the literature examining nanostructure-mechanical property relationships focuses on the lamellar morphology as this is the primary morphology that is observed in well-known polymers such as polyethylene (PE), polyethylene terephthalate (PET), polytetrafluoroethylene (PTFE), and isotactic polypropylene (PP).^{81,82} Recently, much work has been done to establish methods of accessing other polymer morphologies by designing the structure of block copolymers to drive the self-assembly of a particular or desired liquid crystalline morphology.

Researchers have begun to establish relationships between the particular LLC phase and the corresponding mechanical properties of the system. For example, the structure of poly(ethylene glycol) was controlled by photopolymerization in different LLC phases and correlated to the compressive modulus of the polymer.¹⁴ An astonishing three-fold increase in the compressive modulus compared to the isotropic polymer of the same chemical composition was observed. Moreover, the compressive modulus was found to increase as the degree of dimensional order changed from hexagonal to bicontinuous cubic to lamellar. Although these results suggest that the LLC phase has a non-negligible impact on the mechanical properties, it is important to note that it is both degree of parent structure retained and LLC phase order that dictate the final mechanical properties. Based on the above discussions relating polymer structure to mechanical

properties, both the degree of LLC template structure transferred to the polymer (i.e. degree of crystallinity) and the phase geometry (i.e. connectivity of LLC structures) can impact final polymer properties. Thus, in practice a convolution between the degree of structure and ultimate polymer morphology must be considered when analyzing structure-property relationships in LLC templated polymer systems. Because the synthesis of polymers with a wide-range of controllable nanostructures is still a relatively recent and ongoing development in polymer science, exact relationships between the particular liquid crystalline phases and corresponding properties are not yet established.

The properties of LLC templated nanostructured polymers are not orientationally dependent. In other words, properties such as the modulus do not change based on the direction of the sample axis in relation to the applied mechanical stress. This differs from samples that have liquid crystalline order that is generated through a shearing or flow induced arrangements of polymer chains. In these cases, the chains are often aligned along an axis, known as the director, which is parallel to the induced flow. The macroscopic alignment of polymer chains generates differences in the mechanical properties depending on the direction of the applied force in relation to chain alignment. Often, the modulus of the polymer is larger when the applied force is parallel to the alignment of polymer chain. LLC templated polymers have mechanical properties that are independent of the applied stress. No macroscopic alignment or preferential direction of LLC structures is induced. For example, the hexagonal phase contains cylinders with a length that are approximately 20-30 times the length of the surfactant used to form the self-assembled phase.³³ The directionality can extend for several hundred micrometers or even millimeters in some cases as evidenced by the size of grain boundaries observed through crossed polarizers. The bulk hexagonal structure of the polymer is comprised of random arrangements of hexagonally packed cylinders that permeate throughout the polymer matrix. In other words, LLC templated polymers are anisotropic on the nanometer size scale and isotropic on macroscopic size scales (i.e. millimeters).

A particularly useful property relationship often observed in LLC templated polymers is a higher compressive modulus for hydrogel materials than predicted by classical polymer science. Classical polymer science has established the decrease in mechanical properties that occur as water is incorporated into the polymer network. Water molecules act like a plasticizer and decrease the polymers resistance to deformation to an applied mechanical stress. In fact, there is a logarithmic dependence of the compressive modulus on the swelling ratio of the hydrogel. Dramatic decreases in the stiffness of the hydrogel with small increases in water uptake are well-established. However, LLC templated hydrogels display mechanical behavior that is much different from classical polymer science. For LLC templated hydrogels, the compressive modulus of the polymer is often larger than that predicted by classical polymer science established for isotropic hydrogels.⁸³ For example, the hydrated compressive modulus of LLC nanostructured poly(ethylene glycol) was found to be similar to that of the isotropic hydrogel of the same chemical composition despite the higher degree of water uptake for the nanostructured gel.¹⁴ Clearly, a number of mechanical property improvements can be achieved by controlling polymer network structure using LLCs as structure directed photopolymerization platforms.

Transport Properties of LLC Nanostructured Polymers

In addition to the improvement in mechanical properties afforded by the LLC templating process, significant improvements in transport properties are also observed. Transport of molecules throughout the polymer matrix is largely governed by the mesh size of the network and the hydrodynamic radius of the diffusing solute. Inevitably, there is a distribution of mesh sizes throughout the polymer matrix with an average mesh size that is used to establish scaling laws for the diffusion of solute through the network. In the following discussion we assume the interaction of the solute with the polymer is

negligible. If the ratio of the average mesh size to the hydrodynamic radius of the solute is large, the solute will diffuse through the network rather quickly.⁸⁴ As the hydrodynamic radius of the solute approaches the average mesh size the diffusivity is reduced. The primary factors that govern the mesh size of the polymer network are the crosslinking density and the solvent uptake of the network. Figure 1.6 shows a representation of an LLC templated and isotropic polymer network with the average mesh size denoted by ξ .

The crosslinking density of the network is determined by the monomer molecular weight and functionality, with higher crosslinking densities leading to lower mesh sizes. The solvent uptake is determined by the chemistry and hydrophilicity of the network in comparison to the solvent and the crosslinking density. Increases in solvent uptake generate increases in the transport properties of the polymer by increases the network mesh size. These parameters can be used to control and tune the diffusive properties of drugs and dyes through the polymer. The fastest transport is readily achieved by a loosely crosslinked network that can uptake significant quantities of solvent.⁸⁵ This scenario is often unpractical in industrial and biomedical applications because the resulting polymer would be extremely weak. LLC nanostructured materials have unique property relationships such as simultaneous increases in transport and mechanical strength that are useful in a number of industrial and biomedical applications. For example, membranes with a high throughput are useful in water purification and chemical protection suits. Hydrogel materials that can readily facilitate the transport of nutrients and waste to growing tissues as well as drug delivery systems based on hydrogel materials are particularly useful in biomedical applications.⁸⁶⁻⁸⁸ Increases in diffusive transport properties have been established in LLC nanostructured systems. These increases in diffusivity are likely due to the increased mesh size and directed route for solute transport through the network.

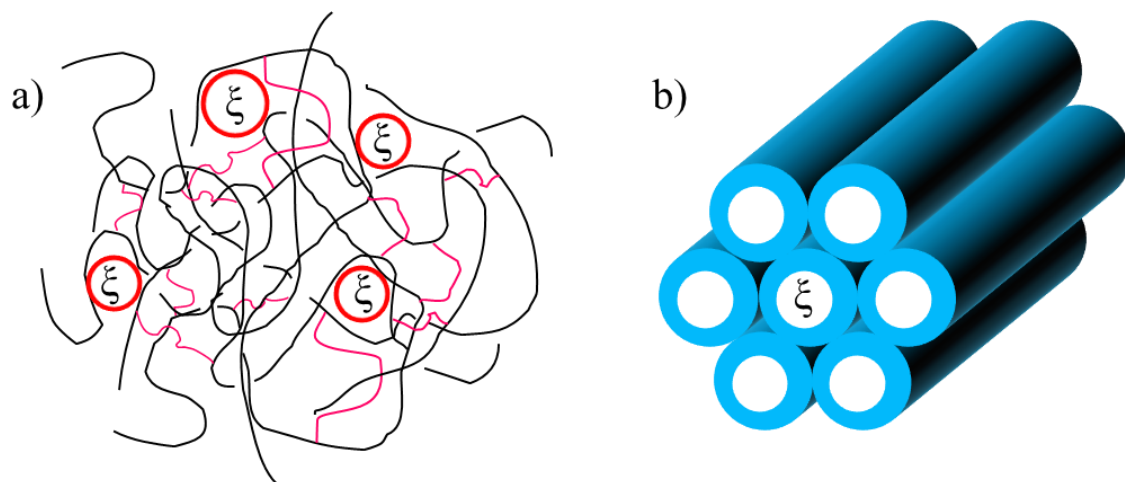


Figure 1.6. Representation of the average mesh size, ξ , which largely dictates the diffusive properties of the polymer network. Shown are a) representative average mesh size for an isotropic network and b) hexagonal LLC nanostructured network

The increased pore uniformity of the hexagonal, bicontinuous cubic, and lamellar nanostructures can increase the average mesh size of the network and increase solute diffusivity. Additionally, the directed pore structure can serve to decrease the tortuosity of the network and decrease mass transport resistance through the polymer matrix, similar to the manner in which a lower tortuosity factor in packed beds leads to a lower pressure drop. Researchers have utilized the directed route of solute transport to increase the diffusivity of light gasses through a polymer membrane by generating a hexagonal structure in the polymer system.^{69,89} Additionally, the bicontinuous cubic phase has been cited to have particular advantages over other LLC phases at increasing solute diffusivity through the polymer for use in membrane and contact lens applications. There is a 3-dimensional symmetry inherent in the cubic phase that can dramatically increase pore alignment and facilitate transport through the polymer.⁹⁰ Increasing pore alignment by generating a bicontinuous cubic or other LLC nanostructure can dramatically improve the diffusive properties relative to an isotropic polymer network.

Stimuli-sensitive Polymers

A particular class of polymers often referred to as “smart” polymers are the topic of considerable research in polymer science. These smart polymers are being examined for use in a wide-variety of applications ranging from controlled drug-delivery systems, chemical sensors, optical displays, and artificial muscles.^{91,92} Stimuli-responsive or smart polymers are polymeric systems that undergo a reversible chemical or physical change in response to an external stimulus. The stimulus that generates the chemical or physical change in the polymer network can range from temperature, pressure, ionic strength, pH, and light. Using these polymers, a particular class of materials have been designed that can change their physical or transport properties in a manner dependent on the external environment. For example, the pH of the gastrointestinal track varies ranging from a pH of 1-2 in a fasting state up to a pH of 4 during digestion.⁹³ Using pH sensitive hydrogels, there is the potential to deliver insulin orally instead of the syringe system currently in use.

Oral administration of insulin without an appropriate delivery vehicle is not effective because insulin cannot survive the acidic conditions of the stomach. However, using a pH sensitive poly(methacrylic-ethylene glycol) graft copolymer, researchers were able to protect the insulin from the acidic conditions of the stomach. After passing through the acidic conditions of the stomach the copolymer began to swell in the increasingly basic conditions of the intestine, allowing the insulin cargo to be released. Other examples of stimuli-sensitive polymers for use in industrial and biomedical applications include the use of shape-memory polymers in which the polymer can “remember” their structure after being deformed and can readopt the original geometry after a temperature change. Applications of shape-memory polymers are being explored for use as industrial fastening applications and minimally invasive wound closures sutures.

One of the most heavily studied stimuli-sensitive polymers is poly(*N*-isopropylacrylamide) (PNIPAM).^{94,95} PNIPAM is a temperature sensitive polymer that undergoes a reversible volume transition in water when heated above the lower critical solution temperature (LCST) of 33 °C. Below the LCST the polymer is hydrophilic and can absorb significant quantities of water and collapses to expel the absorbed water when heated above the LCST. PNIPAM has been examined for use in a variety of applications ranging from drug-delivery, tissue engineering, actuators, and sensors.^{96,97} The use of PNIPAM as a drug delivery vehicle stems from the fact that whole or local body temperature can change based on particular infections or diseases which can trigger the release of therapeutic agents.

Another particularly innovative use of PNIPAM is to control the delivery of insulin in response to glucose concentration. When copolymerized with acrylamidophenylboronic acid moieties, a useful polymer that responds to glucose concentration at normal human body temperature is attained.⁹⁸ The phenylboronic acid moieties in the polymer network form complexes with glucose with a particularly high affinity over other polyols found in the body. The formation of this complex with glucose generates a partial charge on the phenylboronic acid moiety causing the polymer to become hydrophilic and swell. The increase in mesh size that accompanies the swelling process then triggers the release of insulin and can be used as a self-regulating device to control blood sugar. Additionally, the ability to control the hydrophilicity of PNIPAM can be used to entrap hydrophobic drugs in a hydrophilic polymer network for use in controlled drug delivery.

Increasingly complex and “smart” polymer systems that respond to multiple stimuli can be engineered by the copolymerization of multiple monomers each responding to a separate stimulus. Dual responsive hydrogels that respond to both pH and temperature poly(*N*-isopropylacrylamide-co-acrylic acid) have been developed that respond to narrow ranges of temperature or pH, making the polymer useful in drug

delivery and sensor applications.⁹⁹ One of the major problems limiting the functionality of stimuli-sensitive polymers is their slow response to changes in external stimulus. This limits the applications of stimuli-sensitive polymers that require a rapid response to changes in external conditions. Methods of increasing the transition kinetics typically include the generation of a porous structure throughout the polymer by polymerization in surfactant stabilized emulsions, silica beads, grafting of surfactant structures along the polymer backbone, or thermally induced phase separation methods.¹⁰⁰⁻¹⁰⁶ These techniques have been used to dramatically increase the transition kinetics of stimuli-sensitive polymers including a rapid deswelling rate of PNIPAM hydrogels for heating above the LCST.

Another limitation of stimuli-sensitive hydrogels is their weak mechanical properties. Many applications require the hydrogel to withstand significant stresses from the external environment including as well as from the deswelling process itself. A number of methods have been demonstrated to increase the mechanical properties of hydrogels such as incorporation of toughening agents including siloxane moieties, urethane acrylate oligomers, and low molecular weight crosslinking monomers. Other examples include the synthesis of double network hydrogels comprised of acrylamide and a semi-rigid poly(2,2'-disulfonyl-4,4'-benzidine terephthalamide) to generate tougher hydrogel materials.¹⁰⁷ However, these methods often compromise the deswelling rate or the magnitude of the response to changes in external stimuli. It is reasonable to hypothesize that the increase in transport and mechanical properties that are observed in LLC nanostructured polymers could be utilized to overcome many of the difficulties that are associated with stimuli-sensitive polymers.

Compatibility issues are often encountered during the blending of monomer systems to generate a copolymer with intermediate properties of the individual polymer network. These difficulties can arise from the blending of the individual monomer systems or the differences in thermodynamics and reaction kinetics that can occur during

the copolymerization of monomer systems. Differences in solubility between monomers can be overcome by the selection of an appropriate solvent or solvent blend to compatibilize the monomers.^{28,108} Other methods include the use of copolymers with varying block chemistries to selectively solvate and compatibilize the monomer blend. However, identification and design of appropriate solvent or surfactant systems to generate a compatibilized polymer blend can be difficult and time consuming. Emulsion polymerization in which incompatible monomers can be dispersed within continuous or discontinuous domains using surfactants is a promising method of decreasing the size of phase separated domains and generating a polymer with good mechanical integrity.

Other difficulties can arise during the polymerization reaction due to differences in reactivity ratios and changes in molecular weight that occur during the polymerization reaction that can lead to a phase separated polymer with poor mechanical properties. Polymerization of monomers in confined arrangements or using independent polymerization mechanisms that do not interfere or compete with one another is a promising method of generating polymer composites containing properties of the individual polymer networks. Using these methods researchers have generated interpenetrating networks (IPNs) which are comprised of two relatively independent polymer systems through physical entanglements as opposed to covalent chemical bonds.⁶³ IPNs come in different varieties that are used to describe the structure of the polymer networks. Semi-IPNs are comprised of a linear polymer that is interwoven throughout a crosslinked polymer network whereas full-IPNs are made of two intertwined and independent crosslinked polymer networks.

A copolymer formed by the traditional copolymerization of monomers in which both monomer chemistries are incorporated throughout the backbone of the polymer chains will have much different properties when compared to an IPN material of the same chemical composition. Because IPN polymers are two independent polymer systems that are held together by physical entanglements, the resulting polymer material retains

properties of the individual polymer networks instead of properties intermediate of the polymer systems that are obtained by traditional copolymerization. This process has been utilized to improve the tensile properties and elongation and break of poly(vinyl chloride) (PVC) polymers by generating a semi-IPN with a flexible poly(urethane) polymer.¹⁰⁹ In this manner, the toughness inherent in the poly(urethane) was used to increase the elongation at break while maintaining the high modulus of the PVC.

There are two traditional methods of synthesizing IPNs: (1) the crosslinked polymer is swollen with monomer and initiator and polymerized *in-situ* to form a so-called sequential IPN and (2) both polymer networks are synthesized simultaneously by independent and non-interfering routes to form a simultaneous IPN. The use of LLC templates to generate nanostructure IPN polymer materials would fall under the latter case of simultaneous IPNs. The LLC templating method has been utilized to generate IPN materials of otherwise incompatible monomers of hexanediol diacrylate and PEGDA.²⁸ At low surfactant concentrations the polymer composite was phase separated and generated a bar with material properties that were so weak due to macroscopic phase separation that the polymer could not withstand mechanical property testing. As surfactant concentration was increased, the hexagonal LLC phase formed to generate a nano-phase separated polymer network with properties intermediate of the individual polymer networks. In a similar manner, LLCs have been utilized to generate IPN type polymers with incompatible poly(lactic acid-ethylene glycol) copolymers and degradable crosslinker ethoxy succinate dimethacrylate.³⁷ The use of LLCs to modulate the mechanical properties through the confined polymerization in the separate polar and non-polar domains of the LLC phase is a promising method of generating IPN materials in order to improve polymer properties.

Research Summary

The goal of this study is to develop polymeric materials with controlled nanometer sized structures utilizing LLCs as photopolymerization platforms to direct polymer structure. Additionally, the impact of LLC nanostructure on the properties of organic polymers is established in order to understand how polymer structure can be directed to optimized polymer functionality. Much research has focused on the examination of polymerization kinetics to probe the order and structural development of LLC templated systems during polymerization. This work will continue to build upon the rich science of photopolymerization kinetics in LLC templated systems in order to determine the underlying kinetic factors that are dictating polymer structure evolution during the polymerization reaction. Equally or perhaps more important in the synthesis of polymers with controlled LLC nanostructures is the examination of methods that can be used to control polymer structure in systems that tend to phase separate during the polymerization reaction in order to access the useful property relationships dependent on nanostructure.

This work aims at utilizing polymerization kinetics and LLC templating as a tool to synthesize polymers with useful property relationships. The bulk of this research can be categorized into three sections including the use of photopolymerization kinetics as a probe to monitor the evolution of polymer structure during the polymerization reaction, development of methods and photopolymerizable systems that can be used to retain the original LLC nanostructure during polymerization, and the application of LLC nanostructured systems to improve the properties of stimuli-responsive polymers. This work runs the full spectra of LLC templating ranging from fundamental understanding of LLC structure retention factors, to methods of controlling LLC nanostructure in systems that tend to phase separate, and finally to the applications of polymer systems to solve problems associated with a particular class of “smart” polymer materials.

Although the use of photopolymerization kinetics as a tool to probe the order of the LLC structure during polymerization is utilized throughout this work, the majority of this work is presented in chapter 4 which develops a novel method of characterizing changes in polymer structure by analysis of the photopolymerization rate. The development of methods to control LLC nanostructure in polymer systems that tend to phase separate from the parent template upon polymerization are presented in chapter 5. In addition, chapter 5 also contains useful structure property relationships that clearly demonstrate the improved mechanical and transport properties that are attained for LLC systems that retain their template order. Chapters 6 and 7 primarily focus on the application of the LLC templating process to improve the properties of stimuli-sensitive polymer systems. Also inherent in these chapters are additional structure-property relationships that further demonstrate the improved properties of polymers with ordered nanostructured morphologies. Chapter 8 extends the use of LLCs to generate nanostructure in a new class of polymer materials in which the LLC templating process has not yet been applied. This chapter also introduces a unique LLC system and polymerization mechanism which allows for dramatic improvements in structure retention and greatly increases material strength. Photopolymerization and self-assembly provide a promising method of generating nanostructured polymer materials with properties useful in a wide-range of industrial and biomedical applications.

Notes

1. Laslau, C.; Williams, D. E.; Travas-Sejdic, J. *Prog. Polym. Sci.* **2012**, *37*, 1177-1191.
2. Munoz, A.; McConney, M. E.; Kosa, T.; Luchette, P.; Sukhomlinova, L.; White, T. J.; Bunning, T. J.; Taheri, B. *Opt. Lett.* **2012**, *37*, 2904-2906.
3. Schricker, S. R.; Palacio, M. L. B.; Bhushan, B. *Philos. Trans. R. Soc. A-Math. Phys. Eng. Sci.* **2012**, *370*, 2348-2380.
4. Singh, N. K.; Singh, S. K.; Dash, D.; Purkayastha, B. P. D.; Roy, J. K.; Maiti, P. *J. Mater. Chem.* **2012**, *22*, 17853-17863.
5. Wang, Y.; Tran, H. D.; Kaner, R. B. *Macromol. Rapid Commun.* **2011**, *32*, 35-49.
6. Paul, D. R.; Robeson, L. M. *Polymer* **2008**, *49*, 3187-3204.
7. Szleifer, I.; Yerushalmi-Rozen, R. *Polymer* **2005**, *46*, 7803-7818.
8. Wang, X.; Schroeder, H. C.; Wang, K.; Kaandorp, J. A.; Mueller, W. E. G. *Soft Matter* **2012**, *8*, 9501-9518.
9. Avestro, A.; Belowich, M. E.; Stoddart, J. F. *Chem. Soc. Rev.* **2012**, *41*, 5881-5895.
10. Mishra, A.; Aswal, V. K.; Maiti, P. *J Phys Chem B* **2010**, *114*, 5292-5300.
11. Cataldo, S.; Zhao, J.; Neubrech, F.; Frank, B.; Zhang, C.; Braun, P. V.; Giessen, H. *ACS Nano* **2012**, *6*, 979-985.
12. Fujiki, M.; Koe, J.; Terao, K.; Sato, T.; Teramoto, A.; Watanabe, J. *Polym. J.* **2003**, *35*, 297-344.
13. Li, H.; Huck, W. *Curr. Opin. Solid State Mat. Sci.* **2002**, *6*, 3-8.
14. Clapper, J. D.; Guymon, C. A. *Macromolecules* **2007**, *40*, 1101-1107.
15. Forney, B. S.; Guymon, C. A. *Macromol. Rapid Commun.* **2011**, *32*, 765-769.
16. Bara, J. E.; Kaminski, A. K.; Noble, R. D.; Gin, D. L. *J. Membr. Sci.* **2007**, *288*, 13-19.
17. Guo, C.; Wang, J.; Cao, F.; Lee, R. J.; Zhai, G. *Drug Discov. Today* **2010**, *15*, 1032-1040.
18. Hindeleh, A.; Abdo, S. *Polymer Communications* **1989**, *30*, 184-186.

19. Liang, B.; Pan, L.; He, X. *J Appl Polym Sci* **1997**, *66*, 217-224.
20. Xu, J.; Zhu, Y.; Zhang, Y.; Zheng, Y.; Chi, Z.; Xu, J. *J Appl Polym Sci* **2007**, *103*, 3183-3193.
21. Khan, M. B.; Hussain, S.; Hussain, R.; Khan, Z. M. *J. Adv. Mater.* **2010**, *42*, 74-87.
22. Bai, G.; Wang, J.; Yan, H.; Li, Z.; Thomas, R. *J Phys Chem B* **2001**, *105*, 9576-9580.
23. Hentze, H.; Kaler, E. *Curr. Opin. Colloid Interface Sci.* **2003**, *8*, 164-178.
24. Olsen, B. D.; Segalman, R. A. *Mater. Sci. Eng. R-Rep.* **2008**, *62*, 37-66.
25. Clapper, J. D.; Sievens-Figueroa, L.; Guymon, C. A. *Chem. Mat.* **2008**, *20*, 768-781.
26. Hamley, I. *Nanotechnology* **2003**, *14*, R39-R54.
27. Verheyen, E.; Schillemans, J. P.; van Wijk, M.; Demeniex, M.; Hennink, W. E.; van Nostrum, C. F. *Biomaterials* **2011**, *32*, 3008-3020.
28. Clapper, J.; Guymon, C. *Adv Mater* **2006**, *18*, 1575.
29. DePierro, M. A.; Carpenter, K. G.; Guymon, C. A. *Chem. Mat.* **2006**, *18*, 5609-5617.
30. Lester, C.; Smith, S.; Colson, C.; Guymon, C. *Chem. Mat.* **2003**, *15*, 3376-3384.
31. Sievens-Figueroa, L.; Guymon, C. A. *Chem. Mat.* **2009**, *21*, 1060-1068.
32. Collings, P. J.; Hird, M. Introduction to Liquid Crystals: Chemistry and Physics. In *Identification of liquid crystal phases - mesophase characterization*; Gray, G. W., Goodby, J. W. and Fukuda, A., Eds.; Taylor & Francis Inc.: Bristol, PA, 1997; pp 177-190.
33. Lee, Y. S. *Self-Assembly and Nanotechnology: A Force Balance Approach*; John Wiley & Sons, Inc.: Hoboken, NJ, 2008.
34. Neto, A. M. F.; Salinas, S. R. A. *The Physics of Lyotropic Liquid Crystals*; Oxford University Press: New York, 2005.
35. Tortora, L.; Park, H.; Kang, S.; Savaryn, V.; Hong, S.; Kaznatcheev, K.; Finotello, D.; Sprunt, S.; Kumar, S.; Lavrentovich, O. D. *Soft Matter* **2010**, *6*, 4157-4167.
36. Texter, J. *Colloid Polym. Sci.* **2009**, *287*, 313-321.
37. Clapper, J. D.; Sievens-Figueroa, L.; Guymon, C. A. *Chem. Mat.* **2008**, *20*, 768-781.

38. DePierro, M. A.; Carpenter, K. G.; Guymon, C. A. *Chem. Mat.* **2006**, *18*, 5609-5617.
39. Lester, C. L.; Colson, C. D.; Guymon, C. A. *Macromolecules* **2001**, *34*, 4430-4438.
40. Sievens-Figueroa, L.; Guymon, C. A. *Polymer* **2008**, *49*, 2260-2267.
41. Adelhelm, P.; Hu, Y.; Chuenchom, L.; Antonietti, M.; Smarsly, B. M.; Maier, J. *Adv Mater* **2007**, *19*, 4012.
42. Bowman, C. N.; Kloxin, C. J. *AIChE J.* **2008**, *54*, 2775-2795.
43. Lin, Y.; Stansbury, J. J. *J. Polym. Sci. Pol. Chem.* **2004**, *42*, 1985-1998.
44. Ikemura, K.; Endo, T. *Dent. Mater. J.* **2010**, *29*, 481-501.
45. Zhang, Y.; Zhan, F.; Shi, W. *Prog. Org. Coat.* **2011**, *71*, 399-405.
46. Wang, J. J.; Liu, F. *J Appl Polym Sci* **2012**, *127*, 2235-2242.
47. Stansbury, J. W. *J. Esthet. Dent.* **2000**, *12*, 300-308.
48. Ikemura, K.; Endo, T. *Dent. Mater. J.* **2010**, *29*, 481-501.
49. Mauguier-Guyonnet, F.; Burget, D.; Fouassier, J. P. *Progress in Organic Coatings* **2007**, *59*.
50. Jiang, T.; He, Y.; Jian, Y.; Nie, J. *Progress in Organic Coatings* **2012**, *75*.
51. Odian, G. *Principles of Polymerization*; Wiley: Hoboken, NY, 2004.
52. Hoyle, C. E.; Bowman, C. N. *Angewandte Chemie-International Edition* **2010**, *49*.
53. Lowe, A. B. *Polymer Chemistry* **2010**, *1*.
54. Trey, S. M.; Nilsson, C.; Malmstrom, E.; Johansson, M. *Progress in Organic Coatings* **2010**, *67*.
55. Hentze, H.; Goltner, C.; Antonietti, M. *Ber. Bunsen-Ges. Phys. Chem. Chem. Phys.* **1997**, *101*, 1699-1702.
56. Janeschitz-Kriegl, H.; Ratajski, E. *Colloid Polym. Sci.* **2010**, *288*, 1525-1537.
57. Long, Y.; Shanks, R.; Stachurski, Z. *Prog. Polym. Sci.* **1995**, *20*, 651-701.
58. Oya, N.; Saitoh, S.; Furuhashi, Y.; Yoshie, N. *J. Polym. Sci. Pol. Chem.* **2012**, *50*, 1926-1932.

59. Fong, C.; Le, T.; Drummond, C. J. *Chem. Soc. Rev.* **2012**, *41*, 1297-1322.
60. Lester, C.; Colson, C.; Guymon, C. *Macromolecules* **2001**, *34*, 4430-4438.
61. Lester, C.; Smith, S.; Guymon, C. *Macromolecules* **2001**, *34*, 8587-8589.
62. Lester, C.; Smith, S.; Jarrett, W.; Guymon, C. *Langmuir* **2003**, *19*, 9466-9472.
63. Odian, G. *Principles of Polymerization*; John Wiley & Sons: Hoboken, NJ, 2004.
64. DePierro, M.; Guymon, C. *Macromolecules* **2006**, *39*, 617-626.
65. Forney, B. S.; Guymon, C. A. *Macromolecules* **2010**, *43*, 8502-8510.
66. Lester, C.; Guymon, C. *Polymer* **2002**, *43*, 3707-3715.
67. Lester, C.; Guymon, C. *Macromolecules* **2000**, *33*, 5448-5454.
68. Sievens-Figueroa, L.; Guymon, C. A. *Macromolecules* **2009**, *42*, 9243-9250.
69. Hatakeyama, E. S.; Gabriel, C. J.; Wiesenauer, B. R.; Lohr, J. L.; Zhou, M.; Noble, R. D.; Gin, D. L. *J. Membr. Sci.* **2011**, *366*, 62-72.
70. Gin, D. L.; Bara, J. E.; Noble, R. D.; Elliott, B. J. *Macromol. Rapid Commun.* **2008**, *29*, 367-389.
71. Li, M.; Yang, W.; Chen, Z.; Qian, J.; Wang, C.; Fu, S. *J. Polym. Sci. Pol. Chem.* **2006**, *44*, 5887-5897.
72. Sievens-Figueroa, L.; Guymon, C. A. *Polymer* **2008**, *49*, 2260-2267.
73. Ji, B.; Gao, H. *Ann. Rev. Mater. Res.* **2010**, *40*, 77-100.
74. Choi, H. J.; Ray, S. S. *J. Nanosci. Nanotechnol.* **2011**, *11*, 8421-8449.
75. Venkataraman, S.; Hedrick, J. L.; Ong, Z. Y.; Yang, C.; Ee, P. L. R.; Hammond, P. T.; Yang, Y. Y. *Adv. Drug Deliv. Rev.* **2011**, *63*, 1228-1246.
76. Cardoso, D. A.; Jansen, J. A.; Leeuwenburgh, S. C. G. *J. Biomed. Mater. Res. Part B* **2012**, *100B*, 2316-2326.
77. Vuluga, Z.; Panaitescu, D. M.; Radovici, C.; Nicolae, C.; Iorga, M. D. *Polym. Bull.* **2012**, *69*, 1073-1091.
78. Tobolsky, A. V. *Properties and Structure of Polymers*; John Wiley: New York, 1960; pp 71-78.

79. Michler, G. H.; Balta-Calleja, F. J. *Mechanical Properties of Polymers based on Nanostructure and Morphology*; Taylor and Francis Group: Boca Raton, FL, 2005.
80. Ashby, M. *Philos. Trans. R. Soc. A-Math. Phys. Eng. Sci.* **2006**, *364*, 15-30.
81. Seguela, R. J. *Macromol. Sci. -Polym. Rev* **2005**, *C45*, 263-287.
82. Liu, J.; Jungnickel, B. -. *J. Polym. Sci. Pt. B-Polym. Phys.* **2007**, *45*, 1917-1931.
83. Forney, B. S.; Guymon, C. A. *Macromol. Rapid Commun.* **2011**, *32*, 765-769.
84. Lustig, S. R.; Peppas, N. A. *J Appl Polym Sci* **1988**, *36*, 735-747.
85. Dinerman, A. A.; Cappello, J.; Ghandehari, H.; Hoag, S. W. *J. Controlled Release* **2002**, *82*, 277-287.
86. Wei, G.; Ma, P. X. *Adv. Funct. Mater.* **2008**, *18*, 3568-3582.
87. Yang, S. F.; Leong, K. F.; Du, Z. H.; Chua, C. K. *Tissue Eng.* **2001**, *7*, 679-689.
88. Yoon, H.; Choi, M.; Lee, K. A.; Jang, J. *Macromol. Res.* **2008**, *16*, 85-102.
89. Gin, D. L.; Bara, J. E.; Noble, R. D.; Elliott, B. J. *Macromolecular Rapid Communications* **2008**, *29*, 367-389.
90. Hatakeyama, E. S.; Wiesenauer, B. R.; Gabriel, C. J.; Noble, R. D.; Gin, D. L. *Chem. Mat.* **2010**, *22*, 4525-4527.
91. Chaterji, S.; Kwon, I. K.; Park, K. *Prog. Polym. Sci.* **2007**, *32*, 1083-1122.
92. Stuart, M. A. C.; Huck, W. T. S.; Genzer, J.; Mueller, M.; Ober, C.; Stamm, M.; Sukhorukov, G. B.; Szleifer, I.; Tsukruk, V. V.; Urban, M.; Winnik, F.; Zauscher, S.; Luzinov, I.; Minko, S. *Nat. Mater.* **2010**, *9*, 101-113.
93. Alarcon, C.; Pennadam, S.; Alexander, C. *Chem. Soc. Rev.* **2005**, *34*, 276-285.
94. Laszlo, K.; Kosik, K.; Rochas, C.; Geissler, E. *Macromolecules* **2003**, *36*, 7771-7776.
95. Takata, S.; Suzuki, K.; Norisuye, T.; Shibayama, M. *Polymer* **2002**, *43*, 3101-3107.
96. Yoshida, R.; Uchida, K.; Kaneko, Y.; Sakai, K.; Kikuchi, A.; Sakurai, Y.; Okano, T. *Nature* **1995**, *374*, 240-242.
97. Kaneko, Y.; Yoshida, R.; Sakai, K.; Sakurai, Y.; Okano, T. *J. Membr. Sci.* **1995**, *101*, 13-22.

98. Wu, W.; Mitra, N.; Yan, E. C. Y.; Zhou, S. *ACS Nano* **2010**, *4*, 4831-4839.
99. Bromberg, L.; Ron, E. *Adv. Drug Deliv. Rev.* **1998**, *31*, 197-221.
100. Anseth, K. S.; Bowman, C. N.; Brannon Peppas, L. *Biomaterials* **1996**, *17*, 1647-1657.
101. Liu, F.; Urban, M. W. *Prog. Polym. Sci.* **2010**, *35*, 3-23.
102. Serizawa, T.; Wakita, K.; Akashi, M. *Macromolecules* **2002**, *35*, 10-12.
103. Zhang, J.; Liu, X.; Fahr, A.; Jandt, K. D. *Colloid Polym. Sci.* **2008**, *286*, 1209-1213.
104. Zhang, J.; Jandt, K. D. *Macromol. Rapid Commun.* **2008**, *29*, 593-597.
105. Zhang, X. Z.; Wang, F. J.; Chu, C. C. *J. Mater. Sci. -Mater. Med.* **2003**, *14*, 451-455.
106. Zhang, X.; Xu, X.; Cheng, S.; Zhuo, R. *Soft Matter* **2008**, *4*, 385-391.
107. Yang, W.; Furukawa, H.; Gong, J. P. *Adv Mater* **2008**, *20*, 4499-4503.
108. Karaenev, S.; Chilingirjan, M. *Eur. Polym. J.* **1984**, *20*, 1223-1225.
109. Gupta, N.; Srivastava, A. *Polym. Int.* **1994**, *35*, 109-118.

CHAPTER 2

OBJECTIVES

Photopolymerization in lyotropic liquid crystalline (LLC) phases represents a promising method of controlling the nanostructure of organic polymers. Dramatic improvements in transport and mechanical properties can be achieved by applying the LLC templating technology to generate nanostructured polymer materials. The improvements in polymer functionality that can be achieved by controlling polymer nanostructure using LLC templates as photopolymerization platforms has far-reaching benefits in both applied and fundamental polymer science. Although LLC templating is a promising method of synthesizing nanostructured polymers with useful property relationships, several challenges need to be addressed before the LLC templating technique can be applied to large scale applications. The primary problem associated with the LLC templating process is phase separation of the polymer from the parent template. This problem may be addressed from a variety of aspects ranging from the study of polymerization kinetics to probe the underlying factors needed to retain template structure, examination of methods to control polymer structure in LLC systems that tend to phase separate, and design of thermodynamically stable or LLC templated systems that retain their structure during photopolymerization.

As with all research in polymer science and materials engineering, the applications of the synthesized polymers must be worthwhile in order to justify the research. With control of nanostructure, it is anticipated that different and useful properties and property relationships may be possible. Characteristics such as mechanical and transport properties thereby could be controlled through LLC structured polymers. Additionally, the LLC templating process may be useful in solving problems

associated with specific materials that are of great research interest. Although this research examines several problems associated with the LLC templating process, the primary goal is to synthesize polymers with controlled nanometer sized LLC structures and establish useful property relationships that can be applied to solve performance problems of applied polymer materials. This research accomplishes this goal through the following objectives including:

1. Utilize photopolymerization kinetics as a tool to probe the local order of LLC templated polymers systems that phase separate in order to establish how polymer structure evolves during the polymerization reaction.
2. Establish methods that can be utilized to control and retain the LLC nanostructure in polymer systems that tend to phase separate during the polymerization reaction.
3. Establish structure-property relationships to clearly demonstrate the improved properties that can be obtained by incorporating a LLC nanostructure in the polymer network.
4. Apply the LLC templating technology to improve the transport, response, and mechanical properties of stimuli-sensitive polymers.
5. Develop nanostructured polymer systems that retain their LLC structure during the polymerization reaction.

The first objective is addressed in chapter 4 and introduces a novel technique that has been utilized to identify phase separation events that occur during the polymerization reaction. Through careful examination of the photopolymerization kinetics of LLC templated polymer systems that grossly phase separate during polymerization, critical conversions at which the LLC template ceases to be thermodynamically stable are identified. Monomers with contrasting polarity are templated in different LLC

mesophases to establish the breadth in which this technique may be applied to determine how LLC phase structure evolves during the polymerization reaction. Additionally, the impact of polymerization kinetics on final degree of LLC structure retained is also presented in chapter 5.

The second objective is examined in chapter 5. This chapter outlines a method that can be utilized to retain the parent template nanostructure in LLC systems that phase separate during polymerization using combinations of non-reactive and reactive surfactants. A templated polymer that completely phase separates from the parent template during polymerization is examined and techniques of retaining the original nanostructure are established. Through the use of a polymerizable surfactant that retains its LLC structure to a large the degree during polymerization, a systematic study determining the how the template order may be transferred to the polymer is presented.

The third objective is accomplished throughout the remaining chapters (chapters 5 – 8). Chapter 5 presents a clear and systematic examination of the evolution of polymer properties in LLC templated polymer systems. The mechanical and transport properties of phase separated LLC polymers and polymers that retain their LLC structure using methods developed in objective two are presented. Chapters 5 – 8 also establish structure property relationships by comparing the properties of LLC nanostructured polymer systems to corresponding isotropic controls of the same chemical composition. Through characterization of dye release, transient water uptake, and deswelling kinetics the impact of nanostructure on transport properties are clearly established. The compressive modulus, glass transition temperature, and tensile properties of polymers are also characterized to determine the effect of LLC order on polymer mechanical performance.

The fourth objective is addressed in chapters 6 and 7 by applying the LLC templating process to improve the properties associated with the stimuli-sensitive polymer poly(*N*-isopropylacrylamide) (PNIPAM). Using the improvement in mechanical and transport properties than can be obtained by generating a LLC nanostructure in the

polymer the deswelling rate, water uptake, and compressive modulus of PNIPAM are improved. While chapter 6 lays the groundwork and establishes the utility of the LLC templating process to improve the functionality of PNIPAM, chapter 7 demonstrates the full potential of LLCs to improve PNIPAM properties. In particular, nanostructured IPN polymers are produced from PNIPAM and poly(dimethylsiloxane) monomers. Using this method the mechanical properties of PNIPAM are dramatically improved compared to traditional PNIPAM networks without comprising the key performance parameters including rapid deswelling rate and degree of water uptake.

The fifth objective including rapid polymerization rate, insensitivity to oxygen, and step-growth polymerization mechanism is pursued in chapter 8 and utilizes the inherent advantages of the thiol-ene copolymerization to produce robust nanostructured polymer materials. Robust LLC templated polymer systems that retain their structure to a large degree during polymerization are developed by identifying thiol-ene monomer systems that form and retain well-defined LLC phases at high monomer concentration in the absence of water. Examination of the phase formation and mechanical properties establishes the fundamental self-assembly behavior and final LLC order in the nanostructure polymer materials.

Completion of these objectives will establish techniques and fundamental knowledge that can be utilized to overcome many of the challenges associated with producing nanostructure materials via the LLC templating process. Establishing methods to determine where in the polymerization reaction phase separation events occur not only provide a novel characterization technique and model of structure evolution in LLC templated polymer systems, but also provides an experimental method that can be used to verify computational or theoretical investigations into polymer phase evolution. The use of reactive surfactants and thiol-ene photopolymerization to develop robust nanostructured polymer networks with enhanced properties provides the basis to extrapolate the LLC templating technique to improve the properties of a wide-range of

polymer materials. Finally, the direct application of the LLC templating process to improve the properties of stimuli-sensitive polymers establishes the utility of this research to develop materials with enhanced properties. The insights into structure retention and property improvements presented in this research may be utilized to optimize the functionality of polymer materials for use in a wide-range of applications.

CHAPTER 3

MATERIALS AND EXPERIMENTAL METHODS

This chapter describes the synthesis and characterization techniques of isotropic and LLC templated polymers that are used to elucidate the factors needed to produce nanostructured materials with useful property relationships. The chemical structure of surfactants, photoinitiators, and monomers used in this research are presented in the first section along with mixing and fabrication methods used to produce materials for property and structural characterization. The following section describes the kinetic and structural characterization techniques of the polymer materials utilizing differential scanning calorimetry, light microscopy, scanning electron microscopy, and x-ray scattering. The last section in this chapter describes the methods that probe the impact of LLC nanostructure on the physical properties including water uptake, deswelling rate, dye release profiles, and mechanical property characterization.

Materials and Sample Preparation

Several commercially available monomers were used in this study aiming to produce nanostructured polymers with enhanced property relationships. Monofunctional non-mesogenic monomers include acrylamide ($\geq 99\%$, Aldrich) and *N*-isopropylacrylamide (97%, Aldrich). Multifunctional non-mesogenic monomers include *N,N'*-methylenebisacrylamide ($\geq 98\%$, Aldrich), poly(ethylene glycol) diacrylate (PEGDA, $M_n \sim 258$ Aldrich), 1,6-hexanediol diacrylate (HDDA, Sartomer), methacrylate terminated polydimethylsiloxane monomer (DMS-R18, MW 4500-5500, Gelest), 1,3,5-

triallyl-1,3,5-triazine-2,4,6(1H,3H5H)-trione (98%, Aldrich), and pentaerythritol tetrakis(2-mercaptoacetate) (Aldrich). Non-reactive surfactants include polyoxyethylene (10) cetyl ether (Brij 56, Aldrich), polyoxyethylene (2) cetyl ether (Brij 52, Aldrich), and quaternary ammonium surfactant cetyltrimethylammonium bromide (CTAB, $\geq 99\%$, Aldrich). The reactive quaternary ammonium surfactant monomer C12A was prepared by reacting 2-(dimethylamino)ethyl acrylate (98%, Aldrich) with 1-bromododecane ($\geq 99.5\%$, Aldrich) according to previously described methods.^{1,2} Photoinitiators include 2,2-Dimethoxy-1,2-diphenylethan-1-one (Irgacure 651, Ciba Specialty Chemicals) and 2-hydroxy-2-methyl-1-phenyl-propan-1-one (Darocur 1173, Ciba Specialty Chemicals). Ethylene glycol diacetate (Aldrich), acetone ($\geq 99.5\%$, Aldrich), glacial acetic acid (Aldrich), and isopropyl alcohol (Aldrich) were also used as solvents in this study. Figure 3.1 shows the chemical structure of the monomers, photoinitiators, and surfactants that are used in this study.

Lyotropic liquid crystalline templated samples were prepared by mixing particular concentrations of monomer, surfactant, deionized water, and photoinitiator. Isotropic controls were synthesized by replacing the phase forming surfactant with solvent to generate a traditional isotropic polymer network. In other words, isotropic controls contain the same reactive species and photoinitiator concentration but do not contain surfactant. Sample homogeneity was achieved using centrifugation, mechanical agitation, heat sonication, and vortex mixing. Approximately 0.05 wt % of an aluminum salt inhibitor was added to systems that contained thiol monomers to prevent spontaneous polymerization and increase the shelf life of the mixture. Polymer disks were prepared by pipetting samples into borosilicate molds (15 mm diameter, 2 mm height), purging the samples with nitrogen for 8 minutes, and irradiating samples with a medium pressure UV arc lamp (Ace Glass).

Samples were solvent-exchanged with an appropriate solvent to remove unreacted monomer, photoinitiator, and surfactants, then sandwiched between Mylar (DuPont)

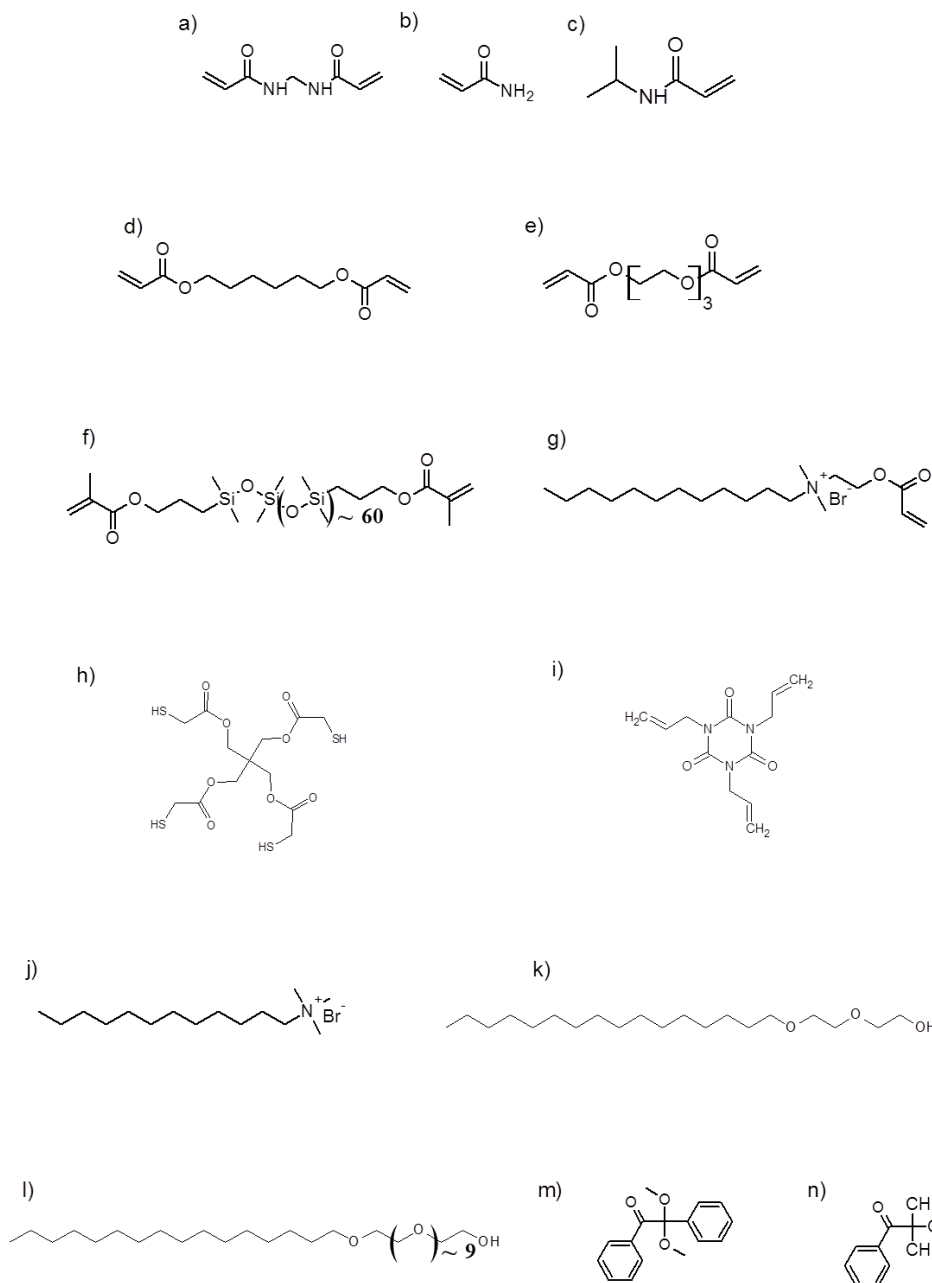


Figure 3.1. Chemical structures of monomers, surfactants, and photoinitiators used in this study. Shown are a) *N,N'*-methylene bisacrylamide, b) acrylamide, c) *N*-isopropylacrylamide, d) hexanediol diacrylate, e) poly(ethylene glycol) diacrylate, f) poly(dimethyl siloxane) dimethacrylate, g) acrylate functionalized quaternary ammonium surfactant, dodecyl-dimethyl-(2-prop-2-enoyloxyethyl)ammonium bromide, (C12A), h) pentaerythritol tetrakis(2-mercaptoacetate) i) 1,3,5-triallyl-1,3,5-triazine-2,4,6(1H,3H,5H)-trione j) quaternary ammonium surfactant cetyltrimethylammonium bromide (CTAB), k) polyoxyethylene (2) cetyl ether (Brij 52), l) polyoxyethylene (10) cetyl ether (Brij 56), m) radical photoinitiators 2,2-Dimethoxy-1,2-diphenylethan-1-one (Irgacure 651) and n) hydroxy-2-methyl-1-phenyl-propan-1-one (Darocur 1173).

sheets to slow solvent evaporation and prevent cracking, and dried under vacuum for 48 hours.³ Solvent was replaced periodically to facilitate surfactant removal. Overall surfactant removal was determined gravimetrically using sample composition information and comparing sample mass immediately after polymerization to the mass obtained after solvent exchange and drying. Dry polymer disks were cut to uniform dimensions prior to transport and mechanical property testing. At least three polymer disks were prepared for each sample formulation and analyzed in property experiments to obtain the standard deviation for each data point represented by error bars in the presented figures.

Polymer bars were fabricated for tensile testing and glass transition temperature measurements. LLC templated polymer bars were fabricated by heating the samples above their clearing temperature and pouring the formulation into bar shaped polytetrafluoroethylene molds. Samples were allowed to cool slowly to room temperature, photopolymerized, and surfactant was removed by solvent exchange unless otherwise noted. Isotropic polymer bars were prepared by injecting monomer solution between glass slides separated by a 1mm spacer in between. Thiol-ene monomer systems were not purged with nitrogen prior to photopolymerization.

Characterization

Photopolymerization Kinetics and Structure Characterization

Photopolymerization kinetics were studied using a Perkin-Elmer differential scanning calorimeter (photo-DSC) equipped with a medium-pressure UV arc lamp (Ace Glass) to initiate polymerization. The emission spectrum was controlled using a 365 nm band-pass filter and light intensity was adjusted with neutral density filters and by varying the distance of the sample from the lamp. Approximately 4 mg of sample was placed into crimped aluminum pans and covered with a thin transparent fluorinated

ethylene propylene copolymer (Teflon[®] Fluorinated Ethylene Propylene, DuPont) film to minimize heat loss resulting from water evaporation. Samples were heated above their clearing temperature to promote uniform thickness and thermal contact. Oxygen inhibition was suppressed by purging samples with nitrogen for eight minutes prior to polymerization. Heat flow, Q , was monitored in real-time, t , by maintaining a constant sample temperature of 30 °C and used to calculate the normalized polymerization rate, R_p , using equation 3.1

$$R_p = \frac{\bar{R}_p}{[M]} = \frac{Q(t) \cdot MW}{n \cdot \Delta H \cdot m} \quad (3.1)$$

where \bar{R}_p is the extensive polymerization rate, $[M]$ is the monomer concentration, MW is the monomer molecular weight, n is the monomer functionality, ΔH_p is the enthalpy of polymerization, and m is the monomer mass.^{4,5} Double bond conversion, p , was calculated by integrating the normalized polymerization rate with respect to time using equation 3.2 and the trapezoidal rule

$$p = \int_0^{\infty} R_p(t) dt \quad (3.2)$$

Polymerization kinetics were also studied using a Thermo Electron Nexus 670 Fourier Transform infrared spectrometer (FTIR). The detector was cooled with liquid nitrogen and the sample chamber was purged with nitrogen gas to eliminate water vapor and carbon dioxide. Double bond and thiol conversion were calculated by monitoring the change in absorption of the thiol and ene peaks at 3100 and 2570 cm^{-1} , respectively. Photopolymerization was initiated using a high-pressure Mercury arc lamp (Exfo Acticure 4000) using 365nm light ($2.5 \text{ mW} \cdot \text{cm}^{-2}$).

The optical anisotropy of LLC samples was characterized before and after polymerization using a polarized light microscope (PLM, Nikon, Eclipse E600W Pol) equipped with a hot stage (Instec, Boulder, CO). PLM images were obtained by placing samples sandwiched between a glass microscope slide and coverslip on the microscope stage, heating above their clearing point, and cooling slowly at room temperature. Samples were photopolymerized with the UV light source described above. Optical textures were examined for birefringent patterns characteristic of the ordered phases formed in the LLC samples.⁶ PLM images obtained before and after photopolymerization were compared to determine the extent of phase disruption that occurred as monomers polymerized into a crosslinked network.

Polymer nanostructure was characterized with a Nonius FR590 small angle X-ray scattering (SAXS) apparatus using a standard copper target Röntgen tube with a Ni-filtered Cu K α line of 1.54 Å as the radiation source, a collimation system of the Kratky type, and a PSD 50M position sensitive linear detector (Hecus M. Braun, Graz). Phases were indexed by calculating the d -spacing ratios of scattering peaks. The scattering vector, q , was calculated from the angle of the scattered radiation, 2θ , and the X-ray wavelength, λ , using eq. 3.3

$$q=4\pi\sin 2\theta/\lambda=2\pi/d \quad (3.3)$$

where d is the lattice or d -spacing. SAXS profiles were desmeared to correct for beam-height effects using a direct transform method described elsewhere.⁷ Desmeared profiles were background corrected and normalized to the invariant, J , calculated using equation 3.4

$$J = \int_0^{\infty} I(q)q^2 dq \quad (3.4)$$

where $I(q)$ is the desmeared intensity.⁸ The invariant represents the scattering power of the sample, is independent of sample morphology, and is used to correct for differences in scattering volume, electron densities, and fluctuations in beam intensity.⁹ In other words, normalizing the scattering profiles to the invariant allows polymer structure to be compared without having to measure absolute intensities. Additionally, the Lorentz correction was applied to correct for the differences in time that individual reciprocal lattice points spend in a diffracting position.¹⁰ Scanning electron microscopy (SEM, Hitachi S-4800) was also used to characterize polymer structure. Samples were freeze-fractured and sputter-coated using a Au/Pd target prior to imaging. SEM images represent the cross-section of LLC templated polymers after surfactant removal.

Transport Property Characterization

Transient water uptake was studied gravimetrically by recording the mass of dried samples, immersing samples in excess deionized water at room temperature, removing the sample at predetermined times, patting the surface dry with damp filter paper to remove surface water, and measuring the sample mass. Hydrogel mass was used to calculate the percentage hydration, %H₂O, or water uptake, W , using equation 3.5 and 3.6 respectively

$$\%H_2O = (W_t - W_o)/W_t \times 100\% < 100\% \quad (3.5)$$

$$W = (W_t - W_o)/W_o \times 100\% \quad (3.6)$$

where W_t is the mass of the hydrogel at time t and W_o is the mass of the dry polymer after solvent-exchange with acetic acid. Note that equation 3.5 represents the weight percentage of the hydrogel that is water while equation 3.6 represents the swelling ratio of the polymer. For temperature dependent swelling studies, polymer disks were

maintained at a given temperature for at least three days in order to assure equilibrium water uptake was achieved. Equilibrium was assumed reached when no significant change in water uptake was observed for measurements taken 48 hours apart.

The diffusivity of LLC templated and isotropic polymer samples was examined by incorporating the solute rhodamine B into the polymer network and measuring the rate of release into water. Dehydrated polymer disks were soaked in a concentrated dye solution for at least 14 days to allow infiltration of the dye into the hydrogel pores. Dye loaded polymer disks were removed from the concentrated dye solution, measured with calipers, rinsed with deionized water to remove excess surface dye, placed in individual containers with 200 ml of deionized water, and sealed to prevent water loss. The release media was gently stirred using a magnetic stir bar to minimize concentration gradients and boundary layer effects. At predetermined times, 2 ml of release media was removed from the individual containers, placed in a quartz cuvette, and the absorbance at 554 nm was measured using a UV-vis spectrometer to determine the concentration of dye released. Release media was returned to the individual containers immediately after measuring dye concentration. Absorption spectrum of release media was measured periodically until no detectable change in dye concentration was observed. Diffusion coefficients for hydrogels were determined by least squares regression of experimental release profiles against the two-dimensional Fickian diffusion equation from a disk given by eq 3.7

$$\frac{M_t}{M_\infty} = 1 - \frac{32}{\pi^2} \sum_{n=1}^{\infty} \frac{1}{a_n^2} \exp\left(-\frac{a_n^2}{r^2} D_e t\right) \times \sum_{p=0}^{\infty} \frac{1}{(2p+1)^2} \exp\left(-\frac{(2p+1)^2 \pi^2}{l^2} D_e t\right) \quad (3.7)$$

where M_t/M_∞ is the fraction dye released at time t , r is the radius of the disk, D_e is the diffusion coefficient, l is the thickness of the disk, and a_n are the roots of the zero order Bessel function of the first kind.¹¹ Assumptions include an initial homogeneous

distribution of dye in the hydrogel, a concentration independent diffusion coefficient, and sink conditions in the release medium. Least-squares regression was performed using MATLAB to estimate diffusion coefficients by fitting experimental release profiles to equation 3.7. Summations were truncated at 1000 terms.

Deswelling kinetics were measured by recording the mass of water swollen hydrogel disks at 22 °C. The equilibrium swollen disks were then transferred to a water bath maintained at 37 °C. At predetermined times, the disks were removed from the warm water bath, patted dry with damp filter paper to remove excess surface water, and the mass of the disk was recorded. Hydrogel masses were used to determine the percent water uptake using equation 3.6.

Mechanical Property Characterization

The hydrated compressive modulus was calculated from the initial slopes of the stress vs. strain profiles using equation 3.7

$$G = \sigma / (\lambda - \lambda^{-2}) \quad (3.7)$$

where G is the compressive modulus, σ is the stress, and λ is the relative deformation.¹² Hydrogel disks were prepared as described above and allowed to equilibrate in water at 22 °C. Typically, swollen hydrogel disks were mounted on the compressive clamp of the dynamic mechanical analyzer (DMA Q800 Series) at 22 °C using a preload force on the order of 0.1N while the force was continually ramped at a rate of about 0.5 N·min⁻¹. Particular conditions of sample testing are given in the corresponding chapters.

The dry compressive modulus was calculated from the linear portion of the stress vs. strain curve using equation 3.8

$$G = \sigma/\lambda \quad (3.8)$$

Dry polymer disks were mounted on the compressive clamp of the dynamic mechanical analyzer using a minimum preload force on the order of 0.1N and the force was continually ramped at a ranging from 0.5 – 2 N·min⁻¹.

Tensile tests measuring the stress-stain behavior of polymer bars subjected to elongation stresses were carried out using DMA. Polymer bars were clamped in the tensile clamp of the DMA and preloaded with the minimum force required for the sample to remain taught in the clamp without creeping to any appreciable extent before the experiment was conducted. The force was continually ramped at a rate of approximately 1 N·min⁻¹. Calipers were used to measure the sample dimensions for input into the DMA for tensile and compression experiments.

Glass transition temperature was characterized using a DMA equipped with a liquid nitrogen gas cooling accessory for sub-ambient material testing. Polymer bars were prepared and mounted in the tensile clamp of the DMA as described above. The polymer was cooled to approximately -90 °C and the temperature was ramped at a rate of 3 °C·min⁻¹ to approximately 200 °C or until the sample yielded. The polymer was subjected to a sinusoidal deformation at a frequency of 1 Hz using a deformation strain of 0.05%. The ratio of the loss to storage modulus was used to calculate the loss tangent (Tan δ).¹³ At the glass transition temperature the loss modulus is at a maximum and the storage modulus is at a minimum leading to a corresponding maximum in the Tan δ. The glass transition temperature is reported as the maximum temperature in the Tan δ vs. temperatures curve.

Notes

1. Sievens-Figueroa, L.; Guymon, C. A. *Polymer* **2008**, *49*, 2260-2267.
2. Hamid, S. M.; Sherrington, D. C. *Polymer* **1987**, *28*, 325-331.
3. Scherer, G. *J Am Ceram Soc* **1990**, *73*, 3-14.
4. Forney, B. S.; Guymon, C. A. *Macromolecules* **2010**, *43*, 8502-8510.
5. Lester, C. L.; Smith, S. M.; Jarrett, W. L.; Guymon, C. A. *Langmuir* **2003**, *19*, 9466-9472.
6. Collings, P. J.; Hird, M. *Introduction to Liquid Crystals Chemistry and Physics*; Taylor & Francis: London, 1997.
7. Singh, M. A.; Ghosh, S. S.; Shannon, R. F. *J. Appl. Crystallogr.* **1993**, *26*, 787-794.
8. Feigin, L. A.; Svergun, D. I. Structure Analysis by Small Angle X-Ray and Neutron Scattering. In Taylor, G. W., Ed.; Plenum Press: New York, NY, 1987; pp 59-63.
9. Glatter, O.; Kratky, O. In *Small Angle X-ray Scattering*. Porod, G., Ed.; General Theory; Academic Press Inc.: New York, NY, 1982.
10. Roe, R. J. In *Methods of X-ray and Neutron Scattering in Polymer Science*. Mark, J. E., Ed.; Oxford University Press, Inc.: New York, NY, 2000.
11. Dinerman, A. A.; Cappello, J.; Ghandehari, H.; Hoag, S. W. *J. Controlled Release* **2002**, *82*, 277-287.
12. Anseth, K. S.; Bowman, C. N.; BrannonPeppas, L. *Biomaterials* **1996**, *17*, 1647-1657.
13. Odian, G. *Principles of Polymerization*; Wiley: Hoboken, NY, 2004.

CHAPTER 4

**NANOSTRUCTURE EVOLUTION DURING
PHOTOPOLYMERIZATION IN LYOTROPIC LIQUID CRYSTAL
TEMPLATES^{1*}**

The ability to direct polymer structure on the nanometer scale has provided access to enhanced material properties that may be tailored to accommodate a growing number of advanced biological and industrial applications. A promising method of generating nanostructure in organic polymers uses self-assembling lyotropic liquid crystalline (LLC) mesophases as templates for polymerization. Unfortunately, thermodynamically driven phase separation often prevents polymer morphology from being precisely controlled. As the demand for polymers with accurately engineered properties increases, a detailed understanding of the phase separation process is needed to control the nanostructure and properties of LLC templated polymers. In this study, photopolymerization kinetics are utilized to identify phase separation events occurring during the photopolymerization of poly(ethylene glycol) diacrylate and hexanediol diacrylate monomers templated in the normal hexagonal or lamellar LLC mesophases. Discontinuities are found in the polymerization rate of anisotropic polymers at several double bond conversions that are not present in the rate profiles of isotropic controls. Polymer morphology was subsequently characterized at particular conversions using small angle X-ray scattering. Changes in polymer nanostructure occur at double bond conversions that coincide with the observed rate discontinuities. These results demonstrate that photopolymerization kinetics can be used as a probe to monitor the evolution of polymer nanostructure during

* Forney, B. S.; Guymon, C. A. *Macromolecules* **2010**, *43*, 8502-8510.

polymerization and optimize the conditions governing the control of polymer morphology to enhance properties dependent on nanostructure.

Introduction

Polymers with nanometer size morphologies are generating significant research interest due to their potential application in areas including tissue engineering, controlled release, and size-selective separation media.¹⁻³ Of particular importance is the potential to improve and tune physical properties by controlling polymer nanostructure as properties ranging from mechanical strength to permeability are highly dependent on local order and size of morphological features.⁴ For example, polymers with sub-micron morphologies have exhibited greater compressive moduli, swelling, permeability, and cell interaction than their isotropic counterparts.⁵⁻⁸ Furthermore, these properties have been tuned by modifying polymer morphology while maintaining the original polymer chemistry. These characteristics could be used to engineer biomedical devices such as tissue scaffolds and hydrogels with the proper mechanical, degradative, and swelling properties needed for successful performance using well-characterized biopolymers.⁹

Methods of directing polymer morphology may use templates to segregate monomers into the desired geometry followed by polymerization to transfer the template structure to the polymer.¹⁰⁻¹² One promising method of generating nanostructure in organic polymers uses self-assembling lyotropic liquid crystals (LLCs) as templates for polymerization.¹³ LLCs are typically low molecular weight surfactants that can self-assemble into a variety of nanometer size mesophases in the presence of a solvent such as water. The highly-ordered LLC mesophases are used to segregate monomers into a variety of different geometries by utilizing the inherent water and oil-soluble domains. In fact, the polar and non-polar domains of LLC templates have been used to compatibilize

otherwise immiscible hydrophobic and hydrophilic monomers, allowing properties intermediate of each polymer to be incorporated into the final polymer network.¹⁴ LLC mesophases are particularly well-suited for templating applications because their morphology and characteristic length depend primarily on the concentration, polarity, and size of surfactant molecules, thus providing a facile method of altering polymer nanostructure.¹⁵

The synthesis of LLC templated polymers is relatively simple and their large-scale production is expected to be more feasible than other templating methods.¹⁶ Ideally, the template can be used to precisely control polymer morphology on the desired size scale during polymerization.¹⁷ In practice, however, it is often difficult to control polymer structure throughout the polymerization reaction. Thermodynamically driven phase separation often occurs as monomer is converted to polymer and frequently yields polymers with poorly defined nanostructures.¹⁸ Phase separation prevents polymer morphology from being precisely controlled and changes properties dependent on nanostructure. A detailed understanding and investigation of the evolution of polymer nanostructure during polymerization is required to determine the kinetic and thermodynamic conditions needed to precisely direct polymer nanostructure and optimize polymer properties.^{19,20}

Polymer-template phase separation is a significant problem in many polymer templating strategies and often prevents the control of polymer nanostructure and properties.^{18,21} The polymerization strategy and initiation method used to generate the templated polymer will often dictate the extent to which template structure is transferred to the polymer and overall success of the templating process. Factors including polymerization rate, propagation mechanism, and local environment in which polymerization occurs must be considered when selecting a polymerization strategy.¹⁹ Rapid initiation rates have been proposed as a method of preserving the original LLC

template order by allowing the polymer to attain sufficient conversion before phase separation can occur.^{22,23}

Photopolymerization is a particularly attractive polymerization strategy for templated systems because the initiation rate is inherently fast, independent of temperature, and readily controlled through light intensity and photoinitiator concentration.²⁴⁻²⁶ The temperature independent initiation rates of photopolymerization allow polymerization to be performed at the temperature at which the template is most stable and could promote the successful transfer of template structure to the polymer.²⁷ In addition to the advantages photopolymerization offers in generating LLC templated polymers, it is also used as a tool to probe the kinetic and structural behavior during polymerization.^{28,29} Because light is used to generate the reactive center, the initiation step can be controlled temporally by regulating irradiation time which provides a robust method of quenching the polymerization to study the relationship between conversion and polymer structure. Furthermore, the initiation rate can be easily adjusted and the impact of polymerization kinetics on polymer structure can be studied more feasibly.

Photopolymerization kinetics provide a considerable amount of information regarding the structure of LLC templated polymers during polymerization. The order imposed on monomers by the parent template significantly affects the local concentration, segregation, and diffusional behavior of reactive species.^{19,23,30-35} Likewise, changes in the LLC mesophase resulting from phase separation events will alter the local concentration, segregation, and diffusional behavior of reactive species and directly impact the polymerization kinetics. Thus, polymerization kinetics are directly related to local order and may be used to elucidate changes in polymer nanostructure occurring during polymerization.

Numerous studies have utilized photopolymerization kinetics to identify changes in polymer morphology by comparing the polymerization rate and kinetic constants of templated systems to those of an appropriate isotropic control.^{23,30,31,34-36} When abrupt

changes in kinetic constants or discontinuities in the polymerization rate are observed in the templated system and not in the isotropic control, these kinetic differences are usually attributed to alterations in the segregation and diffusional behavior of reactive species resulting from changes in polymer structure. Despite this kinetic evidence of structural changes, polymer morphology has been exclusively characterized before and after polymerization, providing limited insight into the evolution of polymer structure during polymerization.

In this study, the nanostructure of LLC templated polymers is characterized at specific conversions to better understand and direct the evolution of polymer structure. The polymerization rate of LLC-monomer solutions that self-assemble into highly-ordered mesophases before polymerization and phase separate during polymerization were investigated for discontinuities relative to isotropic controls. Utilizing the temporal control of photopolymerization, the polymer structure was characterized directly using X-ray diffraction at conversions coinciding with irregular rate behavior. These investigations not only begin to reveal how polymer morphology evolves during polymerization, but also provide methods that may be used to systematically establish how polymerization kinetics and LLC self-assembly can be optimized to control polymer structure. It is hypothesized that characterizing polymer nanostructure during polymerization will provide valuable kinetic and thermodynamic information describing the phase separation process. Such knowledge may be used to direct polymer structure and thus tailor polymer properties to accommodate a number of diverse and advanced applications.

Experimental

Materials

The monomers used in this study were poly(ethylene glycol) diacrylate (PEGDA, $M_n \sim 258$ Aldrich) and 1,6-hexanediol diacrylate (HDDA, Sartomer). The lyotropic liquid

crystal was polyoxyethylene (10) cetyl ether (Brij 56, Aldrich). 2,2-Dimethoxy-1,2-diphenylethan-1-one (Irgacure 651, Ciba Specialty Chemicals) was used as the photoinitiator. Ethylene glycol diacetate (EGDAc, Aldrich) was also used as a solvent in this study. All chemicals were used as received.

Sample Preparation

Samples containing lyotropic liquid crystals were prepared by mixing specific concentrations of monomer, surfactant, deionized water, and photoinitiator. Isotropic samples were prepared by mixing the respective monomer with ethylene glycol diacetate and photoinitiator. All samples contained 20 wt% monomer and 0.5 wt% photoinitiator with respect to monomer mass. Sample homogeneity was achieved using centrifugation, heat sonication, and vortex mixing.

Kinetics

Photopolymerization kinetics were studied using a Perkin-Elmer differential scanning calorimeter (photo-DSC) equipped with a medium-pressure UV arc lamp (Ace Glass) to initiate polymerization. The emission spectrum was controlled using a 365 nm band-pass filter and light intensity was adjusted with neutral density filters and by varying the distance of the sample from the lamp. Approximately 4 mg of sample was placed into crimped aluminum pans and covered with a thin transparent fluorinated ethylene propylene copolymer (Teflon[®] FEP, DuPont) film to minimize heat loss resulting from water evaporation. Samples were heated above their clearing temperature to promote uniform thickness and thermal contact. Oxygen inhibition was suppressed by purging samples with nitrogen for eight minutes prior to polymerization. Heat flow, Q , was monitored in real-time, t , by maintaining a constant sample temperature of 30°C and used to calculate the normalized polymerization rate, R_p , using equation 4.1

$$R_p = \frac{\bar{R}_p}{[M]} = \frac{Q(t) \cdot MW}{n \cdot \Delta H \cdot m} \quad (4.1)$$

where \bar{R}_p is the extensive polymerization rate, $[M]$ is the monomer concentration, MW is the monomer molecular weight, n is the monomer functionality, ΔH_p is the enthalpy of polymerization, and m is the monomer mass.³⁷ Double bond conversion, p , was calculated by integrating the normalized polymerization rate with respect to time.

Characterization

The optical anisotropy of LLC samples was characterized before and after polymerization using a polarized light microscope (PLM, Nikon, Eclipse E600W Pol) equipped with a hot stage (Instec, Boulder, CO). PLM images were obtained by placing samples sandwiched between a glass microscope slide and coverslip on the microscope stage, heating above their clearing point, and allowing to cool slowly at room temperature. Samples were photopolymerized with the UV light source described above. Optical textures were examined for birefringent patterns characteristic of the ordered phases formed in the LLC samples. PLM images obtained before and after photopolymerization were compared to determine the extent of phase disruption that occurred as monomers polymerized into a crosslinked network.

Polymer nanostructure was characterized with a Nonius FR590 small angle X-ray scattering (SAXS) apparatus using a standard copper target Röntgen tube with a Ni-filtered Cu K α line of 1.54 Å as the radiation source, a collimation system of the Kratky type, and a PSD 50M position sensitive linear detector (Hecus M. Braun, Graz). Phases were indexed by calculating the d -spacing ratios of scattering peaks. The scattering vector, q , was calculated from the angle of the scattered radiation and the X-ray wavelength. SAXS profiles were desmeared to correct for beam-height effects using a

direct transform method described elsewhere.³⁸ Desmeared profiles were background corrected and normalized to the invariant, J , calculated using equation 4.2

$$J = \int_0^{\infty} I(q)q^2 dq \quad (4.2)$$

where $I(q)$ is the desmeared intensity.³⁹ The invariant represents the scattering power of the sample, is independent of sample morphology, and is used to correct for differences in scattering volume, electron densities, and fluctuations in beam intensity.⁴⁰ In other words, normalizing the scattering profiles to the invariant allows polymer structure to be compared without having to measure absolute intensities. Additionally, the Lorentz correction was applied to correct for the differences in time that individual reciprocal lattice points spend in a diffracting position.⁴¹

Results and Discussion

An encouraging method of generating nanostructure in polymers uses LLC mesophases as templates for polymerization. However, thermodynamically driven phase separation typically prevents polymer nanostructure from being precisely controlled. A detailed description regarding the evolution of polymer morphology during polymerization is needed to optimize the thermodynamic and kinetic conditions necessary to accurately direct polymer nanostructure. Numerous studies have utilized photopolymerization kinetics to study polymer morphology during polymerization.^{19,27,30,32,33,36} Discontinuities in polymerization rate and kinetic constants are often observed during the polymerization of LLC templated monomers and have been suggested to result from changes in local order. However, because the structure of LLC

templated systems is usually characterized before and after the polymerization reaction, there is little direct evidence supporting that such kinetic behavior is due to changes in polymer structure. Herein, photopolymerization kinetics are utilized to identify changes in polymer structure occurring during polymerization in order to understand and control polymer-temple phase separation. A complete description of the kinetic and thermodynamic factors governing the structure of LLC templated polymers could lead to the synthesis of polymers with precisely engineered physical properties.

To illustrate the effect of local order on photopolymerization kinetics, the polymerization rate of LLC-monomer solutions containing 20 wt% poly(ethylene glycol) diacrylate (PEGDA) or 20 wt% 1,6-hexanediol diacrylate (HDDA) and varying concentrations of the surfactant Brij 56 in water were investigated. The impact of liquid crystalline order on polymerization kinetics is evident from the rate profiles for PEGDA polymerized in the isotropic, normal hexagonal, and lamellar mesophases (Figure 4.1a). The polymerization of PEGDA is fastest in the normal hexagonal mesophase formed at 40 wt% surfactant with the maximum rate being approximately a factor of three greater than that observed for the isotropic polymerization of PEGDA in EGDAC.

As the concentration of surfactant increases to 50 wt%, the maximum polymerization rate of PEGDA is less than half of that observed at 40 wt% surfactant even though both samples have a normal hexagonal morphology before polymerization. Also, the maximum polymerization rate for PEGDA templated in the lamellar LLC mesophases formed at 60 and 70 wt% surfactant is greater than the maximum polymerization rate of PEGDA in solvent. Similar trends are observed in the rate profiles of HDDA polymerized in the isotropic, normal hexagonal, and lamellar phases (Figure 4.1b). The polymerization rate of HDDA is greatest in the normal hexagonal phase formed at 30 wt% surfactant and decreases with increasing surfactant concentration. For both PEGDA and HDDA monomers, the polymerization rate is faster at lower surfactant

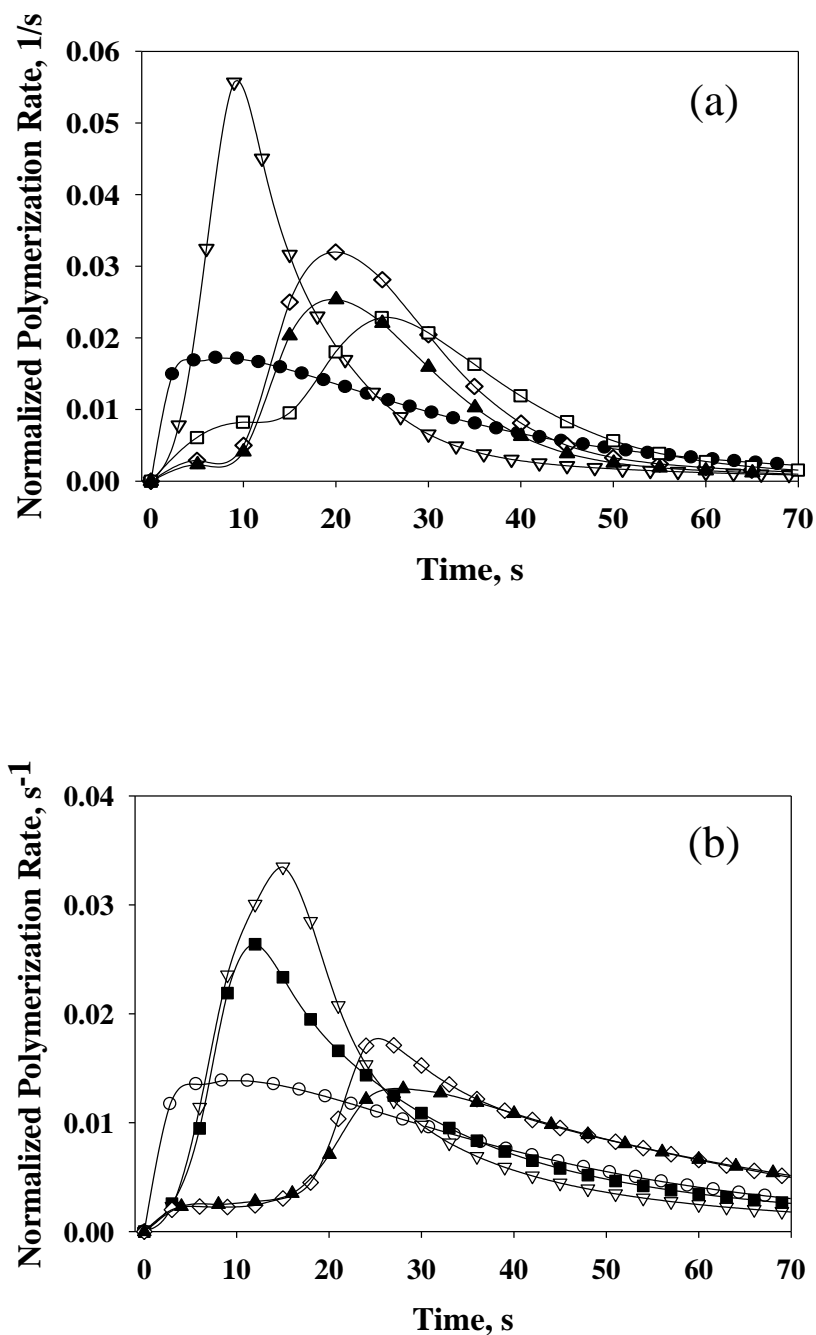


Figure 4.1. Photopolymerization kinetics for LLC templated and isotropic polymer systems. Shown are (a) Polymerization rate as a function of time for 20 wt% PEGDA in EGDAC (isotropic – ●), and with 40 wt% (normal hexagonal – ▽), 50 wt% (normal hexagonal – □), 60 wt% (lamellar – ◇), and 70 wt% (lamellar – ▲) Brij 56 in water. (b) Polymerization rate as a function of time for 20 wt% HDDA in EGDAC (isotropic – ○), and with 30 wt% (normal_hexagonal – ▽), 40 wt% (normal hexagonal – ■), 50 wt% (lamellar – ◇), and 60 wt% (lamellar – ▲) Brij 56 in water. Polymerization was initiated with 0.5 wt% Irgacure 651 at a light intensity of 3.27 mW/cm².

concentration within a given LLC mesophase. This behavior is likely due to a decrease in local monomer concentration at higher surfactant concentrations. This kinetic behavior has been reported for similar LLC-monomer systems and is discussed in greater detail elsewhere.^{23,32,33}

It is clear from the rate profiles in Figure 4.1 that LLC order has a significant impact on polymerization kinetics. Interestingly, rate profiles of anisotropic samples show kinetic behavior that is much different than their isotropic counterparts. For example, a deceleration in polymerization rate is observed at low double bond conversion for both PEGDA and HDDA samples templated with 50 wt% surfactant. This behavior differs from traditional isotropic photopolymerization kinetics of diacrylate monomers in which the polymerization rate is relatively continuous.⁴² These differences in polymerization rate appear to be due to the segregation of acrylate functional groups as directed by the LLC template. It has often been suggested that rate discontinuities in LLC systems result from phase separation events which alter the local concentration, segregation, and diffusional behavior of monomers. However, because polymer structure is typically characterized before and after polymerization, little structural data is available to support this hypothesis.

The morphology of each system in Figure 4.1 was characterized before and after polymerization using PLM and SAXS to determine if a significant change in polymer structure is occurring during polymerization. With phase separation occurring during polymerization, the conversion at which polymer nanostructure changes may be identified by studying the systems photopolymerization kinetics, thus providing insight into the evolution of polymer nanostructure. Because faster polymerization kinetics can increase the degree of structure retained, polymerization was initiated using a low light intensity. Reducing the light intensity facilitated phase separation events and increased the sensitivity of the photo-DSC, allowing discontinuities in heat flow due to changes in local order to be identified.^{23,31,36}

To demonstrate how photopolymerization kinetics can be utilized to identify changes in polymer morphology, two systems with significantly different morphologies before and after polymerization were chosen for detailed kinetic and structural characterization studies. Figure 4.2 shows the PLM images before and after polymerization for 20 wt% PEGDA with 50 wt% surfactant in water and 20 wt% HDDA with 50 wt% surfactant in water, referred to hereafter as PEGDA-50 and HDDA-50, respectively. These two systems were chosen for detailed analysis because each was found to markedly phase separate during polymerization. It is expected that a larger change in polymer structure will have a greater impact on photopolymerization kinetics, thus providing straightforward insight into the evolution of polymer structure.^{33,35} A high birefringence and fan-like optical texture is observed before polymerization of PEGDA-50 (Figure 4.2a) and is indicative of a highly-ordered hexagonal morphology.⁴³ However, after photopolymerization the birefringence decreases and the fan-like optical texture is less defined (Figure 4.2b), suggesting that the original hexagonal structure has not been retained during polymerization. Similarly, the Maltese cross optical texture and high birefringence of the HDDA-50 sample before polymerization (Figure 4.2c) indicates a well-defined lamellar morphology. Yet after polymerization, the original lamellar morphology is lost and a nearly isotropic polymer is obtained, indicated by the decrease in birefringence and ill-defined optical texture (Figure 4.2d).

To corroborate PLM results, the morphology of PEGDA-50 and HDDA-50 samples were characterized before and after polymerization using SAXS. Figure 4.3a shows the SAXS profile of PEGDA-50 before and after polymerization. The *d*-spacing ratios calculated from the SAXS profile of PEGDA-50 before polymerization is indicative of a highly-ordered normal hexagonal morphology.³⁹ After polymerization, the scattering intensity decreases and the positions of the scattering peaks change, confirming that the structure of the PEGDA-50 polymer has been significantly disrupted during polymerization. A decrease in scattering intensity indicates a less ordered polymer due to

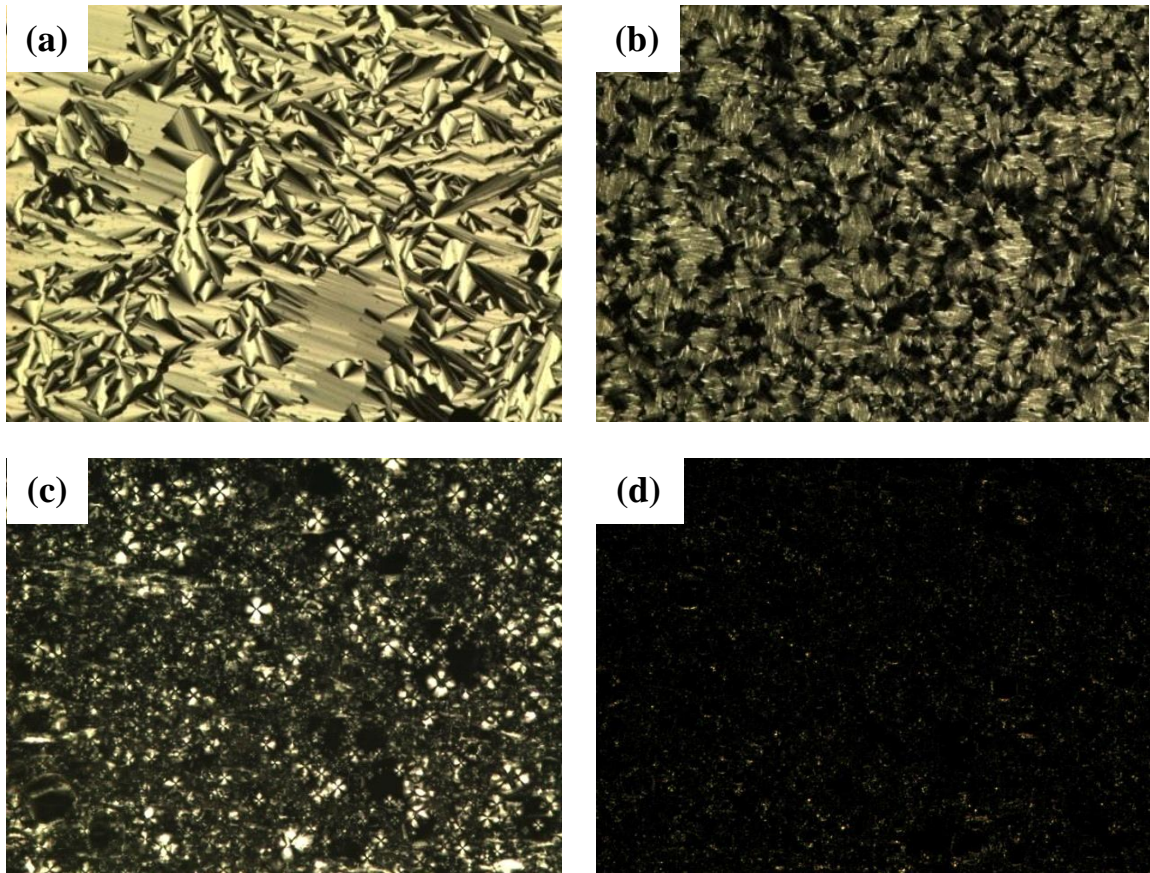


Figure 4.2. Polarized light micrographs of LLC templated samples before and after photopolymerization at 10X magnification. Shown are samples of 20 wt% PEGDA with 50 wt% Brij 56 in water (a) before and (b) after polymerization and a sample of 20 wt% HDDA with 50 wt% Brij 56 in water (c) before and (d) after polymerization. Polymerization was initiated with 0.5 wt% Irgacure 651 at a light intensity of 0.5 mW/cm².

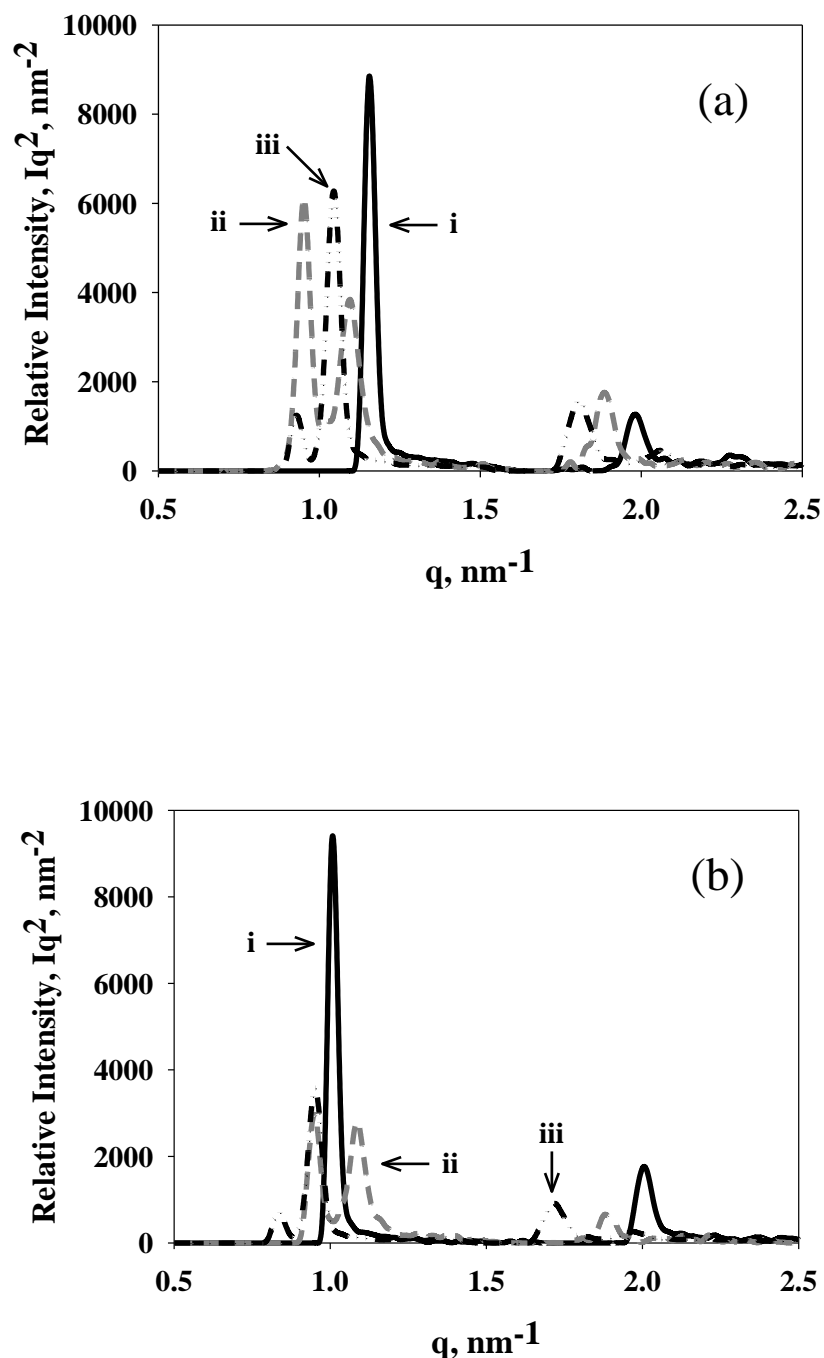


Figure 4.3. SAXS profiles before and after photopolymerization of LLC templated PEGDA and HDDA. Shown are (a) SAXS profile of a 20 wt% PEGDA with 50 wt% Brij 56 in water (normal hexagonal) before polymerization (i) and after polymerization (ii) as well as Brij 56-water mixture (iii) containing the same surfactant to water ratio. (b) SAXS profile for a 20 wt% HDDA with 50 wt% Brij 56 in water (lamellar) before polymerization (i) and after polymerization (ii) as well as Brij 56-water mixture (iii) containing the same surfactant to water ratio. Polymerization was initiated with 0.5 wt% Irgacure 651 at a light intensity of 0.5 mW/cm^2 .

the increased contribution of isotropic scatter to the invariant.^{44,45} A similar analysis of SAXS profiles before and after polymerization for HDDA-50 (Figure 4.3b) supports that the original lamellar morphology is not retained during polymerization. The degree of phase separation is further illustrated by comparing the diffraction profile of a 5:3 weight ratio Brij 56:water solution shown in Figure 4.3a and 4.3b to the SAXS profile for the fully cured PEGDA-50 and HDDA-50 polymers. The Brij 56-water solution contains the same ratio of surfactant to water that would be present if the surfactant-water template completely phase separated from, and did not interact with, the PEGDA-50 or HDDA-50 polymers. The similar intensities and positions of the diffraction peaks of these SAXS profiles suggests that each polymer has phase separated to a large degree during polymerization and the resulting polymer structure is ill-defined and poorly ordered.

It is evident from PLM and SAXS data that the PEGDA-50 and HDDA-50 samples phase separate during polymerization. Utilizing photopolymerization kinetics, the critical conversion(s) at which the parent LLC template ceases to be thermodynamically stable may be identified. This was done by comparing the rate profiles of the PEGDA-50 and HDDA-50 samples to the rate profiles for the isotropic polymerization of the respective monomer in EGDAC in order to identify rate discontinuities that could signal the onset of phase separation. The sensitivity of the photo-DSC to changes in heat flow was increased by lowering the light intensity relative to kinetic studies presented in Figure 4.1.

Discontinuities found in the rate profiles of LLC templated polymers and not in the rate profiles of isotropic controls are hypothesized to result from changes in monomer concentration, segregation, and diffusional behavior brought about by phase separation.^{23,31,35,36} To test this hypothesis, the polymer morphology was characterized at double bond conversions near rate discontinuities to determine if such kinetic behavior coincides with changes in polymer structure. Polymers of specific double bond conversions were acquired by irradiating a sample in an aluminum DSC pan for an

appropriate time and then closing the light shutter. Heat flow was monitored with photo-DSC and used to calculate double bond conversion. After the light shutter was closed, a steady baseline heat flow was established, the sample was removed from the DSC pan, placed into a lead sample holder, covered with X-ray transparent film (Mylar[®], DuPont), sealed with rubber O-rings, and the nanostructure was analyzed using SAXS. For clarity, the kinetic and structural analysis for PEGDA-50 and HDDA-50 samples will be presented separately.

Nanostructure Evolution of Hexagonal Templated PEGDA (PEGDA-50)

To demonstrate how photopolymerization kinetics can be utilized to monitor the evolution of polymer nanostructure, the polymerization rate of anisotropic PEGDA-50 was compared to the polymerization rate of isotropic PEGDA in EGDAC to identify any rate discontinuities that could result from phase separation. Figure 4.4a shows the polymerization rate as a function of double bond conversion for PEGDA-50 and PEGDA in EGDAC. There are several differences between the rate profiles of the hexagonal templated PEGDA-50 sample and the isotropic PEGDA control. Specifically, polymerization rate discontinuities are observed in the first 10% conversion and between 40 and 55% conversion for the PEGDA-50 sample. The derivative of polymerization rate with respect to conversion, dR_p/dp , was calculated to reveal rate fluctuations that are not directly visible from the undifferentiated rate profile and is analogous to data analysis techniques used in Auger electron spectroscopy and X-ray photoelectron spectroscopy.⁴⁶ The rate derivative for the isotropic PEGDA control (Figure 4.4b) is rather smooth, indicating that there are no significant deviations in polymerization rate. However, there are several abrupt changes in the polymerization rate of PEGDA-50, illustrated by peaks in the rate derivative at 10, 45, and 55% double bond conversion.

Polymer nanostructure for double bond conversions preceding and following these rate discontinuities were characterized directly using SAXS to determine if rate

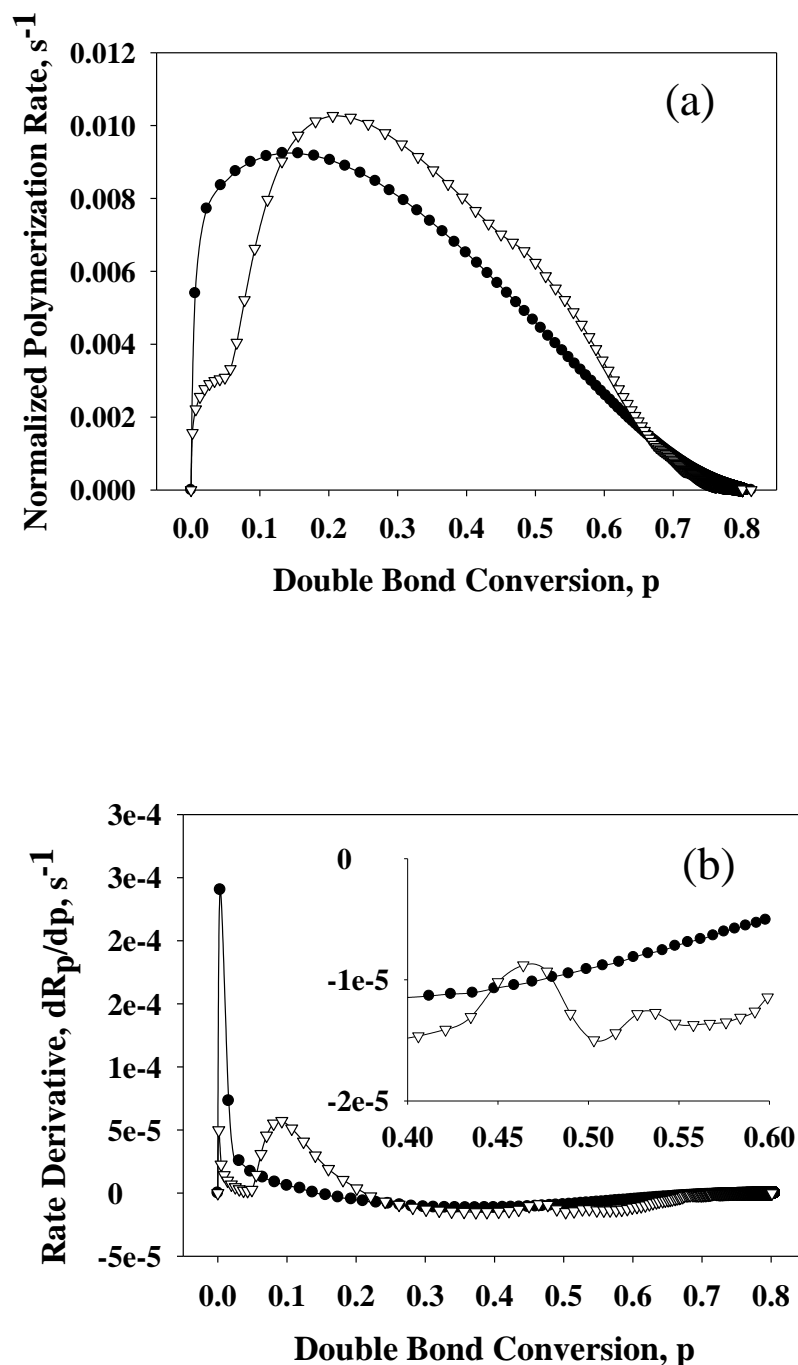


Figure 4.4. Photopolymerization rate and rate derivative for LLC templated and isotropic PEGDA. Shown are (a) Polymerization rate as a function of conversion of 20 wt% PEGDA in EGDAC (isotropic – ●) and with 50 wt% Brij 56 in water (normal hexagonal – ▽). (b) First derivative of polymerization rate shown in (a) with respect to conversion as a function of conversion of 20 wt% of 20 wt% PEGDA in EGDAC (isotropic – ●) and with 50 wt% Brij 56 in water (normal hexagonal – ▽). Inset shows the rate derivative between 40 and 60% conversion. Polymerization was initiated with 0.5 wt% Irgacure 651 at a light intensity of 0.5 mW/cm².

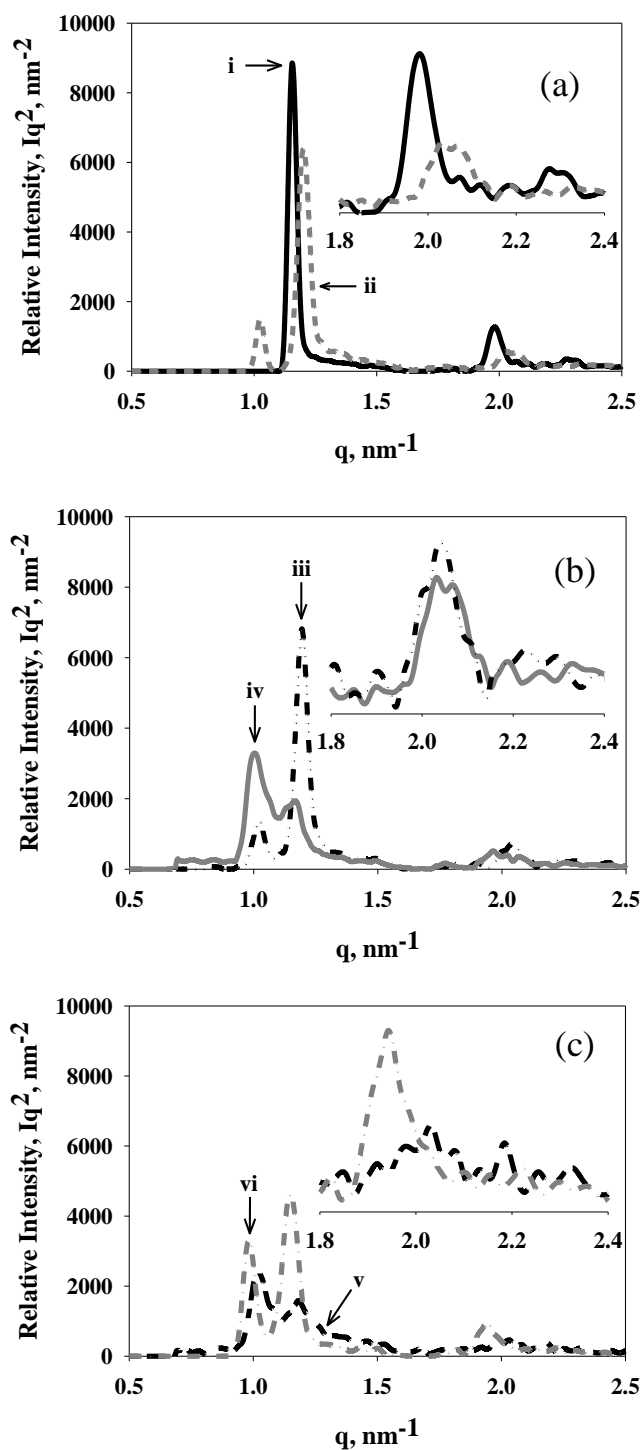


Figure 4.5. SAXS profiles before, during, and after photopolymerization of PEGDA. Shown are (a) SAXS profile for a 20 wt% PEGDA with 50 wt% Brij 56 in water (PEGDA-50, normal hexagonal) before polymerization (i) and at 15% conversion (ii), (b) 40% (iii) and 50% conversion (iv), and (c) 55% (v) and 70% conversion (vi). Insets show higher order scattering peaks. Polymerization was initiated with 0.5 wt% Irgacure 651 at a light intensity of 0.5 mW/cm².

fluctuations correspond to disruptions in polymer structure. Figure 4.5 summarizes the SAXS profiles obtained at conversions near the rate fluctuations shown in Figure 4.4b. A plateau in the polymerization rate was found in the rate profile of PEGDA-50 during the first 10% conversion and was not found in the rate profile for the isotropic PEGDA control. The SAXS profile at 15% conversion (Figure 4.5a) shows a decrease in intensity and shifts in the scattering peaks relative to the scattering profile obtained before polymerization, indicating that the original normal hexagonal morphology is significantly disrupted within the first 15% conversion. Interestingly, this large disruption in PEGDA-50 polymer structure coincides with the rate plateau seen in Figure 4.4 during the first 10% conversion.

The rate derivative in Figure 4.4b decreases monotonically between 10 and 40% conversion for both the isotropic and anisotropic PEGDA samples. This indicates that the segregation behavior of double bonds has not been altered significantly between 10 and 40% conversion. Moreover, the absence of rate discontinuities suggests that no large changes in polymer structure have occurred. The scattering peaks in the SAXS profiles for PEGDA-50 at 15 and 40% conversion are very similar in position and intensity (Figure 4.5a and 4.5b), supporting that polymer morphology has not changed significantly between these conversions. On the other hand, the scattering profile at 50% conversion (Figure 4.5b) is much different than the profile observed at 40% conversion. Namely, the relative intensity of the secondary scattering peak at 50% conversion is much lower and the positions of the secondary and tertiary scattering peaks have shifted, indicating that a significant change in polymer morphology has occurred between 40 and 50% conversion. Furthermore, this change in polymer structure coincides with the rate discontinuity between 40 and 50% conversion shown in the inset of Figure 4.4b.

The structure of the PEGDA-50 polymer appears to evolve in a discrete manner with two significant phase separation events occurring during the first 50% conversion. Furthermore, disruptions in polymer structure appear to give rise to fluctuations in the

polymerization rate. The inset of Figure 4.4b shows an additional rate fluctuation observed between 50 and 55% conversion. Comparison of the SAXS profiles at 50 and 55% conversion (Figure 4.5b and 4.5c) reveals a less defined tertiary scattering peak and a small decrease in intensity for the primary and secondary scattering peaks at 55% conversion. Thus, the rate fluctuation seen between 50 and 55% conversion coincides with a change in polymer morphology. The SAXS profile for PEGDA-50 at 70% conversion (Figure 4.5c) indicates that the structure continues to change. In fact, the scattering intensity increases and the tertiary scattering peak is more defined at 70% conversion compared to the SAXS profile at 55% conversion. Similar trends are observed during the final 10% double bond conversion. The scattering peaks for the fully cured PEGDA-50 polymer (Figure 4.3a) are well-defined and show an increase in scattering intensity relative to the SAXS profile at 70% conversion. It is unlikely that the PEGDA polymer is becoming more ordered at higher conversions because the network is highly crosslinked and structural rearrangement would require the breaking of covalent bonds.^{23,32} Therefore, the increase in scattering intensity observed at 80% conversion is likely due to the self-assembly of surfactant and water into an ordered mesophase as a result of phase separation from the polymer network.

SAXS profiles at specific double bond conversions support that phase separation events occur in a stepwise manner for the PEGDA-50 polymer. For example, polymer structure changes significantly within the first 15% conversion, is similar between 15 and 40% conversion, is disrupted between 40 and 50% conversion, and is further altered between 50 and 55% conversion. Interestingly, significant disruptions in PEGDA-50 polymer nanostructure coincide with fluctuations in the polymerization rate shown in Figure 4.4b. Comparison of the SAXS profiles shown in Figure 4.5 reveal changes in the position and intensity of scattering peaks at conversions preceding and following rate discontinuities, supporting that disruption in polymer structure occurs in conjunction with rate discontinuities.

Nanostructure Evolution of Lamellar Templated HDDA (HDDA-50)

The structural evolution of the HDDA-50 polymer was investigated to determine if photopolymerization kinetics could be used to identify disruptions in polymer structure during polymerization in a system having different order and monomer segregation behavior than the PEGDA-50 sample. The PLM images and SAXS profiles for HDDA-50 before and after polymerization indicate that the original lamellar morphology is lost during polymerization. Critical double bond conversions that may signal the onset of phase separation were identified by comparing the polymerization rate of the HDDA-50 sample to the isotropic polymerization rate of HDDA in solvent. Specifically, the HDDA-50 polymerization rate profile was analyzed for discontinuities not present in the rate profile of the isotropic HDDA control.

Figure 4.6a and 4.6b show the polymerization rate as a function of double bond conversion and the rate derivative with respect to conversion for the HDDA-50 sample and isotropic HDDA control. Although the polymerization rate of HDDA-50 is similar to that of HDDA dissolved in EGDAC, there are several differences in the polymerization behavior of these systems. Two subtle rate discontinuities were found in the rate profile of the anisotropic HDDA-50 sample that are not present in the isotropic rate profile of HDDA in EGDAC. Specifically, a deceleration in polymerization rate is observed at very low conversions in the HDDA-50 sample which is reflected as an initial rise and subsequent fall in the rate derivative shown in Figure 4.6b. It is unlikely that this shoulder is due to oxygen inhibition because samples were purged with nitrogen before polymerization and this behavior is not observed in the rate profile of the isotropic HDDA control.

The morphology of the partially polymerized HDDA-50 sample was characterized using SAXS at approximately 10% conversion that corresponds to the rate deceleration shown in the inset of Figure 4.6a. Figure 4.7a shows the SAXS profile for the HDDA-50 sample before polymerization and at 10% double bond conversion.

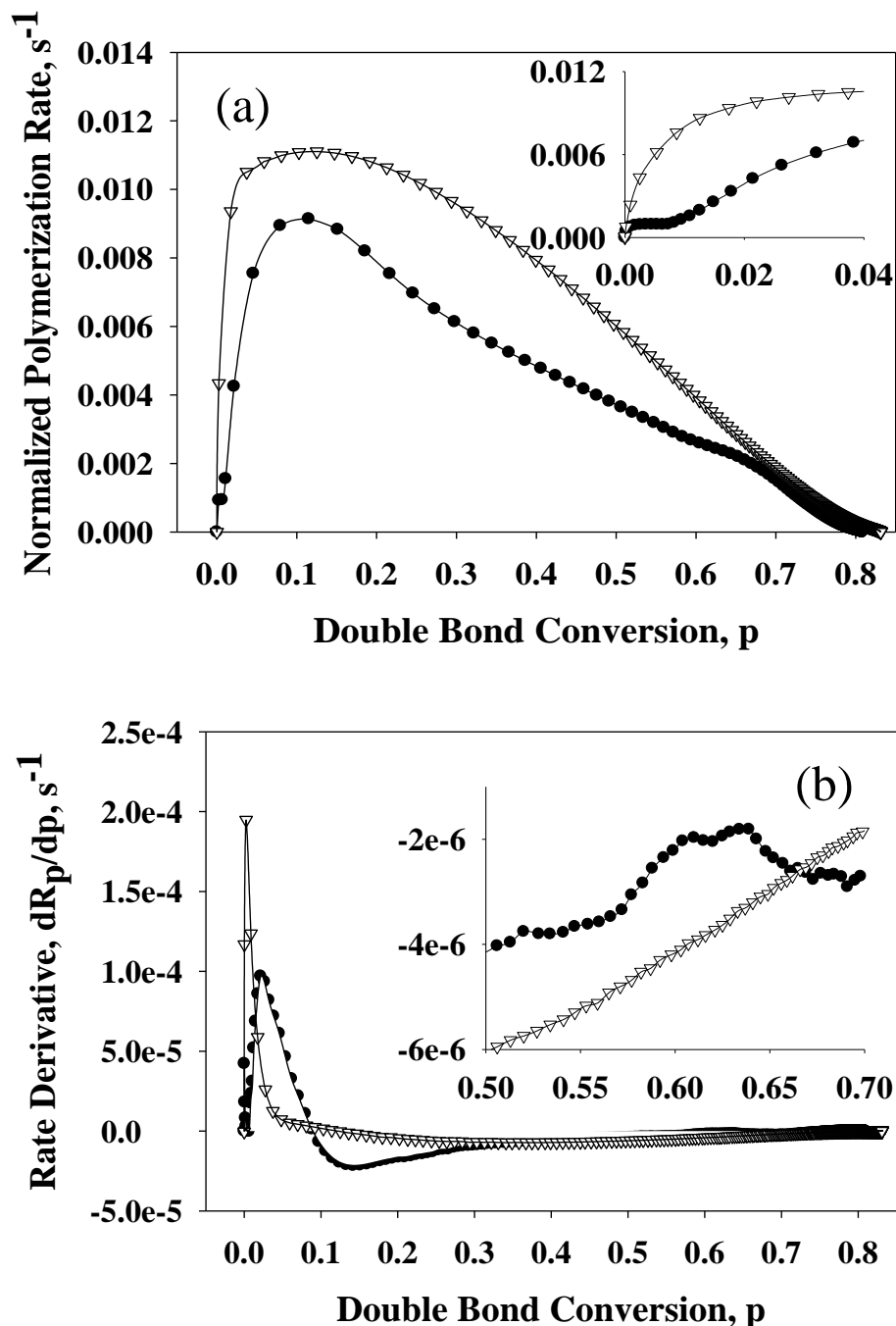


Figure 4.6. Photopolymerization rate and rate derivative for LLC templated and isotropic HDDA. Shown are (a) Polymerization rate as a function of conversion for 20 wt% HDDA in EGDAC (isotropic – ∇) and with 50 wt% Brij 56 in water (lamellar – \bullet). Inset shows rate behavior at low conversion. (b) First derivative of the polymerization rate shown in (a) with respect to conversion as a function of conversion for 20 wt% HDDA in EGDAC (isotropic – ∇) and with 50 wt% Brij 56 in water (lamellar – \bullet). Inset shows the rate derivative between 50 and 70% conversion. Polymerization was initiated with 0.5 wt% Irgacure 651 at a light intensity of 0.5 mW/cm^2 .

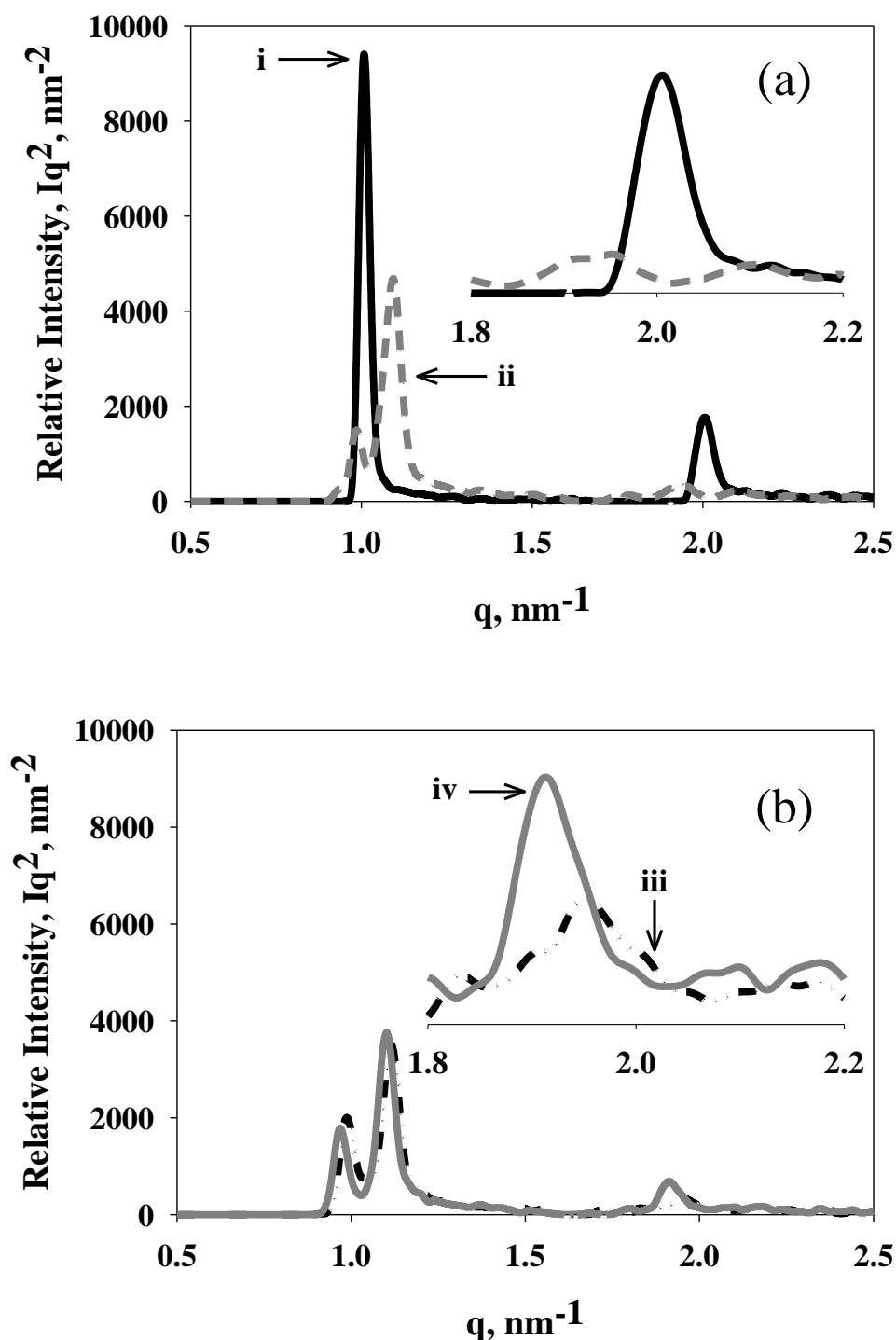


Figure 4.7. SAXS profiles before, during, and after photopolymerization of HDDA. Shown are (a) SAXS profile for 20 wt% HDDA with 50 wt% Brij 56 in water (lamellar) before polymerization (i) 10% conversion (ii) and (b) 55% conversion (iii) and 65% conversion (iv). Insets show higher order scattering peaks. All polymerization were initiated with 0.5 wt% Irgacure 651 at a light intensity of 0.5 mW/cm^2 .

It is evident from the SAXS profile for HDDA-50 at this conversion that the polymer structure is significantly disrupted early in the polymerization, indicated by a decrease in intensity and shifts in the diffraction peaks relative to the SAXS profile obtained before polymerization. Hence, the plateau in polymerization rate for HDDA-50 at low double bond conversion is accompanied by a significant change in polymer structure. The rate derivative for HDDA-50 and isotropic HDDA control (Figure 4.6b) is rather smooth between 10 and 55% conversion and no large changes in polymerization rate are observed. A smooth rate derivative was also seen for the PEGDA-50 and isotropic PEGDA control between 15 and 40% conversion (Figure 4.4b). In addition, the structure of the PEGDA-50 polymer was found to be very similar at 15 and 40% conversion which suggests that no large change in structure has occurred between 10 and 55% conversion for the HDDA-50 sample. Comparison of the SAXS profile for HDDA-50 at 55% conversion (Figure 4.7b) to the SAXS profile at 10% conversion (Figure 4.7a) indicates that polymer structure has not changed significantly between these conversions. Specifically, the scattering intensities are similar and the positions of the diffraction peaks have not changed. Thus, the order of the HDDA-50 polymer has not been altered significantly between 10 and 55% conversion.

The polymerization kinetics and SAXS profiles for the PEGDA-50 and HDDA-50 systems show that rate fluctuations coincide with disruptions in polymer structure. From the results presented thus far, rate fluctuations appear to accompany significant changes in polymer structure. The subtle rate acceleration between 55 and 65% conversion shown in the inset of Figure 4.6b provides insight into the usefulness of photopolymerization kinetics in detecting small changes in polymer structure. The intensity of the tertiary scattering peak for HDDA-50 at 65% conversion (Figure 4.7b) is greater than at 55% conversion. Additionally, the positions of the tertiary peaks at 55 and 65% conversion are different, implying that the HDDA-50 polymer structure has been disrupted between these conversions. The increase in intensity at 65% conversion is probably due to the

self-assembly of surfactant and water into an ordered mesophase as a result of phase separation from the HDDA polymer.^{23,32} Polymer structure continues to change during the final 15% conversion. The intensity of the primary and secondary scattering peaks is greater for the fully cured HDDA-50 polymer (Figure 4.3b) compared to the SAXS profile at 65% conversion. Although the polymer is not completely phase separated, the morphology has changed significantly throughout polymerization and the final structure of the HDDA-50 polymer is much different than the initial order of the parent LLC template.

The SAXS profiles of HDDA-50 at discrete double bond conversions support that disruptions in polymer structure coincide with fluctuations in polymerization rate. Specifically, a fluctuation in the polymerization rate was observed within the first 10% conversion and is accompanied by a significant change in polymer structure; no rate discontinuities or changes in polymer morphology are observed between 10% and 55% conversion; and a disruption in polymer structure coincides with the subtle rate discontinuity between 55 and 65% conversion. Polymer morphology does not appear to change substantially during the final 15% conversion with only slight decreases in order. These results demonstrate that photopolymerization kinetics are useful in monitoring the structural evolution of LLC templated polymers during polymerization and discontinuities in polymerization rate are likely due to changes in polymer nanostructure.

Conclusions

Phase separation events of polymers templated in LLC mesophases were identified during polymerization by studying photopolymerization kinetics and characterizing polymer structure at specific conversions using SAXS. Several fluctuations were found in the polymerization rate of normal hexagonal templated

PEGDA and lamellar templated HDDA monomers which were not present in the rate profiles of isotropic controls. A deceleration in polymerization rate was observed at low double bond conversions while rate accelerations are found at intermediate conversions during photopolymerization of the LLC templated mixtures. The nanostructure of anisotropic polymers was characterized using SAXS at conversions immediately preceding and following the observed rate discontinuities. SAXS data indicates that polymer structure is significantly different at conversions immediately following a rate fluctuation. These results support that polymerization rate discontinuities in LLC templated polymers result from phase separation events. Additionally, polymer structure was found to be very similar between conversions in which no rate discontinuities were present. Large changes in phase morphology appear to occur in conjunction with rate decelerations observed at low conversions. Additional changes in local order appear to coincide with rate accelerations found at intermediate conversions in the systems studied. Phase separation events were found to occur at low double bond conversions and again at intermediate conversions in the systems studied. These results show that photopolymerization kinetics can be used to identify changes in polymer nanostructure occurring during polymerization in LLC templates. This knowledge can be used to determine how LLC self-assembly and photopolymerization kinetics can be optimized to control polymer structure on the nanometer scale.

Notes

1. Chung, H. J.; Park, T. G. *Nano Today* **2009**, *4*, 429-437.
2. Wei, G.; Ma, P. X. *Adv. Funct. Mater.* **2008**, *18*, 3568-3582.
3. Lu, X.; Nguyen, V.; Zeng, X.; Elliott, B. J.; Gin, D. L. *J. Membr. Sci.* **2008**, *318*, 397-404.
4. Michler, G. H.; Balta-Calleja, F. J. *Mechanical Properties of Polymers based on Nanostructure and Morphology*; Taylor and Francis Group: Boca Raton, FL, 2005.
5. Clapper, J. D.; Pearce, M. E.; Guymon, C. A.; Salem, A. K. *Biomacromolecules* **2008**, *9*, 1188-1194.
6. Gin, D. L.; Bara, J. E.; Noble, R. D.; Elliott, B. J. *Macromol. Rapid Commun.* **2008**, *29*, 367-389.
7. Clapper, J. D.; Guymon, C. A. *Macromolecules* **2007**, *40*, 1101-1107.
8. Tsang, E. M. W.; Zhang, Z.; Yang, A. C. C.; Shi, Z.; Peckham, T. J.; Narimani, R.; Frisken, B. J.; Holdcroft, S. *Macromolecules* **2009**, *42*, 9467-9480.
9. Yang, S. F.; Leong, K. F.; Du, Z. H.; Chua, C. K. *Tissue Eng.* **2001**, *7*, 679-689.
10. Tierno, P.; Thonke, K.; Goedel, W. A. *Langmuir* **2005**, *21*, 9476-9481.
11. Li, W.; Li, S. *Oligomers Polymer Composites Molecular Imprinting* **2007**, *206*, 191-210.
12. Yoon, H.; Choi, M.; Lee, K. A.; Jang, J. *Macromol. Res.* **2008**, *16*, 85-102.
13. Hentze, H. P.; Antonietti, M. *Curr. Opin. Solid State Mat. Sci.* **2001**, *5*, 343-353.
14. Clapper, J. D.; Guymon, C. A. *Adv Mater* **2006**, *18*, 1575-1860.
15. Sel, O.; Kuang, D. B.; Thommes, M.; Smarsly, B. *Langmuir* **2006**, *22*, 2311-2322.
16. Adelhelm, P.; Hu, Y.; Chuenchom, L.; Antonietti, M.; Smarsly, B. M.; Maier, J. *Adv Mater* **2007**, *19*, 4012-4017.
17. Liu, T. B.; Burger, C.; Chu, B. *Prog. Polym. Sci.* **2003**, *28*, 5-26.

18. Antonietti, M.; Caruso, R. A.; Goltner, C. G.; Weissenberger, M. C. *Macromolecules* **1999**, *32*, 1383-1389.
19. Clapper, J. D.; Sievens-Figueroa, L.; Guymon, C. A. *Chem. Mat.* **2008**, *20*, 768-781.
20. Kumaraswamy, G.; Wadekar, M. N.; Agrawal, V. V.; Pasricha, R. *Polymer* **2005**, *46*, 7961-7968.
21. Antonietti, M.; Basten, R.; Lohmann, S. *Macromol. Chem. Phys.* **1995**, *196*, 441-466.
22. Hentze, H. P.; Kaler, E. W. *Curr. Opin. Colloid Interface Sci.* **2003**, *8*, 164-178.
23. Lester, C. L.; Colson, C. D.; Guymon, C. A. *Macromolecules* **2001**, *34*, 4430-4438.
24. Odian, G. *Principles of Polymerization*; John Wiley & Sons: Hoboken, NJ, 2004.
25. Decker, C. *Polym. Int.* **2002**, *51*, 1141-1150.
26. Kaur, M.; Srivastava, A. K. *J. Macromol. Sci. -Polym. Rev* **2002**, *C42*, 481-512.
27. DePierro, M. A.; Carpenter, K. G.; Guymon, C. A. *Chem. Mat.* **2006**, *18*, 5609-5617.
28. Matuszewska-Czerwik, J.; Polwin'ski, S. *Eur. Polym. J.* **1991**, *27*, 743-746.
29. Matuszewska-Czerwik, J.; Polwinski, S. *Eur. Polym. J.* **1990**, *26*, 549-552.
30. DePierro, M. A.; Guymon, C. A. *Macromolecules* **2006**, *39*, 617-626.
31. Guymon, C. A.; Hoggan, E. N.; Clark, N. A.; Rieker, T. P.; Walba, D. M.; Bowman, C. N. *Science* **1997**, *275*, 57-59.
32. Lester, C. L.; Guymon, C. A. *Polymer* **2002**, *43*, 3707-3715.
33. Lester, C. L.; Smith, S. M.; Jarrett, W. L.; Guymon, C. A. *Langmuir* **2003**, *19*, 9466-9472.
34. Sievens-Figueroa, L.; Guymon, C. A. *Chem. Mat.* **2009**, *21*, 1060-1068.
35. Sievens-Figueroa, L.; Guymon, C. A. *Polymer* **2008**, *49*, 2260-2267.
36. Guymon, C. A.; Bowman, C. N. *Macromolecules* **1997**, *30*, 5271-5278.
37. Anseth, K. S.; Wang, C. M.; Bowman, C. N. *Macromolecules* **1994**, *27*, 650-655.
38. Singh, M. A.; Ghosh, S. S.; Shannon, R. F. *J. Appl. Crystallogr.* **1993**, *26*, 787-794.

39. Feigin, L. A.; Svergun, D. I. In *Structure Analysis by Small Angle X-Ray and Neutron Scattering*, Taylor, G., Ed.; Plenum Press: New York, NY, 1987; pp 59-63.
40. Glatter, O.; Kratky, O. In *Small Angle X-ray Scattering*. Porod, G., Ed.; General Theory; Academic Press Inc.: New York, NY, 1982.
41. Cser, F. *J Appl Polym Sci* **2001**, *80*, 2300-2308.
42. Andrzejewska, E. *Progress in Polymer Science* **2001**, *26*, 605-665.
43. Collings, P. J.; Hird, M. *Introduction to Liquid Crystals: Chemistry and Physics*; Taylor & Francis, Inc.: Philadelphia, PA, 1997.
44. Junker, M.; Walther, J.; Braun, D.; Alig, I. *Angew. Makromol. Chem.* **1997**, *250*, 119-131.
45. Page, K. A.; Landis, F. A.; Phillips, A. K.; Moore, R. B. *Macromolecules* **2006**, *39*, 3939-3946.
46. Briggs, D.; Seah, M. P. *Practical Surface Analysis by Auger and X-ray Photoelectron Spectroscopy*; Wiley: New York, NY, 1983.

CHAPTER 5

CONTROLLED HYDROGEL NANOSTRUCTURE AND PROPERTIES THROUGH PHOTOPOLYMERIZATION IN LYOTROPIC LIQUID CRYSTAL TEMPLATES

A promising method of synthesizing polymers with useful property relationships utilizes self-assembling lyotropic liquid crystals (LLCs) as photopolymerization templates to direct polymer structure on the nanometer scale. Unfortunately, thermodynamically driven phase separation of the polymer from the LLC template often occurs during polymerization and prevents control over final polymer nanostructure and properties. In this work, the nanostructure of polyacrylamide is controlled through photopolymerization in LLC templates formed using specific concentrations of polymerizable and nonreactive surfactants. Polymer structure information obtained using electron microscopy, X-ray scattering, and polarized light microscopy indicates that LLC nanostructure is retained during photopolymerization at particular reactive surfactant concentrations. Physical properties including water uptake, diffusivity, and mechanical strength are greater in polyacrylamide systems that exhibit nanostructure compared to isotropic controls of the same chemical composition. Useful property relationships typically unattainable in traditional hydrogel systems are also observed for nanostructured hydrogels including simultaneous increases in water uptake and mechanical strength. These results demonstrate methods of generating and retaining polymer nanostructure during photopolymerization in systems that otherwise phase separate from the LLC template and may be utilized to synthesize nanostructured polymers with property relationships useful in a growing number of advanced applications.

Introduction

Hydrogels are useful in a wide variety of applications including contact lenses, tissue scaffolds, separation membranes, and drug delivery systems which utilize characteristic hydrogel properties such as high water content, biocompatibility, porosity, and permeability.¹⁻³ Typically, properties required for proper hydrogel performance are generated through careful adjustment of monomer concentration, functionality, and chemistry.⁴ A particularly important and commonly adjusted parameter determining ultimate hydrogel properties is the network cross-link density.

Significant and simultaneous changes in hydrogel properties including swelling, porosity, mesh-size, and mechanical strength are produced with changes in cross-link density.⁵ Unfortunately, the dependence of numerous hydrogel properties on this single parameter can make synthesis of hydrogels with specific properties difficult. As a result, undesirable compromises between the preferred material properties are often necessary in order for the hydrogel to remain functional.⁶ For example, biomaterials based on hydrogels may require lower cross-link densities to achieve higher degrees of swelling in order to facilitate nutrient and waste transport to a tissue.⁷ On the other hand, higher cross-link densities are often needed to generate the mechanical strength required to withstand biological forces. These property relationships ultimately limit hydrogel design and functionality due to the difficulty or inability to generate specific properties without eliciting unwanted changes in others.

To avoid undesirable properties in hydrogels that can result from changes in cross-link density, other methods of regulating final polymer properties have been examined such as addition of clay nanoparticles,⁸ ionization of polymer chains,⁹ generating interpenetrating or stratified polymer networks,¹⁰ and controlled crystallization.¹¹ These strategies have produced hydrogels with property relationships typically not attainable through the adjustment of cross-link density as the primary design

consideration. Another promising strategy of regulating hydrogel properties focuses on controlling polymer morphology as properties ranging from mechanical strength to molecular transport and electrical conductivity are highly-dependent on the local order of the polymer network and size of morphological features.¹²

Hydrogels with directed network structures on the micron and nanometer size scale can display property relationships much different from traditional hydrogel systems. In particular, hydrogels containing periodic sub-micrometer sized structures can exhibit concurrent increases in strength, biological response, permeability, and swelling compared to hydrogels with random or isotropic network architectures.¹³⁻¹⁶ In other words, controlling polymer structure on the nanometer size scale can allow valuable structure-property relationships that may be utilized to improve hydrogel performance.

Methods of directing polymer nanostructure can use templates to segregate monomers into ordered geometries followed by polymerization to transfer the template structure to the polymer.¹⁷ A promising method of generating nanostructure in organic polymers utilizes self-assembling lyotropic liquid crystals (LLCs) as polymerization platforms to direct polymer structure.^{18,19} The self-organized LLC phases, typically formed at higher concentrations of surfactant or amphiphilic molecules in a polar solvent such as water, contain nanometer sized domains that can be used as polymerization templates to direct polymer network structure. LLC phase geometry is largely controlled by surfactant concentration with spherical micelles forming at lower surfactant concentrations and the higher dimensionally ordered hexagonal, bicontinuous cubic, and lamellar mesophases typically assembling at progressively higher surfactant concentrations.²⁰ Nanostructured polymers generated through polymerization in and of LLC phases have been utilized to produce significant changes in final polymer properties, including increases in water uptake, mechanical strength, surface area, and permeability relative to isotropic polymer systems of the same chemical composition.¹³⁻¹⁶

Although LLCs have been utilized to direct polymer morphology and improve polymer functionality, retention of the original LLC template nanostructure throughout the polymerization reaction can be difficult.²¹ Thermodynamically driven phase separation events often occur during polymerization and can generate polymers with network structures that are much larger and more disordered than the original LLC template. Phase separation of the polymer from the parent template is a substantial problem in LLC templating applications and can prevent control of polymer nanostructure and properties. Efforts to elucidate the factors governing LLC nanostructure retention have examined how the polymerization environment impacts the evolution of polymer nanostructure during the polymerization reaction. Factors including initiation rate, photoinitiator mobility, reaction speed, temperature, monomer segregation behavior, and variations in polymerization rate have been linked to the degree of LLC structure transferred to the polymer.²²⁻²⁷ While these studies provide valuable information describing the underlying factors dictating ultimate polymer structure, a systematic study examining methods of retaining polymer nanostructure for polymer systems that typically undergo phase separation during polymerization in LLC templates has not been conducted. In order to synthesize hydrogels with useful property relationships not attainable in traditional hydrogel systems, a detailed study examining how polymer nanostructure and properties can be controlled through polymerization in LLC templates is needed.

Photopolymerization of LLC phases formed using mesogenic surfactants containing reactive functional groups such as acrylates and methacrylates has also been examined as a method of generating nanostructured polymers.⁶ In particular, polymerization of quaternary ammonium surfactants containing photo-reactive (meth)acrylate moieties attached to the cationic head group can generate polymerizable LLC mesophases which retain to a large degree the original morphology throughout polymerization.^{16,27} It is reasonable to believe that incorporating reactive LLCs into LLC

templates may provide a new avenue for retention of specific nanostructures utilizing a wider selection of monomer chemistries. Therefore, we hypothesize that incorporating low levels of such reactive surfactants may stabilize and facilitate retention of LLC template order in hydrogel materials throughout polymerization in polymer systems that otherwise phase separate when polymerized in nonreactive LLC mesophases. Adding reactive surfactant analogues with strong structure retention properties into non-reactive LLC systems that tend to phase separate could serve to stabilize thermodynamically the template morphology during polymerization through the formation of covalent bonds and attractive interactions between LLC surfactant molecules and monomer. It is further hypothesized that properties differences will be observed between nanostructured and isotropic polymers resulting from retention of the LLC structure through the addition of reactive surfactant.

In this study, the nanostructure of polyacrylamide hydrogels is controlled through photopolymerization in LLC templates formed using a nonreactive surfactant and low concentrations of a polymerizable mesogen to generate and retain nanometer scale order throughout polymerization. The impact of reactive surfactant concentration on the degree of LLC structure transferred to the polyacrylamide hydrogel is characterized to understand how thermodynamically unstable polymer nanostructures can be controlled using LLCs as structure directing polymerization platforms. The network swelling, mechanical strength, and diffusion properties of polyacrylamide systems with varying degrees of LLC order are characterized and related to the degree of LLC template structure retained during photopolymerization. Utilizing low concentrations of reactive mesogens in combination with nonreactive surfactants to control nanostructure of non-mesogenic polymer systems may allow synthesis of a wide variety of materials with versatile properties useful in a growing number of industrial and biomedical applications.

Experimental

Materials

The reactive quaternary ammonium surfactant monomer C12A was prepared by reacting 2-(dimethylamino)ethyl acrylate (98%, Aldrich) with 1-bromododecane ($\geq 99.5\%$, Aldrich) according to previously described methods.^{27,28} Hydrogel forming monomers included acrylamide ($\geq 99\%$, Aldrich) and *N,N'*-methylenebisacrylamide (99%, Aldrich). The nonreactive quaternary ammonium surfactant cetyltrimethylammonium bromide (CTAB, $\geq 99\%$, Aldrich), release solute rhodamine B (dye content $\sim 95\%$, Aldrich), and photoinitiator 2,2-Dimethoxy-1,2-diphenylethan-1-one (Irgacure 651, Ciba Specialty Chemicals) were also used. Glacial acetic acid (Aldrich) was utilized as a solvent. Figure 5.1 shows the chemical structures of monomers and surfactants used. All chemicals were used as received.

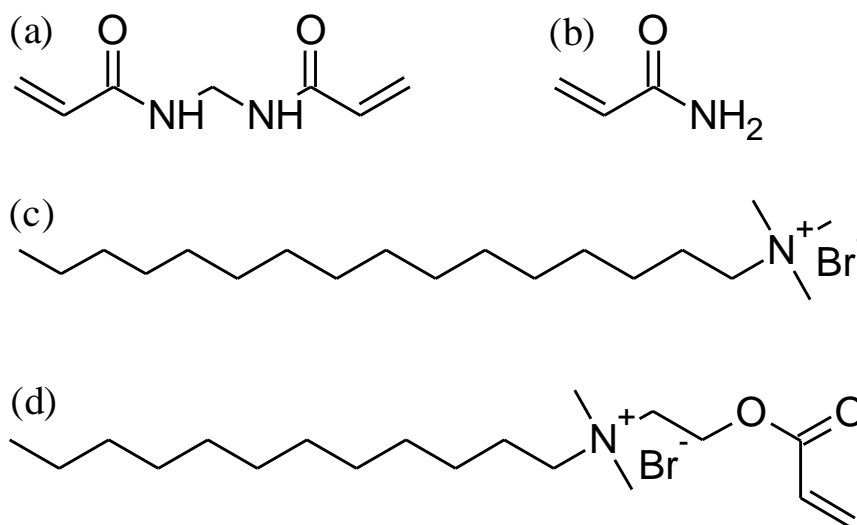


Figure 5.1. Chemical structures of monomers and surfactants used in this study. Shown are (a) *N,N'*-methylenebisacrylamide, (b) acrylamide, (c) cetyltrimethylammonium bromide (CTAB) surfactant, and (d) acrylate functionalized quaternary ammonium surfactant, dodecyl-dimethyl-(2-prop-2-enoyloxyethyl)ammonium bromide, (C12A).

Sample Preparation

Lyotropic liquid crystalline templated samples were prepared by mixing particular concentrations of monomer, surfactant, deionized water, and photoinitiator. Isotropic samples were prepared by mixing specific concentrations of monomer and photoinitiator in deionized water. All samples contained 20 wt % acrylamide (95 wt % acrylamide and 5 wt % *N,N'*-methylenebisacrylamide mixture) and 1 wt % photoinitiator with respect to total monomer mass. Isotropic controls did not contain CTAB surfactant. All LLC templated formulations contained 50 wt % total surfactant which represents the total combined weight percent of CTAB and C12A surfactants.

Sample homogeneity was achieved using centrifugation, mechanical agitation, heat sonication, and vortex mixing. Polymer disks were prepared by pipetting samples into borosilicate molds (15 mm diameter, 2 mm height), purging the samples with nitrogen for 8 minutes, and irradiating samples with a medium pressure UV arc lamp (Ace Glass) with an intensity of 1.5 mW/cm². Samples were solvent-exchanged with acetic acid for 48 hours to remove unreacted monomer, photoinitiator, and surfactants, then sandwiched between Mylar (DuPont) sheets to slow solvent evaporation and prevent cracking, and dried under vacuum for 48 hours.²⁹ Acetic acid was replaced periodically to facilitate surfactant removal. Overall, CTAB surfactant removal was at least 95% as measured gravimetrically. Dry polymer disks were cut to uniform dimensions prior to transport and mechanical testing. At least three polymer disks were prepared for each sample formulation and analyzed in physical property experiments to obtain the standard deviation for each data point represented by error bars in the presented figures.

Kinetics

Photopolymerization kinetics were studied using a Perkin-Elmer differential scanning calorimeter (photo-DSC) equipped with a medium-pressure UV arc lamp (Ace Glass) to initiate polymerization. The emission spectrum was controlled using a 365 nm

band-pass filter. Approximately 4 mg of sample was placed into crimped aluminum pans and covered with a thin transparent fluorinated ethylene propylene copolymer (Teflon[®] FEP, DuPont) film to minimize heat loss resulting from water evaporation. Samples were heated to 90 °C to promote uniform thickness and thermal contact. Oxygen inhibition was suppressed by purging samples with nitrogen for 8 minutes prior to polymerization. Heat flow was monitored in real-time by maintaining a constant sample temperature of 30 °C and used to calculate the normalized polymerization rate.²³ Double bond conversion was calculated by integrating the normalized polymerization rate with respect to time.

Structural Characterization

The optical anisotropy of LLC samples was characterized before and after polymerization using a polarized light microscope (PLM, Nikon, Eclipse E600W Pol) equipped with a hot stage (Instec, Boulder, CO). PLM images were obtained by placing samples sandwiched between a glass microscope slide and coverslip on the microscope stage, heating, and allowing them to cool slowly at room temperature. Samples were photopolymerized with the UV light source described above. Optical textures were examined for birefringent patterns characteristic of ordered phases formed in the LLC samples. PLM images obtained before and after photopolymerization were compared to determine the extent of phase disruption that occurred as monomers polymerized into a cross-linked network.

Polymer nanostructure was also characterized with a Nonius FR590 small angle X-ray scattering (SAXS) apparatus using a standard copper target Röntgen tube with a Ni-filtered Cu K α line of 1.54 Å as the radiation source, a collimation system of the Kratky type, and a PSD 50M position sensitive linear detector (Hecus M. Braun, Graz). Phases were indexed by calculating the *d*-spacing ratios of scattering peaks. The diffraction profiles of the hexagonal phase display a *d*-spacing ratio of 1:1/ $\sqrt{3}$:1/ $\sqrt{4}$...

(corresponding to d_{100} , d_{110} , d_{200} ,...). The scattering vector, q , was calculated from the angle of the scattered radiation and the X-ray wavelength. Additionally, scanning electron microscopy (SEM, Hitachi S-4800) was used to characterize polymer structure. Samples were freeze-fractured and sputter-coated using a Au/Pd target prior to imaging. SEM images represent the cross-section of LLC templated polymers after surfactant removal.

Water Uptake

Water uptake was studied gravimetrically by recording the mass of dried samples, immersing samples in excess deionized water at room temperature, removing the sample at predetermined times, patting the surface dry with damp filter paper to remove surface water, and measuring the sample mass. Hydrogel mass was used to calculate the percent water, W , using equation 5.1

$$W = (W_t - W_o)/W_t \times 100\% < 100\% \quad (5.1)$$

where W_t is the mass of the hydrogel at time t and W_o is the mass of the dry polymer after solvent-exchange with acetic acid. Note that eq 1 represents the weight percentage of the hydrogel that is water.

Release Profiles

The diffusivity of LLC templated and isotropic polymer samples was examined by incorporating the solute rhodamine B into the polymer network and measuring the rate of release into water. Dehydrated polymer disks were soaked in a concentrated dye solution for at least 14 days to allow infiltration of the dye into the hydrogel pores. Dye loaded polymer disks were removed from the concentrated dye solution, measured with

calipers, rinsed with deionized water to remove excess surface dye, placed in individual containers with 200 ml of deionized water, and sealed to prevent water loss. The release media was gently stirred using a magnetic stir bar to minimize concentration gradients and boundary layer effects. At predetermined times, 2 mL of release media was removed from the individual containers, placed in a quartz cuvette, and the absorbance at 554 nm was measured using a UV-vis spectrometer to determine the concentration of dye released. Release media was returned to the individual containers immediately after measuring dye concentration. Absorption spectrum of release media was measured periodically until no detectable change in dye concentration was observed. Diffusion coefficients for hydrogels were determined by least squares regression of experimental release profiles against the two-dimensional Fickian diffusion equation from a disk given by equation 5.2

$$\frac{M_t}{M_\infty} = 1 - \frac{32}{\pi^2} \sum_{n=1}^{\infty} \frac{1}{a_n^2} \exp\left(-\frac{a_n^2}{r^2} D_e t\right) \times \sum_{p=0}^{\infty} \frac{1}{(2p+1)^2} \exp\left(-\frac{(2p+1)^2 \pi^2}{l^2} D_e t\right) \quad (5.2)$$

where M_t/M_∞ is the fraction dye released at time t , r is the radius of the disk, D_e is the diffusion coefficient, l is the thickness of the disk, and a_n are the roots of the zero order Bessel function of the first kind.³⁰ Assumptions include an initial homogeneous distribution of dye in the hydrogel, a concentration independent diffusion coefficient, and sink conditions in the release medium. Least-squares regression was performed using MATLAB to estimate diffusion coefficients by fitting experimental release profiles to equation 5.2. Summations were truncated at 1000 terms.

Mechanical Properties

The compressive modulus of dehydrated and water swollen polymer disks was calculated from the slope of stress-strain curves measured using dynamic mechanical

analysis (TA instruments DMA Q800 series) equipped with a compressive clamp using previously established methods.^{4,15} Dehydrated polymer disks were prepared as described above. Water swollen polymer disks were prepared by immersing dehydrated polymer disks in deionized water at room temperature for approximately 100 hours prior to testing.

Results and Discussion

Recent results have demonstrated that hydrogels with useful property relationships can be synthesized utilizing self-organizing lyotropic liquid crystalline mesophases as polymerization platforms to direct polymer structure on the nanometer scale.¹⁸ Although photopolymerization in and of LLC mesophases is a promising method of generating increases in hydrogel water uptake, strength, diffusivity, surface area, and biological response, it is often difficult to retain the original LLC template nanostructure during the polymerization reaction. The purpose of this work is to describe methods of controlling the nanostructure of LLC templated non-mesogenic polymers that typically undergo phase separation during photopolymerization. This control is enabled using combinations of nonreactive surfactants and their polymerizable analogs to provide a more thermodynamically stable platform for nanostructure development during polymerization. Additionally, properties dependent on polymer nanostructure are examined in order to understand the impact of network architecture on hydrogel performance.

Structure Characterization

To examine if reactive surfactants facilitate greater retention of the original LLC structure, the nanostructure of polyacrylamide photopolymerized in the normal hexagonal phase formed using the unreactive quaternary ammonium surfactant (CTAB) and

polymerizable analogue (C12A) in water was characterized using polarized light microscopy (PLM). The reactive C12A mesogen is similar to CTAB in structure and molecular weight which facilitates incorporation into the nonreactive surfactant template without significant disruptions to the LLC phase. Furthermore, C12A readily forms and retains a hexagonal LLC structure.²⁷ Therefore, it is reasonable to believe that incorporation of a polymerizable amphiphile such as C12A which polymerize with the acrylamide will stabilize the structure during polymerization and reduce phase disruptions and separations. The total surfactant concentration is maintained at 50 wt % for all LLC templated formulations and represents the combined weight percent of CTAB and C12A.

Figure 5.2 shows the PLM images of acrylamide templated with different concentrations of C12A and CTAB before and after photopolymerization. The birefringence pattern and fan-like optical texture observed before polymerization in each of the LLC templated acrylamide samples is characteristic of the hexagonal LLC mesophase.²⁰ After polymerization, acrylamide polymers templated with 0 or 5 wt % C12A (Figures 5.2b and 5.2d) do not retain the characteristic optical texture of the hexagonal phase implying that these samples have phase separated. On the other hand, PLM images of acrylamide templated with 10 or 15 wt % C12A (Figures 5.2f and 5.2h) show a large degree of preservation of the birefringent pattern indicative of the hexagonal LLC phase after polymerization. The strong birefringence intensity and well-defined optical texture observed after polymerization indicate that the parent template structure is preserved during the polymerization reaction when sufficient C12A is incorporated into the nonreactive CTAB template. PLM images shown in Figure 5.2 demonstrate that polyacrylamide samples templated with 0 or 5 wt % C12A have phase separated. PLM images in Figure 5.2 support that incorporating sufficient concentrations of reactive surfactant into the LLC template greatly increases the degree of hexagonal order transferred to polyacrylamide during polymerization. To corroborate PLM results and

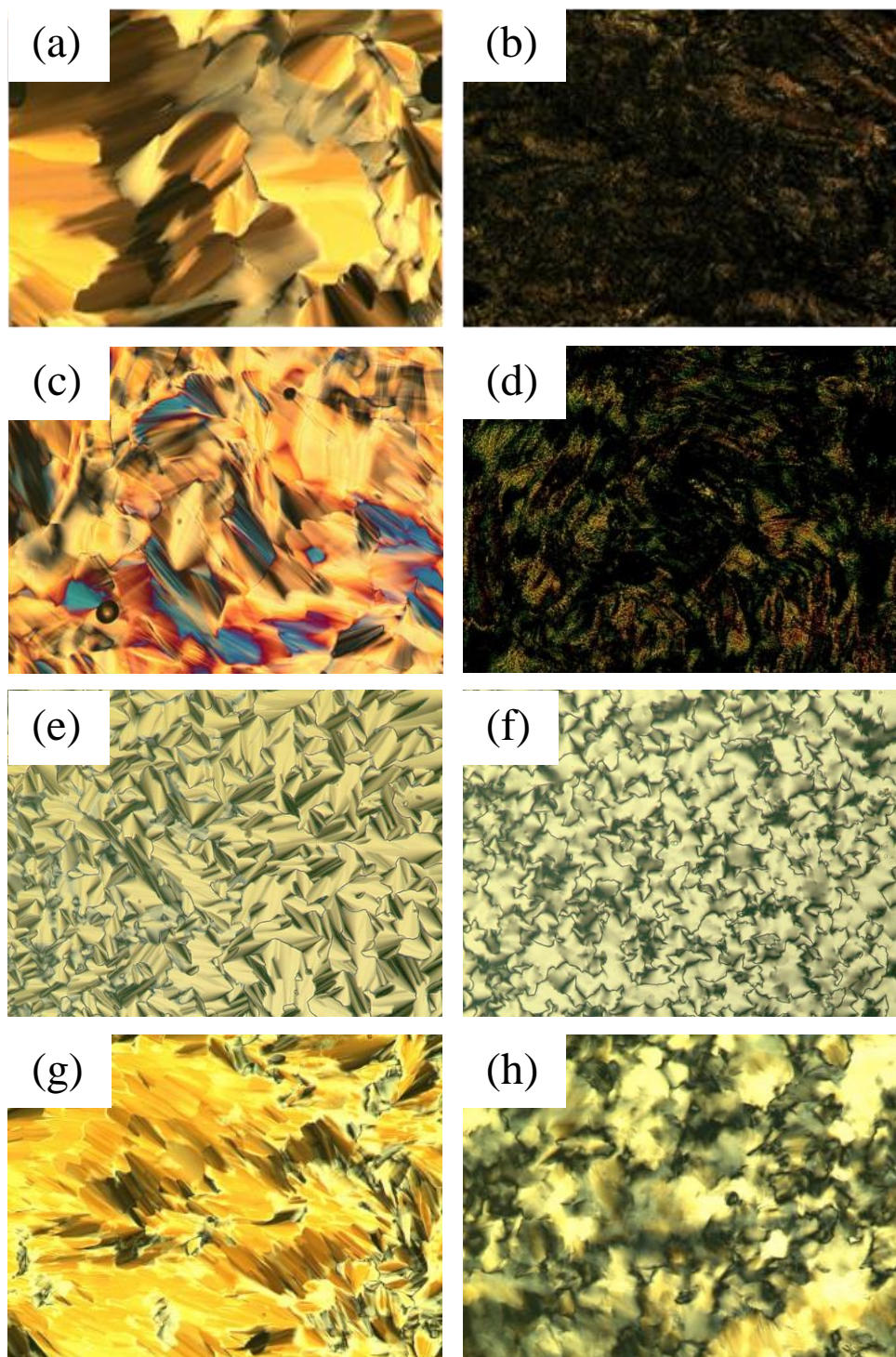


Figure 5.2. Polarized light micrographs of 20 wt % cross-linked acrylamide templated with different concentrations of CTAB and C12A surfactants (50 wt % total) in water before and after photopolymerization. Shown are 0 wt % C12A before (a) and after (b), 5 wt % C12A before (c) and after (d), 10 wt % C12A before (e) and after (f), and 15 wt % C12A before (g) and after (h) polymerization.

confirm the presence of nanometer sized order, small angle X-ray scattering (SAXS) was also performed. Figure 5.3 shows the SAXS profiles before and after photopolymerization of 20 wt % acrylamide templated with 50 wt % surfactant at different concentrations of CTAB and C12A in water. Close examination of the SAXS profiles for LLC templated acrylamide systems before polymerization show primary and secondary scattering peaks (see insert) as would be expected from a hexagonal LLC mesophase.³¹ Retention of the original hexagonal structure and successful transfer of LLC template order to the polymer is examined by comparing the scattering intensities and position of scattering maxima of LLC formulations before and after polymerization.

The SAXS profile observed after photopolymerization of acrylamide templated with 50 wt % CTAB (Figure 5.3a) shows significant decreases in scattering intensity and large changes in the positions of scattering maxima compared to the SAXS profile obtained before polymerization. These differences between the SAXS profiles along with PLM results indicate that the original hexagonal LLC structure is not retained during polymerization of acrylamide templated solely with the nonreactive CTAB surfactant. Similar trends are seen in the SAXS profiles before and after photopolymerization of acrylamide templated with 45 wt % CTAB and 5 wt % C12A shown in Figure 5.3b. The decrease in scattering intensity and loss of the primary scattering peak signify the normal hexagonal structure is not retained by substituting 5 wt % CTAB with the reactive C12A surfactant.²³ The degree of phase separation for acrylamide templated with low percentages of reactive surfactant is further illustrated by comparing the scattering profile of a 5:3 weight ratio CTAB:water formulation shown in Figure 5.3a to the SAXS profile for the cured LLC templated acrylamide polymers. The CTAB-water mixture contains the same ratio of surfactant to water that would be present if the surfactant-water template completely phase separated from, and did not interact with, the polymer network. The similar intensities and positions of the scattering peaks for the CTAB-water mixture

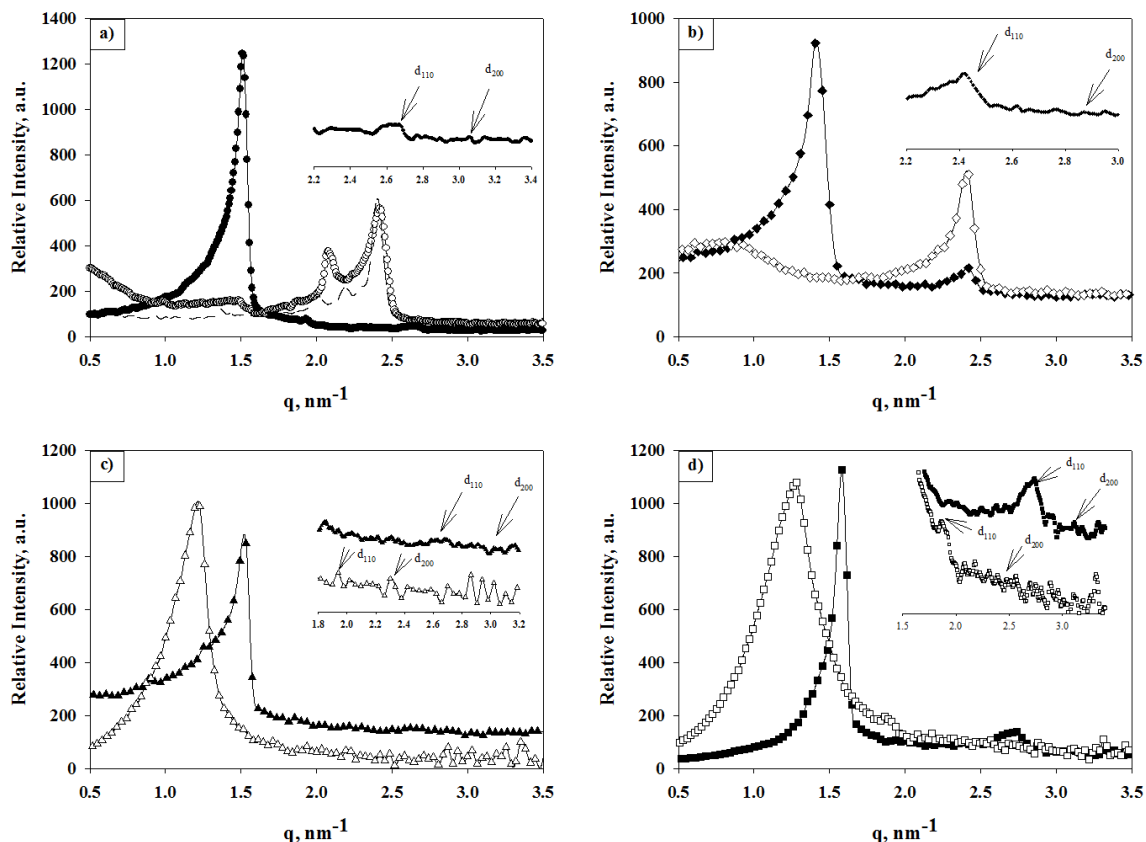


Figure 5.3. Small angle X-ray scattering profiles before and after photopolymerization of acrylamide (95 wt % acrylamide and 5 wt % N,N' -methylenebisacrylamide) templated with varying concentrations of nonreactive CTAB and polymerizable C12A surfactants. Shown are profiles of samples with a) 5:3 weight ratio CTAB:water (---), 0/50 wt % C12A/CTAB before (\bullet), and after polymerization (\circ), b) 5/45 wt % C12A/CTAB before (\blacklozenge) and after polymerization (\diamond), c) 10/40 wt % C12A/CTAB before (\blacktriangle) and after polymerization (Δ), and d) 15/35 wt % C12A/CTAB before (\blacksquare) and after (\square) polymerization. Insets are also shown to indicate the secondary reflections that identify the hexagonal phase.

and the cured polyacrylamide samples templated using CTAB and 0 or 5 wt % C12A supports that the LLC systems templated with 5 wt % or less C12A adopt a polymer network structure that is predominantly isotropic during polymerization.²³

Conversely, the SAXS profiles before and after polymerization of acrylamide templated with CTAB and 10 or 15 wt % C12A (Figure 5.3c and 5.3d) show structural behavior much different than samples templated with lower C12A concentrations. In fact, incorporating 10 or 15 wt % C12A into the LLC template significantly increases the degree of nanostructure retained during photopolymerization. The SAXS profile before polymerization of acrylamide templated with 40 wt % CTAB and 10 wt % C12A shown in Figure 5.3c displays a strong primary reflection and scattering maxima indicative of a nanoporous morphology. Additionally, while the secondary reflections are small, subtle peaks are observed for the 10 wt % C12A system at positions representative of a normal hexagonal LLC mesophase. After polymerization, the intensity and position of the primary scattering peak is retained to a much larger degree compared to acrylamide system templated with 0 or 5 wt % C12A. These results corroborate those from PLM suggesting a well-defined nanoporous structure is generated in the polymer after polymerization with sufficient polymerizable surfactant.

The SAXS profile after polymerization of acrylamide templated with 15 wt % C12A and 35 wt % CTAB (Figure 5.3d) shows similar behavior and maintains the general shape, intensity, and ratio of the primary and secondary scattering reflections observed before polymerization. Retention of the strong primary reflection of the SAXS profiles at 15 wt % C12A concentration indicates that the polymers contain defined nanometer sized structures. While the higher ordered scattering peaks for the 15 wt % C12A system are subtle the PLM images in Figure 5.2h in combination with the SAXS profiles suggest that the polymer has adopted a hexagonal morphology. Concentrations of reactive C12A surfactant above 15 wt % were not examined for structure retention in

detail as the acrylate terminated quaternary ammonium head group interferes with LLC phase formation at greater concentrations.

Both SAXS and PLM results support that the hexagonal LLC structure is transferred to polyacrylamide when sufficient reactive surfactant is incorporated due to the additional thermodynamic stability provided during polymerization. While this structural information is critical to determine the extent of LLC nanostructure retained during polymerization, the bulk structure of the polymer may also be affected by the surfactant template. In order to examine polymer structure on larger size scales, scanning electron microscopy (SEM) was used to analyze the bulk morphology of polymer samples templated with varying concentrations of CTAB and C12A. Figure 5.4 shows the SEM images of polyacrylamide samples photopolymerized in the hexagonal LLC phase formed at different concentrations of CTAB and C12A after removal of unreacted monomer and surfactants by solvent exchange. For SEM analysis, water must also be removed which may allow the polymer structure to collapse. However, the morphology should still show differences in the bulk morphology if nanostructure is present.³²

SEM images show structural information that directly parallels SAXS and PLM data of LLC templated polyacrylamide samples. Specifically, SEM images of polyacrylamide templated using CTAB and 0 or 5 wt % C12A (Figures 5.4a and 5.4b) show an expected smooth and glassy morphology observed for isotropic polyacrylamide systems not influenced significantly by the LLC template.¹⁵ Conversely, SEM images for polyacrylamide templated with 10 or 15 wt % C12A show a more defined and ordered bulk structure than formulations templated with lower C12A concentrations. In fact, micrographs of polyacrylamide templated with 10 wt % C12A shown in Figure 5.4c and 5.4d contain directed sheet-like structures while SEM images of polyacrylamide templated with 15 wt % C12A (Figure 5.4e and 5.4f) show a defined porous structure. These differences in the primary or bulk polymer structure observed by SEM suggest that monomer diffusion and polymer microstructure is directed in a manner dependent on

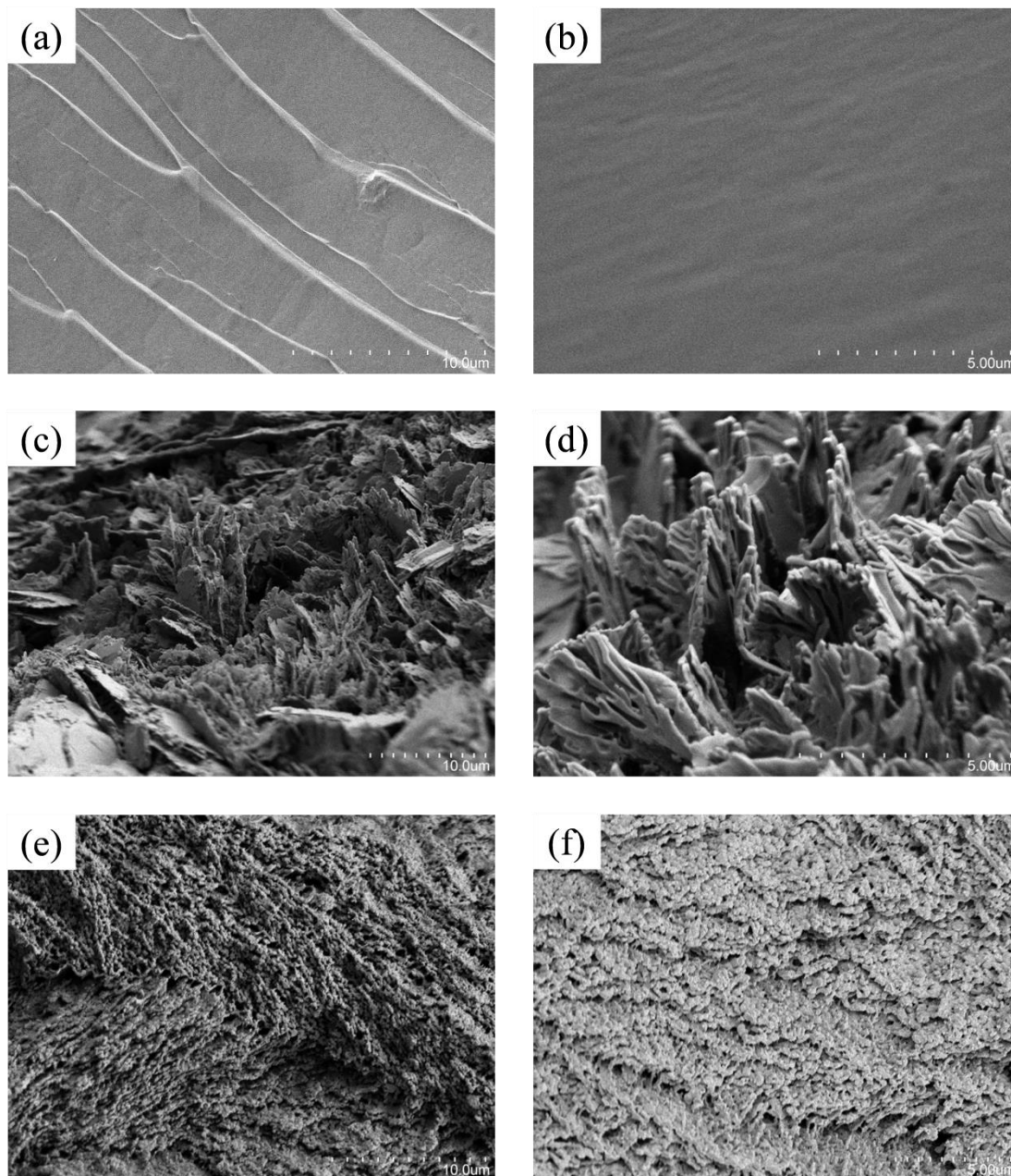


Figure 5.4. Scanning electron micrographs of 20 wt % cross-linked polyacrylamide photopolymerized in the hexagonal LLC phase formed using varying concentrations of unreactive CTAB and polymerizable C12A surfactants. Shown are cross-sections of polyacrylamide templated with (a) 0/50 wt % C12A/CTAB, (b) 5/45 wt % C12A/CTAB, (c) 10/40 wt % C12A/CTAB, (d) (c) at higher magnification, (e) 15/35 wt % C12A/CTAB, and (f) (e) at higher magnification. CTAB surfactant template was removed prior to imaging.

C12A concentration.¹⁷ Differences in monomer diffusional behavior observed on the microscale generate a significant impact on overall photopolymerization rate and the degree of LLC order retained during the polymerization reaction.

The LLC structure retention for polyacrylamide systems was further examined by characterizing the polymerization rate using photo-differential scanning calorimetry (photo-DSC). Photopolymerization kinetic behavior in LLC systems is directly related to the local order of the polymer as directed by the parent template and may be utilized as a tool to probe polymer structure evolution during the polymerization reaction.²³ In fact, faster photopolymerization rates are often observed in systems that retain a high degree of LLC template order.^{15,22,25} Figure 5.5 shows the photopolymerization kinetic profiles for acrylamide templated with different CTAB and C12A concentrations. Interestingly, the polymerization rate appears to depend significantly on the amount of polymerizable surfactant and consequently the degree of hexagonal LLC structure retained. The slowest polymerization rates are observed for acrylamide templated with CTAB and 0 or 5 wt % C12A. Polymerization rate increases considerably for the polyacrylamide systems with 10 and 15 wt % C12A that retain the hexagonal LLC structure. In fact, for the systems that retain nanostructure the polymerization rate increases by 50% over those that phase separate. Additionally, no further increase in rate is observed for systems that retain nanostructure when the concentration is increased from 10 to 15 wt % C12A. The increase in polymerization rate observed in these systems is likely due to a higher reactive species concentration through segregation in the hexagonal phase that is preserved to a much higher extent during the polymerization reaction. Because higher polymerization rates are often detected in ordered LLC systems, the faster photopolymerization rate of acrylamide templated with 10 and 15 wt % C12A corroborate SAXS, PLM, and SEM data demonstrating that the hexagonal LLC structure is preserved during the polymerization reaction. Moreover, the hexagonal LLC nanostructure of polyacrylamide retained at 10 and 15 wt % C12A could

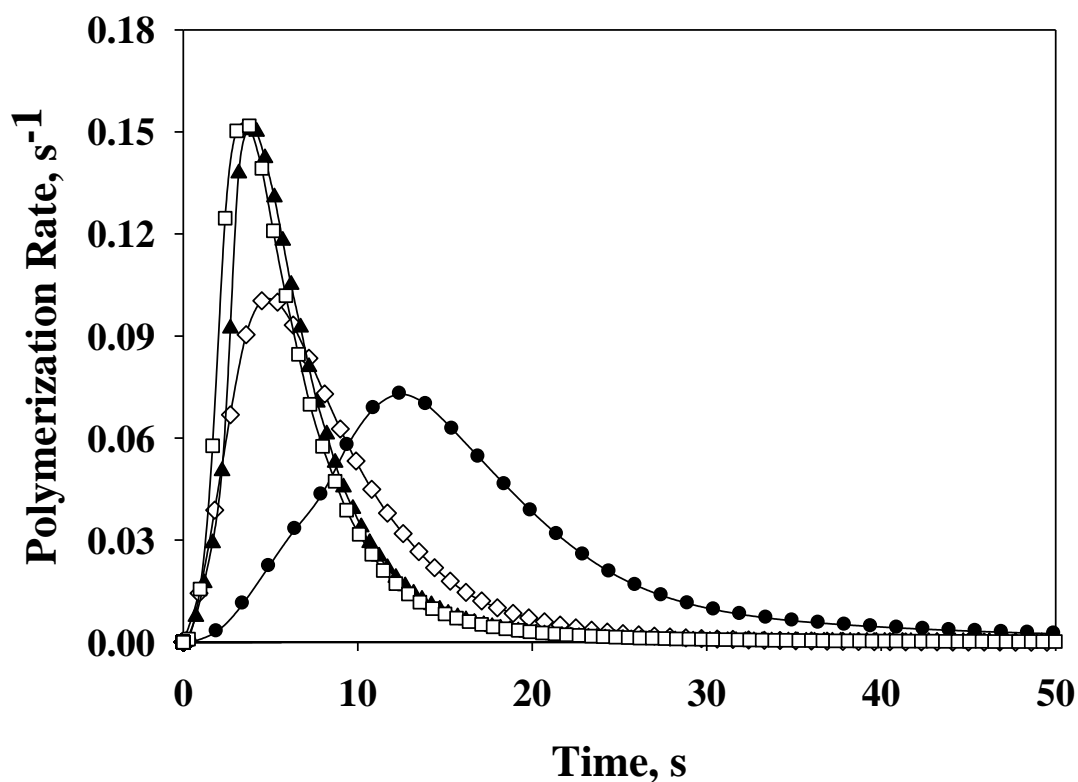


Figure 5.5. Polymerization rate as a function of time for 20 wt % cross-linked polyacrylamide photopolymerized in the hexagonal LLC phase formed using varying concentrations of nonreactive CTAB and polymerizable C12A surfactants. Shown are acrylamide templated with 0/50 wt % C12A/CTAB (●), 5/45 wt % C12A/CTAB (◇), 10/40 wt % C12A/CTAB (▲), and 15/35 wt % C12A/CTAB (□). Photopolymerization was initiated at a light intensity of 1.5 mW/cm² at 365 nm and 1 wt % Irgacure 651 with respect to monomer mass.

generate significant differences in polymer properties that may be useful in biological and industrial applications.

Physical Properties

The mechanical and transport properties of polyacrylamide containing different degrees of hexagonal LLC order were characterized to elucidate the impact of polymer structure on hydrogel properties. Considerable changes in hydrogel properties can result from differences in morphology and may generate useful property relationships that cannot be attained through regulation of hydrogel cross-link density.¹² To examine the impact of LLC structure on hydrogel transport properties, the swelling behavior of polyacrylamide gels templated with different CTAB and C12A concentrations was characterized and compared to the swelling behavior of isotropic controls with the same basic chemical composition. Isotropic controls of LLC templated polymers were synthesized by substituting CTAB surfactant used in LLC formulations with an equivalent concentration of water thereby and do not contain LLC order. The properties observed for isotropic systems represent the material behavior of a polymer system with a random or isotropic network architecture that does not contain long-range order or periodic structures. Property variances between isotropic and LLC templated polymers of the same chemical composition may be attributed to differences in polymer order as directed by the LLC surfactant template.

Figure 5.6 shows the water uptake as a function of time for LLC templated and isotropic polyacrylamide hydrogels upon removal of nonreactive surfactant. It is apparent from Figure 5.6 that the rate and degree of water uptake depends significantly on hydrogel structure. The phase separated polyacrylamide gels that do not retain the hexagonal LLC structure when 0 or 5 wt % C12A is incorporated into the CTAB template have swelling profiles very similar to their respective isotropic controls

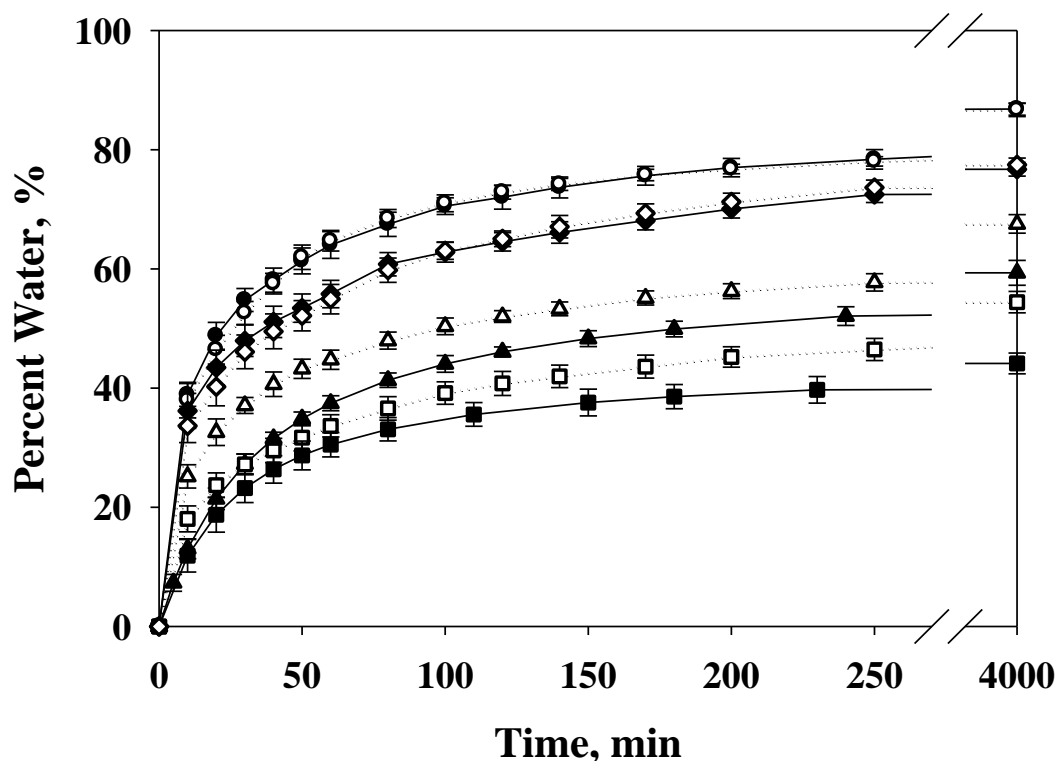


Figure 5.6. Mass percentage water content as a function of time for polyacrylamide hydrogels photopolymerized in the hexagonal LLC phase formed using varying concentrations of unreactive CTAB and polymerizable C12A surfactants. Also included is the transient water uptake of isotropic polyacrylamide controls with the same basic chemical composition of LLC templated systems. Shown are 0/50 wt % C12A/CTAB (○, phase separated), 0/0 wt % C12A/CTAB (●, isotropic), 5/45 wt % C12A/CTAB (◇, phase separated), 5/0 wt % C12A/CTAB (◆, isotropic), 10/40 wt % C12A/CTAB (Δ, hexagonal), 10/0 wt % C12A/CTAB (▲, isotropic), 15/35 wt % C12A/CTAB (□, hexagonal), and 15/0 wt % C12A/CTAB (■, isotropic). CTAB surfactant was removed by solvent exchange prior to analysis.

with identical chemical composition. Water uptake does decrease with increasing C12A concentration for both LLC templated and isotropic hydrogels due to greater incorporation of aliphatic chains from the C12A surfactant which decreases the polarity of the polymer network. The similar swelling behavior between the phase separated LLC templated and isotropic gels indicates that the polymer network structures are disordered

resulting in no significant differences in hydrogel properties. However, LLC templated polymers that retain the nanostructure during polymerization show swelling behavior much different than their isotropic counterparts. Polyacrylamide hydrogels containing nanostructure have larger rates and degrees of water uptake compared to isotropic controls of the same chemical composition. Specifically, hydrogels templated with CTAB and 10 or 15 wt % C12A swell faster and uptake approximately 10% more water than their respective isotropic controls. Although seemingly small, increasing the mass fraction of water in the gel by 10% without changing the polymer chemical composition could facilitate significant transport enhancements in numerous applications including contact lens and drug delivery applications.^{3, 18} The increase in the rate and overall degree of water uptake between isotropic and nanostructured hydrogels is likely due to the templated nanostructure and accompanying nanoporous networks facilitated by incorporating 10 or 15 wt % C12A into the LLC template.

In addition to water uptake, hydrogel structure can also have a significant impact on the diffusive transport through the polymer network. Changes in cross-link density can greatly alter the water uptake and mesh size of the hydrogel network which typically results in differences in diffusivity and transport properties.³³ The porous domains of hydrogels generated by photopolymerization in LLC phases may also impact diffusive transport behavior through a directed network of porous domains. To further examine the impact of LLC structure on polymer transport properties, the diffusivity of polyacrylamide hydrogels was characterized by measuring the dye release rate from the polymer matrix. Figure 5.7 shows the dye fraction released as a function of time for LLC templated hydrogels and their isotropic controls. As is apparent from Figure 5.7, dye release is more rapid for hydrogel systems that contain a hexagonal LLC structure as compared to their respective isotropic counterparts. The fastest release is observed for the highly water swollen polyacrylamide hydrogels containing 0 or 5 wt % C12A.

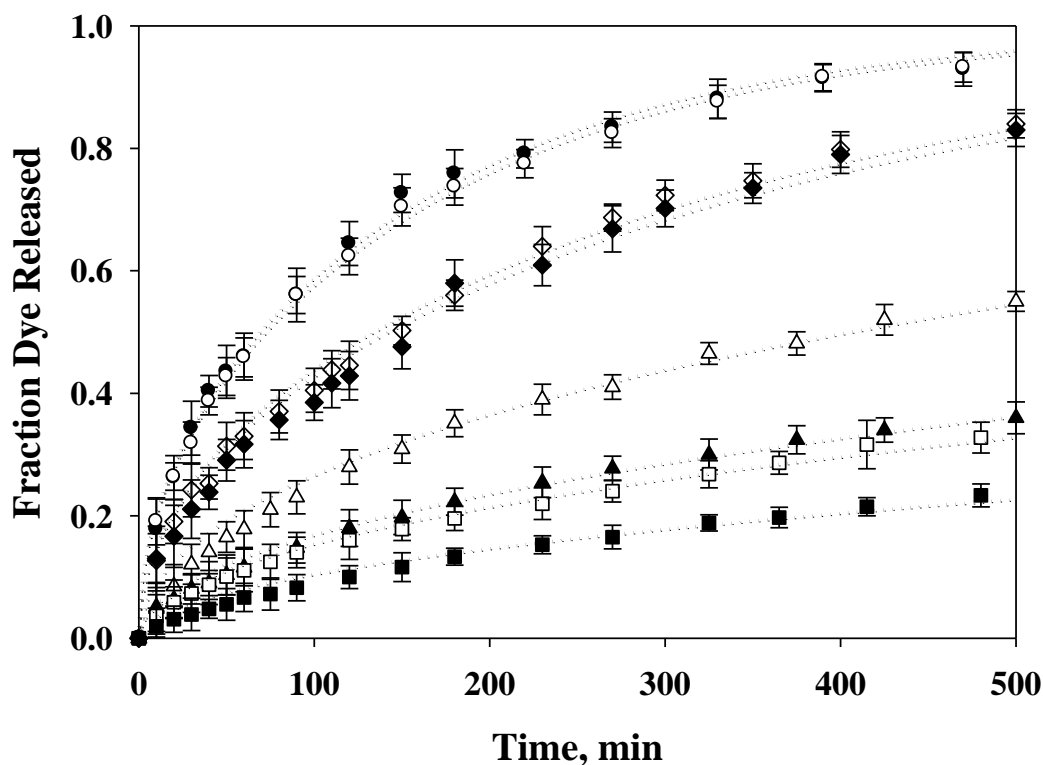


Figure 5.7. Cumulative dye release profiles as a function of time for polyacrylamide hydrogels photopolymerized in the hexagonal LLC phase formed using varying concentrations of nonreactive CTAB and polymerizable C12A surfactants. Also included are the release profiles of isotropic polyacrylamide controls with the same basic chemical composition of LLC templated systems. Shown are 0/50 wt % C12A/CTAB (\circ , phase separated), 0/0 wt % C12A/CTAB (\bullet , isotropic), 5/45 wt % C12A/CTAB (\diamond , phase separated), 5/0 wt % C12A/CTAB (\blacklozenge , isotropic), 10/40 wt % C12A/CTAB (Δ , hexagonal), 10/0 wt % C12A/CTAB (\blacktriangle , isotropic), 15/35 wt % C12A/CTAB (\square , hexagonal), and 15/0 wt % C12A/CTAB (\blacksquare , isotropic). CTAB surfactant was removed by solvent exchange prior to analysis. Trend lines generated by least squares curve fits against equation 2.

These systems have the highest diffusivity due to their larger water content compared to hydrogels containing higher C12A concentrations as shown in Figure 5.6.³⁴ As expected, no differences are observed in the release profiles between the phase separated hydrogels

templated with 0 or 5 wt % C12A and CTAB compared to isotropic controls due to random network structures, similar water contents, and analogous chemical compositions. On the other hand, hydrogels with a templated nanostructure release dye faster than the corresponding isotropic polymers of the same chemical composition. For example, the 10 wt % C12A containing samples release dyes at a rate more than 200% faster compared to isotropic analogues with an overall release 40% greater at 500 minutes. Of particular interest is the similar release profile for nanostructured polyacrylamide templated with 15 wt % C12A compared to the isotropic polyacrylamide hydrogel containing 10 wt % C12A. Even though the nanostructured hydrogel templated with 15 wt % C12A uptakes considerably less water than the isotropic hydrogel containing 10 wt % C12A, the gels have diffusivities within experimental error. This behavior suggests that the increase in release rate between hexagonal nanostructured hydrogels compared to their isotropic controls is not solely due to differences in water uptake.³³ Instead, it is likely that the observed increases in diffusive transport properties of nanostructured gels are due to the directed porous network nanostructure generated through photopolymerization in the hexagonal LLC phase formed using sufficient reactive surfactant. Interestingly, the diffusion coefficient for nanostructured gels is approximately 200% greater than the analogous isotropic samples suggesting a dramatic increase in pore alignment using LLCs as structure directing polymerization platforms.

Mechanical Properties

In addition to changing swelling behavior and diffusivity, the LLC polymer nanostructure may also have a significant impact on polymer mechanical properties.^{13-16,35} To better understand the impact of polymer nanostructure on macroscopic mechanical properties, the compressive strength of polymers with varying degrees of LLC order was characterized using dynamic mechanical analysis. Figure 5.8a shows the compressive stress-strain profiles of hydrated polyacrylamide samples templated with

varying concentrations of C12A and CTAB. Also shown in Figure 5.8a are the stress-strain profiles of isotropic hydrogels with the same basic chemical composition as their LLC templated counterparts. It is apparent from the slope of stress-strain curves in Figure 5.8a that the compressive strength increases with reactive surfactant concentration. These differences in hydrogel mechanical properties at different C12A concentrations are explained by the swelling data of hydrogels presented in Figure 5.6, which displays the general trend of increasing water uptake with decreasing C12A concentration.

The compressive stress-strain profiles for the polymers shown in Figure 5.8a are consistent with the fact that increases in water uptake can generate large decreases in hydrogel mechanical strength.⁴ Interestingly, Figure 5.8a shows that the compressive modulus between LLC templated hydrogels and their isotropic controls is virtually the same. It is well-documented that even small increases in water uptake can generate significant decreases in mechanical strength for traditional hydrogel systems. Even with 10% greater water content the slopes of stress-strain profiles for nanostructured gels templated with 10 or 15 wt % C12A are similar to their isotropic controls. In fact, no statistically significant difference in the compressive modulus between the nanostructured materials with their respective isotropic controls is observed.⁴

To further examine the observed increase in mechanical strength of the nanostructured hydrogels, the compressive strength of LLC templated and isotropic polymers shown in Figure 5.8a were characterized in their dehydrated state. Figure 5.8b shows the compressive stress-strain profiles for polymers templated with varying concentrations of C12A and their appropriate isotropic controls. Similar to the compressive strength of hydrated polymer samples, the slope of the stress-strain curves increases with increasing C12A concentrations for both LLC templated and isotropic polymers. However, the polymers with nanostructure have a significantly larger modulus relative to their isotropic controls. In fact, the nanostructured polyacrylamide samples templated with 10 or 15 wt % C12A display a compressive modulus about

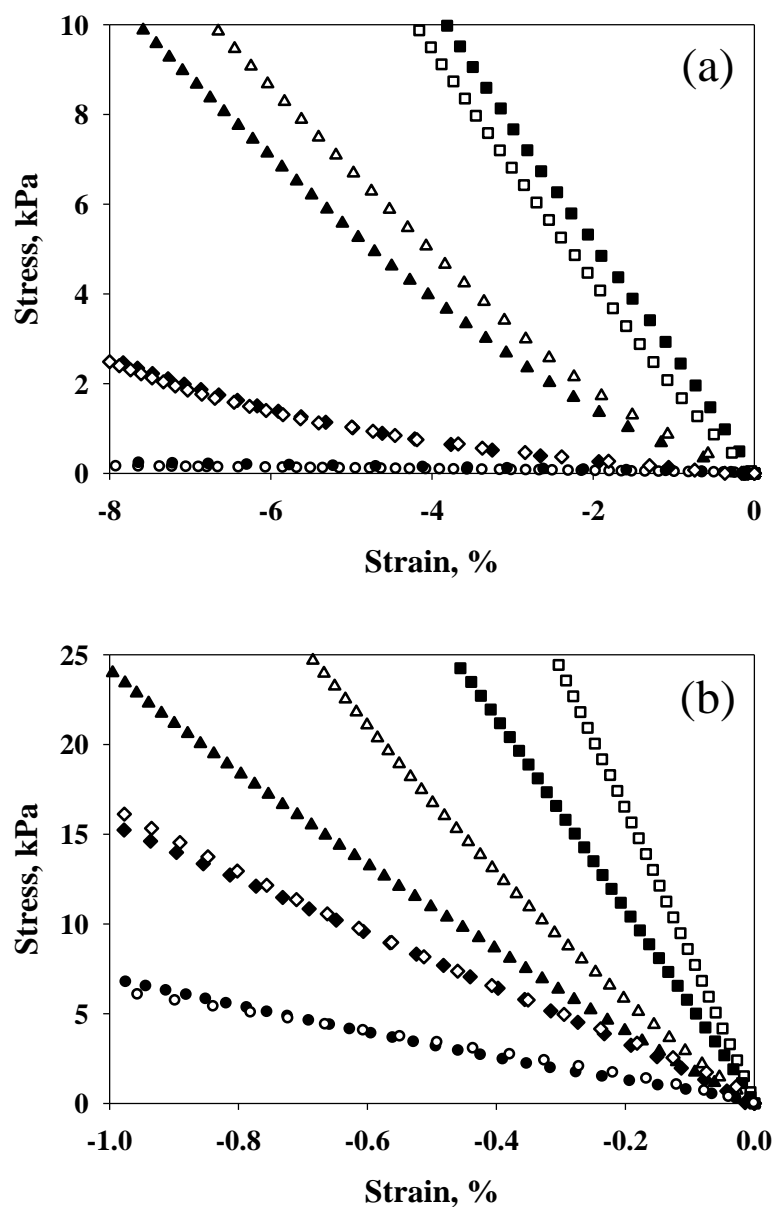


Figure 5.8. Stress-strain profiles of LLC templated and isotropic polyacrylamide systems. Shown are Stress-strain profiles of (a) hydrated and (b) dehydrated polyacrylamide photopolymerized in the hexagonal LLC phase formed using varying concentrations of unreactive CTAB and polymerizable C12A surfactants. Also included are isotropic polyacrylamide controls with the same basic chemical composition of LLC templated counterparts. Shown are 0/50 wt % C12A/CTAB (\circ , phase separated), 0/0 wt % C12A/CTAB (\bullet , isotropic), 5/45 wt % C12A/CTAB (\diamond , phase separated), 5/0 wt % C12A/CTAB (\blacklozenge , isotropic), 10/40 wt % C12A/CTAB (Δ , hexagonal), 10/0 wt % C12A/CTAB (\blacktriangle , isotropic), 15/35 wt % C12A/CTAB (\square , hexagonal), and 15/0 wt % C12A/CTAB (\blacksquare , isotropic). CTAB surfactant was removed by solvent exchange prior to analysis.

50 and 60% greater than their isotropic counterparts of the same chemical composition, respectively. This increase in compressive modulus is derived solely from polymer structure and represents a promising method of improving material properties by controlling nanostructure. Because the nanostructured polymers are compositionally identical to their isotropic controls that contain a random or disordered network structure, it is apparent that the directed LLC structure is more resistant to deformation and generates an increase in mechanical strength.^{13,36}

The impact of organized structures on material properties is well-characterized through relationships developed for architected foams, polymers, and ceramics.³⁵ For architected systems, the compressive modulus is largely dependent on the alignment of support structures in relation to the applied stress. It is likely that the hexagonal LLC structure increases the alignment of polymer chains in a manner that can more effectively resist deformation compared to a disordered or isotropic network. The uniformity and orientation of the polymer network as directed by the LLC template provides additional support likely via the mechanism often observed in architected foams, thereby leading to the increased compressive modulus observed in the LLC templated systems. The structure-property relationships observed in these polymers indicate that improved properties based on nanostructure can be realized. As such, effectively templated LLC polymers may prove useful as biomaterials and tissue scaffolds with combinations in both transport and mechanical properties that cannot be generated using traditional polymerization techniques.

It is clear from SAXS, PLM, microscopy, and kinetic data that incorporating 10 or 15 wt % C12A into the LLC template formed using CTAB and water significantly increases the degree of template structure transferred to the final polymer network during polymerization through enhanced thermodynamic stability. Table 5.1 summarizes the mechanical and transport property measurements presented previously for LLC templated systems and their isotropic controls. Comparison of the properties reviewed in Table 1

indicates that the nanostructure elicits large changes in polymer transport and mechanical properties relative to polymers with random network architectures and the same chemical composition. For example, all properties of phase separated systems are within experimental error of analogous isotropic systems. On the other hand, the nanostructured gels contain at least 25% more water, exhibit an increase of at least 70% for the dry compressive modulus, and at least 200% for the diffusion coefficient when compared to the corresponding isotropic polymer. Additionally, the hydrated compressive modulus of the nanostructured gels is not statistically different than the isotropic gels despite their additional water content. The physical property relationships of nanostructured polyacrylamide hydrogels synthesized in this work by photopolymerization in LLC templates are not possible in traditional hydrogel systems through regulation of cross-link density, chemistry, and chemical composition.^{37,38} These results demonstrate that retaining the original LLC structure during polymerization in polymer systems that typically undergo phase separation from the parent LLC template allows enhancement of transport and mechanical properties dependent on nanostructure. Using polymerizable surfactants allows greater control of structure for LLC templated polymerizations of acrylamide monomer systems.

Table 5.1. Summary of Physical Properties for LLC Templated and Isotropic Polyacrylamide

C12A/CTAB (wt %)	Polymer Structure	Percent Water (%)	Diffusion Coefficient $\times 10^9$ (cm ² /s)	Hydrated Modulus (kPa)	Dehydrated Modulus (kPa)
0/50	Phase Separated	86.7 \pm 1.1	328.2 \pm 40.5	0.8 \pm 1.3	597 \pm 11
0/0	Isotropic	86.2 \pm 1.0	345.9 \pm 51.4	0.6 \pm 1.4	676 \pm 24
5/45	Phase Separated	77.5 \pm 1.1	175.7 \pm 20.9	6.8 \pm 1.8	1547 \pm 30
5/0	Isotropic	76.7 \pm 1.3	165.6 \pm 22.5	7.3 \pm 1.2	1555 \pm 35
10/40	Nanostructured	67.5 \pm 1.6	57.5 \pm 6.6	51.2 \pm 3.6	3946 \pm 50
10/0	Isotropic	59.3 \pm 2.1	23.1 \pm 4.2	50.7 \pm 4.8	2440 \pm 62
15/35	Nanostructured	54.4 \pm 1.8	18.7 \pm 4.0	107.9 \pm 2.7	7966 \pm 51
15/0	Isotropic	44.1 \pm 1.7	8.5 \pm 1.7	114.0 \pm 3.5	5340 \pm 43

Conclusions

The nanostructure of polyacrylamide hydrogels has been controlled through photopolymerization in LLC templates formed using specific concentrations of nonreactive and polymerizable surfactants. Reactive surfactant concentration directly impacts the degree of hexagonal LLC structure transferred to polyacrylamide hydrogels during polymerization. The polymerizable surfactants are incorporated into the polyacrylamide networks and thus impart an additional degree of thermodynamic stability within the LLC phase before and during polymerization. Nanostructure was retained during polymerization using particular concentrations of reactive surfactant. A significant polymerization rate increase is observed in the LLC templated systems that retain nanostructure compared to phase separated polymers. Scanning electron micrographs show a directed porous structure for LLC templated polymers that retain

nanostructure while isotropic polymers contained relatively featureless and glassy morphologies. Improved transport properties of nanostructured polymers are observed relative to isotropic polymers of the same chemical composition including increases in the rate and degree of water uptake as well as much faster release profiles. Additionally, the hydrated compressive modulus of nanostructured gels is within experimental error of isotropic polymers despite the additional water content. Furthermore, the dry compressive modulus of nanostructured gels is about 70% greater than the corresponding isotropic control. The observed increases in mechanical properties and transport for nanostructure polymers are analogous to those seen in architected ceramics and cellular foams, where ordered assemblies provide greater mechanical stability and the continuous pores allow faster transport. These results may be used to develop hydrogels with highly-ordered nanostructures and property relationships useful in a growing number of advanced biological and industrial applications.

Notes

1. McMahon, T. T.; Zadnik, K. *Cornea* **2000**, *19*, 730-740.
2. Sagle, A. C.; Ju, H.; Freeman, B. D.; Sharma, M. M. *Polymer* **2009**, *50*, 756-766.
3. Wang, C.; Varshney, R. R.; Wang, D. *Adv. Drug Deliv. Rev.* **2010**, *62*, 699-710.
4. Anseth, K. S.; Bowman, C. N.; Brannon Peppas, L. *Biomaterials* **1996**, *17*, 1647-1657.
5. Peppas, N. A.; Khare, A. R. *Adv. Drug Deliv. Rev.* **1993**, *11*, 1-35.
6. Yang, S. F.; Leong, K. F.; Du, Z. H.; Chua, C. K. *Tissue Eng.* **2001**, *7*, 679-689.
7. Hoffman, A. S. *Adv. Drug Deliv. Rev.* **2002**, *54*, 3-12.
8. Ma, J.; Zhang, L.; Fan, B.; Xu, Y.; Liang, B. *J. Polym. Sci. Pt. B-Polym. Phys.* **2008**, *46*, 1546-1555.
9. Zhao, Q.; Sun, J.; Chen, S.; Zhou, Q. *J Appl Polym Sci* **2010**, *115*, 2940-2945.
10. Yin, L.; Fei, L.; Tang, C.; Yin, C. *Polym. Int.* **2007**, *56*, 1563-1571.
11. Sanabria-DeLong, N.; Agrawal, S. K.; Bhatia, S. R.; Tew, G. N. *Macromolecules* **2006**, *39*, 1308-1310.
12. Michler, G. H.; Balta-Calleja, F. J. *Mechanical Properties of Polymers based on Nanostructure and Morphology*; Taylor and Francis Group: Boca Raton, FL, 2005.
13. Clapper, J. D.; Guymon, C. A. *Macromolecules* **2007**, *40*, 1101-1107.
14. Forney, B. S.; Guymon, C. A. *Macromol. Rapid Commun.* **2011**, *32*, 765-769.
15. DePierro, M. A.; Carpenter, K. G.; Guymon, C. A. *Chem. Mat.* **2006**, *18*, 5609-5617.
16. Sievens-Figueroa, L.; Guymon, C. A. *Chem. Mat.* **2009**, *21*, 1060-1068.
17. Hentze, H. P.; Antonietti, M. *Curr. Opin. Solid State Mat. Sci.* **2001**, *5*, 343-353.
18. Clapper, J. D.; Sievens-Figueroa, L.; Guymon, C. A. *Chem. Mat.* **2008**, *20*, 768-781.
19. Antonietti, M.; Caruso, R. A.; Goltner, C. G.; Weissenberger, M. C. *Macromolecules* **1999**, *32*, 1383-1389.

20. Collings, P. J.; Hird, M. Introduction to Liquid Crystals: Chemistry and Physics. In *Identification of liquid crystal phases - mesophase characterization*; Gray, G. W., Goodby, J. W. and Fukuda, A., Eds.; Taylor & Francis Inc.: Bristol, PA, 1997; pp 177-190.
21. Texter, J. *Colloid Polym. Sci.* **2009**, *287*, 313-321.
22. DePierro, M. A.; Guymon, C. A. *Macromolecules* **2006**, *39*, 617-626.
23. Forney, B. S.; Guymon, C. A. *Macromolecules* **2010**, *43*, 8502-8510.
24. Guymon, C. A.; Bowman, C. N. *Macromolecules* **1997**, *30*, 5271-5278.
25. Lester, C. L.; Colson, C. D.; Guymon, C. A. *Macromolecules* **2001**, *34*, 4430-4438.
26. Lester, C. L.; Smith, S. M.; Jarrett, W. L.; Guymon, C. A. *Langmuir* **2003**, *19*, 9466-9472.
27. Sievens-Figueroa, L.; Guymon, C. A. *Polymer* **2008**, *49*, 2260-2267.
28. Hamid, S. M.; Sherrington, D. C. *Polymer* **1987**, *28*, 325-331.
29. Scherer, G. *J Am Ceram Soc* **1990**, *73*, 3-14.
30. Dinerman, A. A.; Cappello, J.; Ghandehari, H.; Hoag, S. W. *J. Controlled Release* **2002**, *82*, 277-287.
31. Feigin, L. A.; Svergun, D. I. Structure Analysis by Small Angle X-Ray and Neutron Scattering. In Taylor, G. W., Ed.; Plenum Press: New York, NY, 1987; pp 59-63.
32. Zhang, J.; Xie, Z.; Hill, A. J.; She, F. H.; Thornton, A. W.; Hoang, M.; Kong, L. X. *Soft Matter* **2012**, *8*, 2087-2094.
33. Lustig, S. R.; Peppas, N. A. *J Appl Polym Sci* **1988**, *36*, 735-747.
34. Mason, M. N.; Metters, A. T.; Bowman, C. N.; Anseth, K. S. *Macromolecules* **2001**, *34*, 4630-4635.
35. Ashby, M. *Philos. Trans. R. Soc. A-Math. Phys. Eng. Sci.* **2006**, *364*, 15-30.
36. Meuler, A. J.; Hillmyer, M. A.; Bates, F. S. *Macromolecules* **2009**, *42*, 7221-7250.
37. Wei, G.; Ma, P. X. *Adv. Funct. Mater.* **2008**, *18*, 3568-3582.
38. Gin, D. L.; Bara, J. E.; Noble, R. D.; Elliott, B. J. *Macromol. Rapid Commun.* **2008**, *29*, 367-389.

CHAPTER 6

FAST DESWELLING KINETICS OF NANOSTRUCTURED POLY(*N*-ISOPROPYLACRYLAMIDE) PHOTOPOLYMERIZED IN A LYOTROPIC LIQUID CRYSTAL TEMPLATE*

The thermal-response and mechanical properties of poly(*N*-isopropylacrylamide) (PNIPAm) are improved by controlling the polymer nanostructure through photopolymerization in a bicontinuous cubic lyotropic liquid crystal template. The bicontinuous cubic nanostructure increases the rate and amount of water expelled from PNIPAm for heating above the lower critical solution temperature (LCST) relative to an isotropic PNIPAm hydrogel while maintaining the mechanical integrity of the polymer. These results could allow development of PNIPAm hydrogels with proper water uptake, deswelling kinetics, volume transition, and mechanical properties required for successful performance in a growing number of advanced biological and industrial applications.

Introduction

Hydrogels that undergo reversible physical or chemical changes in response to external stimuli are generating significant research interest due to their potential application as artificial muscles, membranes, actuators, drug delivery vehicles, and chemical sensors.¹ Poly(*N*-isopropylacrylamide) (PNIPAm) is a widely investigated temperature responsive hydrogel that undergoes a reversible volume transition at a lower

* Forney, B. S.; Guymon, C. A. *Macromol. Rapid Commun.* **2011**, *32*, 765-769.

critical solution temperature (LCST) of 33 °C. PNIPAm can uptake significant quantities of water below the LCST and shrinks to expel water when heated above the LCST. The close proximity of PNIPAm LCST to common physiological temperatures may provide a promising method of controlling drug release using thermoregulation.² Unfortunately, a thick and dense polymer layer typically forms on the surface of traditional PNIPAm hydrogels at temperatures above the LCST and the deswelling rate is often too slow for many of the abovementioned applications which require a rapid response to external thermal stimuli.³ Herein, a bicontinuous nanostructure is generated in PNIPAm through photopolymerization in a lyotropic liquid crystal template yielding an increase in the volume transition rate and quantity of water expelled above the LCST relative to an isotropic PNIPAm hydrogel. The bicontinuous cubic nanostructure also significantly improves PNIPAm mechanical properties compared to traditional or macroporous PNIPAm hydrogels. Direct fabrication of nanostructured materials through photopolymerization in lyotropic liquid crystal templates may provide a promising method of optimizing the functionality of stimuli-responsive polymers useful in a growing number of advanced biological and industrial applications.

The slow deswelling kinetics of PNIPAm may be increased through various chemical and physical strategies. These strategies often increase the rate of deswelling by precluding the thick and dense polymer layer that forms on the gels surface above the LCST.⁴ For example, macroporous PNIPAm hydrogels have been synthesized by polymerization at high temperature, low pressure, or in mixed solvents to induce phase separation.⁵⁻⁷ The interconnected network of micrometer sized pores generated through the phase separation process can prevent the formation of the dense polymer layer and allow water to diffuse outward rapidly from PNIPAm above the LCST. Polymerization in the presence of pore-forming templates such as silicon spheres or surfactant stabilized emulsions can also generate porous structures in PNIPAm and increase the deswelling rate.⁸⁻¹⁰ Incorporating hydrophilic or surfactant polymers into PNIPAm networks

through grafting, copolymerization, or generating interpenetrating networks are promising chemical strategies to improve volume transition kinetics.¹¹⁻¹³ However, the increased deswelling rate produced by the above methods typically generates an undesirable decrease in mechanical properties or degree of water expulsion and compromises PNIPAm functionality in many applications such as actuators, chemical sensors, drug delivery vehicles, and artificial muscles which require a high degree of mechanical strength or large changes in volume.⁴

Although numerous methods of improving PNIPAm deswelling rate by controlling polymer microstructure are well-characterized, the utility of periodic nanometer-sized structures generated using self-assembling lyotropic liquid crystal (LLC) mesophases as polymerization templates to improve PNIPAm functionality has not been investigated. LLC mesophases are typically formed at high concentrations of low molecular weight surfactants that self-organize into geometries with nanometer dimensions in the presence of a solvent such as water. The hexagonal, bicontinuous cubic, and lamellar LLC phases formed at higher surfactant concentrations can be utilized as polymerization templates to control the morphology and properties of organic polymers. Interestingly, properties including water uptake, mechanical strength, and solute release rate may be controlled by directing polymer nanostructure using LLC mesophases as polymerization templates without changing the original polymer chemistry.¹⁴

The ordered nanometer-sized structures generated through polymerization in LLC mesophases can increase the equilibrium water uptake and swelling rate of hydrophilic polymers including poly(ethylene glycol) and poly(acrylamide) without sacrificing mechanical properties.^{15,16} In particular, the interconnected three-dimensional porous structure of the bicontinuous cubic LLC phase could better facilitate solvent transport through the polymer matrix relative to lower dimensionally ordered LLC phases such as the lamellar, hexagonal, or micellar phases.¹⁷ A network of interconnected nanometer-

sized pores could potentially improve water expulsion from PNIPAm above the LCST. Analogous to methods of synthesizing macroporous PNIPAm hydrogels using low surfactant concentrations or pore-forming templates to control the shrinkage rate, the periodic nanostructures generated through polymerization in a bicontinuous cubic LLC mesophase could generate a network structure with the long-range order necessary for rapid water expulsion. Additionally, the ordered bicontinuous cubic morphology may increase hydrogel water uptake below the LCST while preventing the significant and problematic decrease in mechanical properties typically observed in macroporous and traditional PNIPAm hydrogels.^{3,4} A mechanically robust PNIPAm hydrogel with a large volume transition and rapid thermal response would provide significant advantages in many biomedical and industrial applications.

Experimental

Materials

The monomers used in this study were *N*-isopropylacrylamide (97%, Aldrich) and *N,N'*-methylenebisacrylamide ($\geq 98\%$, Aldrich). The lyotropic liquid crystal was polyoxyethylene (2) cetyl ether (Brij 52, Aldrich). 2,2-Dimethoxy-1,2-diphenylethan-1-one (Irgacure 651, Ciba Specialty Chemicals) was used as the photoinitiator. Acetone ($\geq 99.5\%$, Aldrich) was also used as a solvent in this study. All materials were used as received.

Hydrogel Synthesis

Lyotropic liquid crystalline templated samples were prepared by mixing monomer, surfactant, photoinitiator, and water (19.5 wt.-% *N*-isopropylacrylamide, 0.5

wt.-% *N,N'*-methylenebisacrylamide, 50 wt.-% polyoxyethylene (2) cetyl ether, and 1 wt.-% photoinitiator with respect to monomer mass in deionized water). Isotropic solutions were prepared by dissolving monomer and photoinitiator in water (19.5 wt.-% *N*-isopropylacrylamide, 0.5 wt.-% *N,N'*-methylenebisacrylamide, and 1 wt.-% photoinitiator with respect to monomer mass in deionized water). Sample homogeneity was achieved using centrifugation, heat sonication, and vortex mixing. Polymer disks were prepared by pipetting samples into borosilicate molds (15 mm diameter, 3 mm height), purging the samples with nitrogen for 8 minutes, and irradiating samples with a medium pressure UV arc lamp (Ace Glass) with an intensity of 1.5 mW cm⁻² for 45 minutes. Samples were solvent-exchanged with acetone for 48 hours to remove unreacted monomer, photoinitiator, and surfactant and then dried under vacuum for 48 hours. Acetone was replaced periodically to facilitate surfactant removal. Overall surfactant removal was at least 95 % as measured gravimetrically.

Structure Characterization

Polymer nanostructure was characterized with a Nonius FR590 small angle X-ray scattering (SAXS) apparatus using a standard copper target Röntgen tube with a Ni-filtered Cu K α line of 1.54 Å as the radiation source, a collimation system of the Kratky type, and a PSD 50M position sensitive linear detector (Hecus M. Braun, Graz). The scattering vector, q , was calculated from the angle of the scattered radiation, 2θ , and the X-ray wavelength, λ , using eq. 6.1

$$q=4\pi\sin 2\theta/\lambda=2\pi/d \quad (6.1)$$

where d is the lattice or d -spacing. Phases were indexed by calculating the d -spacing ratios of scattering peaks. SAXS profiles were desmeared to correct for beam-height effects using a direct transform method described elsewhere.¹⁸

Network Swelling

Water uptake was studied gravimetrically by recording the mass of dried samples, immersing samples in excess deionized water in a temperature controlled oven, removing the sample at predetermined times, patting the surface dry with damp filter paper to remove surface water, and measuring the sample mass. Polymer disks were soaked in water for at least 96 hours at a given temperature and massed periodically to ensure equilibrium water uptake was attained. Hydrogel mass was used to calculate the percent water uptake, W , using eq. 6.2

$$W = (W_t - W_o)/W_o \times 100\% \quad (6.2)$$

where W_t is the mass of the hydrogel at time t and W_o is the mass of the dry polymer after solvent-exchange with acetone. At least three polymer disks were analyzed for swelling, deswelling, and mechanical property experiments to obtain the standard deviation for each data point represented by error bars in the presented figures.

Deswelling Kinetics

The rate of deswelling was investigated gravimetrically by transferring water swollen gels at 22 °C to a water bath maintained at 37 °C. At predetermined times the gel was removed from the water bath, patted with damp filter paper to remove surface water, and the sample mass was measured and used to calculate the percent water uptake.

Mechanical Properties

Compressive modulus of swollen polymer disks was calculated from the slope of stress-strain curves measured using dynamic mechanical analysis (TA instruments DMA Q800 series) at 22 °C.¹⁵ Samples were prepared by cutting 4 mm thick uniform disks

from water swollen gels. Swollen polymer disks were mounted on the compressive clamp of the DMA using a preload force of 0.05 N and compressed at a rate of 0.10 N min⁻¹. An independent two-sample *t*-test was used to compare the compressive moduli of swollen hydrogels at a confidence level of 95 %.

Results and Discussion

To improve the thermal response and mechanical properties of PNIPAm, a nanostructured PNIPAm hydrogel was synthesized by photopolymerizing *N*-isopropylacrylamide in a bicontinuous cubic LLC mesophase formed using the non-ionic surfactant polyoxyethylene (2) cetyl ether (Brij 52) in water. The self-organized bicontinuous cubic structure contains co-continuous hydrophilic and hydrophobic domains with nanometer-sized dimensions that may be used to segregate monomers into ordered geometries based on polarity. Specifically, water-soluble *N*-isopropylacrylamide monomers segregate primarily in the hydrophilic regions of the LLC template and adopt a geometry that directly resembles the bicontinuous cubic morphology.¹⁹ The fast initiation rates inherent in photopolymerization are then utilized to transfer the order of the parent LLC template to PNIPAm. After photopolymerization, the structure directing LLC template is removed by solvent-exchange, yielding a nanostructured PNIPAm hydrogel. Although direct fabrication of materials with bicontinuous cubic morphologies on the nano- and micrometer length scales is typically difficult and expensive, utilizing LLC mesophases as polymerization templates represents a potentially simple and inexpensive method of fabricating hydrogels containing a three-dimensional bicontinuous cubic structure with nanometer scale dimensions.²⁰

The morphology of PNIPAm photopolymerized in the bicontinuous cubic LLC mesophase was characterized using small angle X-ray scattering (SAXS). Figure 6.1

shows the SAXS profiles before and after photopolymerization of LLC templated *N*-isopropylacrylamide. The SAXS profile before polymerizations shows a strong primary peak with distinct secondary and tertiary reflections indicative of a highly-ordered bicontinuous cubic morphology.¹⁷ The same triply periodic structure, *d*-spacing ratios ($\sqrt{2}:\sqrt{3}:\sqrt{4}:\sqrt{6}$, *Pn3m*), and similar scattering intensity observed after photopolymerization supports that the original LLC template structure is retained during the polymerization

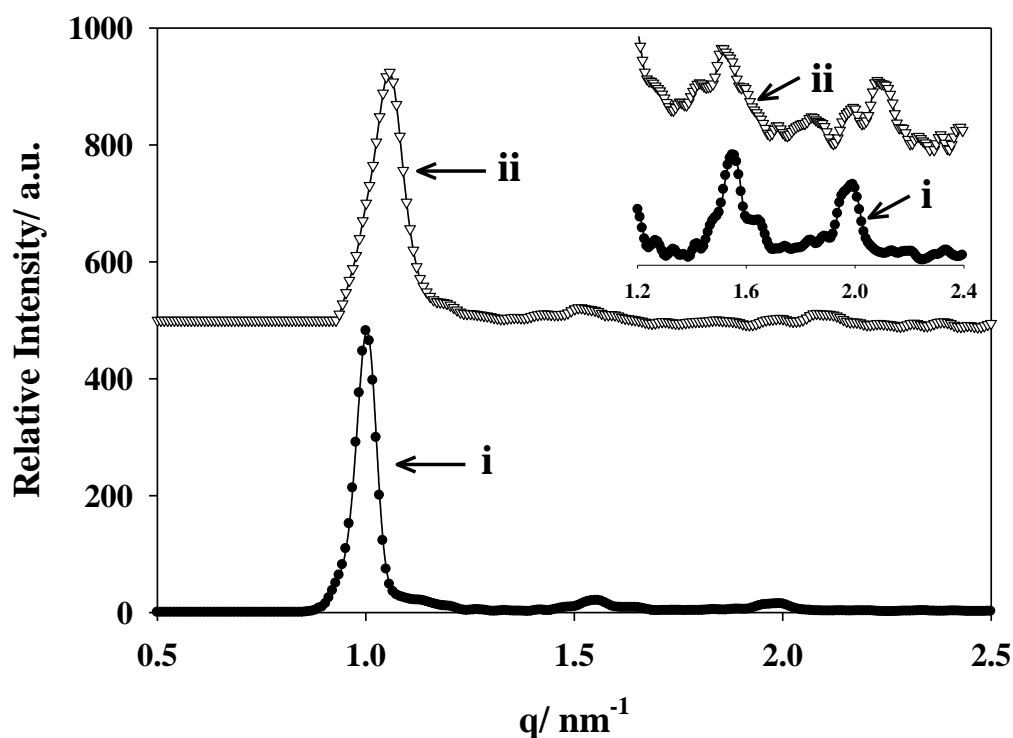


Figure 6.1. Small angle X-ray scattering profile of 20 wt.-% *N*-isopropylacrylamide (97.5 wt.-% *N*-isopropylacrylamide and 2.5 wt.-% *N,N'*-methylenebisacrylamide mixture) templated in the bicontinuous cubic LLC mesophase formed with 50 wt.-% polyoxyethylene (2) cetyl ether in water. Shown are SAXS profiles (i) before (●) and (ii) after (∇) photopolymerization. Inset shows higher order scattering peaks.

reaction and the resulting PNIPAm hydrogel has adopted a bicontinuous cubic morphology.

The impact of cubic nanostructure on PNIPAm properties was examined by measuring the equilibrium water uptake at different temperatures. For comparison, the water uptake of an isotropic PNIPAm hydrogel prepared by photopolymerization in water was also examined. The polymers were solvent-exchanged with acetone to remove unreacted monomer, photoinitiator, and LLC surfactant template to yield PNIPAm hydrogels with the same basic chemical composition. Figure 6.2a shows the equilibrium percent water uptake of nanostructured and isotropic PNIPAm for temperatures between 22 and 45 °C. Interestingly, the swelling behavior of nanostructured PNIPAm is significantly different than the isotropic hydrogel at the temperatures studied. Although each hydrogel is highly swollen below 33 °C, the bicontinuous cubic templated hydrogel absorbs 400 wt.-% more water than isotropic PNIPAm at 22 °C. The equilibrium percent water uptake decreases sharply around 33 °C for each polymer and no apparent difference in LCST between hydrogels is observed. Thermal scans obtained using differential scanning calorimetry verifies further that the LCST of the hydrogels are very similar at approximately 33 °C.

The bicontinuous cubic nanostructure also impacts the amount of water expelled from PNIPAm. For example, LLC templated PNIPAm loses almost 900 wt.-% water when heated from 22 to 37 °C. On the other hand, the water loss of isotropic PNIPAm for the same change in temperature is only about 200 wt.-%. The similar LCST of the hydrogels supports that their chemical composition is virtually identical and differences in water uptake are likely due to contrasting polymer morphologies.

To elucidate the impact of bicontinuous cubic nanostructure on PNIPAm deswelling kinetics, the water loss of hydrogels after transfer to temperatures above the LCST was examined. Figure 6.2b shows the weight percent water as a function of time

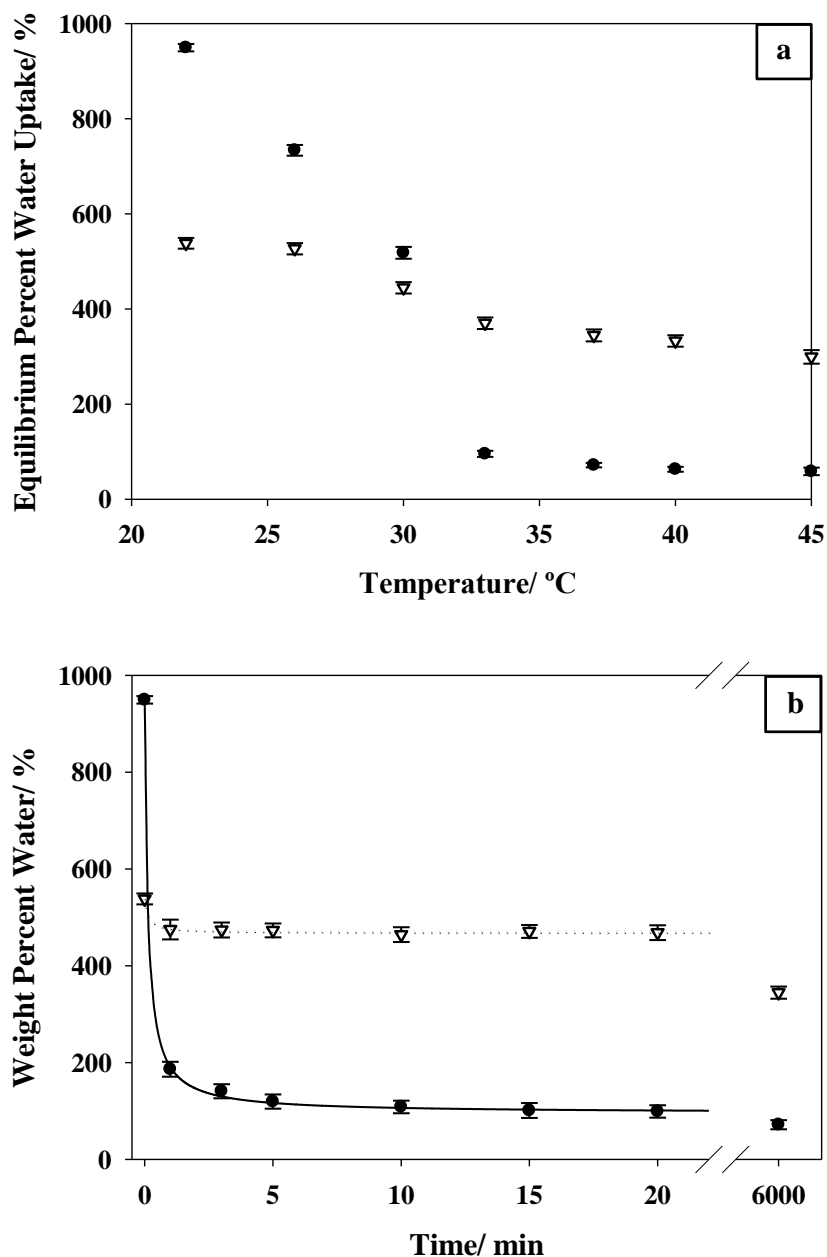


Figure 6.2. Equilibrium water uptake for polymer hydrogels. Shown are a) Equilibrium percent water uptake as a function of temperature for isotropic (∇) and bicontinuous cubic LLC templated (●) PNIPAM hydrogels. (b) Weight percent water of isotropic (∇) and bicontinuous cubic LLC templated (●) PNIPAM hydrogels as a function of time after transfer from 22 to 37 °C water at time zero. Trendlines represent least squares curve fits.

for the isotropic and nanostructured PNIPAm hydrogels after transfer from water at 22 °C to 37 °C. The deswelling rate of nanostructured PNIPAm photopolymerized in the LLC template is much faster than the isotropic hydrogel. Specifically, nanostructured PNIPAm loses at least 750 wt.-% water in 1 minute while the isotropic gel expels only 50 wt.-% water over the same time frame. Furthermore, LLC templated PNIPAm loses an additional 90 wt.-% water between 1 and 20 minutes while no further water loss is detected for the isotropic PNIPAm control. As is apparent from the deswelling kinetics presented in Figure 6.2b, the symmetry inherent in the bicontinuous cubic mesophase improves water transport through an open-network of interconnected nanometer sized pores and increases the rate and amount of water expelled from PNIPAm above the LCST.¹⁷

In addition to the increase in deswelling rate and amount of water lost, the bicontinuous cubic nanostructure also significantly improves PNIPAm mechanical properties. Figure 6.3 shows the compressive stress-strain profiles of the water swollen LLC templated and isotropic PNIPAm hydrogels at 22 °C. Interestingly, the stress-strain profiles for both hydrogels are very similar. The comparable slopes of the stress vs. strain curves indicate there is little difference in hydrogel mechanical properties. Despite absorbing 400 wt.-% more water, the compressive modulus of nanostructured PNIPAm is not statistically different than the isotropic PNIPAm control. This differs from mechanical behavior typically observed in conventional hydrogels where an increase in water uptake results in substantial decreases in compressive modulus. In fact, a similar difference in water uptake can generate a three-fold difference in the compressive modulus between isotropic hydrogels.²¹ The exceptionally large compressive modulus of nanostructured PNIPAm is likely due to the continuous network of ordered polymer domains as directed by the bicontinuous cubic LLC template that combine to resist mechanical deformation.²² These results demonstrate that directing PNIPAm

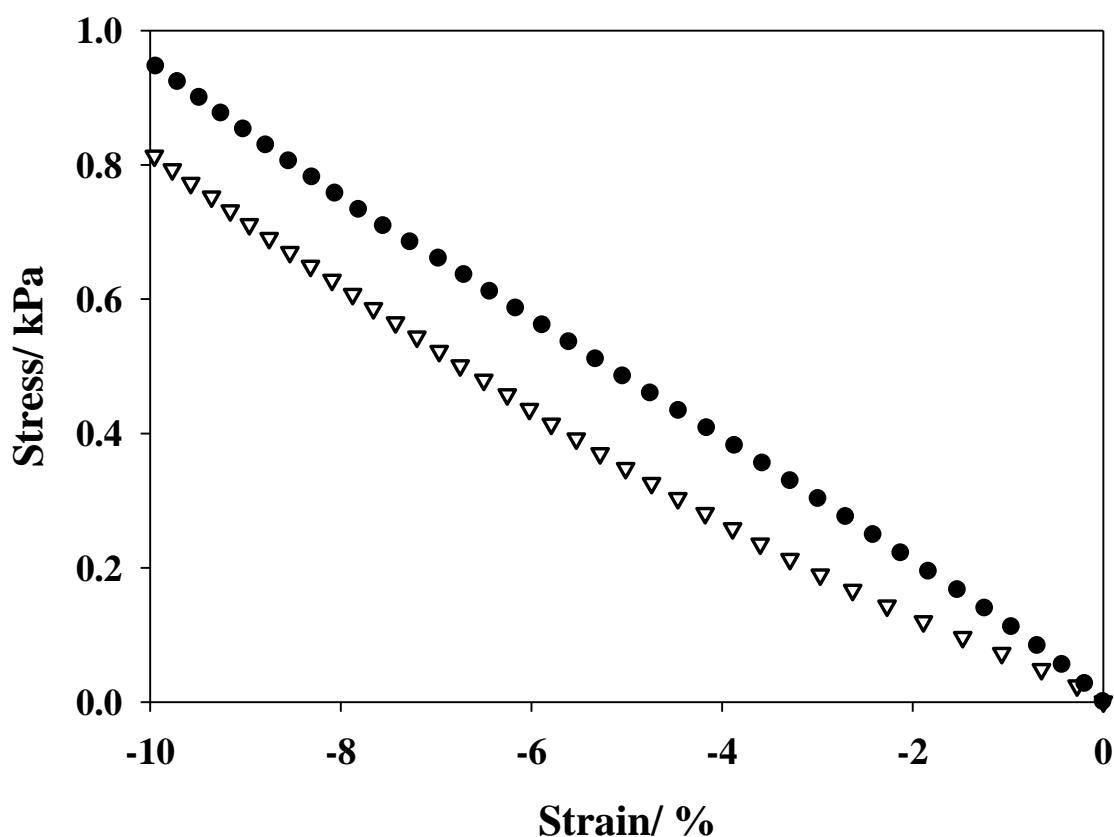


Figure 6.3. Stress-strain profiles for water swollen hydrogels. Shown are typical stress vs. strain curves of water swollen isotropic (▽) and bicontinuous cubic LLC templated (●) PNIPAm hydrogels at 22 °C. No statistically significant difference in compressive modulus between the isotropic (2.42 ± 0.29 kPa) and bicontinuous cubic LLC templated (2.64 ± 0.39 kPa) hydrogels is observed as determined using a *t*-test at a confidence level of 95 %.

nanostructure utilizing LLC mesophases as polymerization templates can greatly increase the rate and degree of PNIPAm deswelling without compromising the mechanical integrity of the network. Additionally, the properties of nanostructured PNIPAm address a major drawback reported for macroporous or traditional PNIPAm hydrogels where an increase in water uptake can considerably weaken the polymer network or reduce the degree of water expulsion.^{3,4}

Conclusions

In summary, a nanostructured PNIPAm hydrogel was directly fabricated by photopolymerization in a bicontinuous cubic LLC template. The bicontinuous cubic nanostructure of PNIPAm increases the (1) water uptake at temperatures below the LCST, (2) rate of deswelling above the LCST, and (3) amount of water expelled above the LCST relative to an isotropic PNIPAm hydrogel of the same chemical composition while (4) maintaining the mechanical integrity of the polymer network. The improved performance of nanostructured PNIPAm is likely due to the ordered network of interconnected pores as directed by the bicontinuous cubic LLC template. These results could allow development and optimization of PNIPAm hydrogels with proper water uptake, deswelling kinetics, volume transition, and mechanical properties required for successful performance in a growing number of advanced biological and industrial applications.

Notes

1. Stuart, M. A. C.; Huck, W. T. S.; Genzer, J.; Mueller, M.; Ober, C.; Stamm, M.; Sukhorukov, G. B.; Szleifer, I.; Tsukruk, V. V.; Urban, M.; Winnik, F.; Zauscher, S.; Luzinov, I.; Minko, S. *Nat. Mater.* **2010**, *9*, 101-113.
2. Chaterji, S.; Kwon, I. K.; Park, K. *Prog. Polym. Sci.* **2007**, *32*, 1083-1122.
3. Liu, F.; Urban, M. W. *Prog. Polym. Sci.* **2010**, *35*, 3-23.
4. Zhang, X.; Xu, X.; Cheng, S.; Zhuo, R. *Soft Matter* **2008**, *4*, 385-391.
5. Takata, S.; Suzuki, K.; Norisuye, T.; Shibayama, M. *Polymer* **2002**, *43*, 3101-3107.
6. Zhang, X. Z.; Wang, F. J.; Chu, C. C. *J. Mater. Sci. -Mater. Med.* **2003**, *14*, 451-455.
7. Laszlo, K.; Kosik, K.; Rochas, C.; Geissler, E. *Macromolecules* **2003**, *36*, 7771-7776.
8. Wu, X. S.; Hoffman, A. S.; Yager, P. *J. Polym. Sci. Pol. Chem.* **1992**, *30*, 2121-2129.
9. Serizawa, T.; Wakita, K.; Akashi, M. *Macromolecules* **2002**, *35*, 10-12.
10. Zhang, J.; Jandt, K. D. *Macromol. Rapid Commun.* **2008**, *29*, 593-597.
11. Yoshida, R.; Uchida, K.; Kaneko, Y.; Sakai, K.; Kikuchi, A.; Sakurai, Y.; Okano, T. *Nature* **1995**, *374*, 240-242.
12. Kaneko, Y.; Yoshida, R.; Sakai, K.; Sakurai, Y.; Okano, T. *J. Membr. Sci.* **1995**, *101*, 13-22.
13. Kaneko, Y.; Nakamura, S.; Sakai, K.; Aoyagi, T.; Kikuchi, A.; Sakurai, Y.; Okano, T. *Macromolecules* **1998**, *31*, 6099-6105.
14. Clapper, J. D.; Sievens-Figueroa, L.; Guymon, C. A. *Chem. Mat.* **2008**, *20*, 768-781.
15. Lester, C. L.; Smith, S. M.; Colson, C. D.; Guymon, C. A. *Chem. Mat.* **2003**, *15*, 3376-3384.
16. Clapper, J. D.; Guymon, C. A. *Macromolecules* **2007**, *40*, 1101-1107.
17. Hatakeyama, E. S.; Wiesenauer, B. R.; Gabriel, C. J.; Noble, R. D.; Gin, D. L. *Chem. Mat.* **2010**, *22*, 4525-4527.
18. Singh, M. A.; Ghosh, S. S.; Shannon, R. F. *J. Appl. Crystallogr.* **1993**, *26*, 787-794.

19. Lester, C. L.; Smith, S. M.; Jarrett, W. L.; Guymon, C. A. *Langmuir* **2003**, *19*, 9466-9472.
20. Matthew N. Lee; Ali Mohraz *Adv Mater* **2010**, *22*, 4836-4841.
21. Anseth, K. S.; Bowman, C. N.; BrannonPeppas, L. *Biomaterials* **1996**, *17*, 1647-1657.
22. Meuler, A. J.; Hillmyer, M. A.; Bates, F. S. *Macromolecules* **2009**, *42*, 7221-7250.

CHAPTER 7

**IMPROVED STIMULI-RESPONSE AND MECHANICAL
PROPERTIES OF NANOSTRUCTURED POLY(*N*-
ISOPROPYLACRYLAMIDE-CO-DIMETHYLSILOXANE)
HYDROGELS GENERATED THROUGH
PHOTOPOLYMERIZATION IN LYOTROPIC LIQUID CRYSTAL
TEMPLATES**

Temperature sensitive poly(*N*-isopropylacrylamide) (PNIPAM) hydrogels are the most widely studied stimuli-responsive systems due to their significant volume changes at biologically relevant temperatures and wide range of applications including drug delivery, cell cultures, chemical sensors, and desalination systems. The successful performance of PNIPAM gels often requires a rapid response rate when heated above the lower critical solution temperature with a significant degree of deswelling. However, it is often difficult to design PNIPAM hydrogels with appropriate mechanical strength for the gels to remain functional in a working environment. Herein, lyotropic liquid crystals (LLCs) are utilized to generate a hexagonal nanostructure in PNIPAM hydrogels in order to improve material properties and transport characteristics. Methacrylated poly(dimethylsiloxane) (PDMS) was incorporated into PNIPAM gels at varying concentrations through photopolymerization in the hexagonal LLC phase in order to modulate water content and mechanical properties. The hexagonal LLC nanostructure dramatically increases hydrogel deswelling rate compared to traditional isotropic PNIPAM-PDMS hydrogels of the same chemical composition. Additionally, the ordered LLC structure allows for considerable incorporation of PDMS into the hydrogel without significantly decreasing the water content of the gels. Interestingly, the hexagonal

nanostructured hydrogels exhibit similar compressive moduli compared to isotropic hydrogel controls despite having considerably higher water content. These results may be utilized to generate stimuli-sensitive hydrogels with the proper rate and degree of deswelling while maintaining the necessary mechanical integrity of the gel for use in numerous biomedical and industrial applications.

Introduction

Polymers that demonstrate physical or chemical changes in response to external stimuli are generating significant research interest due to their potential use in a wide variety of applications ranging from drug-delivery systems to chemical sensors.¹⁻³ Critical to the proper functioning of these materials is a rapid response to changes in external stimuli. Poly(*N*-isopropylacrylamide) (PNIPAM) has been extensively examined as a temperature sensitive polymer. The water molecules associated with the isopropyl moiety are expelled into the bulk solution when PNIPAM is heated above a critical temperature. The temperature at which PNIPAM transitions from a hydrophilic polymer that can uptake significant quantities of water to a hydrophobic polymer that expels water from the matrix is known as the lower critical solution temperature (LCST). For PNIPAM the LCST is approximately 32 °C and can be increased above and below human body temperature by co-polymerization with various hydrophilic monomers, making PNIPAM particularly well-suited for a variety of biomedical applications. Unfortunately, the deswelling rate of traditional PNIPAM hydrogels is often too slow for many uses that require a rapid response to thermal stimuli.

Several factors are critical in determining the performance of stimuli-sensitive polymers.⁴ These include the rate of response to changes in environmental conditions, the dynamic range of physical change in response to stimuli, and the mechanical

properties of the polymer at all stages of the transition.⁵ Appropriate mechanical stability is especially important as properties such as water content, volume, and modulus can change quite dramatically through the phase transition.⁶ The modulus of hydrogels depends significantly on water content and even small differences in water content can generate substantial changes in mechanical properties. For example, it is common for the modulus of PNIPAM hydrogels to decrease two or more orders of magnitude when the hydrogel is cooled below the LCST. The significant volume of water that PNIPAM hydrogels absorb below the LCST considerably compromises the strength of the material and can limit the functionality of the gel.

The large change in PNIPAM mechanical strength at the transition temperature is directly related to the amount of water expelled or absorbed.⁶ In order to achieve sufficient mechanical stability in PNIPAM hydrogels, the degree of crosslinking of the material can be controlled. Additionally, incorporating particular monomers or moieties into the polymer network through copolymerization or grafting onto polymer chains has been used to produce desired material properties.⁷⁻⁹ Crosslinking PNIPAM does modulate the mechanical properties of the gel, but also significantly restricts the magnitude of the volume transition. Controlling the chemistry of the PNIPAM network by incorporating particular moieties into or onto the polymer backbone can also generate PNIPAM hydrogels with a very wide range of properties.¹⁰ In fact, PNIPAM hydrogels with appropriate mechanical properties are readily achieved using these strategies of controlling hydrogel chemistry and crosslinking density. However, the changes in water uptake both above and below the LCST as well as the dynamics of the transition are inevitably compromised when the chemistry of the network is modulated using these methods. For example, researchers have examined incorporation of poly(dimethylsiloxane) (PDMS) into the PNIPAM polymer network to increase the mechanical toughness of the gel.^{11,12} However, incorporating even small concentrations into the network can dramatically decrease the dynamic range and magnitude of

deswelling from the network upon heating above the LCST due to the hydrophobicity of PDMS. For example, PNIPAM has been crosslinked with a multifunctional epoxide terminated oligomeric silsesquioxane in order to improve hydrogel performance.¹³ Incorporating just 20 wt % of the oligomeric silsesquioxane decreased the water uptake below the LCST nearly a factor of five and significantly decreased the quantity of water expelled for heating above the LCST, illustrating the sensitivity of PNIPAM properties on the concentration of hydrophobic crosslinking agents.

A PNIPAM hydrogel with mechanical properties that could be tuned over a large range without significantly compromising the degree of water uptake below the LCST or the rate of volume transition for heating above the LCST is highly desirable and would facilitate expanded use of temperature sensitive gels.¹⁴ To overcome the difficulties in designing PNIPAM hydrogels with the proper degree of deswelling, rapid response rate, and mechanical stability, methods of modulating material properties in a manner that does not give rise to traditional changes in polymer properties may be useful.¹⁵ Controlling polymer nanostructure in order to modulate material properties is receiving significant research interest due to the strong dependence of mechanical and transport properties on the morphology of the polymer network.¹⁶ In particular, photopolymerization of monomers in lyotropic liquid crystal (LLC) phases has generated nanostructured polymers with properties that are much different than isotropic polymers.^{15,17-21} For example, the bicontinuous cubic LLC phase has been utilized to generate a cubic morphology in a PNIPAM hydrogel.²² The bicontinuous cubic nanostructure dramatically increases both the rate and degree of volume transition for heating above the LCST compared to a traditional PNIPAM gel. Additionally, the bicontinuous cubic nanostructured system absorbs over 400 wt % more water than an isotropic control below the LCST and the compressive modulus of the LLC gel was not compromised. This behavior is very atypical of traditional hydrogel systems where such

a similar difference in water uptake between isotropic gels can generate over a three-fold decrease in mechanical strength.⁶

LLC templating can be used to control the morphology of organic polymers by utilizing the self-assembled surfactant mesophases as structure directing polymerization platforms.²³⁻²⁸ The parent LLC template may be used to segregate monomers into ordered geometries based on their solubility in the mesophase. Photopolymerization has shown great promise in curing the polymer and transferring the order of the mesophase to the final polymer network.^{17,19,22,29-32} This templating method has been utilized to generate nanophase separated polymers containing two distinct polymer chemistries. Similar to interpenetrating networks (IPNs), the nanophase separated polymer composite may be designed to contain two discrete polymer networks that impart particular properties inherent to the individual polymers in the final material. For example, the hexagonal LLC phase has been used to generate an IPN-like polymer network using the two immiscible monomers hexanediol diacrylate (HDDA) and poly(ethylene glycol) diacrylate (PEGDA).³³ The polar PEGDA network was confined primarily to the continuous domain of the hexagonal LLC mesophase while the hydrophobic HDDA network was segregated in the discontinuous cores of hexagonal packed cylinders. This hexagonal IPN nanocomposite imparted useful properties associated with each polymer network to the final working polymer. Specifically, the continuous PEGDA hydrogel domain provided an interconnected polymer network that was capable of absorbing water while the discontinuous HDDA network imparted mechanical stability to the polymer composite.

The LLC templating process can generate IPN copolymers with properties of multiple polymer networks can be of great use in improving the properties of stimuli-sensitive PNIPAM hydrogels. Generating a LLC nanostructured and continuous PNIPAM network could facilitate water uptake by providing a directed route for water to access the polymer pores and void space. The directed pore structure and improved void

space accessibility are often the reported mechanisms of increased water uptake for nanostructured hydrogels fabricated using LLCs as photopolymerization templates.^{17-19,22} The directed pore structure can also increase the transport of water through the network by decreasing the tortuosity and diffusion resistance through an aligned pore structure produced by the LLC templating process. A separate discontinuous polymer network may also be incorporated into the polymer using LLC templating to improve the mechanical stability of the hydrogel without interfering with the transport or water uptake PNIPAM hydrogel network. This would result in an IPN copolymer that contained the stimuli-responsive properties of PNIPAM hydrogels with the inherent mechanical stability of tough polymer materials such as PDMS. A PNIPAM hydrogel with a wide dynamic range, fast deswelling rate, and appropriate degree of mechanical stability is of great utility in many biomedical applications.^{5,12,34}

In this study, the hexagonal LLC mesophase is utilized to generate nanostructured IPN PNIPAM-PDMS copolymers containing a continuous PNIPAM domain to increase transport and water uptake and a discontinuous PDMS domain to impart mechanical stability to the network. Numerous studies have demonstrated increases in water uptake, transport, and mechanical strength for polymers containing LLC morphologies.^{17,19-22,32,35} It is hypothesized that generating a LLC nanostructure will lessen the impact of PDMS on the degree of water uptake while allowing a high-degree of mechanical stability. A continuous and directed hexagonal pore structure produced by the LLC templated process has been used to improve the swelling and transport properties of PNIPAM hydrogels.¹⁷ Additionally, a PDMS network is incorporated into the discontinuous domains of the hexagonal LLC mesophase to generate an nanostructured IPN copolymer in order to increase the mechanical properties of the hydrogel without significantly compromising the degree of water uptake below the LCST. The utility of the hexagonal LLC mesophase in generating IPN materials with the stimuli-sensitive properties of PNIPAM and mechanical stability of PDMS is examined in this work by characterizing equilibrium

swelling, deswelling rate, and compressive modulus of the hydrogels at varying concentrations of PNIPAM and PDMS. The performance of isotropic controls containing the same chemical composition of IPN nanostructured materials are also characterized to elucidate the impact of network structure on the properties of PDMS-PNIPAM copolymers. The hexagonal LLC mesophase provides an ideal platform for the synthesis of interpenetrating networks of PDMS and PNIPAM that can be utilized to tune the mechanical properties as well as the degree of deswelling for heating above the LCST.³³ It is expected that the nanostructure will provide a more directed route for water transport from the polymer matrix for heating above the LCST, thereby increasing the rate of deswelling. A mechanically stable PNIPAM hydrogel with a fast response rate and significant degree of water uptake is of substantial use in a growing number of industrial and biomedical applications.

Experimental

Materials

Hydrogel forming monomers used included *N*-isopropylacrylamide (97%, Aldrich) and the crosslinker *N,N'*-methylenebisacrylamide (99%, Aldrich). The methacrylate terminated siloxane monomer (DMS-R18, MW 4500-5500, Gelest) was used to incorporate siloxane linkages into the hydrogel. The non-ionic surfactant polyoxyethylene (2) cetyl ether (Brij 52, Aldrich) was used to generate the lyotropic liquid crystalline phase in deionized water. The photoinitiator 2-hydroxy-2-methyl-1-phenyl-propan-1-one (Darocur 1173, Ciba Specialty Chemicals) was used to initiate polymerization. All chemicals were used as received.

Sample Preparation

Lyotropic liquid crystalline templated samples were prepared by mixing particular concentrations of monomer, surfactant, deionized water, and photoinitiator. LLC templated samples contained 50 wt % Brij 52 surfactant, 40 wt % monomer, and 1 wt % photoinitiator with respect to monomer mass in water. The ratio of *N*-isopropylacrylamide to DMS-R18 monomer was varied to modulate the siloxane content of the hydrogels. The concentration of the crosslinker *N,N'*-methylenebisacrylamide was maintained at approximately 6 wt % of the *N*-isopropylacrylamide concentration. For isotropic samples, the phase forming Brij 52 surfactant and water was replaced with an equivalent mass of isopropyl alcohol which dissolves the monomer system and does not form an LLC phase with monomer and photoinitiator concentrations equal to that of the analogous LLC templated sample. Sample homogeneity was achieved using centrifugation, mechanical agitation, heat, sonication, and vortex mixing. Polymer disks were prepared by transferring samples into polystyrene molds, purging the samples with nitrogen for 8 minutes, and irradiating samples with a medium pressure UV arc lamp (Ace Glass) at an intensity of 2.5 mW/cm². Samples were solvent-exchanged with isopropyl alcohol for at least 48 hours to remove unreacted monomer, photoinitiator, and surfactant. The samples were then sandwiched between Mylar (DuPont) sheets to slow solvent evaporation and prevent cracking while under vacuum.³⁶ Overall surfactant removal was greater than 95% as measured gravimetrically. Three or more polymer disks were prepared for each sample formulation and analyzed in water uptake and deswelling experiments to obtain the standard deviation for each data point represented by error bars in the presented figures. The reported siloxane concentration reported on the x-axis for several of the plots in this work represents the total weight percent siloxane in the polymer after removal of surfactant by solvent exchange and drying.

Structural Characterization

Polymer nanostructure was characterized with a Nonius FR590 small angle X-ray scattering (SAXS) apparatus using a standard copper target Röntgen tube with a Ni-filtered Cu K α line of 1.54 Å as the radiation source, a collimation system of the Kratky type, and a PSD 50M position sensitive linear detector (Hecus M. Braun, Graz). Phases were indexed by calculating the *d*-spacing ratios of scattering peaks. Diffraction profiles of the hexagonal phase exhibit a *d*-spacing ratio of 1:1/√3:1/√4... (corresponding to d_{100} , d_{110} , d_{200} ,...). The scattering vector, *q*, was calculated from the angle of the scattered radiation and the X-ray wavelength.

Equilibrium Water Uptake

Water uptake was studied gravimetrically by recording the mass of dried samples, immersing samples in excess deionized water at a particular temperature, removing the sample at predetermined times, patting the surface dry with damp filter paper to remove surface water, and measuring the sample mass. Hydrogel mass was used to calculate the percent water uptake, *W*, using equation 7.1

$$W = (W_t - W_o)/W_o \times 100\% \quad (7.1)$$

where W_t is the mass of the hydrogel at time *t* and W_o is the mass of the polymer after solvent-exchange with isopropyl alcohol and drying. Polymer disks were maintained at a given temperature for at least three days in order to assure equilibrium water uptake was achieved. Equilibrium was assumed to be reached when no significant change in water uptake was observed for measurements taken 48 hours apart.

Deswelling Kinetics

Deswelling kinetics were measured by recording the mass of water swollen hydrogel disks at 22 °C. The equilibrium swollen disks were then transferred to a water bath maintained at 37 °C. At predetermined times, hydrogel masses were measured as described above and hydrogel masses were used to determine the percent water uptake using equation 1.

Mechanical Properties

The hydrated compressive modulus was calculated from the initial slopes of the stress vs. strain profiles using equation 7.2

$$G = \sigma / (\lambda - \lambda^{-2}) \quad (7.2)$$

where G is the compressive modulus, σ is the stress, and λ is the relative deformation.⁶ Hydrogel disks were prepared as described previously and allowed to equilibrate in water at 22 °C. Swollen hydrogel disks were mounted on the compressive clamp of the dynamic mechanical analyzer (DMA Q800 Series) at 22 °C using a preload force of 0.1N while the force was continually ramped at a rate of 0.5 N·min⁻¹. At least three polymer disks were analyzed and used to calculate the standard deviation.

Results and Discussion

The proper functionality of temperature sensitive PNIPAM hydrogels requires a delicate balance between the rate and degree of deswelling in response to thermal stimuli as well as a proper degree of mechanical strength to withstand the stresses of the working environment.¹² However, it is difficult to generate higher mechanical strength without

eliciting significant and undesirable changes in other properties including dynamic range of water uptake and rate of deswelling. Oftentimes, a compromise between the desired hydrogel properties is required in order for the hydrogel to remain functional. Herein, the ordered nanostructured domains generated through photopolymerization in a LLC template are utilized to improve PNIPAM hydrogel properties. We hypothesize that the improved water uptake and transport properties often observed in LLC templated hydrogels will allow control over the mechanical properties through incorporation of PDMS into the polymer network and promote a rapid response rate and large degree of water uptake.

Figure 7.1 shows a representation of the LLC templating process utilized to generate a hexagonal nanostructure in the PDMS-PNIPAM hydrogels. The LLC surfactant template contains both polar and non-polar domains that may be used to segregate monomers into ordered geometries based on their polarity.¹⁹ For example, when polar *N*-isopropylacrylamide is introduced to the hexagonal mesophase the monomers will likely preferentially segregate into the continuous water-soluble domains of the template and adopt a geometry that directly resembles that of the LLC phase. Likewise, hydrophobic PDMS monomers will primarily segregate in the discontinuous oil-soluble domains of the hexagonal template. Photopolymerization is then utilized to transfer the order of the LLC parent template to the polymer, followed by subsequent removal of the non-reactive surfactant template by solvent exchange. This process has been utilized to generate nanostructured hydrogels that display enhanced transport properties including greater water uptake, faster dye release, and increased deswelling rate of PNIPAM gels for heating above the LCST.^{17,18,20,31}

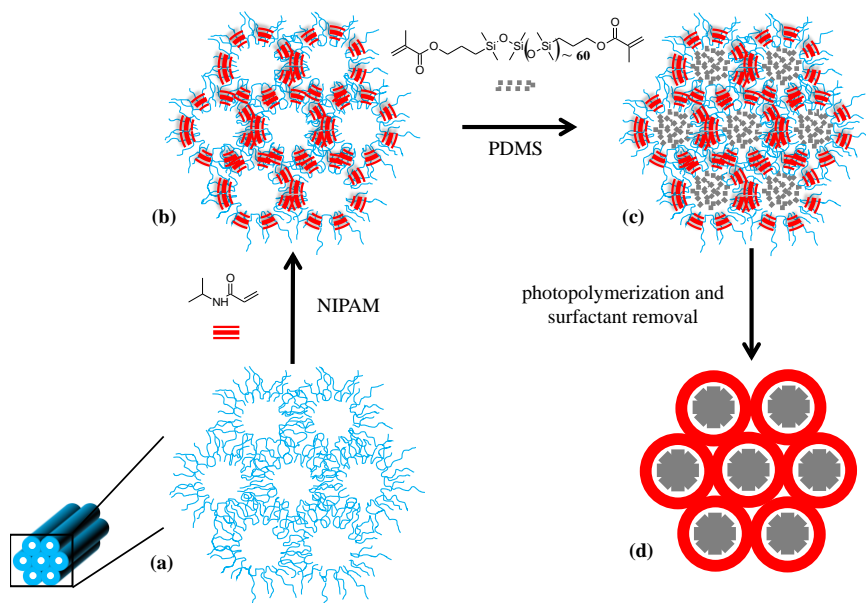


Figure 7.1. Representative LLC templating process used to generate a hexagonal nanostructure in PDMS-PNIPAM hydrogels. Shown clockwise from the bottom left is (a) cross-section of the hexagonal phase, (b) segregation of polar *N*-isopropylacrylamide in the continuous water-soluble domains of the template, (c) segregation of non-polar PDMS monomers in the discontinuous oil-soluble domains of the template, (d) photopolymerization of monomers and removal of the non-reactive surfactant template.

The nanostructure of LLC templated PDMS-PNIPAM hydrogels was characterized before and after photopolymerization using small angle X-ray scattering (SAXS) to determine the degree of LLC order transferred to the polymer during the polymerization reaction. The degree of structure retention was examined by comparing the positions and ratios of scattering peaks in SAXS profiles before and after polymerization. The ratio of PDMS to *N*-isopropylacrylamide was varied to achieve a range of water content and mechanical properties. Figure 7.2 shows the SAXS profiles for LLC templated PDMS-PNIPAM hydrogels before and after polymerization containing different concentrations of PDMS. In all the SAXS profiles shown in Figure 7.2, a strong primary reflection is observed both before and after polymerization, suggesting that a significant degree of nanostructure is transferred to the working

polymer.³¹ Moreover, a ratio of scattering peaks indicative of the hexagonal phase ($1:1/\sqrt{3}:1/\sqrt{4}...$) is clearly observed before and after polymerization.

The position of the primary scattering peak shifts to slightly higher scattering vectors after polymerization for all concentrations of PDMS examined. Shifts in the positions of primary scattering peaks to higher scattering vectors corresponds to a decrease in the d -spacing in the systems and is likely due to polymerization induced shrinkage. Interestingly, the ratio of PDMS to PNIPAM does not have a significant impact on the morphology of the system as the ratio of scattering peaks indicative of the hexagonal phase is observed before and after polymerization for all PDMS concentrations examined. Although PDMS concentration does not impact the formation of the hexagonal LLC mesophase, it does appear to have a slight impact on the intensity of the primary scattering peak after curing the polymer. The intensity of the scattering peak observed in the SAXS profiles after polymerization increases with PDMS concentration which may be due to the higher electron density contrast of the PDMS polymer that gives rise to the observed increase in primary scattering peak intensity.³⁷ The strong primary reflection and consistent ratio of scattering peaks observed before and after polymerization indicates that the original LLC structure is retained during polymerization and the polymer has adopted a hexagonal structure.

It is apparent from the SAXS profiles in Figure 7.2 that the hexagonal LLC structure is retained throughout photopolymerization at all concentrations of PDMS examined. To determine the impact of the hexagonal nanostructure of IPN hydrogels containing distinct PDMS and PNIPAM domains, the equilibrium water uptake at different temperatures was characterized. For comparison, the equilibrium water uptake of isotropic hydrogel controls containing the same chemical composition as LLC templated samples was also characterized. These controls were synthesized by replacing the phase forming Brij 52 surfactant and water with isopropyl alcohol and exhibit no observed nanostructure.

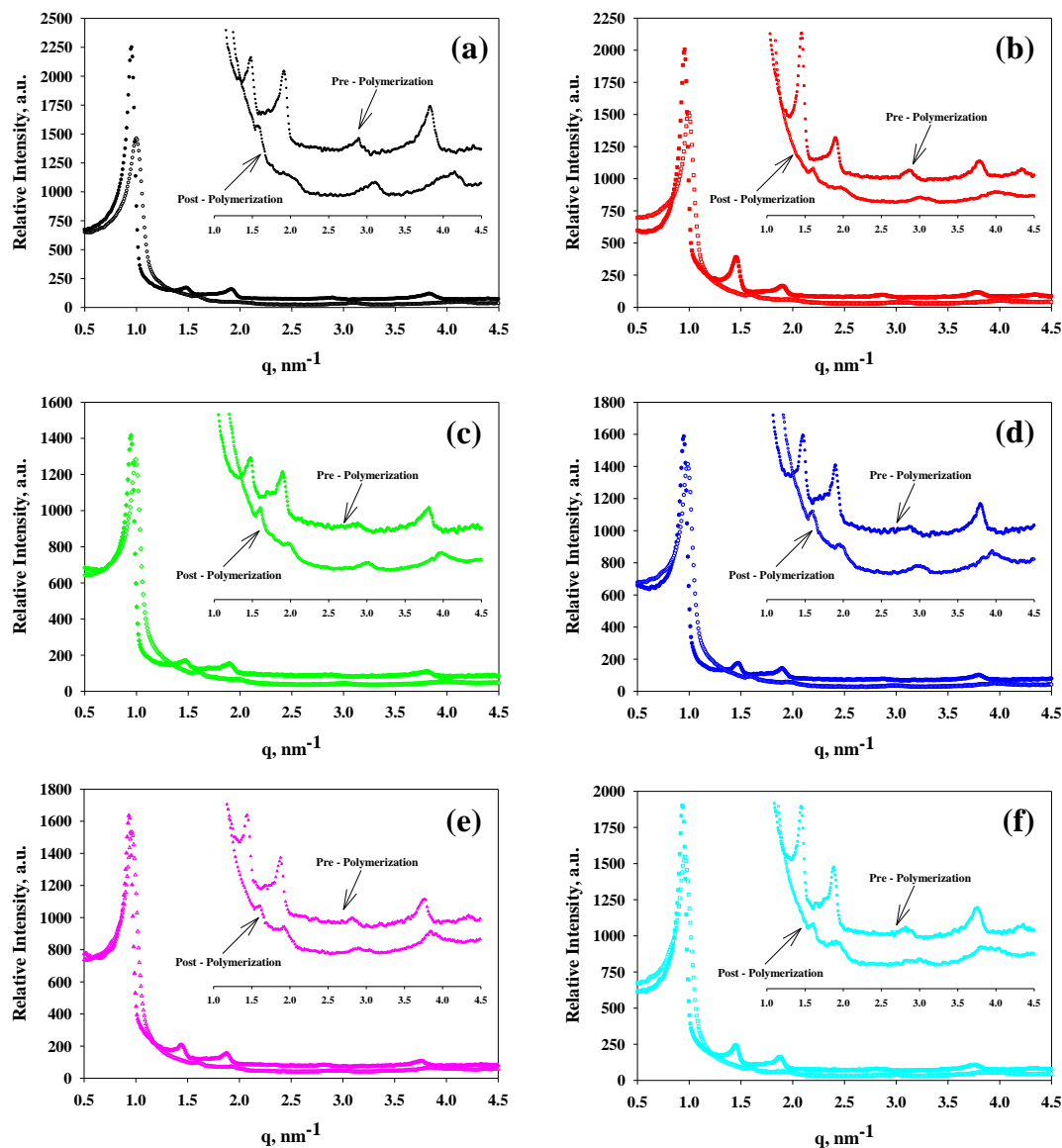


Figure 7.2. Small angle X-ray scattering profiles for hexagonal LLC templated PDMS-PNIPAM hydrogels with varying concentrations of PDMS monomer before and after photopolymerization. Samples contained 50 wt % Brij 52 surfactant, 40 wt % total monomer, and 1 wt % photoinitiator with respect to monomer mass in water. Shown are (a) 0% PDMS before (\bullet) and after (\circ), (b) 6.7% PDMS before (\blacksquare) and after (\square), (c) 12.5% PDMS before (\blacklozenge) and after (\lozenge), (d) 25.0% PDMS before (\bullet) and after (\circ), (e) 33.0% PDMS before (\blacktriangle) and after (\triangle), (f) 50.0% PDMS before (\blacksquare) and after (\square) photopolymerization. PDMS concentration represents the weight percentage of the total monomer. Insets show higher order scattering reflections in greater detail.

Figure 7.3 shows the equilibrium water uptake for LLC templated and isotropic PDMS-PNIPAM hydrogels with varying PDMS concentrations between 22 and 50 °C. The hydrogels display water uptake behavior typical of PNIPAM hydrogels, with networks swollen with water for temperatures below the LCST and water then expelled from the network when heated above the LCST. No apparent changes in the LCST between LLC templated and isotropic polymers for all PDMS concentrations are observed as the LCST of the hydrogels are within the commonly reported range of 32-34 °C for both neat and LLC templated PNIPAM gels. Additionally, incorporating the hydrophobic PDMS moiety into the hydrogel network decreases the equilibrium water uptake of the network for both nanostructured and isotropic gels, albeit to different degrees.

Significant differences in the water uptake between the LLC templated gels and their isotropic counterparts are evident. Although only a small difference in equilibrium water uptake is seen between the ordered and disordered gels at 22 °C for the gels that do not contain PDMS, incorporating small concentrations of PDMS enhances the impact of the LLC template geometry on the water uptake properties of the gels. For the isotropic systems, incorporating 6.7% siloxane into the network dramatically decreases the equilibrium water uptake below the LCST. In fact, the equilibrium water uptake for the isotropic gel that contains 6.7% siloxane is 150 wt% less than that for the LLC nanostructured PNIPAM gel at the same temperature and siloxane concentration. It is apparent from Figure 7.3 that the water uptake for the LLC templated gels is much less sensitive to changes in siloxane concentration than the analogous isotropic controls of the same chemical composition. For the hexagonal nanostructured gel, incorporating 6.7% siloxane into the network only decreases the water uptake by approximately 25 wt% compared to the LLC gel that does not contain siloxane. This represents a six-fold difference in the change in the equilibrium water uptake between the LLC templated and isotropic hydrogels at 22 °C and 6.7% siloxane concentration. The trend of significantly decreasing water uptake with increasing siloxane concentrations continues for the

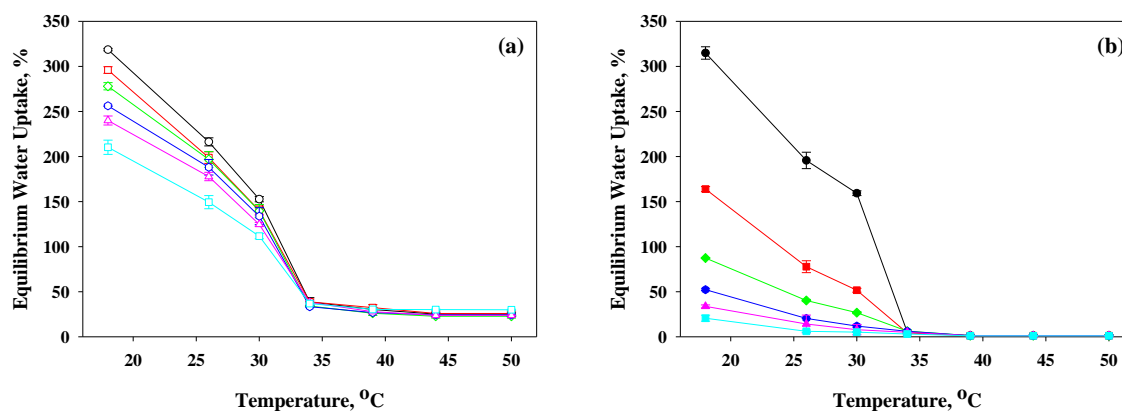


Figure 7.3. Equilibrium water uptake for polymer hydrogels. Shown are Equilibrium water uptake for (a) hexagonal LLC templated and (b) isotropic PDMS-PNIPAM hydrogels with varying concentrations of PDMS monomer at temperatures between 22 and 50 °C. Shown are LLC templated hydrogels (a) containing 0% PDMS (\circ), 6.7% PDMS (\square), 12.5% PDMS (\diamond), 25% PDMS (\circ), 33.3% PDMS (\triangle), 50% PDMS (\square). Also shown are isotropic hydrogels (b) containing 0% PDMS (\bullet), 6.7% PDMS (\blacksquare), 12.5% PDMS (\blacklozenge), 25% PDMS (\bullet), 33.3% PDMS (\blacktriangle), 50% PDMS (\blacksquare). PDMS concentrations represent the weight percentage of the polymer that is siloxane after surfactant removal and drying. Surfactant was removed prior to analysis.

isotropic hydrogels. Although the hexagonal nanostructured systems decrease in water uptake with increasing siloxane concentration, the change is not nearly as significant as that of the isotropic systems. For example at 50% siloxane, the highest concentration of siloxane system, the water uptake for the isotropic PDMS-PNIPAM hydrogel is only 20 wt % water at 22 °C while the nanostructured gel uptakes over 200 wt % water at the same temperature and siloxane concentration. The ten-fold increase in water uptake at the same temperature and siloxane concentration represents a significant improvement in hydrogel properties utilizing LLC templating, allowing considerable amounts of PDMS to be incorporated into the network without reducing the water content to a nearly useless level as is seen in the isotropic gel. The significant increase in hydrogel water uptake for LLC templated gels compared to isotropic counterparts of the same chemical

composition can be attributed to differences in polymer network structure.^{17,22} Specifically, the ordered porous structure of hexagonal nanostructured gels contain directed pore structures that allow more water to infiltrate and occupy the voids and pores of the hydrogel compared to an isotropic gel.^{17,22}

Unlike the nanostructured gel, the isotropic copolymer incorporates siloxane and NIPAM chemistries into the polymer network throughout the backbone of polymer chains as opposed to distinct and independent domains of different polymer chemistries. On the other hand, the nanostructured IPN copolymer contains independent polymer networks consisting of a continuous PNIPAM rich region and a separate discontinuous PDMS network. It is likely that the increased continuous free volume of the PNIPAM phase provides an additional mechanism for increased water uptake by allowing the network to expand in a less restricted manner compared to the isotropic network in which the siloxane chemistries in the polymer backbone prevent significant expansion and swelling of the network. The pore structure of the LLC nanostructured hydrogels also explains why these hydrogels do not fully deswell when heated above the LCST. Although all gels lose significant amounts of water when heated above the LCST, the hexagonal gels contain 30 wt % water while the isotropic gels contain about 1 wt %. This difference in water uptake is likely due to water occupying the pore volume of the LLC hexagonal nanostructured polymers while the network of the isotropic gels is completely collapsed.

It is apparent from Figure 7.3 that the hexagonal nanostructure allows for the incorporation of considerable concentrations of PDMS without significantly reducing the amount of water the gel can absorb. This result is of substantial utility in the design and proper functioning of stimuli-sensitive hydrogels in that the chemistry of the system can be varied over a wide range while maintaining a functional level of network swelling necessary for a sufficiently large range of hydrogel deswelling. Also critical to the proper functioning of stimuli-responsive PNIPAM gels is the rate at which the hydrogel

deswells when heated above the LCST. To examine how the directed pore structure generated by photopolymerization in the hexagonal LLC phase impacts the network transport, the deswelling rate for heating above the LCST was characterized and compared to the deswelling rate of isotropic controls.

Figure 7.4 shows deswelling profiles for LLC templated and isotropic PDMS-PNIPAM hydrogels at varying siloxane concentrations after transfer from 22 to 37 °C water. Significant differences are evident in the rate of deswelling between the LLC nanostructured gels and their isotropic analogs. The rate and degree of deswelling for the nanostructured gels is significantly faster and more dramatic than for the isotropic controls in all PDMS concentrations. For example, at 6.7% PDMS the nanostructured gel loses about 200 wt % water after one minute in 37 °C water while the isotropic gel only loses about 30 wt % water in the same deswelling time. These differences in the magnitude and rate of deswelling are enhanced at siloxane concentrations of 12.5% and greater where the isotropic gels lose less than 20 wt % water after 30 minutes of deswelling while the nanostructured gels lose at least 150 wt % for the same deswelling time. It is also important to note that the LLC templated gels are at their equilibrium water uptake after approximately 30 minutes while the isotropic PDMS-PNIPAM hydrogels take many hours to reach equilibrium.

The substantial increase in the rate and degree of hydrogel deswelling is likely due to the ordered pore structure as directed by the LLC template.¹⁵ The pore structure of LLC nanostructured gels provides a more directed route of water transport to bulk solution for heating above the LCST and facilitates the deswelling process. The increase in deswelling rate resulting from the orientated pore structure has been reported elsewhere for nanostructured LLC PNIPAM hydrogels.^{20,22} It is likely that the continuous PNIPAM hydrogel network in the nanostructured LLC templated copolymer allows water to be rapidly expelled from the matrix by precluding the thick and dense

layer of collapsed polymer chains that inhibits the deswelling process. In addition to the aligned porous structure that provides an uninterrupted path for water transport, the pore

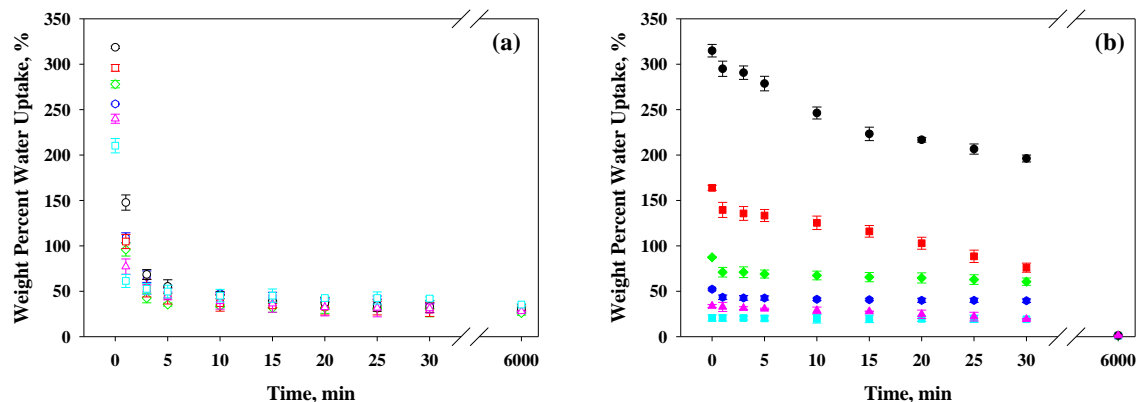


Figure 7.4. Transient water uptake profiles for polymer hydrogels. Shown are water uptake as a function of time for (a) hexagonal LLC templated and (b) isotropic PDMS-PNIPAM hydrogels with varying ratios of PDMS monomer after transfer from 22 to 37 °C water. Shown are LLC templated hydrogels containing (a) 0 % PDMS (\circ), 6.7 % (\square), 12.5 % PDMS (\diamond), 25 % PDMS (\circ), 33.3 % PDMS (\triangle), 50 % PDMS (\square). Also shown are isotropic hydrogels containing (b) 0 % PDMS (\bullet), 6.7 % PDMS (\blacksquare), 12.5 % PDMS (\blacklozenge), 25 % PDMS (\bullet), 33.3 % PDMS (\blacktriangle), 50 % PDMS (\blacksquare). PDMS concentration represents the total weight percentage of the polymer that is siloxane after surfactant removal and drying. Surfactant was removed prior to analysis.

structure also allows water to flow through the thick polymer skin that can form during the deswelling process. Interestingly, the deswelling rate for the LLC nanostructured copolymers is not significantly changed by PDMS concentration. On the other hand, the deswelling profiles for the isotropic hydrogels show increases in the time needed for the gel to lose significant fractions of water with increasing PDMS concentrations. A decrease in deswelling rate is often reported for other studies of PNIPAM hydrogels that incorporate toughening agents into the network to enhance mechanical properties.^{5,9,13} In contrast to traditional PNIPAM copolymers often reported in the literature and the isotropic copolymers presented in the deswelling profiles of Figure 4b, the LLC

templated gels deswell rapidly and reach equilibrium in 30 minutes at all PDMS concentrations examined.

It is apparent from Figures 7.3 and 7.4 that the LLC template substantially increases the rate and degree of PDMS-PNIPAM hydrogel deswelling. Although these properties show great potential in the design of functional hydrogels for use in biomedical and chemical sensing applications, the mechanical properties must also be considered for the proper performance of these materials.^{3,12} To characterize the effect of LLC order on the mechanical properties of the PDMS-PNIPAM hydrogels, the compressive modulus of the hydrogels in their most swollen state at 22 °C was measured. Figure 5a shows the compressive modulus of water swollen LLC templated and isotropic hydrogels measured at 22 °C as a function of siloxane concentration. Interestingly, the mechanical behavior of the nanostructured and isotropic hydrogels for different PDMS concentrations is very similar. The compressive modulus increases with increasing siloxane concentrations for all hydrogel systems. This is partially due to the decrease in water uptake that accompanies the addition of PDMS monomer to the polymer network as well as the increase in toughness that is associated with incorporation of the difunctional PDMS monomer.

The compressive modulus shown as a function of PDMS concentration for the ordered and disordered PDMS-PNIPAM systems in Figure 7.5a is very atypical of traditional hydrogel mechanical behavior. This is because the LLC templated gels contain significantly more water than the isotropic gels at all PDMS concentrations. Because the LLC nanostructured and isotropic PDMS-PNIPAM hydrogel controls are of the same chemical composition, it is expected that the nanostructured gels would be weaker than isotropic gels due to the higher water content of the LLC hydrogels.^{6,17} Decreases in hydrogel mechanical strength with increasing water content are well-established and occur because water plasticizes the network, generating significant decreases in mechanical strength. In fact, even small changes in water content can

dramatically change the mechanical properties of the gel. Even though the LLC nanostructured gels contain more water than isotropic PDMS-PNIPAM hydrogels, the

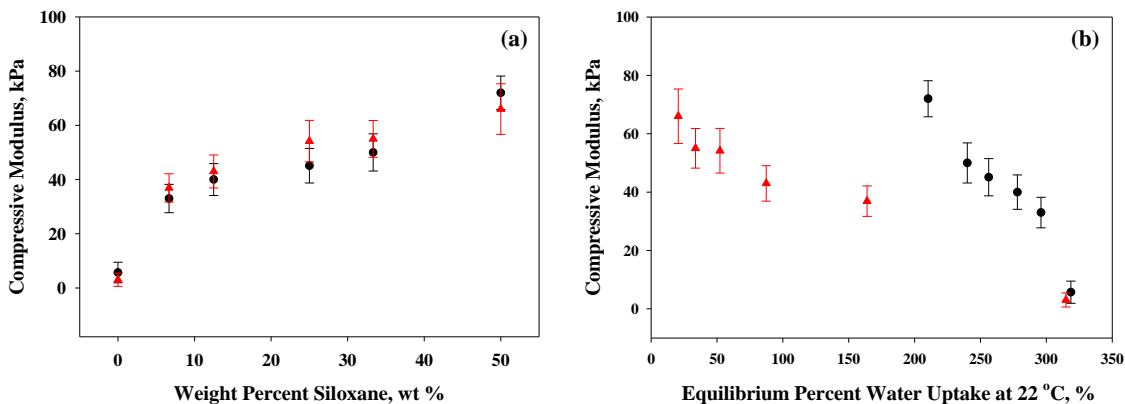


Figure 7.5. Compressive modulus for polymer hydrogels. Shown are compressive modulus of hexagonal LLC templated (●) and isotropic (▲), PDMS-PNIPAM hydrogels as a function of (a) PDMS concentration and (b) equilibrium percent water uptake at 22 °C. PDMS concentration represents the total weight percentage of the polymer that is siloxane after surfactant removal and drying. Surfactant was removed prior to analysis.

hexagonal order appears to resist compressive forces and increase the modulus of the hydrogels. To more clearly illustrate this point, the compressive modulus of the hydrogel systems is plotted as a function of equilibrium water content at 22 °C in Figure 7.5b. It is clear from this relation of mechanical properties to degree of hydrogel swelling that for a given compressive modulus, the LLC nanostructured gels contain more water than the isotropic controls. For example, for a median compressive modulus of approximately 45 kPa the isotropic hydrogel uptakes about 90 wt% water while the LLC nanostructured hydrogel absorbs about 255 wt% water for a similar compressive modulus. Figure 7.5b demonstrates that the water uptake of the LLC templated hydrogels is larger than the isotropic gels without compromising the mechanical stability of the network. Even though traditional hydrogel behavior and theory would predict a lower modulus, the ordered LLC nanostructure maintains the strength of the network despite the increase in

water uptake.⁶ The increase in mechanical properties observed for the hexagonal LLC structure may be characterized through the relationships developed for architected foams.³⁸ For architected systems, the compressive modulus is largely dependent on the alignment of support structures in relation to the applied stress. It is likely that the hexagonal LLC structure increases the alignment of polymer chains in a manner that can better resist deformation compared to a disordered or isotropic network. The uniformity and orientation of the polymer network as directed by the LLC template may better withstand mechanical stresses via the mechanism often observed in architected foams leading to the increased compressive modulus observed in the LLC templated systems.¹⁷ These structure-property relationships provide a significant degree of control over the functionality of the hydrogel, allowing the chemistry to be modulated over a wide range while maintaining to a large degree the water uptake and mechanical strength of the network and improving the response rate to thermal stimuli.

Conclusions

A hexagonal LLC nanostructure was generated in PNIPAM hydrogels containing different concentrations of PDMS. The deswelling rate and degree of water uptake for LLC nanostructured PDMS-PNIPAM hydrogels was enhanced while maintaining the mechanical stability of the network. SAXS profiles confirm that the hexagonal LLC nanostructure is retained during the photopolymerizations reaction for all examined PDMS concentrations. The equilibrium water uptake for the hexagonal nanostructured gels is significantly greater than that for isotropic controls of the same chemical composition for all PDMS concentrations studied. The rate of deswelling is also significantly faster for all hexagonal LLC templated hydrogels compared to their isotropic counterparts, decreasing the time needed for the hydrogel to deswell and reach

equilibrium by over an order of magnitude. Moreover, the mechanical strength of the hydrogels was maintained for LLC systems despite their significantly greater water uptake. These results represent how ordered nanostructures generated through photopolymerization in LLC templates may be utilized to improve material properties. In particular, the improved properties observed for nanostructured systems provide a facile method of modulating the chemistry of stimuli-responsive PNIAPM hydrogels while improving the rate and degree of deswelling and maintaining the gels mechanical strength. This work may be useful in developing stimuli-responsive hydrogels with a rapid rate of deswelling, enhanced dynamic range, and the required mechanical strength needed for proper functionality for use in biomedical, drug delivery, and chemical sensor applications.

Notes

1. Alarcon, C.; Pennadam, S.; Alexander, C. *Chem. Soc. Rev.* **2005**, *34*, 276-285.
2. Liu, L.; Sheardown, H. *Biomaterials* **2005**, *26*, 233-244.
3. Stuart, M. A. C.; Huck, W. T. S.; Genzer, J.; Mueller, M.; Ober, C.; Stamm, M.; Sukhorukov, G. B.; Szleifer, I.; Tsukruk, V. V.; Urban, M.; Winnik, F.; Zauscher, S.; Luzinov, I.; Minko, S. *Nat. Mater.* **2010**, *9*, 101-113.
4. Zhang, J.; Liu, X.; Fahr, A.; Jandt, K. D. *Colloid Polym. Sci.* **2008**, *286*, 1209-1213.
5. Zhang, X.; Xu, X.; Cheng, S.; Zhuo, R. *Soft Matter* **2008**, *4*, 385-391.
6. Anseth, K. S.; Bowman, C. N.; BrannonPeppas, L. *Biomaterials* **1996**, *17*, 1647-1657.
7. Kaneko, Y.; Nakamura, S.; Sakai, K.; Aoyagi, T.; Kikuchi, A.; Sakurai, Y.; Okano, T. *Macromolecules* **1998**, *31*, 6099-6105.
8. Laszlo, K.; Kosik, K.; Rochas, C.; Geissler, E. *Macromolecules* **2003**, *36*, 7771-7776.
9. Zhang, X. Z.; Wang, F. J.; Chu, C. C. *J. Mater. Sci. -Mater. Med.* **2003**, *14*, 451-455.
10. Chaterji, S.; Kwon, I. K.; Park, K. *Prog. Polym. Sci.* **2007**, *32*, 1083-1122.
11. Lin, J. B.; Isenberg, B. C.; Shen, Y.; Schorsch, K.; Sazonova, O. V.; Wong, J. Y. *Colloids and surfaces.B, Biointerfaces* **2012**, *99*, 108-115.
12. Liu, F.; Urban, M. W. *Prog. Polym. Sci.* **2010**, *35*, 3-23.
13. Mu, J.; Zheng, S. *J. Colloid Interface Sci.* **2007**, *307*, 377-385.
14. Li, D.; Zhang, X.; Yao, J.; Simon, G. P.; Wang, H. *Chem. Commun.* **2011**, *47*, 1710-1712.
15. Clapper, J. D.; Sievens-Figueroa, L.; Guymon, C. A. *Chem. Mat.* **2008**, *20*, 768-781.
16. Michler, G. H.; Balta-Calleja, F. J. *Mechanical Properties of Polymers based on Nanostructure and Morphology*; Taylor and Francis Group: Boca Raton, FL, 2005.
17. Clapper, J. D.; Guymon, C. A. *Macromolecules* **2007**, *40*, 1101-1107.
18. Clapper, J. D.; Iverson, S. L.; Guymon, C. A. *Biomacromolecules* **2007**, *8*, 2104-2111.

19. DePierro, M. A.; Carpenter, K. G.; Guymon, C. A. *Chemistry of Materials* **2006**, *18*, 5609-5617.
20. Lester, C. L.; Smith, S. M.; Colson, C. D.; Guymon, C. A. *Chem. Mat.* **2003**, *15*, 3376-3384.
21. Sievens-Figueroa, L.; Guymon, C. A. *Chem. Mat.* **2009**, *21*, 1060-1068.
22. Forney, B. S.; Guymon, C. A. *Macromol. Rapid Commun.* **2011**, *32*, 765-769.
23. Bender, F.; Chilcott, T. C.; Coster, H. G. L.; Hibbert, D. B.; Gooding, J. J. *Electrochim. Acta* **2007**, *52*, 2640-2648.
24. Gong, X.; Sagnella, S.; Drummond, C. J. *Int. J. Nanotechnol.* **2008**, *5*, 370-392.
25. Hintze-Bruening, H.; Troutier, A.; Leroux, F. *Prog. Org. Coat.* **2011**, *70*, 240-244.
26. Zhang, J.; Xie, Z.; Hill, A. J.; She, F. H.; Thornton, A. W.; Hoang, M.; Kong, L. X. *Soft Matter* **2012**, *8*, 2087-2094.
27. Zhang, J.; Xie, Z.; She, F. H.; Hoang, M.; Hill, A. J.; Gao, W. M.; Kong, L. X. *J Appl Polym Sci* **2011**, *120*, 1817-1821.
28. Texter, J. *Colloid Polym. Sci.* **2009**, *287*, 313-321.
29. Sievens-Figueroa, L.; Guymon, C. A. *Polymer* **2008**, *49*, 2260-2267.
30. DePierro, M. A.; Guymon, C. A. *Macromolecules* **2006**, *39*, 617-626.
31. Forney, B. S.; Guymon, C. A. *Macromolecules* **2010**, *43*, 8502-8510.
32. Gin, D. L.; Bara, J. E.; Noble, R. D.; Elliott, B. J. *Macromolecular Rapid Communications* **2008**, *29*, 367-389.
33. Clapper, J. D.; Guymon, C. A. *Adv Mater* **2006**, *18*, 1575-+.
34. Bushetti, S. S.; Singh, V.; Raju, S. A.; Atharjaved; Veermaram *Indian J. Pharm. Educ. Res.* **2009**, *43*, 241-250.
35. Clapper, J. D.; Pearce, M. E.; Guymon, C. A.; Salem, A. K. *Biomacromolecules* **2008**, *9*, 1188-1194.
36. Scherer, G. *J Am Ceram Soc* **1990**, *73*, 3-14.
37. Feigin, L. A.; Svergun, D. I. Structure Analysis by Small Angle X-Ray and Neutron Scattering. In Taylor, G. W., Ed.; Plenum Press: New York, NY, 1987; pp 59-63.

38. Ashby, M. *Philos. Trans. R. Soc. A-Math. Phys. Eng. Sci.* **2006**, 364, 15-30.

CHAPTER 8

NANOSTRUCTURED THIOL-ENE POLYMERS GENERATED THROUGH PHOTOPOLYMERIZATION IN WATER FREE LYOTROPIC LIQUID CRYSTALLINE PHASES

Photopolymerization in lyotropic liquid crystalline (LLC) templates is a promising method of generating nanostructure in organic polymers to optimize material performance. Although the LLC templating process has been applied to control the nanostructure and improve the properties of many (meth)acrylate polymers, several challenges such as poor retention of LLC order during polymerization and low polymer volume fraction have not been examined. Herein, the unique advantages of thiol-ene copolymerizations are used to produce LLC nanostructured polymers with improved material properties. Polymerization thermodynamics inherent in the thiol-ene copolymerization are utilized to overcome phase separation and structure retention issues observed in traditional LLC templated systems. A LLC nanostructured thiol-ene formulation with high polymer concentration and large degree of nanostructure retention is identified. Whereas traditional LLCs utilize water as a cosolvent to form the phase, this system self-assembles into an inverse hexagonal LLC phase in the absence of water. In fact, the polar ene monomer behaves as a cosolvent and facilitates formation of the inverse hexagonal phase. The ordered polymer network, as directed by the LLC template, increases the glass transition temperature and mechanical properties compared to an isotropic control of the same chemical composition. These results may be used to synthesize nanostructured polymers with improved properties using thiol-ene copolymerizations and LLCs as photopolymerization platforms.

Introduction

Photopolymerization is a useful polymerization technique utilizing a light mediated process to produce polymer materials with a wide range of properties.¹ The use of light to cure polymers is becoming increasingly popular due to numerous advantages including rapid initiation rate, energy efficiency, spatial and temporal control, and solvent free polymerizations.² The capability to produce polymer materials at the desired time and location by irradiation of monomers and photoinitiator mixtures with light is particularly useful in a wide-range of biomedical applications that require polymerization in cumbersome or biologically sensitive locations.³⁻⁵ These advantages make photopolymerization an attractive method for *in-situ* curing of polymer materials such as dental composites, artificial corneas, and tissue scaffolds.⁶⁻⁹ Although photopolymerization may be utilized to cure a wide-range of monomer functionalities, a particularly useful class of polymers generated through the light mediated reaction of thiol and ene monomers has received particular interest in the past decade.¹⁰⁻¹⁴

Thiol-ene copolymerizations have been examined to overcome some of the shortcomings associated with classical radical photopolymerization reactions including oxygen inhibition, high degrees of shrinkage stress, and inhomogeneous network structures.^{1,10-13} Radical mediated thiol-ene copolymerizations are characterized by the addition of thiol functional groups to electron rich double bonds such as vinyl ethers. The molecular weight buildup proceeds in a step-growth manner to form low molecular weight dimers and trimers at low to moderate conversions and high molecular weight polymers at relatively high conversions. This reaction is not significantly affected by oxygen, has low shrinkage stress, rapid polymerization kinetics, and a narrow glass transition range when compared to classical radical photopolymerizations of (meth)acrylates. The radical mediated thiol-ene photopolymerization reaction could be particularly useful in industrial coating applications because the polymerization rate is

inherently rapid and the insensitivity to oxygen eliminates the need to purge with expensive inert gasses.²

The wide range of monomer chemistries and uniform network structures generated by thiol-ene copolymerizations have led to polymer materials that span a wide range of glass transition temperatures and mechanical properties. A range of physical properties have been developed using thiol-ene technology from compliant poly(ethylene glycol) networks for use as tissue scaffolds and cell cultures to high-strength industrial adhesives.¹⁵⁻¹⁹ Recently, the alternating step-growth reaction has been extended to thiol-yne polymerizations where two thiol functional groups can add across the triple bond of an yne monomer. The thiol-yne reaction has further expanded the use of radical mediated addition of thiol functional groups across electron rich unsaturated alkyl compounds to produce highly-crosslinked polymer networks with high moduli for use in advanced applications.²⁰⁻²² The success of thiol-ene “click” reactions is largely due to fundamental work examining the reaction mechanism and physical property development by the Hoyle and Bowman groups.^{10,12,23-25} Several reviews have recently examined the improved properties and tremendous range of applications of thiol-ene reactions ranging from surface modification, 3D printing, and lithography.²⁶⁻²⁸

Despite the wide-range of applications and large breadth of research utilizing thiol-enes in polymer science, little work has examined the effect of periodic nanostructured polymer networks on thiol-ene copolymer systems. Significant research efforts investigating the impact of nanostructure and crystallinity of polymer materials has been conducted in the past decade. Much work has focused on the synthesis of block copolymers, mechanisms of assembly into ordered geometries, and to a lesser extent, properties imparted to the materials by ordered nanostructured domains.²⁹⁻³²

Considering the wide range of applications for thiol-ene polymers, it could be useful to further expand the properties and performance of these materials through incorporation of nanostructure. Much research has focused on methods of generating

periodic nanostructured domains throughout the polymer network.^{33,34} Although periodic nanometer sized domains throughout the polymer can be beneficial, synthesis and design of polymers with proper stereochemistry and interaction parameters needed to drive the self-assembly process can be difficult, time consuming, and expensive.³⁵ Other promising methods of generating nanostructure in polymers include the use of templates as polymerization platforms to direct polymer morphology.³⁶⁻³⁸

Molecular imprinting (MIP), in which a polymer is formed around a template or host molecule such as a protein or enzyme that interacts with functional groups on the monomer shows great promise in many biosensing and separation applications.³⁹ By polymerizing around a host or template molecule followed by subsequent removal of the molecule from the polymer matrix, MIP generates a specific site containing the precise geometry needed for proper interaction to favor strong association and binding affinity to the template molecule, similar to the “lock and key” mechanism of enzyme binding in a biological environment.^{40,41} However, MIP often requires functionalization of particular monomers with functional groups or proteins that bind to the target molecule in order to form a pocket with high binding affinity. It is highly desirable to develop a synthesis process that may be applied to a range of monomers to generate nanostructured networks without the use of lengthy or expensive synthesis schemes often reported in the literature.

A particularly promising method of generating nanostructure in organic polymers utilizes self-assembling lyotropic liquid crystals (LLCs) as photopolymerization platforms to direct polymer structure on the nanometer size scale.⁴²⁻⁵¹ This method has been used to produce liquid crystalline order in a wide-range of polymers including poly(ethylene glycol), acrylamide, *N*-isopropylacrylamide, hexanediol diacrylate, poly(lactic acid), and other (meth)acrylate systems. The utility of the LLC templating technique stems largely from the ability to apply the templating technology to generate nanostructure in polymers with a range of chemistries using commercially available monomers. This method has been used to improve the mechanical and transport

properties of polymer materials by incorporating nanostructure into the network. For example, the compressive modulus of poly(ethylene glycol) increased by a factor of three compared to an isotropic polymer of the same chemical composition by generating a lamellar nanostructure in the polymer network architecture.⁵² The nanoporous network as directed by the LLC template has also been used to improve the transport properties of temperature sensitive poly(*N*-isopropylacrylamide) hydrogels, decreasing the time needed for the polymer to deswell when heated above the lower critical solution temperature by two orders of magnitude.⁵³

Lyotropic liquid crystals are typically formed at higher concentrations of surfactant or amphiphilic molecules in a polar solvent such as water.⁵⁴ The self-assembled LLC phases contain polar and non-polar domains that can be used to segregate monomers into ordered geometries based on polarity.^{55,56} For example, water soluble monomers such as acrylamide segregate near the polar head groups of surfactant molecules and adopt a geometry that directly resembles that of the LLC phase. Likewise, non-polar monomers primarily segregate in the oil-soluble domains of the LLC phase. Photopolymerization is then utilized to transfer the order of the LLC phase to the polymer network. Examples of LLC phases that have been used as templates to direct polymer network structure include the hexagonal, bicontinuous cubic, and lamellar phases.⁵⁷

Despite the utility of LLC templates in generating nanostructure to improve polymer properties, a number of disadvantages are inherent in the LLC templating process. The most notable problem in LLC templating is retention of the original nanostructure during the polymerization reaction. The polymerization brings about a thermodynamically unfavorable decrease in entropy that can lead to a disruption in LLC order. It is not uncommon for the resulting polymer to have a structure that is much different from the original LLC template or on much larger size scales than the parent LLC phase.^{36,48} Much research in LLC nanostructured polymer networks has examined the impact of kinetics on the degree of template order retained during polymerization.

Research suggests that the polymerization speed has a significant impact on the degree of LLC structure transferred to the polymer during the polymerization reaction.⁴⁹⁻⁵¹ Faster initiation rates have been correlated to higher degrees of LLC template structure transferred to the polymer. However, the final degree of structure transferred to the polymer varies and is highly dependent on the particular monomer/surfactant system. Even small changes in monomer structure or polarity can lead to a reaction environment that favors phase separation from the parent template. Identification of robust LLC templated monomer systems that retain their structure during polymerization is highly desirable in the synthesis of nanostructured polymers with improved properties.

Another factor that limits the functionality of the LLC templating process is the relatively low monomer concentrations that can be incorporated in LLC formulations. Because higher ordered LLC phases including the hexagonal, bicontinuous cubic, and lamellar phase are typically formed at higher surfactant concentrations in water, the monomer concentration is often limited to 40 wt % or less in order to prevent phase disruptions that occur in the self-assembled surfactant template at higher monomer concentrations.⁵⁷ The low monomer concentrations and high concentration of plasticizing surfactants can lead to a material with poor mechanical properties. For instance, the modulus of a polymer is directly proportional to the volume fraction of the polymer.⁵⁸ As polymer concentration decreases the material becomes more porous and subsequently weaker. LLC templated polymers are thus difficult to develop preventing the full potential of nanostructured polymers from being realized. Despite these limitations, LLC templating remains a promising method of producing nanostructure in organic polymers because the templating process is rapid, cost-effective, and may be applied to a wide-range of polymer chemistries that otherwise lack the stereochemistry needed to form self-assembled liquid crystalline nanostructures.⁵⁹ Coupling the unique properties and reaction mechanism of thiol-ene photopolymerizations with the property

enhancements achieved using LLCs as nanostructure directing polymerization platforms may lead to a useful polymer with optimized performance.

Herein, we utilize the advantages of thiol-ene copolymerizations to generate nanostructured polymers with LLC surfactant templates and photopolymerization to direct polymer network structure. A robust thiol-ene monomer system that retains its structure to a large degree during polymerization is identified. This system is unique from a fundamental liquid crystalline perspective because it forms a well-defined hexagonal structure in the absence of a traditional solvent. Additionally, the hexagonal phase is formed using an unprecedentedly low surfactant concentration with thiol-ene monomers. The phase behavior of LLC templated systems is examined using small angle X-ray scattering to determine the segregation behavior of thiol and ene monomers. Photopolymerization kinetics are characterized to probe the local order of templated polymer systems. Additionally, the mechanical properties are examined in order to determine the impact of LLC order on mechanical performance. This work introduces the utility of thiol-ene copolymerizations to retain the nanostructure of LLC templated polymer systems and presents a system with greater mechanical stability due to high polymer volume fraction.

Experimental

Monomers used in this study include 1,3,5-triallyl-1,3,5-triazine-2,4,6(1H,3H,5H)-trione (TTT, 98%, Aldrich) and pentaerythritol tetrakis(2-mercaptoacetate) (4-SH, Aldrich). The non-reactive surfactant polyoxyethylene (2) cetyl ether (Brij 52, Aldrich) was also used to facilitate LLC phase formation. Photoinitiator 2,2-Dimethoxy-1,2-diphenylethan-1-one (Irgacure 651, Ciba Specialty Chemicals) was used to initiate polymerization. Isopropyl alcohol (Aldrich) and dimethyl sulfoxide

(DMSO, Aldrich) were used as solvents. An aluminum salt (*N*-nitroso-*N*-phenylhydroxylamine aluminum salt) was incorporated as an inhibitor at a concentration of 0.05 wt % to increase the shelf-life of thiol-ene mixtures. Figure 8.1 shows the chemical structure of monomers, photoinitiator, and surfactant.

Lyotropic liquid crystalline templated samples were prepared by mixing particular concentrations of monomer, surfactant, inhibitor, and photoinitiator. A one-to-one molar ratio of thiol and ene monomers based on functional groups was used for all kinetic and mechanical property testing in this study. Isotropic controls were synthesized by replacing the phase forming surfactant with DMSO solvent to generate an isotropic polymer network. Sample homogeneity was achieved using centrifugation, mechanical agitation, heat, sonication, and vortex mixing. Polymer bars were prepared by transferring samples into bar shaped Teflon molds and irradiating the samples with a medium pressure UV arc lamp for 20 minutes at an intensity of $2.5 \text{ mW}\cdot\text{cm}^{-2}$.

LLC nanostructured formulations containing Brij 52 surfactant were solvent-exchanged with isopropyl alcohol to remove unreacted monomer, photoinitiator, and surfactant, sandwiched between Mylar (DuPont) sheets to slow solvent evaporation and prevent cracking, and dried under vacuum for 48 hours.⁶⁰ Solvent was replaced periodically to facilitate surfactant removal. Overall surfactant removal was determined gravimetrically using sample composition information and comparing sample mass immediately after polymerization to the mass obtained after solvent exchange and drying. LLC templated polymer bars were fabricated for tensile testing by heating the samples above their clearing temperature and pouring the formulation into bar shaped Teflon molds. Samples were allowed to cool slowly to room temperature, photopolymerized, and surfactant was removed by solvent exchange.

Isotropic polymer bars were prepared by injecting monomer solution between glass slides clamped together with a 1mm spacer. Isotropic samples were solvent exchanged with DMSO/water mixtures by allowing the bar to soak in a 75 / 25 %

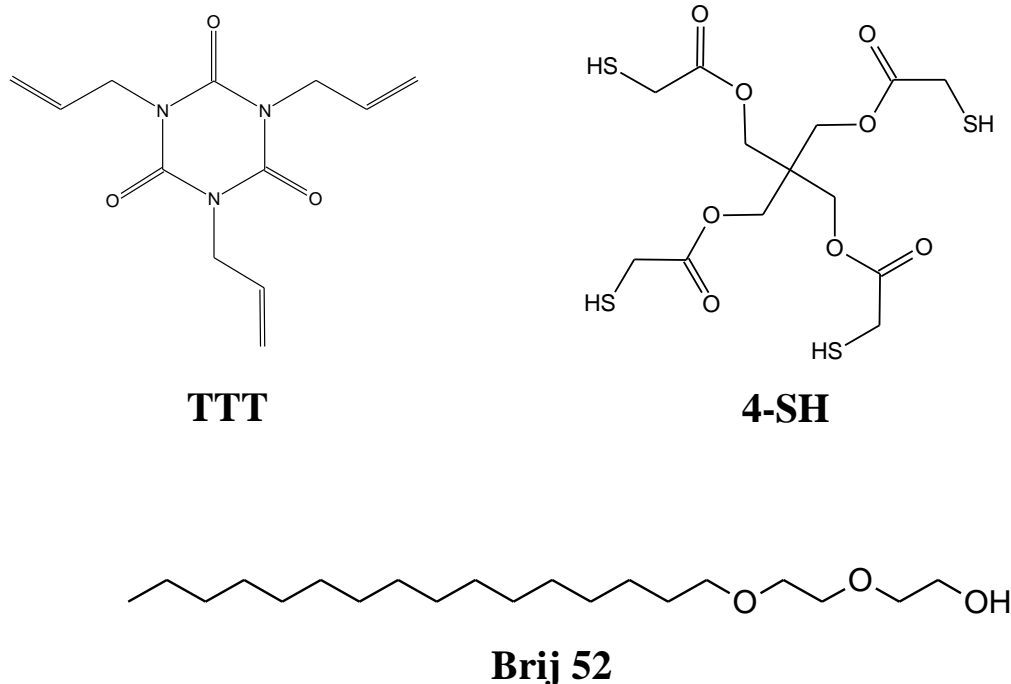


Figure 8.1. Chemical structures of monomers and surfactants used in this study. Shown are trifunctional ene monomer 1,3,5-triallyl-1,3,5-triazine-2,4,6(1H,3H5H)-trione (TTT) tetrafunctional thiol monomer pentaerythritol tetrakis(2-mercaptoacetate) (4-SH), and non-reactive surfactant polyoxyethylene (2) cetyl ether (Brij 52)

DMSO/water solution and continually adding water to the solution at predetermined intervals. Water dilution was completed when the sample reached about 5 / 95 % at which time the bar was transferred to a pure water bath to soak and dried under vacuum. At least three polymer bars were prepared for each sample formulation and analyzed in property experiments to obtain the standard deviation for each data point represented by error bars in the presented figures.

Polymerization kinetics were studied using a Thermo Electron Nexus 670 Fourier Transform infrared spectrometer (FTIR). The detector was cooled with liquid nitrogen and the sample chamber was purged with nitrogen gas to eliminate water vapor and carbon dioxide. Double bond and thiol conversion were calculated by monitoring the

change in absorption of the thiol and ene peaks at 3100 and 2570 cm^{-1} , respectively. Photopolymerization was initiated using a high-pressure Mercury arc lamp (Exfo Acticure 4000) using 365nm light ($2.5 \text{ mW}\cdot\text{cm}^{-2}$).

Polymer nanostructure was characterized with a Nonius FR590 small angle X-ray scattering (SAXS) apparatus using a standard copper target Röntgen tube with a Ni-filtered Cu K α line of 1.54 Å as the radiation source, a collimation system of the Kratky type, and a PSD 50M position sensitive linear detector (Hecus M. Braun, Graz). Phases were indexed by calculating the d -spacing ratios of scattering peaks. The scattering vector, q , was calculated from the angle of the scattered radiation, 2θ , and the X-ray wavelength, λ , using equation 8.1

$$q=4\pi\sin 2\theta/\lambda=2\pi/d \quad (8.1)$$

where d is the lattice or d -spacing.⁶¹ Glass transition temperature characterization was carried out using dynamic mechanical analysis (DMA, Q800, TA Instruments) equipped with a liquid nitrogen gas cooling accessory for sub-ambient material testing. Polymer bars were prepared and examined in tensile mode. The polymer was cooled to approximately -90 °C and the temperature was increased at a rate of 3 °C·min⁻¹ to approximately 200 °C or until the sample yielded. The polymer was subjected to a sinusoidal deformation at a frequency of 1 Hz using a deformation strain of 0.05%. The ratio of the loss to storage modulus was used to calculate the loss tangent (Tan δ). The glass transition temperature is reported as the maximum temperature in the Tan δ vs. temperature curve.⁶²

Results and Discussion

Utilizing LLCs as photopolymerization platforms to direct polymer nanostructure shows great promise in improving polymer functionality for use in a wide-range of applications. Unfortunately, difficulties in retaining LLC nanostructure during polymerization and low polymer volume fraction limit the large scale use of LLC templating. Although much research has examined how the polymerization reaction can be used to control polymer morphology, little has examined how the unique advantages of thiol-ene polymerization may be used to retain order in LLC templated polymer systems. Because low molecular weights are maintained until relatively higher conversions in thiol-ene copolymerizations, the thermodynamic driving force for self-assembly is reduced and may allow LLC structure to be retained during polymerization. In fact, the gradual buildup of molecular weight coupled with inherently fast polymerization kinetics make thiol-enes a promising reaction mechanism for the synthesis of nanostructured polymer materials using LLCs and photopolymerization.

The rapid reaction rates of thiol-ene copolymerizations may provide a useful method of retaining LLC template order in polymer systems by kinetically trapping thermodynamically unstable nanostructures. In one study, the use of a highly efficient photoinitiator facilitated retention of the hexagonal LLC structure after photopolymerization whereas the system polymerized with the slower and less efficient photoinitiator did not retain the LLC order during polymerization.⁶³ While most work examining LLC templating has focused on the use of radical mediated chain polymerizations of (meth)acrylate based monomers, the thiol-ene copolymerization proceeds by an inherently different mechanism.^{1,20} The thiol-ene polymerization proceeds by a step-growth polymerization mechanism which is characterized by the gradual build-up of molecular weight at lower conversions. The beginning stages of the step-growth polymerization are dominated by the formation of dimer and trimer units and

the molecular weight remains very low. The point at which a cross-linked and insoluble polymer is formed, or the gel point, occurs at later stages in the polymerization reaction where the molecular weight increases exponentially with conversion. The gel point for a step-growth polymerization may be estimated by the functionality of reactive monomers. For an equimolar mixture of thiol and ene functional groups of monomers shown in Figure 8.1, a gel point conversion of approximately 60% is predicted. This conversion is much greater than in radical chain polymerizations in which gelation occurs within the first few percent conversion.^{64,65}

Because faster polymerization rates may better preserve LLC structure, it is hypothesized that the fast reaction speed of thiol-ene photopolymerizations may provide a useful method of controlling phase separation and allow LLC template structure to be successfully transferred to the polymer after curing. Additionally, the gradual buildup of molecular weight characteristic of the thiol-ene step-growth copolymerization may decrease the entropic driving force for phase separation from the parent template and allow retention of the original LLC structure. It is hypothesized that the delayed gel point and rapid polymerization rate will aid in transferring the original LLC template order to the polymer.

Previous work has demonstrated that polymer structure changes at distinct conversions throughout the polymerization reaction. Utilizing photopolymerization kinetics as a tool to probe the local order in a LLC templated poly(ethylene glycol) and hexanediol diacrylate systems, researchers found that polymer structure was disrupted at specific conversions coinciding with phase separation events.⁴⁸ In particular, changes in polymer structure occurred throughout the polymerization reaction including during the first 5% conversion and again at later stages (~ 50% conversion) in the polymerization reaction. The continuous change in polymer structure could be due to the increasing crosslinking density that occurs as the polymerization reaction progresses. Because the phase separation process is driven by the buildup of molecular weight, delaying the onset

of gelation to higher conversions could allow for much of the polymerization reaction to occur before the increase in molecular weight gives rise to phase separation from the parent template. In other words, the step-growth polymerization could allow for the LLC template to remain thermodynamically stable for much of the polymerization reaction compared to radical chain polymerization and may provide a useful method of retaining LLC structure.^{66,67} Additionally, the fast polymerization rates inherent in thiol-ene photopolymerizations provide could allow successful transfer of LLC template structure to the polymer by kinetically trapping the template order before phase separation occurs.

For the development of nanostructured thiol-ene copolymers in this work it became apparent that traditional methods of generating LLC order with surfactant, monomer, and water were not feasible due to incompatibility of commercially available thiol monomers with water. Formulations containing thiol-ene monomers with Brij series surfactants and water macroscopically phase separate leaving a distinct water rich domain and a separate viscous layer with surfactant and thiol-ene monomer. Due to the strong tendency for thiol and ene monomers to macroscopically phase separate from any surfactant system that contains water, it was concluded that water was not a viable solvent to generate LLC order with thiol-ene monomers and Brij surfactants. On the other hand, the monomers in Figure 8.1 contain the proper polarity and molecular weight to act as cosolvents in place of water to generate liquid crystalline order with Brij 52 and 58 series surfactants. Although both Brij 52 and 58 form LLCs phases with thiol-ene monomers, Brij 52 was chosen for further characterization due to stronger phase development at lower surfactant concentration.

The morphology of Brij 52 surfactant with a stoichiometric ratio of thiol and ene monomers was characterized using small angle X-ray scattering (SAXS). Figure 8.2 shows the SAXS profile before and after polymerization for a 15 wt % Brij 52 with an 85 wt % thiol-ene monomer mixture before and after polymerization. A strong primary reflection is observed before polymerization, indicating a preferential ordering and

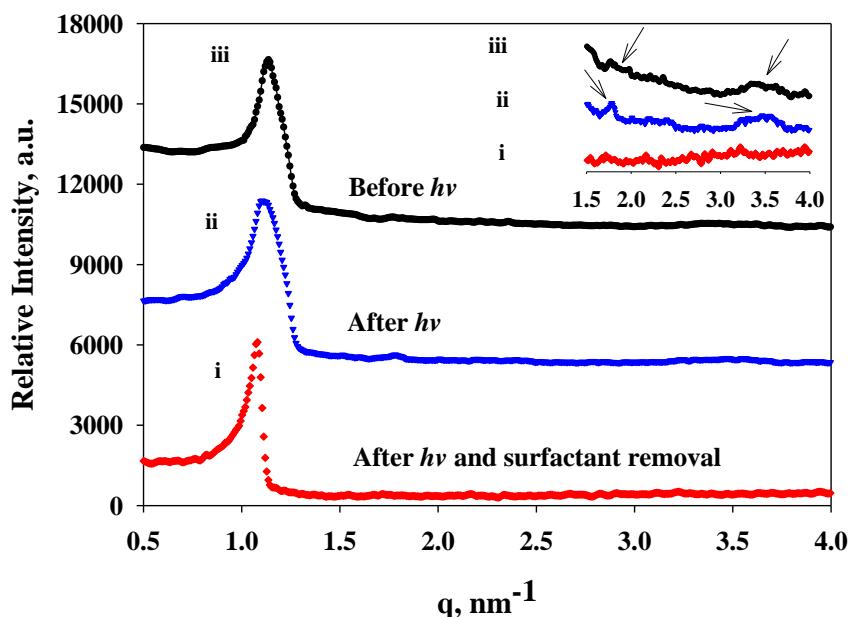


Figure 8.2 Small angle x-ray scattering profiles for the hexagonal phase formed at 85 wt % thiol-ene mixture and 15 wt % Brij 52 surfactant i) before photopolymerization, ii) after photopolymerization, and iii) after photopolymerization and surfactant removal. Insets show higher order scattering peaks in greater detail with secondary and tertiary scattering peaks identified. The thiol-ene mixture includes 1 wt % photoinitiator and a 1:1 molar ratio of thiol and ene functional groups.

domain spacing in the system. Moreover, the d -spacing ratio characteristic of the hexagonal phase ($1:1/\sqrt{3}:1/\sqrt{4}$, corresponding to d_{100} , d_{110} , d_{200}, \dots) is observed before polymerization supporting that monomers have adopted a hexagonal morphology.^{48,50} The original morphology appears to retain well throughout photopolymerization as a similar position and intensity of the primary scattering peak is observed. After polymerization, the position and intensity of the primary scattering reflection are preserved suggesting that the polymer contains preferential and periodic domain spacing of approximately 5.5nm. Additionally, the d -spacing ratios characteristic of the

hexagonal phase are retained after polymerization supporting that the system has adopted a hexagonal structure.

Polymer structure was further characterized after removal of the parent surfactant template to probe the order of the working polymer. Interestingly, a strong primary reflection is present at roughly the same scattering vector observed before and after polymerization of surfactant containing systems, further suggesting that the polymer has a periodic pore structure. Although higher order scattering peaks are not evident in the scattering profile after surfactant removal, the strong primary reflection at the same d -spacing of the pre-polymerization system indicates periodic structures on the nanometer scale are present in the polymer network. The fact that a strong primary scattering peak is observed after surfactant removal further illustrates the large degree of nanostructure in the LLC templated thiol-ene system. The scattering intensity is a function of the electron density distribution and structure factor, with higher electron density contrasts or more ordered structures giving rise to a larger scattering intensities.⁶⁸ Typically, removal of the surfactant template decreases the electron density contrast needed to scatter X-rays. The strong primary reflection present after surfactant removal indicates that the polymer network structure is defined enough to generate a high intensity scattering peak despite the decrease in electron density contrast that accompanies removal of the surfactant template.

The degree of structure retention is particularly impressive when compared to other LLC templated polymer systems in which the network structure is influenced by the presence of the LLC phase but a one-to-one copy of the mesophase is not transferred to the polymer. In this case, it appears that the original hexagonal nanostructure is successfully transferred to the thiol-ene polymer. Formation and retention of a hexagonal LLC phase for the Brij 52 templated thiol-ene system is interesting because LLC phase formation typically requires polar solvents such as water to drive the self-assembly process.⁶⁹ Clearly, the interaction of thiol-ene monomers with the Brij 52 surfactant is

strong enough to drive the self-assembly process and to form the hexagonal phase. To better understand phase formation and segregation behavior of this system, a ternary phase diagram was constructed by varying the ratio of thiol, ene, and surfactant. Figure 8.3 shows the phase diagram of thiol and ene monomers with Brij 52 surfactant.

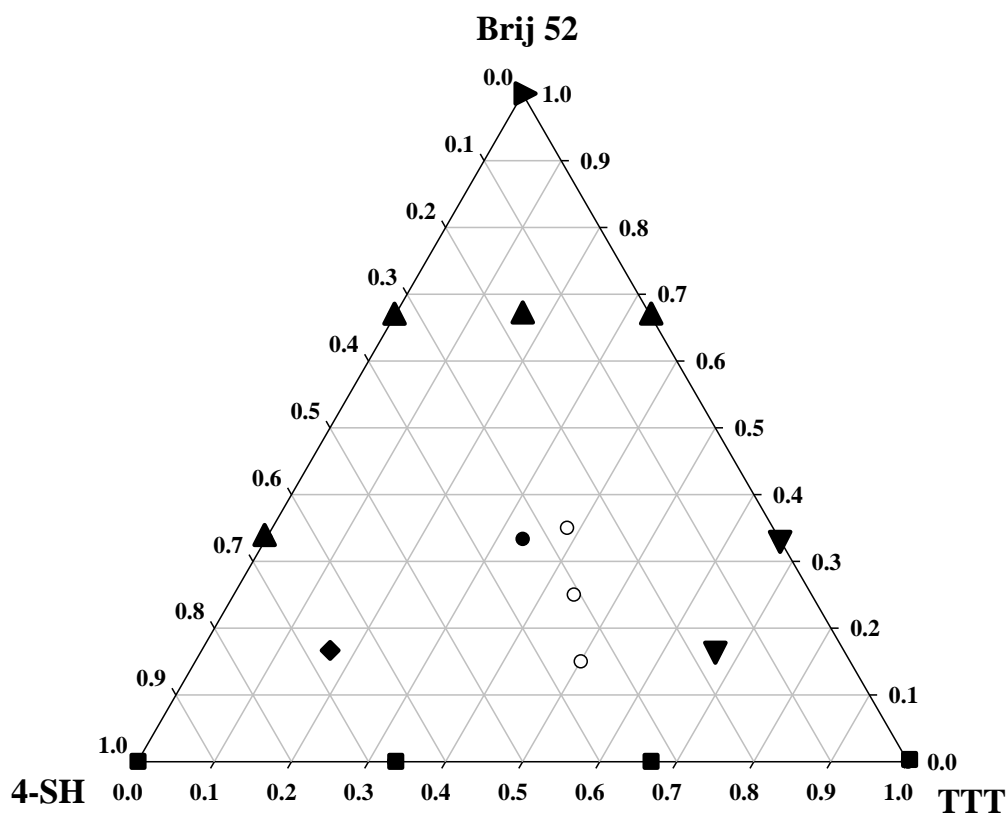


Figure 8.3. Ternary phase diagram for Brij 52 surfactant, thiol monomer 4-SH, and ene monomer TTT. Symbols represent LLC phase including ■-isotropic, ●-hexagonal, ▲-cubic/lamellar, ▼-lamellar, and ►-crystalline solid. Filled symbols represent a disproportional ratio of thiol and ene monomers that would not form a robust polymer after curing where unfilled symbols represent a stoichiometric ratio of thiol and ene functional groups that are cured and used in mechanical property studies.

Due to the stoichiometry of the thiol-ene step growth polymerization reaction the systems that do not contain a 1:1 molar ratio of thiol and ene functional groups were not photopolymerized, as shown by the black symbols in Figure 8.3. The open symbols in Figure 8.3 are for a 1:1 molar ratio of thiol and ene functional groups.

The stoichiometric ratio of thiol-ene monomers shows a defined hexagonal phase geometry with relatively low concentrations of Brij 52 surfactant. For equimolar thiol-ene concentrations between 65 and 85 wt % with Brij 52 surfactant a well-defined hexagonal phase is formed and retained after polymerization. This system represents a much higher monomer concentration that can be typically used for LLC templated polymers. For most literature, monomer concentration only range from 20 to 40 wt %.^{36,47,52} The ability to tune the monomer concentration over a large range may allow modulation of polymer properties while maintaining a hexagonal nanostructure. From Figure 8.3, it is obvious that Brij 52 surfactant is required to form a LLC phase with the thiol-ene monomers. At higher surfactant concentrations a lamellar/cubic mixed phase is formed with the thiol and ene monomers. As surfactant concentration is decreased the phases become less defined and change from the more ordered lamellar and hexagonal phases to the relatively disordered micellar phase.

Further examination of the phase diagram indicates that the more polar ene monomer drives the phase formation more so than the less polar thiol monomer. For the thiol rich 4-SH region of the phase diagram at 15 wt % Brij 52, a less ordered micellar morphology is formed. As 4-SH is replaced with ene monomer at constant Brij 52 concentration (15 wt %), the phase changes from micellar to the higher dimensionally ordered hexagonal and lamellar phases. The transition to ordered LLC phases at higher TTT concentration for 15 wt % Brij 52 surfactant suggests that the ene monomer acts as a co-solvent with the surfactant and drives phase formation to a much higher degree than the 4-SH monomer.⁴² This behavior is not surprising because the TTT monomer is more polar than the thiol monomer due to the electronegative nitrogen and oxygen atoms

present in the chemical structure. The ene monomer is less compatible with the long hydrophobic tails of the Brij 52 surfactant causing the aliphatic carbon chains to segregate and minimize their contact with ene monomer and drive the self-assembly process through the hydrophobic effect.⁶⁹

To further probe the segregation behavior, the d -spacing of the primary scattering peak was measured using SAXS as a function of thiol, ene, and surfactant concentration. Figure 8.4 shows the d -spacing of the primary scattering peak plotted on a ternary diagram at varying concentrations of monomer and surfactant. For a given surfactant

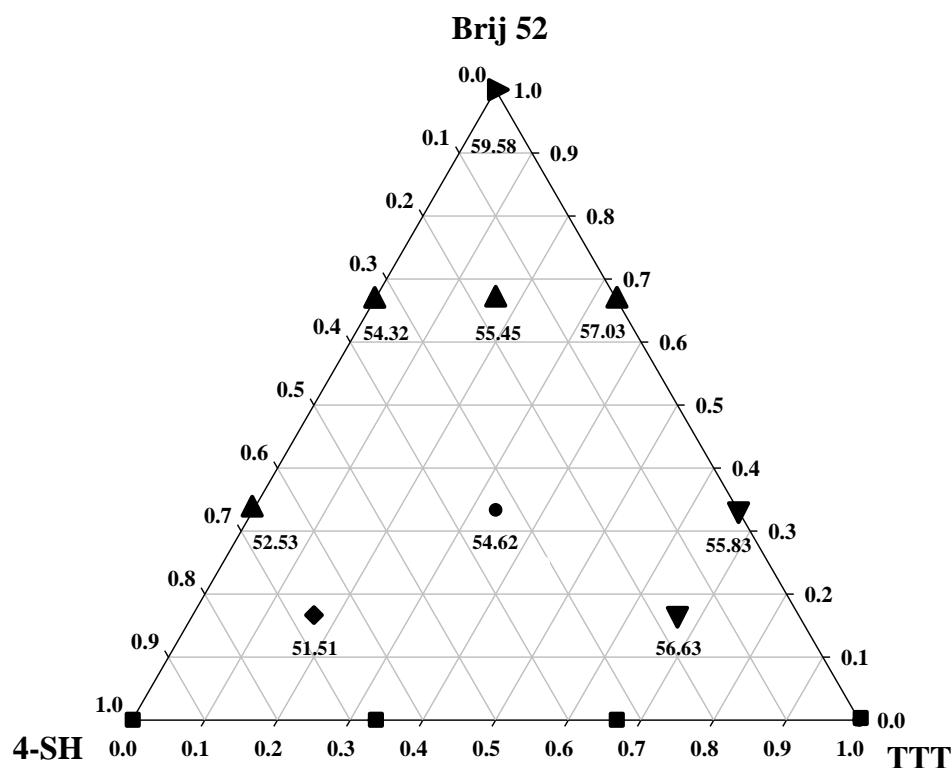


Figure 8.4. Lattice or d -spacings (\AA) of the primary scattering peak in ordered systems for the ternary Brij 52 surfactant, thiol monomer 4-SH, and ene monomer TTT system. Symbols represent LLC phase including ■-isotropic, ●-hexagonal, ▲-cubic/lamellar, ▼-lamellar, and ▶-crystalline solid.

concentration, the d -spacing increases with increasing ene monomer concentration. The increased d -spacing with higher TTT concentration indicates that the ene monomer is swelling the phase and increasing the LLC dimensions. For hexagonal systems, it is likely that the TTT monomer is segregating in the discontinuous cores of the hexagonal phase near the polar head group of the Brij 52 surfactant.⁷⁰ The increase in TTT concentration causes the hexagonal cores to swell and increases the d -spacing ratio of the system. On the other hand, increases in thiol monomer concentration cause decreases in the d -spacing. This decrease arises from segregation of 4-SH monomer near the aliphatic chains of the Brij 52 surfactant in the continuous domain of the hexagonal phase. As TTT is replaced with 4-SH, less ene monomer is available to swell the hexagonal cores causing them to shrink to allow for additional thiol monomer to sequester into the continuous domains. The curvature of this system with the more polar species segregated in the cores of hexagonal rods is known as an inverse hexagonal phase and will be referred to as such throughout the remainder of this chapter.

To better understand the impact of LLC order on polymer mechanical properties, the storage modulus and glass transition temperature (T_g) of the polymers was characterized using dynamic mechanical analysis. Figure 8.5 shows the storage modulus and $\tan \delta$ profiles as a function of temperature for the LLC templated, neat, and solution polymerized thiol-ene systems. It is apparent from Figure 8.5a that LLC order has a significant impact on the glass transition temperature of the polymer. The lowest T_g of the samples examined is for the solution polymerization of 85 wt % thiol-ene monomer mixture in DMSO with a T_g of approximately 25 °C. The T_g of the LLC templated and neat thiol-ene copolymer is higher at approximately 37 °C. Interestingly, there is no observable difference in T_g is observed for the nanostructured and neat thiol-ene polymers. This is surprising because the surfactant has been removed from the LLC templated polymer before property characterization, leading to a significantly higher void fraction compared to the neat system. Typically, a decrease in the polymer volume

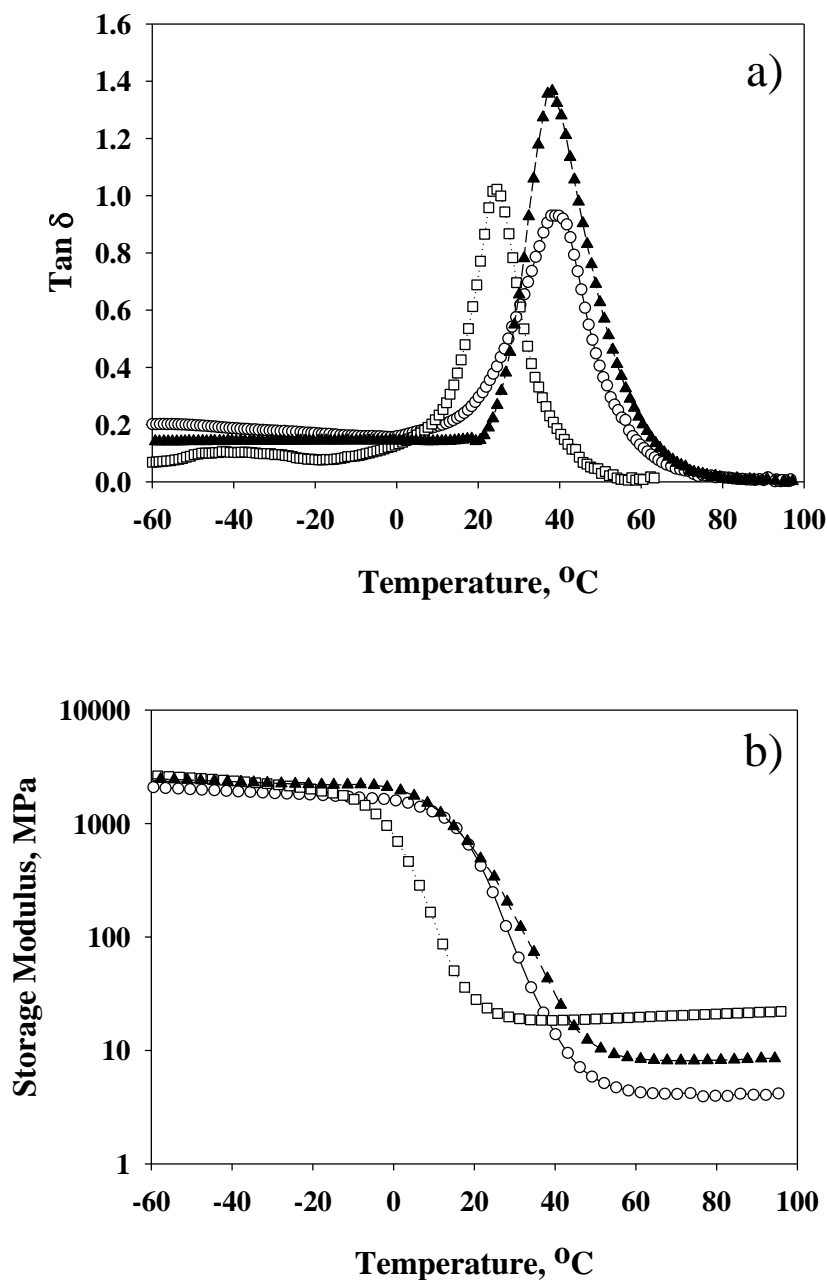


Figure 8.5. Glass transition temperature and $\text{Tan } \delta$ for thiol-ene polymers. Shown are a) $\text{Tan } \delta$ as a function of temperature and b) storage modulus as a function of temperature for LLC templated and isotropic thiol-ene systems. Shown are a 85 wt % thiol-ene mixture cured in 15 wt % DMSO (\square), an LLC templated system cured with 85 wt % thiol-ene mixture and 15 wt % Brij 52 surfactant (\circ), and a neat thiol-ene polymer cured as a 100 wt % mixture of thiol and ene (\blacktriangle). A 1:1 molar ratio of thiol and ene functional groups were used for all thiol-ene mixtures with 1 wt % photoinitiator. Solvent and surfactant were removed prior to analysis.

fraction leads to an increase in polymer chain mobility as more volume is available for polymer chains to partition. The increase in free volume has been used to explain differences in glass transition behavior of polymers using models developed by Eyring.⁷¹ A higher free volume or greater number of “holes” can lower the energy required for polymer chains to achieve coordinated long-range molecular motion associated with the glass transition region.⁷² The net result of an increase in free volume is often a decrease in the glass transition temperature.⁷³ The free volume theory of the glass transition temperature explains why the more porous 85 wt % thiol-ene copolymer cured in solvent has the lower T_g compared to the neat system, but it does not explain the unexpectedly large T_g of the LLC templated polymer. Despite the lower volume fraction, the nanostructured thiol-ene polymer has a T_g similar to the neat polymer. The higher glass transition temperature of the LLC templated polymer could be due to the induced packing of polymer chains as a result of polymerization in the ordered domains of the inverse hexagonal phase.⁷⁴ Even with the lower polymer volume fraction of the LLC system on the macroscopic scale, the packing of polymer chains on the micron and sub-micron scale may be comparable to the neat system. A similar effective volume fraction of polymers due to the induced ordering and packing of polymer chains as directed by the parent LLC template may explain the similar T_g of the LLC templated and neat polymer systems.

Such T_g behavior can have a dramatic impact on the polymer performance and is often described as the most important property that governs polymer functionality. The storage modulus of the polymer drops by several orders of magnitude as the polymer transitions from a glassy to a rubbery state.⁷⁵ Figure 8.5b shows the storage modulus as a function of temperature for the thiol-ene polymer systems. The increase in glass transition temperature for the LLC nanostructured system compared to the 85 wt % thiol-ene copolymer cured in solvent is evident from these profiles. The significant drop in modulus occurring at the glass transition temperature is 12 °C greater for the LLC

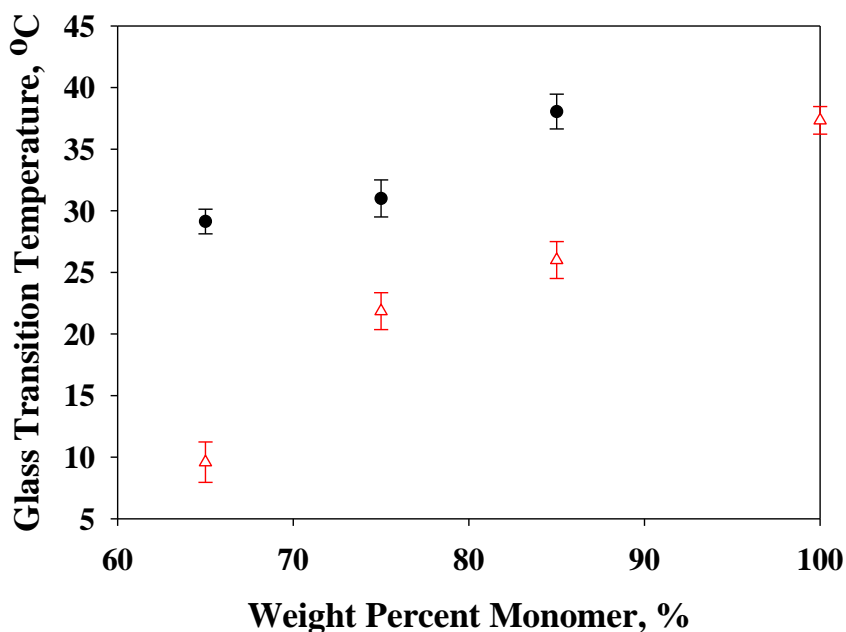


Figure 8.6. Glass transition temperature for LLC templated and isotropic thiol-ene polymers as a function of weight percent monomer used in the initial formulation. Shown are a hexagonal nanostructured thiol-ene copolymers templated using Brij 52 surfactant (●) and an isotropic polymer system cured in varying concentrations of DMSO. A 1:1 molar ratio of thiol and ene functional groups were used for all thiol-ene mixtures with 1 wt % photoinitiator. Brij 52 surfactant comprised the remainder of the sample formulations for the LLC templated system while the remainder of the isotropic solutions was DMSO. Solvent and surfactant were removed prior to testing.

nanostructured and neat thiol-ene polymers when compared to the solution polymerization of thiol-ene in solvent.

The impact of polymer nanostructure and volume fraction was further examined by analyzing the glass transition temperature of LLC templated and isotropic polymers at varying polymer volume fractions. From Figure 8.3, the inverse hexagonal LLC phase is formed at Brij 52 concentrations between 65 and 85 wt % with a stoichiometric ratio of thiol and ene monomers. The glass transition temperature of thiol-ene polymers templated with varying concentrations of Brij 52 surfactants was characterized and compared to the T_g of isotropic polymers cured with equal monomer concentration in

DMSO. Figure 8.6 shows the T_g of isotropic and inverse hexagonal nanostructured thiol-ene photopolymers as a function of monomer concentration used in the formulation. The glass transition temperature appears to be directly related to monomer concentration. Interestingly, the glass transition temperature of the inverse hexagonal nanostructured thiol-enes is higher than the corresponding isotropic thiol-ene control for all monomer concentrations. The largest difference in the glass transition temperature occurs at 65 wt % monomer where the LLC nanostructured polymer has a T_g 20 °C greater than the isotropic polymer. As noted above, the glass transition temperature is likely larger in the nanostructured systems because of the induced packing and ordering and corresponding decrease in mobility of the polymer chains as directed by the LLC template. Enhancing the T_g of polymers using LLCs to control polymer structure could be of great utility as the T_g is one of the key parameters dictating polymer performance and operating temperature.⁷⁵ Additionally, the improvement in T_g is accomplished using LLC templates formed using low cost surfactants. These materials show great economic promise in applications as the concentration of expensive monomer and photoinitiator can be decreased and replaced with low cost surfactants without sacrificing polymer properties.

In addition to differences in T_g for the polymers, the plateau modulus of the three polymer systems shown in Figure 8.5b are also different. The plateau modulus is proportional to the crosslink density of the network, increasing as the molecular weight between crosslinks decreases.⁷⁵ The plateau modulus is highest for the solution polymerization of 85 wt % thiol-ene in solvent and lowest for the nanostructured LLC thiol-ene system. Although the LLC nanostructure could have an impact on the plateau modulus because the orientation of polymer chains as directed by the LLC template has been shown to increase the modulus, differences in plateau modulus can also be explained by the different ultimate conversions and polymer volume fractions. Relative crosslinking density may be estimated from the volume fraction of polymer determined

from monomer concentration in the formulation before polymerization and the ultimate conversion as measured by FTIR.

The degree of conversion for thiol-ene systems was measured using FTIR in order to estimate the relative crosslinking densities of the polymer networks. Figure 8.7 shows the thiol and ene functional group conversion as a function of time for the LLC templated system formed with 85 wt % thiol-ene monomer and 15 wt % Brij 52. Also shown in Figure 8.5 is the neat polymerization of a thiol-ene mixture and the isotropic polymerization of an 85 wt % thiol-ene system in solvent. The highest conversion is observed for the solution polymerization of thiol-ene monomers in DMSO. The second highest conversion is observed for the LLC templated system while the lowest conversion is seen in the neat thiol-ene system. Performing estimated crosslinking density analysis based on FTIR conversion data gives rise to the observed trend in plateau modulus with the highest crosslink density occurring in the solution polymerization of thiol-ene and the lowest crosslink density in the LLC nanostructured system. The higher conversion of the solution cured thiol-ene polymer overcomes the smaller polymer volume fraction and leads to the highest crosslinking density and plateau modulus. Although the LLC templated polymer and neat thiol-ene system attain similar conversions, the higher polymer volume fraction facilitates crosslinking density compared to the nanostructured system.

Interestingly, significant differences in the polymerization rate and conversion between the LLC templated and isotropic thiol-ene systems shown in Figure 8.7. LLC order can have a dramatic impact on the photopolymerization kinetics of the system.⁴⁷⁻⁵⁰ The order imposed on monomers by the parent template can lead to changes in local monomer concentration and kinetic parameters which directly impact the polymerization rate. The highest polymerization rate and ultimate conversion is observed in the isotropic polymerization of thiol-ene in solvent. On the other hand, the lowest polymerization rate is observed for the neat polymerization of the thiol-ene monomers.

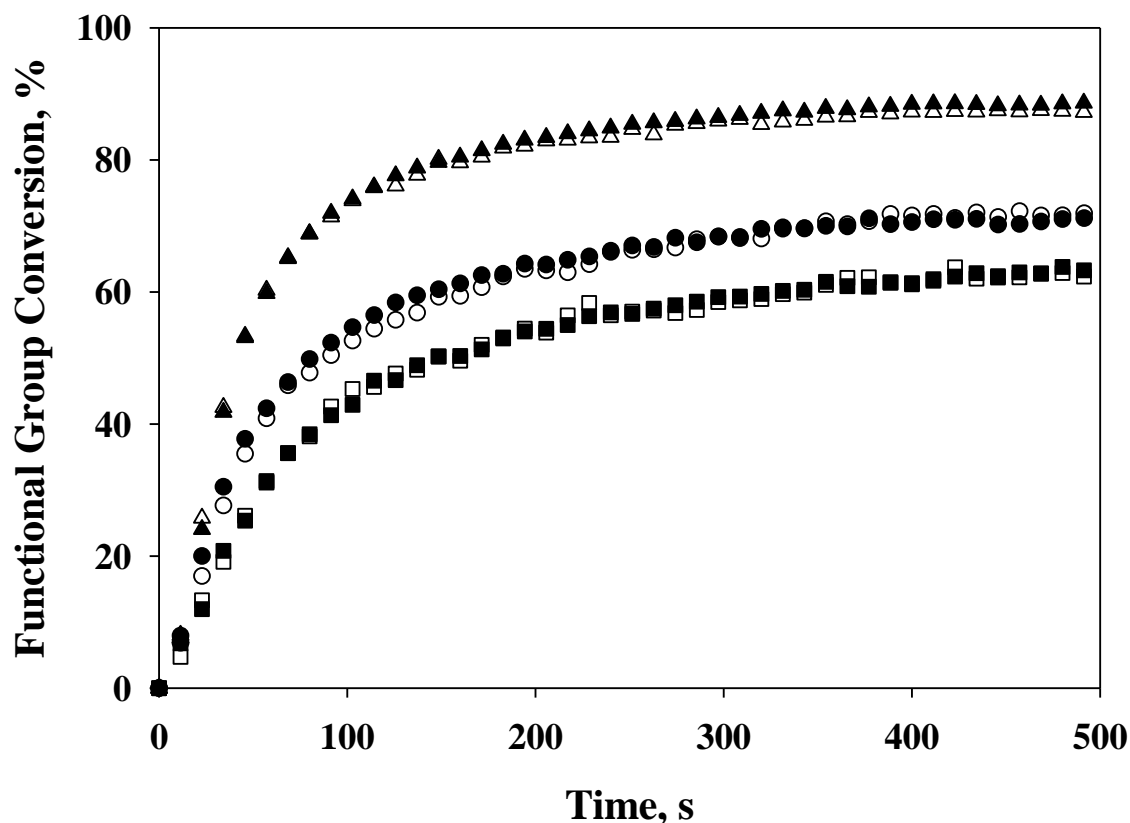


Figure 8.7. FTIR conversion profiles of thiol and ene functional groups for LLC templated and isotropic thiol-ene systems. Shown are thiol (Δ) and ene (\blacktriangle) conversion for a 85 wt % thiol-ene mixture in 15 wt % DMSO, thiol (\circ) and ene (\bullet) conversion for 85 wt % thiol-ene mixture with 15 wt % Brij 52 surfactant, and thiol (\square) and ene (\blacksquare) conversion for a 100 wt % mixture of thiol and ene. A 1:1 molar ratio of thiol and ene functional groups were used for all thiol-ene mixtures with 1 wt % photoinitiator. Photopolymerization was initiated using 365nm light at an intensity of $2.5 \text{ mW}\cdot\text{cm}^{-2}$.

These differences in conversion and rate are likely due to mass transfer limitations between the systems. The DMSO solvent used to solubilize the 85 wt % thiol-ene system increases the mobility of the reactive species and aids in the translational diffusion of reactive functional groups leading to a higher polymerization rate and conversion compared to the LLC templated and neat thiol-ene systems.

The polymerization rate of the neat thiol-ene mixture is slowest which could be due to greater mass transfer limitations that occur as monomer is converted to polymer in this system.⁷⁵ The polymerization rate of the LLC templated system is faster than the neat thiol-ene polymerization and lower than the isotropic polymerization in solvent. The slower rate of the LLC templated system compared to the isotropic polymerization in DMSO is likely due to greater monomer mobility as a result of DMSO plasticizing the network.^{2,65} The LLC templated system displays polymerization behavior more similar to the neat system which may be induced by the segregation of thiol and ene monomers in the LLC template and leads to an increase in local monomer concentration. The slower polymerization rate of the templated system compared to the isotropic polymerization of thiol-ene in solvent may be due to mass transfer limitations that result from differences in thiol and ene segregation behavior in the inverse hexagonal LLC phase as discussed above. For the LLC templated system, thiol and ene monomers are segregated from each other to a larger degree compared to the isotropic system and may need to diffuse larger distances to react which could explain the slower polymerization rate.^{64,76-78}

Conclusions

Generating nanostructure in organic polymers using LLCs as structure directing polymerization templates has shown great promise in the synthesis of polymers with useful property relationships based on nanostructure. In this work, the LLC templating process has been extended to step-growth thiol-ene polymers. The kinetics and mechanism of the polymerization allows greater structure retention and polymer volume fractions than previously possible in LLC templating. The phase behavior of ene

monomer 1,3,5-triallyl-1,3,5-triazine-2,4,6(1H,3H5H)-trione with thiol monomer pentaerythritol tetrakis(2-mercaptoacetate) and non-ionic Brij 52 surfactant was examined to understand the segregation and self-assembly behavior of the system. The ene monomer behaved as a cosolvent with thiol and surfactant to facilitate LLC phase formation in the absence of water. The inverse hexagonal LLC phase formed with a stoichiometric ratio of thiol-ene monomers is present over a wide range of surfactant concentrations for this system. Utilizing an ene monomer facilitate generation of the LLC phase instead of water allows more than double the monomer concentration and polymer volume fraction compared to previously examined LLC templated systems. Additionally, the inverse hexagonal structure of self-assembled thiol-ene/surfactant systems is retained after the photopolymerization reaction providing useful insight into factors governing polymer structure retention. Analysis of the photopolymerization kinetics and *d*-spacing ratios suggest that the segregation behavior of thiol and ene monomers is strongly influenced by the presence of an inverse hexagonal LLC phase. Dynamic mechanical analysis of LLC templated thiol-ene polymers up to a 20 °C increase in the glass transition temperature compared to a corresponding isotropic control of the same chemical composition and volume fraction. These results are useful in the design of robust polymer systems with high polymer volume fraction, improved mechanical properties, and controlled nanometer sized structures as directed by photopolymerization in LLC templates.

Notes

1. Bowman, C. N.; Kloxin, C. J. *AIChE J.* **2008**, *54*, 2775-2795.
2. Kaur, M.; Srivastava, A. *J. Macromol. Sci. -Polym. Rev* **2002**, *C42*, 481-512.
3. Baroli, B. *J. Chem. Technol. Biotechnol.* **2006**, *81*, 491-499.
4. Wang, H.; Feng, Y.; An, B.; Zhang, W.; Sun, M.; Fang, Z.; Yuan, W.; Khan, M. *J. Mater. Sci. -Mater. Med.* **2012**, *23*, 1499-1510.
5. Bader, R. A. *Acta Biomater.* **2008**, *4*, 967-975.
6. Catel, Y.; Degrange, M.; Le Pluart, L.; Madec, P.; Pham, T.; Chen, F.; Cook, W. D. *J. Polym. Sci. Pol. Chem.* **2009**, *47*, 5258-5271.
7. Elisseeff, J.; Anseth, K.; Sims, D.; McIntosh, W.; Randolph, M.; Yaremchuk, M.; Langer, R. *Plast. Reconstr. Surg.* **1999**, *104*, 1014-1022.
8. Pathak, C.; Sawhney, A.; Hubbell, J. *J. Am. Chem. Soc.* **1993**, *115*, 2548-2548.
9. Stansbury, J. W. *J. Esthet. Dent.* **2000**, *12*, 300-308.
10. Kwisnek, L.; Nazarenko, S.; Hoyle, C. E. *Macromolecules* **2009**, *42*.
11. Lwisnek, L.; Kaushik, M.; Hoyle, C. E.; Nazarenko, S. *Macromolecules* **2010**, *43*.
12. Li, Q.; Zhou, H.; Hoyle, C. E. *Polymer* **2009**, *50*.
13. Shin, J.; Nazarenko, S.; Phillips, J. P.; Hoyle, C. E. *Polymer* **2009**, *50*.
14. Zhou, J.; Zhang, Q.; Zhang, H.; Chen, S.; Liu, Q. *Journal of Polymer Research* **2012**, *19*, 9984.
15. Fu, Q.; Liu, J.; Shi, W. *Progress in Organic Coatings* **2008**, *63*.
16. Clark, T.; Kwisnek, L.; Hoyle, C. E.; Nazarenko, S. *Journal of Polymer Science Part A-Polymer Chemistry* **2009**, *47*.
17. Aimetti, A. A.; Machen, A. J.; Anseth, K. S. *Biomaterials* **2009**, *30*.
18. Acosta Ortiz, R.; Ruiz Martinez, A. Y.; Garcia Valdez, A. E. *Journal of Biobased Materials and Bioenergy* **2012**, *6*.

19. Acosta Ortiz, R.; Garay Flores, R. V.; Garcia Valdez, A. E.; Berlanga Duarte, M. L. *Progress in Organic Coatings* **2010**, 69.
20. Bowman, C. N.; Fairbanks, B. D.; Cramer, N. B.; Anseth, K. S. *Abstracts of Papers of the American Chemical Society* **2010**, 240.
21. Fairbanks, B. D.; Sims, E. A.; Anseth, K. S.; Bowman, C. N. *Macromolecules* **2010**, 43.
22. Lomba, M.; Oriol, L.; Alcala, R.; Sanchez, C.; Moros, M.; Grazu, V.; Luis Serrano, J.; De la Fuente, J. M. *Macromolecular Bioscience* **2011**, 11.
23. Cramer, N. B.; Reddy, S. K.; Cole, M.; Hoyle, C.; Bowman, C. N. *Journal of Polymer Science Part A-Polymer Chemistry* **2004**, 42.
24. Okay, O.; Reddy, S. K.; Bowman, C. N. *Macromolecules* **2005**, 38.
25. Reddy, S. K.; Cramer, N. B.; Bowman, C. N. *Macromolecules* **2006**, 39.
26. Hoyle, C. E.; Bowman, C. N. *Angewandte Chemie-International Edition* **2010**, 49.
27. Liu Qing; Zhang Qiuyu; Chen Shaojie; Zhou Jian; Lei Xingfeng *Chinese Journal of Organic Chemistry* **2012**, 32.
28. Lowe, A. B. *Polymer Chemistry* **2010**, 1.
29. Hussein, M. A.; Abdel-Rahman, M. A.; Asiri, A. M.; Alamry, K. A.; Aly, K. I. *Designed Monomers and Polymers* **2012**, 15.
30. Pilla, P.; Cusano, A.; Cutolo, A.; Giordano, M.; Mensitieri, G.; Rizzo, P.; Sanguigno, L.; Venditto, V.; Guerra, G. *Sensors* **2009**, 9.
31. Wei, J.; Yu, Y. *Soft Matter* **2012**, 8.
32. Hikmet, R.; Lub, J. *Prog. Polym. Sci.* **1996**, 21, 1165-1209.
33. Carfagna, C.; Amendola, E.; Giamberini, M. *Progress in Polymer Science* **1997**, 22.
34. Hussein, M. A.; Abdel-Rahman, M. A.; Asiri, A. M.; Alamry, K. A.; Aly, K. I. *Designed Monomers and Polymers* **2012**, 15.
35. Olson, D. A.; Chen, L.; Hillmyer, M. A. *Chemistry of Materials* **2008**, 20.
36. Clapper, J. D.; Sievens-Figueroa, L.; Guymon, C. A. *Chemistry of Materials* **2008**, 20.

37. Pulko, I.; Krajnc, P. *Macromolecular Rapid Communications* **2012**, *33*.
38. Wan, Y.; Shi, Y.; Zhao, D. *Chemistry of Materials* **2008**, *20*.
39. Verheyen, E.; Schillemans, J. P.; van Wijk, M.; Demeniex, M.; Hennink, W. E.; van Nostrum, C. F. *Biomaterials* **2011**, *32*, 3008-3020.
40. Lorenzo, R. A.; Carro, A. M.; Alvarez-Lorenzo, C.; Concheiro, A. *International Journal of Molecular Sciences* **2011**, *12*.
41. Ewen, S. L.; Steinke, J. H. G. *Recognition of Anions* **2008**, *129*.
42. Claesson, M.; Engberg, K.; Frank, C. W.; Andersson, M. *Soft Matter* **2012**, *8*.
43. Wiesenauer, B. R.; Gin, D. L. *Polym. J.* **2012**, *44*, 461-468.
44. Zhang, J.; Xie, Z.; Hill, A. J.; She, F. H.; Thornton, A. W.; Hoang, M.; Kong, L. X. *Soft Matter* **2012**, *8*.
45. Zhang, J.; Xie, Z.; She, F. H.; Hoang, M.; Hill, A. J.; Gao, W. M.; Kong, L. X. *J Appl Polym Sci* **2011**, *120*.
46. Clapper, J. D.; Guymon, C. A. *Macromolecules* **2007**, *40*.
47. DePierro, M. A.; Carpenter, K. G.; Guymon, C. A. *Chemistry of Materials* **2006**, *18*.
48. Forney, B. S.; Guymon, C. A. *Macromolecules* **2010**, *43*.
49. Lester, C. L.; Colson, C. D.; Guymon, C. A. *Macromolecules* **2001**, *34*.
50. Lester, C. L.; Smith, S. M.; Jarrett, W. L.; Guymon, C. A. *Langmuir* **2003**, *19*.
51. Sievens-Figueroa, L.; Guymon, C. A. *Polymer* **2008**, *49*.
52. Clapper, J. D.; Guymon, C. A. *Macromolecules* **2007**, *40*.
53. Forney, B. S.; Guymon, C. A. *Macromolecular Rapid Communications* **2011**, *32*.
54. Odijk, T. *Macromolecules* **1986**, *19*.
55. Wiesenauer, B. R.; Gin, D. L. *Polym. J.* **2012**, *44*.
56. Kotz, J.; Kosmella, S. *Current Opinion in Colloid & Interface Science* **1999**, *4*.
57. Wang, C.; Chen, D.; Jiao, X. *Science and Technology of Advanced Materials* **2009**, *10*, 023001.

58. Queslel, J. P.; Mark, J. E. *Advances in Polymer Science* **1984**, *65*.
59. Yoon, H.; Choi, M.; Lee, K. A.; Jang, J. *Macromol. Res.* **2008**, *16*, 85-102.
60. Scherer, G. *J Am Ceram Soc* **1990**, *73*, 3-14.
61. Glatter, O.; Kratky, O. In *Small Angle X-ray Scattering*. Porod, G., Ed.; General Theory; Academic Press Inc.: New York, NY, 1982.
62. Clapper, J. D.; Guymon, C. A. *Adv Mater* **2006**, *18*, 1575.
63. Sievens-Figueroa, L.; Guymon, C. A. *Macromolecules* **2009**, *42*.
64. Jakubiak, J.; Rabek, J. *Polimery* **2001**, *46*, 10-22.
65. Jakubiak, J.; Rabek, J. *Polimery* **2000**, *45*, 485-495.
66. Hentze, H. P.; Kaler, E. W. *Curr. Opin. Colloid Interface Sci.* **2003**, *8*, 164-178.
67. Hentze, H. P.; Antonietti, M. *Curr. Opin. Solid State Mat. Sci.* **2001**, *5*, 343-353.
68. Feigin, L. A.; Svergun, D. I. Structure Analysis by Small Angle X-Ray and Neutron Scattering. In Taylor, G. W., Ed.; Plenum Press: New York, NY, 1987; pp 59-63.
69. Collings, P. J.; Hird, M. Introduction to Liquid Crystals: Chemistry and Physics. In *Identification of liquid crystal phases - mesophase characterization*; Gray, G. W., Goodby, J. W. and Fukuda, A., Eds.; Taylor & Francis Inc.: Bristol, PA, 1997; pp 177-190.
70. Sievens-Figueroa, L.; Guymon, C. A. *Chemistry of Materials* **2009**, *21*.
71. Faerber, G. L.; Kim, S. W.; Eyring, H. *J. Phys. Chem.* **1970**, *74*.
72. Binder, K.; Baschnagel, J.; Paul, W. *Progress in Polymer Science* **2003**, *28*, PII S0079-6700(02)00030-8.
73. Aharoni, S. M. *Polym. Adv. Technol.* **1998**, *9*.
74. Lu, H. B.; Nutt, S. *Macromolecules* **2003**, *36*.
75. Odian, G. *Principles of Polymerization*; John Wiley & Sons: Hoboken, NJ, 2004.
76. Herrera-Ordonez, J.; Olayo, R.; Carrol, S. *Journal of Macromolecular Science-Polymer Reviews* **2004**, *C44*.
77. Nomura, M. *Journal of Industrial and Engineering Chemistry* **2004**, *10*.

78. Thickett, S. C.; Gilbert, R. G. *Polymer* **2007**, *48*.

CHAPTER 9

CONCLUSIONS AND RECOMMENDATIONS

Nanostructured polymers generated through photopolymerization in lyotropic liquid crystalline templates show great promise in enhancing the functionality of a wide range of polymer materials. The property relationships of these systems are not traditionally observed in classical polymers with isotropic structures and represent a new class of polymer materials with enhanced properties based on nanostructure. The simultaneous increases in polymer transport and mechanical properties achieved using the LLC templated process are of considerable use in numerous applications including hydrogels, drug delivery, coatings, and sensors. Even with the promise of improved polymer performance by generating structure in polymer materials, there are several difficulties that need to be addressed in order to utilize LLCs to control polymer nanostructure. Many of the problems associated with the LLC templating technique have been addressed in this research. From a basic understanding of the phase separation process to the development and application of methods to control polymer structure, this research contributes a significant and useful body of knowledge that can be applied to synthesize polymers with controlled nanostructure. A significant portion of this research has applied the LLC templating procedure to improve the performance of stimuli-responsive hydrogels for use in drug delivery, sensor, and membrane applications. The nanostructured network as directed by the LLC template shows dramatic increases in key performance parameters including deswelling rate, mechanical properties, and dynamic range of water uptake. Expanding upon previous work regarding nanocomposites generated using LLCs, the functionality of poly(*N*-isopropylacrylamide) was improved through generation of a nanostructured interpenetrating network with poly(dimethyl

siloxane) to improve the mechanical properties of the hydrogel. Ultimately, the fundamental development and application of LLC templating technology has been greatly expanded as a result of this research and can be applied to develop nanostructured polymers with property relationships that are not attainable in traditional polymer systems.

One of the primary difficulties in applying the LLC templating methodology to generate nanostructured polymer materials is phase separation from the parent template. Phase separation and structural development in LLC systems has been studied in great detail, primarily through detailed examination of the photopolymerization kinetics. Building upon previous research relating the local order imposed on monomers by the parent template, the photopolymerization kinetics of hexanediol diacrylate and poly(ethylene glycol) diacrylate templated in the lamellar and hexagonal LLC phases were characterized and used to determine the structure evolution during polymerization. The phase separation process was found to produce significant changes in the polymerization rate that are not explained by classical polymerization kinetics of isotropic polymer systems. Small angle x-ray scattering (SAXS) of the polymers at particular conversions show dramatic changes in polymer structure occur in a step wise manner throughout the polymerization reaction. In fact, the most significant phase separation events occur within the first 10% conversion and again at later stages in the reaction at about 40-50% conversion. These data suggest that the phase separation process is driven partially by the gelation effect that occurs at low conversions and higher crosslinking densities that occur at later stages of radical mediated acrylate chain photopolymerizations. Additionally, these results provide a novel method that can be used to probe the local order in the system and identify the phase separation processes directly through characterization of the photopolymerization kinetics. This tool is particularly useful in establishing the effectiveness of methods to control polymer structure by examining the impact of factors dictating LLC structure retention on phase evolution during polymerization.

While fundamental characterization of the structural development in LLC templated systems is critical to the synthesis of nanostructured polymers, perhaps more important is the development of methods that can be used to control the polymer structure in systems that phase separate during polymerization. Such control was achieved by examining an LLC templated acrylamide monomer system that has a high tendency to phase separate from the parent template during polymerization. This system served as a model system to examine how the original phase structure may be transferred to the polymer for an unstable LLC templated system. A reactive surfactant known to retain its structure during polymerization was added to the LLC phase to aid in structure preservation. By adding the reactive surfactant to the hexagonal LLC phase the original structure was transferred to the polymer during polymerization.

The impact of LLC nanostructure on polymer properties was characterized extensively to demonstrate the enhancement in performance that may be achieved by incorporating nanostructure in the polymer network. The water uptake and diffusivity of acrylamide polymers that retain the hexagonal LLC nanostructure is significantly improved compared to isotropic controls of the same chemical composition. The compressive moduli of hexagonal nanostructured polymers are 70% greater than the moduli of corresponding isotropic controls. The significant increase in modulus for LLC nanostructured polymers illustrates the improved mechanical performance that can be attained by the LLC templating process. Unique property relationships that are not observed in traditional polymer systems were also established in this work. Despite the higher water uptake of the LLC nanostructured polymers, the compressive modulus of LLC hydrogels in their swollen state is not different than the modulus of isotropic controls containing less water. This behavior is very different from the behavior often reported for traditional hydrogels in which an increase in water uptake will decrease the compressive modulus in accordance with classical polymer science. These property

relationships represent a new paradigm of performance useful in a tremendous range of hydrogel applications.

An essential basis for research in polymer science is application of acquired knowledge to solve problems encountered in material development. Utilizing the property relationships established for the acrylamide hydrogels with hexagonal LLC nanostructure including simultaneous increases in water uptake, transport, and mechanical stability, the LLC templating technology was used to improve the performance of stimuli-sensitive polymers. The widely studied temperature sensitive polymer poly(*N*-isopropylacrylamide) (PNIPAM) was chosen for examination due to limitations in the mechanical and transport properties that are often reported in literature. To demonstrate the utility of LLC templating technology to control polymer structure and optimize polymer properties, a bicontinuous cubic morphology was generated in a PNIPAM network and the swelling and deswelling properties of the nanostructured hydrogel were compared to a traditional isotropic PNIPAM gel. Significant increases in water uptake were observed for the cubic nanostructured hydrogel below the lower critical solution temperature (LCST). In fact, a near two fold increase in equilibrium water uptake at 22 °C is seen for the LLC templated gel compared to the isotropic PNIPAM hydrogel of the same chemical composition.

The deswelling rate of PNIPAM is dramatically increased using LLC templating technology. In fact, using the time needed for the hydrogel to lose half of the water for heating above the LCST as a reference, the nanostructured gel deswells two orders of magnitude faster than the isotropic gel. Of particular interest in this LLC system that differs from other research in stimuli-sensitive PNIPAM hydrogels is the mechanical properties of the network. Despite the increase in water uptake observed for the cubic hydrogel, the compressive modulus is not statistically different from the isotropic PNIPAM gel. Even though classical polymer science would predict a near three-fold decrease in the compressive modulus given the additional water absorbed by the LLC

templated gel, the directed pore structure of the nanostructured gel better resists mechanical deformation and preserves the mechanical stability of the network. This stability represents a significant improvement in PNIPAM properties that may be of great utility in the design of hydrogels with appropriate mechanical properties for use in biomedical and sensor applications.

To further demonstrate the usefulness of LLC templating to improve the properties of temperature sensitive PNIPAM hydrogels, the hexagonal mesophase was used to produce interpenetrating networks (IPN) of poly(dimethyl siloxane) (PDMS) and PNIPAM to further enhance the mechanical stability of the network. The LLC template allows for rapid synthesis of PDMS-PNIPAM IPN copolymers with the temperature sensitive hydrogel properties inherent in PNIPAM and the toughness associated with PDMS networks. The swelling, deswelling, and mechanical properties of the LLC templated PDMS-PNIPAM copolymers with varying PDMS concentrations were examined and compared to the properties of an isotropic copolymer network of the same chemical composition. The equilibrium water uptake for the hexagonal nanostructured gels was significantly greater than that of the isotropic controls for all PDMS concentrations examined. The rate of deswelling was also significantly faster for all hexagonal LLC templated hydrogels compared to their isotropic counterparts, decreasing the time needed for the hydrogel to deswell and reach equilibrium by at least an order of magnitude. Moreover, the mechanical stability of the hydrogels was maintained for LLC templated IPN systems despite their significantly greater water uptake. These results further illustrate the utility of LLC templating to produce useful polymer materials including the facile synthesis of IPN copolymers with useful property relationships that cannot be attained by traditional bulk polymerization methods.

The utility of LLC templating to generate nanostructured polymers with improved properties was expanded by applying the templating methodology to a new class of polymer materials. Specifically, LLC nanostructure was incorporated into a useful class

of polymers known as thiol-enes which are widely used in coating applications. The thiol-ene copolymerization proceeds by a very different radical mediated step-growth polymerization mechanism compared to the previously studied radical mediated chain polymerizations of (meth)acrylates. By comparing the structure retention and phase behavior of the thiol-ene step-growth polymerization to radical mediated chain polymerizations, critical thermodynamic and kinetic information dictating the underlying factors governing polymer structure control were examined. In order to apply the LLC templating method to hydrophobic thiol-ene copolymers, the strong incompatibility of thiol monomers with water was overcome using an ene monomer to act as the cosolvent for the LLC phase to avoid compatibility issues with water and to allow self-assembly into an ordered LLC phase. The phase behavior and photopolymerization kinetics of the water-free LLC templated thiol-ene system was characterized to elucidate the segregation behavior and phase formation of the system. The strong degree of structure retention observed for the thiol-ene templated system provides a useful tool in the synthesis of robust LLC nanostructured polymers that retain the parent template structure during polymerization. Additionally, the improved glass transition temperature and mechanical properties of the LLC nanostructured thiol-ene copolymers compared to isotropic controls of the same chemical composition further illustrates how polymer nanostructure may be directed to improve polymer performance.

While control of polymer nanostructure using LLCs as structure directing polymerization platforms to improve polymer functionality has been advanced by this research, much work remains in the development of robust LLC nanostructured systems containing useful property relationships. Although significant information including methods of determining nanostructure evolution during polymerization, identification of several systems that retain LLC structure, and a method of retaining LLC structure in systems that phase separate have been developed, the degree of structure retained remains a largely experimental observation with little theoretical basis. In order to predict final

polymer morphology, degree of structure retention, and achieve greater control over the final polymer nanostructure, a theoretical model that predicts LLC phase retention and stability should be developed.

One method that may be used to predict phase stability is based on the cohesive energy density (CED) of the LLC templated system. The cohesive energy density of the system is described as the energy needed to remove a given molecule from its nearest neighboring molecules. Because the phase separation process involves molecular rearrangement and disruption of order in the system through the diffusion of molecules, it is likely that higher CEDs could lead to more stable LLC templated systems and a greater degree of structure transferred to the polymer during polymerization. An LLC template with a higher CED would require the system to overcome a larger energy barrier in order to phase separate. By increasing the CED of the LLC templated polymer, the thermodynamic driving force for phase separation can be minimized and the LLC structure may be successfully transferred to the polymer. Through theoretical estimations of the CED based on group contribution methods, the solubility parameters that describe the CED can be approximated. LLC templated systems containing varying degrees of CED can then be designed based on the selection of commercially available surfactants and monomers with different polarities and chemical structures. The degree of LLC phase structure retention can then be correlated through qualitative and quantitative analysis of the small angle x-ray scattering (SAXS) profiles before and after polymerization. Qualitative structure information can be extracted from SAXS profiles by characterizing the phase morphology of the system before and after polymerization. Quantitative structural information can also be obtained from SAXS by calculating shifts in the primary scattering peaks and changes in the degree of disorder in the system based on the scattering peak position and full-width at half maximum. By comparing the CED to the degree of structure retained as examined by SAXS the thermodynamics of the LLC

templated system needed to control and retain the original morphology may be determined.

A CED model may also be used to determine the underlying factors that govern the high degree of structure retention observed in the thiol-ene LLC system discussed above. At present, it is unclear if the high degree of structure retention is due to the polymerization mechanism and kinetics or the thermodynamics and stability of the self-assembled system. Utilizing the CED model to decouple thermodynamic and kinetic stability of the thiol-ene and other LLC systems will provide great insight into the development and expansion of polymer chemistries in which the LLC templating process may be successfully applied. Another problem that the CED model may prove useful in solving is the poor mechanical stability that can result in LLC templated systems due to low monomer concentrations. Although the thiol-ene system contains monomer concentrations up to 85 wt%, typically LLC formulations contain at most 40 wt% monomer. The low monomer concentration can lead to low polymer volume fractions which can compromise the mechanical stability of the system and limit the functionality of LLC nanostructured polymers. The CED model may provide insight into methods of increasing monomer concentrations while maintaining the LLC order of the system by estimating CED thresholds and identifying particular monomers that are required to achieve the self-assembled order. Another method that can be used to increase monomer concentration in the system is the development and use of reactive surfactants to template common monomers. By acrylate capping hydroxyl terminated Brij surfactants with an acrylate using isocyanate or acryloyl chloride chemistries the fraction of polymerizable material can be greatly increased and mechanical stability of the LLC templated system may be significantly improved.

Due to the intimate relationships between polymer structure and properties, it is important that the final working structure of the polymer be characterized directly. While SAXS is important in examining polymer morphology, results can be misleading because

phase separated polymers still allow LLC phase formation between surfactant and water. Thus, the structural information obtain using SAXS is inherently convoluted with multiple-phase scattering resulting from LLC-water and LLC-polymer interactions. In order to understand the thermodynamic factors governing polymer morphology and the relationship between nanostructure and properties, it is critical that polymer structure be characterized directly before, during, and after polymerization using neutron scattering. The order of polymer and water should be probed in real-time during photopolymerization using small-angle neutron scattering (SANS). Contrast variation can be utilized to extract the specific structures of polymer and water from the measured scattering profiles by modulating the deuteration level of water and monomer. Deuterated monomers may be templated using a non-deuterated surfactant in water to elucidate how polymer nanostructure changes during photopolymerization. Similarly, deuterium oxide could be used as the solvent to template non-deuterated monomers in an LLC template and provide important thermodynamic information regarding solvent interactions with polymer and surfactant during polymerization.

Deuterated compounds should be used at high concentration to provide maximum contrast and structural information regarding the compound of interest. LLC templated systems that self-assemble into highly-ordered mesophases before polymerization and phase separate during polymerization identified in our lab using SAXS should be characterized comprehensively using neutron scattering to gather explicit structural and thermodynamic information describing phase separation events. An ultraviolet (UV) light source could irradiate LLC templated samples mounted in a UV transparent sample holder and initiate the photopolymerization reaction. The intensity and emission spectrum of the UV light source will be directly related to the rate of monomer conversion and the intense neutron pulses will provide time-resolved structures of water and polymer throughout the photopolymerization reaction. As the polymerization progresses, phase separation events may be identified directly from the time-resolved

neutron scattering profiles. Utilizing the inherent advantages of photopolymerization, the UV light intensity can be adjusted to achieve a polymerization rate sufficiently slow to allow structural characterization on time-scales accessible to the neutron scattering instrumentation. Additional thermodynamic information can be obtained by monitoring the zero-angle scattering intensity, $I(0)$, which is inversely related to the curvature of the Gibbs free energy density of the system. Monitoring the zero-angle scattering intensity in time will provide fundamental thermodynamic information including stable, metastable, and spinodal regimes of the Gibbs free energy density as a function of monomer conversion. Knowledge gathered from the proposed neutron scattering experiments will be utilized to identify and optimize the thermodynamic factors governing the control of polymer nanostructure to enhance properties dependent on nanometer sized structures.

To further expand the use of LLCs in improving the properties of stimuli-sensitive systems for use in biomedical applications, the templating methods should be applied to other stimuli-sensitive polymers that respond to pH or ionic strength. These systems share many of the problems associated with traditional PNIPAM hydrogels including slow response rates and weak mechanical properties. It is likely that the improved mechanical and transport properties observed for the LLC templated PNIPAM hydrogels in this work can be extrapolated to solve problems associated with other classes of stimuli-sensitive polymers. Similar to the use of LLC templates to generate PNIPAM-PDMS IPNs, the templating methods can be used to generate IPN materials with multiple stimuli-responsive polymers. For example, multiple responsive hydrogels that respond to different combinations of stimuli including temperature, pH, and ionic strength may be produced by utilizing the LLC template to segregate polymer with a particular stimuli into distinct domains. The properties of multiple individual polymer networks that respond to particular stimuli can be incorporated into a single polymer material to produce a novel class of hydrogels that respond to several stimuli. It is likely that these

novel hydrogels could contain useful property relationships generated by the LLC network for use in a wide variety of applications.

Another particularly innovative application of LLC templating is the use of PNIPAM-acrylamidophenylboronic acid copolymers to control insulin delivery in response to glucose concentration. When PNIPAM is copolymerized with acrylamidophenylboronic acid moieties, a useful polymer that responds to glucose concentration at normal human body temperature is attained. The phenylboronic acid moieties in the polymer network form complexes with glucose with a particularly high affinity over other polyols found in the body. The formation of this complex with glucose generates a partial charge on the phenylboronic acid moiety causing the polymer to become hydrophilic and swell. The increase in mesh size that accompanies the swelling process then triggers the release of insulin and can be used as a self-regulating device to control blood sugar. A rapid on-off insulin delivery system may be attainable by the fast collapse of the polymer network as aided by the LLC nanostructure that shuts off insulin delivery quickly as glucose concentration decreases. This innovative polymer would have great functionality in the prevention of hypoglycemia in diabetic patients and could save lives.

In summary, many problems associated with the control of polymer structure using LLCs as structure directing polymerization platforms have been examined in this research. The use of photopolymerization kinetics as a probe to elucidate nanostructure evolution during polymerization, development of novel methods to preserve LLC structure, identification of systems that retain LLC structure during polymerization, and application of the LLC templating process to generate useful stimuli-responsive polymers has been achieved. Continuation of this work can lead to tremendous advancements in the functionality of polymers by controlling polymer network structure using LLCs as polymerization templates and applied to a growing number of advanced industrial and biomedical applications.

BIBLIOGRAPHY

- Acosta Ortiz, R.; Garay Flores, R. V.; Garcia Valdez, A. E.; Berlanga Duarte, M. L. *Progress in Organic Coatings* **2010**, *69*.
- Acosta Ortiz, R.; Ruiz Martinez, A. Y.; Garcia Valdez, A. E. *Journal of Biobased Materials and Bioenergy* **2012**, *6*.
- Adelhelm, P.; Hu, Y.; Chuenchom, L.; Antonietti, M.; Smarsly, B. M.; Maier, J. *Adv Mater* **2007**, *19*, 4012-+.
- Aharoni, S. M. *Polym. Adv. Technol.* **1998**, *9*.
- Aimetti, A. A.; Machen, A. J.; Anseth, K. S. *Biomaterials* **2009**, *30*.
- Alarcon, C.; Pennadam, S.; Alexander, C. *Chem. Soc. Rev.* **2005**, *34*, 276-285.
- Alexandridis, P.; Holmqvist, P.; Lindman, B. *Colloid Surf. A-Physicochem. Eng. Asp.* **1997**, *130*, 3-21.
- Andrzejewska, E. *Prog. Polym. Sci.* **2001**, *26*, 605-665.
- Anseth, K. S.; Bowman, C. N.; BrannonPeppas, L. *Biomaterials* **1996**, *17*, 1647-1657.
- Antonietti, M.; Caruso, R. A.; Goltner, C. G.; Weissenberger, M. C. *Macromolecules* **1999**, *32*, 1383-1389.
- Avestro, A.; Belowich, M. E.; Stoddart, J. F. *Chem. Soc. Rev.* **2012**, *41*, 5881-5895.
- Bader, R. A. *Acta Biomater.* **2008**, *4*, 967-975.
- Bai, G.; Wang, J.; Yan, H.; Li, Z.; Thomas, R. *J Phys Chem B* **2001**, *105*, 9576-9580.
- Bara, J. E.; Kaminski, A. K.; Noble, R. D.; Gin, D. L. *J. Membr. Sci.* **2007**, *288*, 13-19.
- Baroli, B. *J. Chem. Technol. Biotechnol.* **2006**, *81*, 491-499.
- Bates, F. S. *Science* **1991**, *251*, 898-905.
- Beatty, S.; Eong, K. G. A. *J. Accid. Emerg. Med.* **2000**, *17*, 324-329.
- Becquart, F.; Taha, M.; Zerroukhi, A.; Kaczun, J.; Stebani, U. *J. Polym. Sci. Pol. Chem.* **2004**, *42*, 1618-1629.
- Bender, F.; Chilcott, T. C.; Coster, H. G. L.; Hibbert, D. B.; Gooding, J. J. *Electrochim. Acta* **2007**, *52*, 2640-2648.
- Binder, K.; Baschnagel, J.; Paul, W. *Progress in Polymer Science* **2003**, *28*, PII S0079-6700(02)00030-8.

- Bowman, C. N.; Fairbanks, B. D.; Cramer, N. B.; Anseth, K. S. *Abstracts of Papers of the American Chemical Society* **2010**, 240.
- Bowman, C. N.; Kloxin, C. J. *AIChE J.* **2008**, 54, 2775-2795.
- Bromberg, L.; Ron, E. *Adv. Drug Deliv. Rev.* **1998**, 31, 197-221.
- Bushetti, S. S.; Singh, V.; Raju, S. A.; Atharjaved; Veermaram *Indian J. Pharm. Educ. Res.* **2009**, 43, 241-250.
- Campbell, G. C.; Vanderhart, D. L. *J. Magn. Reson.* **1992**, 96, 69-93.
- Canal, T.; Peppas, N. A. *J. Biomed. Mater. Res.* **1989**, 23, 1183-1193.
- Cardoso, D. A.; Jansen, J. A.; Leeuwenburgh, S. C. G. *J. Biomed. Mater. Res. Part B* **2012**, 100B, 2316-2326.
- Carfagna, C.; Amendola, E.; Giamberini, M. *Progress in Polymer Science* **1997**, 22.
- Cataldo, S.; Zhao, J.; Neubrech, F.; Frank, B.; Zhang, C.; Braun, P. V.; Giessen, H. *ACS Nano* **2012**, 6, 979-985.
- Catel, Y.; Degrange, M.; Le Pluart, L.; Madec, P.; Pham, T.; Chen, F.; Cook, W. D. *J. Polym. Sci. Pol. Chem.* **2009**, 47, 5258-5271.
- Chamarthy, S. P.; Pinal, R. In *In Plasticizer concentration and the performance of a diffusion-controlled polymeric drug delivery system*; Colloids and Surfaces A-Physicochemical and Engineering Aspects; Elsevier Science BV: Amsterdam; PO BOX 211, 1000 AE Amsterdam, Netherlands, 2008; Vol. 331, pp 25-30.
- Chaterji, S.; Kwon, I. K.; Park, K. *Prog. Polym. Sci.* **2007**, 32, 1083-1122.
- Choi, H. J.; Ray, S. S. *J. Nanosci. Nanotechnol.* **2011**, 11, 8421-8449.
- Chung, H. J.; Park, T. G. *Nano Today* **2009**, 4, 429-437.
- Claesson, M.; Engberg, K.; Frank, C. W.; Andersson, M. *Soft Matter* **2012**, 8.
- Clapper, J. D.; Guymon, C. A. *Macromolecules* **2007**, 40, 1101-1107.
- Clapper, J. D.; Iverson, S. L.; Guymon, C. A. *Biomacromolecules* **2007**, 8, 2104-2111.
- Clapper, J. D.; Pearce, M. E.; Guymon, C. A.; Salem, A. K. *Biomacromolecules* **2008**, 9, 1188-1194.
- Clapper, J. D.; Sievens-Figueroa, L.; Guymon, C. A. *Chemistry of Materials* **2008**, 20.
- Clapper, J.; Guymon, C. *Adv Mater* **2006**, 18, 1575.
- Clark, T.; Kwisnek, L.; Hoyle, C. E.; Nazarenko, S. *Journal of Polymer Science Part A-Polymer Chemistry* **2009**, 47.
- Collings, P. J.; Hird, M. *Introduction to Liquid Crystals Chemistry and Physics*; Taylor & Francis: London, 1997.

- Cramer, N. B.; Reddy, S. K.; Cole, M.; Hoyle, C.; Bowman, C. N. *Journal of Polymer Science Part A-Polymer Chemistry* **2004**, *42*.
- DePierro, M.; Guymon, C. *Macromolecules* **2006**, *39*, 617-626.
- DePierro, M.; Olson, A.; Guymon, C. *Polymer* **2005**, *46*, 335-345.
- DePierro, M. A.; Carpenter, K. G.; Guymon, C. A. *Chemistry of Materials* **2006**, *18*.
- Dinerman, A. A.; Cappello, J.; Ghandehari, H.; Hoag, S. W. *J. Controlled Release* **2002**, *82*, 277-287.
- Dos Santos, E. P.; Tokumoto, M. S.; Surendran, G.; Remita, H.; Bourgaux, C.; Dieudonne, P.; Prouzet, E.; Ramos, L. *Langmuir* **2005**, *21*, 4362-4369.
- Elabd, Y. A.; Baschetti, M. G.; Barbari, T. A. *J. Polym. Sci. Pt. B-Polym. Phys.* **2003**, *41*, 2794-2807.
- Elisseeff, J.; Anseth, K.; Sims, D.; McIntosh, W.; Randolph, M.; Yaremchuk, M.; Langer, R. *Plast. Reconstr. Surg.* **1999**, *104*, 1014-1022.
- El-Safty, S. A.; Hanaoka, T.; Mizukami, F. *Acta Mater.* **2006**, *54*, 899-908.
- Ewen, S. L.; Steinke, J. H. G. *Recognition of Anions* **2008**, *129*.
- Faerber, G. L.; Kim, S. W.; Eyring, H. *J. Phys. Chem.* **1970**, *74*.
- Fairbanks, B. D.; Sims, E. A.; Anseth, K. S.; Bowman, C. N. *Macromolecules* **2010**, *43*.
- Feigin, L. A.; Svergun, D. I. Structure Analysis by Small Angle X-Ray and Neutron Scattering. In Taylor, G. W., Ed.; Plenum Press: New York, NY, 1987; pp 59-63.
- Feng, P. Y.; Bu, X. H.; Pine, D. J. *Langmuir* **2000**, *16*, 5304-5310.
- Fong, C.; Le, T.; Drummond, C. J. *Chem. Soc. Rev.* **2012**, *41*, 1297-1322.
- Forney, B. S.; Guymon, C. A. *Macromolecules* **2010**, *43*.
- Forney, B. S.; Guymon, C. A. *Macromolecular Rapid Communications* **2011**, *32*.
- Frisch, H. L.; Stern, S. A. *Crc Critical Reviews in Solid State and Materials Sciences* **1983**, *11*, 123-187.
- Fu, Q.; Liu, J.; Shi, W. *Progress in Organic Coatings* **2008**, *63*.
- Fujiki, M.; Koe, J.; Terao, K.; Sato, T.; Teramoto, A.; Watanabe, J. *Polym. J.* **2003**, *35*, 297-344.
- Funari, S. S.; Holmes, M. C.; Tiddy, G. J. T. *J. Phys. Chem.* **1994**, *98*, 3015-3023.
- Ge, L.; Guo, R.; Zhang, X. *J Phys Chem B* **2009**, *113*, 1993-2000.

Gin, D.; Smith, R.; Deng, H.; Leising, G. In *In Synthesis of PPV nanocomposites using lyotropic liquid crystal monomers*; Synthetic Metals; Elsevier Science SA: Lausanne; PO Box 564, 1001 Lausanne, Switzerland, 1999; Vol. 101, pp 52-55.

Gin, D. L.; Bara, J. E.; Noble, R. D.; Elliott, B. J. *Macromol. Rapid Commun.* **2008**, *29*, 367-389.

Glatter, O.; Kratky, O. In *Small Angle X-ray Scattering*. Porod, G., Ed.; General Theory; Academic Press Inc.: New York, NY, 1982.

Gong, X.; Sagnella, S.; Drummond, C. J. *Int. J. Nanotechnol.* **2008**, *5*, 370-392.

Graeser, M.; Pippel, E.; Greiner, A.; Wendorff, J. H. *Macromolecules* **2007**, *40*, 6032-6039.

Gray, G. W.; Winsor, P. A. *Liquid Crystals & Plastic Crystals*; John Wiley & Sons, Inc.: New York, 1974.

Gregg, S. J.; Sing, K. S. *Surface Area and Porosity*; Academic Press: London, 1982.

Guo Ruijie; Zhang Baoquan; Sun Yuan; Liu Xiufeng *Prog. Chem.* **2007**, *19*, 1695-1702.

Guo, C.; Wang, J.; Cao, F.; Lee, R. J.; Zhai, G. *Drug Discov. Today* **2010**, *15*, 1032-1040.

Gupta, N.; Srivastava, A. *Polym. Int.* **1994**, *35*, 109-118.

Guymon, C. A.; Bowman, C. N. *Macromolecules* **1997**, *30*, 5271-5278.

Guymon, C. A.; Hoggan, E. N.; Clark, N. A.; Rieker, T. P.; Walba, D. M.; Bowman, C. N. *Science* **1997**, *275*, 57-59.

Haberstroh, K. M.; Thapa, A.; Miller, D. C.; Webster, T. J. In *In Polymers with nanostructured surface features for soft tissue replacement applications*; Chandra, T., Torralba, J. M. and Sakai, T., Eds.; Thermec'2003, Pts 1-5; Materials Science Forum; Trans Tech Publications LTD: Zurich-Uetikon; Brandrain 6, CH-8707 Zurich-Uetikon, Switzerland, 2003; Vol. 426-4, pp 3115-3120.

Hamid, S. M.; Sherrington, D. C. *Polymer* **1987**, *28*, 325-331.

Hamley, I. *Nanotechnology* **2003**, *14*, R39-R54.

Hatakeyama, E. S.; Gabriel, C. J.; Wiesenauer, B. R.; Lohr, J. L.; Zhou, M.; Noble, R. D.; Gin, D. L. *J. Membr. Sci.* **2011**, *366*, 62-72.

Hatakeyama, E. S.; Wiesenauer, B. R.; Gabriel, C. J.; Noble, R. D.; Gin, D. L. *Chem. Mat.* **2010**, *22*, 4525-4527.

Hentze, H. P.; Antonietti, M. *Curr. Opin. Solid State Mat. Sci.* **2001**, *5*, 343-353.

Hentze, H. P.; Kaler, E. W. *Chem. Mat.* **2003**, *15*, 708-713.

Hentze, H.; Goltner, C.; Antonietti, M. *Ber. Bunsen-Ges. Phys. Chem. Chem. Phys.* **1997**, *101*, 1699-1702.

- Hentze, H.; Kaler, E. *Chem. Mat.* **2003**, *15*, 708-713.
- Hentze, H.; Kaler, E. *Curr. Opin. Colloid Interface Sci.* **2003**, *8*, 164-178.
- Herrera-Ordóñez, J.; Olayo, R.; Carrol, S. *Journal of Macromolecular Science-Polymer Reviews* **2004**, *C44*.
- Hikmet, R.; Lub, J. *Prog. Polym. Sci.* **1996**, *21*, 1165-1209.
- Hindeleh, A.; Abdo, S. *Polymer Communications* **1989**, *30*, 184-186.
- Hintze-Bruening, H.; Troutier, A.; Leroux, F. *Prog. Org. Coat.* **2011**, *70*, 240-244.
- Hoag, B. P.; Gin, D. L. *Macromolecules* **2000**, *33*, 8549-8558.
- Hoffman, A. S. *Adv. Drug Deliv. Rev.* **2002**, *54*, 3-12.
- Hoyle, C. E.; Bowman, C. N. *Angewandte Chemie-International Edition* **2010**, *49*.
- Huang, W. E.; Smith, C. C.; Lerner, D. N.; Thornton, S. F.; Oram, A. *Water Res.* **2002**, *36*, 1843-1853.
- Hussein, M. A.; Abdel-Rahman, M. A.; Asiri, A. M.; Alamry, K. A.; Aly, K. I. *Designed Monomers and Polymers* **2012**, *15*.
- Ikemura, K.; Endo, T. *Dent. Mater. J.* **2010**, *29*, 481-501.
- Israelachvili, J. N.; Mitchell, D. J.; Ninham, B. W. *Journal of the Chemical Society-Faraday Transactions II* **1976**, *72*, 1525-1568.
- Jakubiak, J.; Rabek, J. *Polimery* **2000**, *45*, 485-495.
- Jakubiak, J.; Rabek, J. *Polimery* **2001**, *46*, 10-22.
- Janeschitz-Kriegl, H.; Ratajski, E. *Colloid Polym. Sci.* **2010**, *288*, 1525-1537.
- Ji, B.; Gao, H. *Ann. Rev. Mater. Res.* **2010**, *40*, 77-100.
- Jiang, T.; He, Y.; Jian, Y.; Nie, J. *Progress in Organic Coatings* **2012**, *75*.
- Junker, M.; Walther, J.; Braun, D.; Alig, I. *Angew. Makromol. Chem.* **1997**, *250*, 119-131.
- Kaneko, Y.; Nakamura, S.; Sakai, K.; Aoyagi, T.; Kikuchi, A.; Sakurai, Y.; Okano, T. *Macromolecules* **1998**, *31*, 6099-6105.
- Kaneko, Y.; Yoshida, R.; Sakai, K.; Sakurai, Y.; Okano, T. *J. Membr. Sci.* **1995**, *101*, 13-22.
- Karaenev, S.; Chilingirjan, M. *Eur. Polym. J.* **1984**, *20*, 1223-1225.
- Kaur, M.; Srivastava, A. *J. Macromol. Sci. -Polym. Rev* **2002**, *C42*, 481-512.
- Khan, M. B.; Hussain, S.; Hussain, R.; Khan, Z. M. *J. Adv. Mater.* **2010**, *42*, 74-87.

- Kotz, J.; Kosmella, S. *Current Opinion in Colloid & Interface Science* **1999**, *4*.
- Kumaraswamy, G.; Wadekar, M. N.; Agrawal, V. V.; Pasricha, R. *Polymer* **2005**, *46*, 7961-7968.
- Kwisnek, L.; Nazarenko, S.; Hoyle, C. E. *Macromolecules* **2009**, *42*.
- Laslau, C.; Williams, D. E.; Travas-Sejdic, J. *Prog. Polym. Sci.* **2012**, *37*, 1177-1191.
- Laszlo, K.; Kosik, K.; Rochas, C.; Geissler, E. *Macromolecules* **2003**, *36*, 7771-7776.
- Lee, Y. S. *Self-Assembly and Nanotechnology: A Force Balance Approach*; John Wiley & Sons, Inc.: Hoboken, NJ, 2008.
- Lester, C. L.; Guymon, C. A. *Polymer* **2002**, *43*, 3707-3715.
- Lester, C. L.; Smith, S. M.; Colson, C. D.; Guymon, C. A. *Chem. Mat.* **2003**, *15*, 3376-3384.
- Lester, C. L.; Smith, S. M.; Guymon, C. A. *Macromolecules* **2001**, *34*, 8587-8589.
- Lester, C. L.; Smith, S. M.; Jarrett, W. L.; Guymon, C. A. *Langmuir* **2003**, *19*, 9466-9472.
- Lester, C.; Colson, C.; Guymon, C. *Macromolecules* **2001**, *34*, 4430-4438.
- Lester, C.; Guymon, C. *Macromolecules* **2000**, *33*, 5448-5454.
- Li, D.; Zhang, X.; Yao, J.; Simon, G. P.; Wang, H. *Chem. Commun.* **2011**, *47*, 1710-1712.
- Li, H.; Huck, W. *Curr. Opin. Solid State Mat. Sci.* **2002**, *6*, 3-8.
- Li, M.; Yang, W.; Chen, Z.; Qian, J.; Wang, C.; Fu, S. *J. Polym. Sci. Pol. Chem.* **2006**, *44*, 5887-5897.
- Li, Q.; Zhou, H.; Hoyle, C. E. *Polymer* **2009**, *50*.
- Li, W.; Li, S. *Oligomers Polymer Composites Molecular Imprinting* **2007**, *206*, 191-210.
- Li, X.; Zhang, J.; Dong, B.; Zheng, L.; Tung, C. *Colloid Surf. A-Physicochem. Eng. Asp.* **2009**, *335*, 80-87.
- Liang, B.; Pan, L.; He, X. *J Appl Polym Sci* **1997**, *66*, 217-224.
- Lin, J. B.; Isenberg, B. C.; Shen, Y.; Schorsch, K.; Sazonova, O. V.; Wong, J. Y. *Colloids and surfaces.B, Biointerfaces* **2012**, *99*, 108-115.
- Lin, Y.; Stansbury, J. *J. Polym. Sci. Pol. Chem.* **2004**, *42*, 1985-1998.
- Liu Qing; Zhang Qiuyu; Chen Shaojie; Zhou Jian; Lei Xingfeng *Chinese Journal of Organic Chemistry* **2012**, *32*.
- Liu, F.; Urban, M. W. *Prog. Polym. Sci.* **2010**, *35*, 3-23.

- Liu, J.; Jungnickel, B. -. *J. Polym. Sci. Pt. B-Polym. Phys.* **2007**, *45*, 1917-1931.
- Liu, L.; Sheardown, H. *Biomaterials* **2005**, *26*, 233-244.
- Liu, T. B.; Burger, C.; Chu, B. *Prog. Polym. Sci.* **2003**, *28*, 5-26.
- Lomba, M.; Oriol, L.; Alcala, R.; Sanchez, C.; Moros, M.; Grazu, V.; Luis Serrano, J.; De la Fuente, J. M. *Macromolecular Bioscience* **2011**, *11*.
- Long, Y.; Shanks, R.; Stachurski, Z. *Prog. Polym. Sci.* **1995**, *20*, 651-701.
- Lorenzo, R. A.; Carro, A. M.; Alvarez-Lorenzo, C.; Concheiro, A. *International Journal of Molecular Sciences* **2011**, *12*.
- Lowe, A. B. *Polymer Chemistry* **2010**, *1*.
- Lu, H. B.; Nutt, S. *Macromolecules* **2003**, *36*.
- Lu, X.; Nguyen, V.; Zeng, X.; Elliott, B. J.; Gin, D. L. *J. Membr. Sci.* **2008**, *318*, 397-404.
- Lustig, S. R.; Peppas, N. A. *J Appl Polym Sci* **1988**, *36*, 735-747.
- Lwisnek, L.; Kaushik, M.; Hoyle, C. E.; Nazarenko, S. *Macromolecules* **2010**, *43*.
- Ma, J.; Zhang, L.; Fan, B.; Xu, Y.; Liang, B. *J. Polym. Sci. Pt. B-Polym. Phys.* **2008**, *46*, 1546-1555.
- Mao, G.; Ober, C. K. *Handbook of Liquid Crystals*; Wiley-VCH: Weinheim, 1998.
- Mason, M. N.; Metters, A. T.; Bowman, C. N.; Anseth, K. S. *Macromolecules* **2001**, *34*, 4630-4635.
- Matthew N. Lee; Ali Mohraz *Adv Mater* **2010**, *22*, 4836-4841.
- Mauguiere-Guyonnet, F.; Burget, D.; Fouassier, J. P. *Progress in Organic Coatings* **2007**, *59*.
- Mautner, A.; Qin, X.; Wutzel, H.; Ligon, S. C.; Kapeller, B.; Moser, D.; Russmueller, G.; Stampfl, J.; Liska, R. *Journal of Polymer Science Part A-Polymer Chemistry* **2013**, *51*.
- McCormick, D. T.; Stovall, K. D.; Guymon, C. A. *Macromolecules* **2003**, *36*, 6549-6558.
- McMahon, T. T.; Zadnik, K. *Cornea* **2000**, *19*, 730-740.
- Meuler, A. J.; Hillmyer, M. A.; Bates, F. S. *Macromolecules* **2009**, *42*, 7221-7250.
- Michler, G. H.; Balta-Calleja, F. J. *Mechanical Properties of Polymers based on Nanostructure and Morphology*; Taylor and Francis Group: Boca Raton, FL, 2005.
- Mishra, A.; Aswal, V. K.; Maiti, P. *J Phys Chem B* **2010**, *114*, 5292-5300.
- Mu, J.; Zheng, S. *J. Colloid Interface Sci.* **2007**, *307*, 377-385.

- Munoz, A.; McConney, M. E.; Kosa, T.; Luchette, P.; Sukhomlinova, L.; White, T. J.; Bunning, T. J.; Taheri, B. *Opt. Lett.* **2012**, *37*, 2904-2906.
- Napoli, A.; Tirelli, N.; Wehrli, E.; Hubbell, J. A. *Langmuir* **2002**, *18*, 8324-8329.
- Narayanan, J.; Jungman, M. J.; Patton, D. L. *Reactive & Functional Polymers* **2012**, *72*.
- Neto, A. M. F.; Salinas, S. R. A. *The Physics of Lyotropic Liquid Crystals*; Oxford University Press: New York, 2005.
- Nielsen, E. L. *Mechanical Properties of Polymers and Composites*; Marcel Ceker, Inc.: New York, 1974.
- Niu, G.; Song, L.; Zhang, H.; Cui, X.; Kashima, M.; Yang, Z.; Cao, H.; Wang, G.; Zheng, Y.; Zhu, S.; Yang, H. *Polym. Eng. Sci.* **2010**, *50*.
- Nomura, M. *Journal of Industrial and Engineering Chemistry* **2004**, *10*.
- Odian, G. *Principles of Polymerization*; John Wiley & Sons: Hoboken, NJ, 2004.
- Odijk, T. *Macromolecules* **1986**, *19*.
- Okay, O.; Reddy, S. K.; Bowman, C. N. *Macromolecules* **2005**, *38*.
- Okumura, Y.; Ito, K. *Adv Mater* **2001**, *13*, 485-+.
- Olsen, B. D.; Segalman, R. A. *Mater. Sci. Eng. R-Rep.* **2008**, *62*, 37-66.
- Olson, D. A.; Chen, L.; Hillmyer, M. A. *Chemistry of Materials* **2008**, *20*.
- Oya, N.; Saitoh, S.; Furuhashi, Y.; Yoshie, N. *J. Polym. Sci. Pol. Chem.* **2012**, *50*, 1926-1932.
- Pathak, C.; Sawhney, A.; Hubbell, J. *J. Am. Chem. Soc.* **1993**, *115*, 2548-2548.
- Paul, D. R.; Robeson, L. M. *Polymer* **2008**, *49*, 3187-3204.
- Pellizer, G.; Asaro, F. *Magn. Reson. Chem.* **2008**, *46*, S80-S85.
- Peppas, N. A.; Khare, A. R. *Adv. Drug Deliv. Rev.* **1993**, *11*, 1-35.
- Perla, V.; Webster, T. J. *Journal of Biomedical Materials Research Part a* **2005**, *75A*, 356-364.
- Pilla, P.; Cusano, A.; Cutolo, A.; Giordano, M.; Mensitieri, G.; Rizzo, P.; Sanguigno, L.; Venditto, V.; Guerra, G. *Sensors* **2009**, *9*.
- Pulko, I.; Krajnc, P. *Macromolecular Rapid Communications* **2012**, *33*.
- Queslel, J. P.; Mark, J. E. *Advances in Polymer Science* **1984**, *65*.
- Reddy, S. K.; Cramer, N. B.; Bowman, C. N. *Macromolecules* **2006**, *39*.

- Reppy, M. A.; Gray, D. H.; Pindzola, B. A.; Smithers, J. L.; Gin, D. L. *J. Am. Chem. Soc.* **2001**, *123*, 363-371.
- Sagle, A. C.; Ju, H.; Freeman, B. D.; Sharma, M. M. *Polymer* **2009**, *50*, 756-766.
- Sanabria-DeLong, N.; Agrawal, S. K.; Bhatia, S. R.; Tew, G. N. *Macromolecules* **2006**, *39*, 1308-1310.
- Scherer, G. *J Am Ceram Soc* **1990**, *73*, 3-14.
- Schricker, S. R.; Palacio, M. L. B.; Bhushan, B. *Philos. Trans. R. Soc. A-Math. Phys. Eng. Sci.* **2012**, *370*, 2348-2380.
- Seguela, R. *J. Macromol. Sci. -Polym. Rev* **2005**, *C45*, 263-287.
- Serizawa, T.; Wakita, K.; Akashi, M. *Macromolecules* **2002**, *35*, 10-12.
- Settle, F. *Handbook of Instrumental Techniques for Analytical Chemistry*; Prentice Hall PTR: Upper Saddle River, NJ, 1997.
- Shin, J.; Nazarenko, S.; Phillips, J. P.; Hoyle, C. E. *Polymer* **2009**, *50*.
- Sievens-Figueroa, L.; Guymon, C. A. *Polymer* **2008**, *49*.
- Sievens-Figueroa, L.; Guymon, C. A. *Chem. Mat.* **2009**, *21*, 1060-1068.
- Sievens-Figueroa, L.; Guymon, C. A. *Macromolecules* **2009**, *42*, 9243-9250.
- Singh, M. A.; Ghosh, S. S.; Shannon, R. F. *J. Appl. Crystallogr.* **1993**, *26*, 787-794.
- Singh, N. K.; Singh, S. K.; Dash, D.; Purkayastha, B. P. D.; Roy, J. K.; Maiti, P. *J. Mater. Chem.* **2012**, *22*, 17853-17863.
- Sonpatki, M.; Chien, L. C. In *In Lyo-mesophases from self-assembled disk-shaped molecules*; Molecular Crystals and Liquid Crystals; Gordon Breach Publishing, Taylor & Francis Group: Philadelphia; 325 Chestnut St, 8TH FL, Philadelphia, PA 19106 USA, 2001; Vol. 367, pp 3333-3341.
- Stansbury, J. W. *J. Esthet. Dent.* **2000**, *12*, 300-308.
- Stuart, M. A. C.; Huck, W. T. S.; Genzer, J.; Mueller, M.; Ober, C.; Stamm, M.; Sukhorukov, G. B.; Szleifer, I.; Tsukruk, V. V.; Urban, M.; Winnik, F.; Zauscher, S.; Luzinov, I.; Minko, S. *Nat. Mater.* **2010**, *9*, 101-113.
- Szleifer, I.; Yerushalmi-Rozen, R. *Polymer* **2005**, *46*, 7803-7818.
- Takata, S.; Suzuki, K.; Norisuye, T.; Shibayama, M. *Polymer* **2002**, *43*, 3101-3107.
- Texter, J. *Colloid Polym. Sci.* **2009**, *287*, 313-321.
- Thapa, A.; Webster, T. J.; Haberstroh, K. M. *Journal of Biomedical Materials Research Part a* **2003**, *67A*, 1374-1383.
- Thickett, S. C.; Gilbert, R. G. *Polymer* **2007**, *48*.

Tobolsky, A. V. *Properties and Structure of Polymers*; John Wiley: New York, 1960; pp 71-78.

Tortora, L.; Park, H.; Kang, S.; Savaryn, V.; Hong, S.; Kaznatcheev, K.; Finotello, D.; Sprunt, S.; Kumar, S.; Lavrentovich, O. D. *Soft Matter* **2010**, *6*, 4157-4167.

Trey, S. M.; Nilsson, C.; Malmstrom, E.; Johansson, M. *Progress in Organic Coatings* **2010**, *67*.

Venkataraman, S.; Hedrick, J. L.; Ong, Z. Y.; Yang, C.; Ee, P. L. R.; Hammond, P. T.; Yang, Y. Y. *Adv. Drug Deliv. Rev.* **2011**, *63*, 1228-1246.

Verheyen, E.; Schillemans, J. P.; van Wijk, M.; Demeniex, M.; Hennink, W. E.; van Nostrum, C. F. *Biomaterials* **2011**, *32*, 3008-3020.

Vuluga, Z.; Panaitescu, D. M.; Radovici, C.; Nicolae, C.; Iorga, M. D. *Polym. Bull.* **2012**, *69*, 1073-1091.

Wan, Y.; Shi, Y.; Zhao, D. *Chemistry of Materials* **2008**, *20*.

Wang, C.; Varshney, R. R.; Wang, D. *Adv. Drug Deliv. Rev.* **2010**, *62*, 699-710.

Wang, C.; Chen, D.; Jiao, X. *Science and Technology of Advanced Materials* **2009**, *10*, 023001.

Wang, H.; Feng, Y.; An, B.; Zhang, W.; Sun, M.; Fang, Z.; Yuan, W.; Khan, M. J. *Mater. Sci. -Mater. Med.* **2012**, *23*, 1499-1510.

Wang, J. J.; Liu, F. *J Appl Polym Sci* **2012**, *127*, 2235-2242.

Wang, X.; Schroeder, H. C.; Wang, K.; Kaandorp, J. A.; Mueller, W. E. G. *Soft Matter* **2012**, *8*, 9501-9518.

Wang, Y.; Tran, H. D.; Kaner, R. B. *Macromol. Rapid Commun.* **2011**, *32*, 35-49.

Wei, G.; Ma, P. X. *Adv. Funct. Mater.* **2008**, *18*, 3568-3582.

Wei, J.; Yu, Y. *Soft Matter* **2012**, *8*.

Wiesnauer, B. R.; Gin, D. L. *Polym. J.* **2012**, *44*, 461-468.

Wu, W.; Mitra, N.; Yan, E. C. Y.; Zhou, S. *ACS Nano* **2010**, *4*, 4831-4839.

Wu, X. S.; Hoffman, A. S.; Yager, P. J. *Polym. Sci. Pol. Chem.* **1992**, *30*, 2121-2129.

Xu, J.; Zhu, Y.; Zhang, Y.; Zheng, Y.; Chi, Z.; Xu, J. *J Appl Polym Sci* **2007**, *103*, 3183-3193.

Xu, Y. J.; Gu, W. Q.; Gin, D. L. *J. Am. Chem. Soc.* **2004**, *126*, 1616-1617.

Yan, F.; Texter, J. *Adv. Colloid Interface Sci.* **2006**, *128*, 27-35.

Yang, S. F.; Leong, K. F.; Du, Z. H.; Chua, C. K. *Tissue Eng.* **2001**, *7*, 679-689.

- Yang, W.; Furukawa, H.; Gong, J. P. *Adv Mater* **2008**, *20*, 4499-4503.
- Yin, L.; Fei, L.; Tang, C.; Yin, C. *Polym. Int.* **2007**, *56*, 1563-1571.
- Yoon, H.; Choi, M.; Lee, K. A.; Jang, J. *Macromol. Res.* **2008**, *16*, 85-102.
- Yoshida, R.; Uchida, K.; Kaneko, Y.; Sakai, K.; Kikuchi, A.; Sakurai, Y.; Okano, T. *Nature* **1995**, *374*, 240-242.
- Zhang, J.; Jandt, K. D. *Macromol. Rapid Commun.* **2008**, *29*, 593-597.
- Zhang, J.; Liu, X.; Fahr, A.; Jandt, K. D. *Colloid Polym. Sci.* **2008**, *286*, 1209-1213.
- Zhang, J.; Xie, Z.; Hill, A. J.; She, F. H.; Thornton, A. W.; Hoang, M.; Kong, L. X. *Soft Matter* **2012**, *8*, 2087-2094.
- Zhang, J.; Xie, Z.; She, F. H.; Hoang, M.; Hill, A. J.; Gao, W. M.; Kong, L. X. *J Appl Polym Sci* **2011**, *120*.
- Zhang, X. Z.; Wang, F. J.; Chu, C. C. *J. Mater. Sci. -Mater. Med.* **2003**, *14*, 451-455.
- Zhang, X.; Xu, X.; Cheng, S.; Zhuo, R. *Soft Matter* **2008**, *4*, 385-391.
- Zhao, Q.; Sun, J.; Chen, S.; Zhou, Q. *J Appl Polym Sci* **2010**, *115*, 2940-2945.
- Zhou, J.; Zhang, Q.; Zhang, H.; Chen, S.; Liu, Q. *Journal of Polymer Research* **2012**, *19*, 9984.